



Greenhouse gas emissions from and storm impacts on wastewater treatment plants: Process modelling and control

Thèse

Li Sha Guo

Doctorat en génie des eaux
Philosophiae doctor (Ph.D)

Québec, Canada

© Li Sha Guo, 2014

Résumé

Cette thèse étudie l'interaction entre les stations d'épuration (STEP) et le changement climatique: soit en premier lieu la production ainsi que les émissions de gaz à effet de serre (GES), en particulier le protoxyde d'azote (N_2O), généré à la STEP et en second lieu l'effet des pluies plus intenses dues aux changements climatiques sur la STEP. Des campagnes de mesure sur le terrain et la modélisation à échelle réelle ont été utilisées conjointement dans cette recherche.

Une campagne de mesure d'une durée d'un mois a été réalisée dans une STEP traitant les eaux usées de 750,000 équivalents habitants, soit la STEP d'Eindhoven aux Pays-Bas. Des capteurs en ligne ont été installés dans la zone d'aération du bioréacteur.

Une usine virtuelle de grande échelle, soit la STEP décrit par le Benchmark Simulation Model No.2 (BSM2), ainsi qu'une usine réelle de grande échelle, soit la STEP d'Eindhoven aux Pays-Bas, étaient incluses dans cette étude. Dans les deux cas, les modèles ont été modifiés afin de prendre en compte les GES, en particulier la production de N_2O . Deux modèles de boues activées (ASM) ont été développés, soit l'ASMG1 et l'ASMG2d. En plus de la conversion de N_2O par les bactéries hétérotrophes, les deux modèles sont en mesure de simuler la production de N_2O par la dénitrification catalysée par les bactéries oxydant l'ammoniac (AOB). Les modèles décrivent aussi l'effet de l'oxygène dissous (OD) sur la cinétique de production de N_2O par les AOB grâce à une modification de la cinétique d'Haldane.

Les résultats montrent que les AOB produisent beaucoup de N_2O tandis que les hétérotrophes en consomment considérablement. Les émissions de N_2O augmentent lorsque les concentrations de NH_4^+ sont élevées et que les concentrations d'OD sont modérées (jusqu'à 2.5 mg O_2/l dans cette étude). Ces conditions peuvent avoir été créées

par le contrôle en cascade de NH_4^+ -OD qui vise à réduire la consommation d'énergie en diminuant les concentrations d'OD lorsque la concentration de NH_4^+ est suffisamment faible. En outre, ce contrôleur en cascade est une stratégie de réaction à gain faible. C'est-à-dire, un retard significatif se produit entre la détection d'une augmentation de NH_4^+ et l'accroissement de l'aération. Toutes ces propriétés produisent des conditions favorables à la production de N_2O par les bactéries AOB.

Différents scénarios alternatifs ainsi que des stratégies de contrôle ont été comparés selon la qualité de l'effluent, le coût d'opération et les émissions de GES. Dans le cadre de BSM2, un bon équilibre entre la qualité de l'effluent, le coût d'opération et les émissions de GES a été obtenu avec à la mise en œuvre d'un contrôleur rétroactif pur de l'OD sur la première zone d'aération et d'un contrôleur en cascade de NH_4^+ -DO sur les deux zones d'aération suivantes et en utilisant soit une stratégie d'alimentation étagée ou le contrôle du recyclage des boues afin de gérer les pics de débits.

Mots-clés:

Traitement des eaux usées par boues activées, contrôle de procédé, campagne de mesures en terrain, modélisation mathématique à échelle grandeur réelle, gaz à effet de serre, protoxyde d'azote, temps de pluie

Abstract

This PhD thesis studied the interaction between wastewater treatment plants (WWTPs) and climate change, i.e. the production and emission of greenhouse gases (GHGs), especially nitrous oxide (N_2O), from WWTPs and the effect of the climate change induced more intense rain events on WWTPs. Both field measurements and full-scale modelling were pursued in this research.

A one-month measurement campaign was performed by installing on-line sensors at the aeration zone of the bioreactor of a 750,000 person equivalents WWTP, i.e. the Eindhoven WWTP in the Netherlands. The models of a full-scale virtual plant, i.e. the Benchmark Simulation Model No.2 (BSM2), and a full-scale real plant, i.e. the Eindhoven WWTP in the Netherlands, were extended with respect to GHG emissions, especially the pathways involving N_2O . Two types of extended Activated Sludge Models (ASM) were developed, i.e. ASMG1 for COD/N removal and ASMG2d for COD/N/P removal. Besides heterotrophic N_2O production, both proposed models include N_2O production by nitrite denitrification by ammonia-oxidizing bacteria (AOB) and describe the DO effect on AOB N_2O production by a modified Haldane kinetics term.

Results showed that AOB are the major producer of N_2O while the heterotrophs consume N_2O considerably. The high N_2O emissions occurred under high NH_4^+ and intermediate DO concentrations (up to 2.5 mg O_2/l in this work). Such conditions can be created by NH_4^+ -DO cascade control which aims at reducing energy consumption by lowering the DO concentrations when the NH_4^+ concentration is sufficiently low. Moreover, this cascade controller is a low-gain feedback control strategy, i.e. a significant delay will occur between the detection of a NH_4^+ increase and the increase in aeration. All these properties lead to conditions favourable to N_2O production by AOB.

Different alternative scenarios and control strategies were compared in terms of effluent quality, operational cost and GHG emissions. In the framework of BSM2, a good balance among effluent quality, operational cost and GHG emissions was realized by implementing a pure DO feedback controller in the first aeration zone and a NH_4^+ -DO cascade controller in the following two aeration zones and using either step feed or sludge recycling control to deal with hydraulic shocks.

Keywords:

Activated sludge, wastewater treatment, process control, field measurements, full-scale mathematical modelling, greenhouse gases, nitrous oxide, wet weather conditions

Table of Contents

Résumé	III
Abstract	V
Table of Contents	VII
List of Tables	XI
List of Figures	XIII
Nomenclature	XV
Foreword.....	XXV
1 Introduction	1
2 Literature review.....	3
2.1 GHGs emissions from WWTPs	3
2.1.1 WWTPs borne GHGs: classification and evaluation framework	3
2.1.2 Full-scale N ₂ O emissions.....	6
2.2 N₂O production pathways	7
2.2.1 Biochemical pathways	7
2.2.2 Chemical pathway	14
2.3 Modelling of N₂O emissions.....	15
2.3.1 Model structures.....	18
2.3.2 Model applications in full-scale plants.....	31
2.4 Control of N₂O emissions.....	38
2.4.1 Control in BSM2	38
2.4.1 Alternative N ₂ O mitigation strategies	39
2.5 Controlling under rain events	40
2.6 Problem statement.....	41
2.6.1 Insufficient full-scale measurement data.....	41
2.6.2 Insufficient model development	42
2.6.3 Lack of control strategy studies including GHGs models	42
2.7 Objectives	43
3 Benchmark GHG modelling and controlling	45
3.1 Introduction.....	45
3.2 ASMG1 model calibration and validation using BSM2.....	46

3.2.1 Implementation and calibration/validation approaches.....	46
3.2.2 Results	54
3.2.3 Discussion.....	63
3.3 Control of GHG emissions in BSM2	69
3.3.1 Methods	69
3.3.2 Results and discussion.....	75
3.4 Conclusion	79
4 Measuring and modelling N₂O emissions from a real WWTP	81
4.1 Introduction.....	81
4.2 Measuring N₂O emissions from a real WWTP	82
4.2.1 Materials and methods	82
4.2.2 N ₂ O emissions under dry weather conditions	91
4.2.3 N ₂ O emissions under wet weather conditions.....	95
4.2.4 Relationship between N ₂ O emissions and control strategies	98
4.2.5 Control improvement	105
4.3 Modelling N₂O emissions from a real WWTP	109
4.3.1 ASMG2d model and implementation of a real WWTP	109
4.3.2 Simulation results of a real WWTP	125
4.3.3 Discussion.....	133
4.4 Conclusion	140
5 Conclusions and perspectives.....	143
5.1 Conclusions	143
5.1.1 Full-scale measurement experience	143
5.1.2 DO effect on AOB denitrification	144
5.1.3 Model calibration and validation.....	145
5.1.4 Model discrimination.....	147
5.1.5 Contribution from AOB denitrification.....	147
5.1.6 N ₂ O emissions under wet-weather conditions.....	149
5.1.7 Control strategies	150
5.2 Perspectives.....	152
5.2.1 A unified model of AOB N ₂ O production	152
5.2.2 Wet-weather studies.....	153
5.2.3 Sensitivity analysis of ASMG2d	154

5.2.4 Other GHGs besides N ₂ O.....	155
5.2.5 Integrated models.....	156
References	157
Appendix A Calculation of N ₂ O emissions.....	175
Appendix B Contribution of AOB pathway to N ₂ O emissions.....	179
Appendix C Liquid-gas equilibrium of N ₂ O	183
Appendix D Stoichiometric matrix of ASMG1	185
Appendix E Kinetic equations of ASMG1	189
Appendix F Component matrix of ASMG1	191
Appendix G Stoichiometric matrix of ASMG2d	193
Appendix H Kinetic equations of ASMG2d	203
Appendix I Component matrix of ASMG2d.....	209
Appendix J Publications and conferences.....	211

List of Tables

Table 2.1	Structures of models	16
Table 2.2	Stoichiometric matrices of the different AOB N ₂ O production models.....	27
Table 3.1	Summary of the two ASMG1-BSM2 models	46
Table 3.2	Open loop BSM2 results obtained with ASMN with default and calibrated parameters	55
Table 3.3	Tuned parameters of the ASMN submodel and corresponding target of each parameter tuning.....	56
Table 3.4	Tuned parameters of the two AOB denitrification submodels and corresponding target of each parameter tuning.....	57
Table 3.5	Calibration results of ASMG1 BSM2 in open loop	57
Table 3.6	Validation of calibrated ASMG1 in BSM2 control strategies	61
Table 3.7	Comparison of average heterotrophic and autotrophic N ₂ O production rates and the emission rate for the two AOB models	61
Table 3.8	Control strategies tested in the thesis	71
Table 3.9	Parameters of the PI controllers.....	71
Table 4.1	Average N ₂ O emission rates and emission factors.....	91
Table 4.2	Parameters of ASMG2d ^a	118
Table 4.3	Average contribution to N ₂ O production (%)......	135

List of Figures

Figure 2.1	GHG emission sources from a WWTP. The GWP values are from the IPCC report (2013).....	5
Figure 2.2	Scheme of biochemical N removal and N ₂ O productions	8
Figure 2.3	Illustration of the MLE process configuration for nitrogen removal	9
Figure 2.4	Scheme of the chemical NO ₂ ⁻ reduction	14
Figure 2.5	Maximum specific growth rate of heterotrophs expressed by the Arrhenius equation (dashed) and the Ratkowsky equation (solid).	20
Figure 2.6	Scheme of the model proposed by Pan et al. (2013).....	22
Figure 2.7	Scheme of the model proposed by Ni et al. (2011) (a) and the model proposed by Ni et al. (2013a) (b)	24
Figure 2.8	Scheme of the model proposed by Law et al. (2012)	24
Figure 2.9	Scheme of the models proposed by Mampaey et al. (2013)	25
Figure 2.10	BSM2 plant layout.....	34
Figure 2.11	BSM2 default control strategies	35
Figure 3.1	Illustration of kinetic relationship between S _O and DO _{Haldane} in the modified Haldane term.	48
Figure 3.2	The calibration procedure and the sub-targets of each step.....	53
Figure 3.3	Comparison of daily averaged dynamic results of ASU4 obtained with the original, the modified ASMG1-BSM2 and the finalized ASM1-BSM2 in open loop (a) and with 1-DO strategy (b).	58
Figure 3.4	Comparison of total dynamic N ₂ O emissions in the two warmest (a) and the two coldest weeks (b) in open loop and under the three tested control strategies.	62
Figure 3.5	Comparison of daily averaged N ₂ O emissions in open loop under steady-state simulation and dynamic simulation with the modified ASMG1-BSM2. .	64
Figure 3.6	Comparison of daily averaged dynamic N ₂ O production rates by different bacteria groups simulated with the modified ASMG1-BSM2 in open loop. ...	67
Figure 3.7	NH ₄ ⁺ -DO cascade with minimal DO requirement strategy	72
Figure 3.8	NH ₄ ⁺ -DO cascade plus 1 DO controller strategy	72
Figure 3.9	Comparison of different control strategies using the current influent file.....	75
Figure 3.10	Comparison of different control strategies using the future influent file.....	75
Figure 4.1	Bird view of bioreactor (a), location of N ₂ O sampling points	84

Figure 4.2	Temporal variation of N ₂ O emission rate at the beginning (a), the middle (b) and the end section (c) of the summer package.....	87
Figure 4.3	Comparison of N ₂ O emission rates at the end section of the summer package with influent flow rate and influent NH ₄ ⁺ concentrations and loads (a), local aeration flow rate and DO concentration (b), and N component concentrations at the end of the summer package (c).....	88
Figure 4.4	Comparison of N ₂ O emission rates at the end section of the summer package with the local aeration flow rate and the DO concentration (a), and with N components concentrations at the end of the summer package and influent NH ₄ ⁺ concentrations and loads (b) for one typical dry day.....	89
Figure 4.5	Off-line measurement of NO ₂ ⁻ concentration under three dry-weather days (a-c) and two wet-weather days (d-e).....	90
Figure 4.6	Comparison of aeration flow rate, NH ₄ ⁺ concentration and influent flow rate for the wet weather day August 25 th (a) and comparison of N ₂ O emission rate, NH ₄ ⁺ concentration, DO concentration and NO ₃ ⁻ concentration for the same wet weather day (b).	100
Figure 4.7	Comparison of aeration flow rate, NH ₄ ⁺ concentration and influent flow rate for the wet weather day August 26 th (a) and comparison of N ₂ O emission rate, NH ₄ ⁺ concentration, DO concentration and NO ₃ ⁻ concentration for the same wet weather day (b).	104
Figure 4.8	Scheme of control strategies.....	107
Figure 4.9	Comparison of different μ_{PAO} values in ASM2d based on the Arrhenius temperature dependency ($\mu_{A,T,PAO}$) and in ASMG2d based on the Ratkowsky temperature dependency ($\mu_{R,PAO}$).....	112
Figure 4.10	ASMG2d influent fractionation model.....	114
Figure 4.11	Comparison of $k_L a$ calculated by original aeration model and the modified model at 20.26 °C with sludge age of 5.74 d.	116
Figure 4.12	Comparison in terms of DO and N ₂ O simulation results between using original aeration model (a and c) and modified aeration model (b and d) ...	124
Figure 4.13	Comparison of the measured DO concentrations near the outlet of the bioreactor with the simulation results.	125
Figure 4.14	Comparison of the measurement results with the simulation results of NH ₄ ⁺ (a), NO ₃ ⁻ (b) and NO ₂ ⁻ (c).....	126
Figure 4.15	Comparison of simulated and measured N ₂ O emissions at the beginning (BM) (a), the middle (MM) (b) and the end section (EM) (c) of the summer aeration package.	128
Figure 4.16	Comparison of the internal recycle flow rate from the middle ring to the inner ring (Q _A) and the internal recycling flow rate from the outer ring to the middle ring (Q _B) on August 16 th -17 th (b) with the values under two normal dry days (a).....	132

Nomenclature

ANRA	Assimilative NO_3^- reduction to ammonia
AMO	Ammonia monooxygenase
AOB	Ammonia-oxidizing bacteria
ASM1, ASM2d, ASM3	Activated sludge model No. 1, No. 2d No. 3
ASMN	Activated sludge model for Nitrogen
ASMG1	Activated sludge model for GHG No. 1
ASMG2d	Activated sludge model for GHG No. 2d
ASMN-BSM2	BSM2 implemented with ASMN
ASMG1-BSM2	BSM2 implemented with ASMG1
ASM1-BSM2	BSM2 implemented with ASM1
ASU1-5	Activated sludge unit 1-5
BSM1	Benchmark simulation model No. 1
BSM2	Benchmark simulation model No. 2
C/N	Ratio between organic carbon and nitrogen
CODs	Soluble chemical oxygen demand
CODt	Total chemical oxygen demand
CSTR	Completely stirred tank reactors
DN-N	Denitrification-nitrification
DO	Dissolved oxygen
EPRI	Electric Power Research Institute
EQI	Effluent quality index
GAOs (DGAOs)	Glycogen accumulating organisms (Denitrifying GAOs)
GHG	Greenhouse gas
GWP	Global warming potential
HAO	Hydroxylamine oxidoreductase
HRT	Hydraulic retention time
IPCC	Intergovernmental Panel on Climate Change
MLE process	Modified Ludzack-Ettinger process
NAR	Nitrate reductase
NGGI	National Greenhouse Gas Inventory
NiR	Nitrite reductase

NiRK	Nitrite reductase used by AOB
NOR	Nitric-oxide reductase
NOB	Nitrite-oxidizing bacteria
NOS	Nitrous oxide reductase
NXR	Nitrite oxidoreductase
OCI	Operational cost index
PAOs (DPAOs)	Phosphorous accumulating organisms (Denitrifying PAOs)
PHA	Polyhydroxyalkanoates
SBR	Sequencing batch reactor
SHARON	Single reactor system for High activity Ammonia Removal Over Nitrite
SP	Setpoint
UCT process	University Cape Town process
WWTP	Wastewater treatment plant
$k_{l,a}$	Oxygen transfer coefficient

BOD5	Five-day biochemical oxygen demand
CH ₄	Methane
CO ₂	Carbon dioxide
Fe ²⁺	Ferrous iron
Fe ³⁺	Ferric iron
FNA	Free nitrous acid
FA	Free ammonia
N	Nitrogen
NH ₂ OH	Hydroxylamine
NH ₄ ⁺	Ammonia
NO ₃ ⁻	Nitrate
NO ₂ ⁻	Nitrite
NO	Nitric oxide
NOH	Hyponitrous acid
N ₂ O	Nitrous oxide
N ₂	Dinitrogen
P	Phosphorous

PO_4^-	Phosphate
TKN	Total Kjeldahl nitrogen
TN	Total nitrogen
TSS	Total suspended solids
VFA	Volatile fatty acids
$S_{\text{soluble_component}}$	Concentration of "soluble components"
$X_{\text{partical_component}}$	Concentration of "particle components"

I dedicate this thesis to my parents

谨以此论文献给我的父亲母亲

Acknowledgement

First of all, I would like to express my gratitude to my supervisor Prof. Peter A. Vanrolleghem who taught me a lot in the past four years. With his creative mind and broad knowledge, Peter has achieved high reputation in the field of wastewater treatment. From him I have learnt not only the expertise, but also the way of thinking and the attitude to have in work and life. There are many things for which I would like to thank him. He is a patient advisor who spent great efforts on correcting my papers and thesis. He is a funny person who often came up with jokes and shared them with us. He has a kind heart. I will never forget that during my difficult time, he always encouraged and trusted me. People are often impressed by his enormous energy during work. His enthusiasm also inspired me to be more positive and happier in my studies and life. All these stories, either small or big, were weaved into a warm memory.

I also want to thank Prof. Ingmar Nopens who is my co-supervisor from the Ghent University in Belgium. His knowledge and experience on hydraulic modelling elevated my understanding of wastewater treatment. His comments on my papers and thesis expanded my mind with new ideas. Ingmar is a young and amicable professor, who feels like a friend. During my visiting studies at the Ghent University, I got a lot of help from him and his BIOMATH team. Through discussions with them, I learnt how to design and carry out the field measurements and gathered working experience in the lab.

At the same time, I want to give a special thanks to my committee members, Prof. Ulf Jeppsson, Prof. Paul Lessard and Dr. Stefan Weijers. Thanks for your brilliant comments which profoundly improved my thesis and thanks for joining my defense which gave my PhD study a beautiful ending. I also thank Prof. Kartik Chandran, Prof. Mark C. M. van Loosdrecht, Dr. Sudhir Murthy, Dr. Andrew R. Shaw, Prof. Eveline I.P. Volcke and Prof. Zhiguo Yuan. Conferences and cooperation provided me great opportunities to learn from

those preeminent and reputable scholars, especially in terms of mechanisms and modelling of N₂O production.

modelEAU team is the research group where I did my PhD study with Prof. Peter A. Vanrolleghem. Team members are from different places around the world. They are all helpful and kind persons. This created an enjoyable working environment during my whole PhD period. I want to thank especially Coralie Lamaire-Chad. She worked at the Eindhoven plant with me for a one-month measurement campaign in the summer of 2012. I also want to thank Giulia Bachis, Ji Fan, Sovanna Tik, Cristina Martin, Thibaud Maruejols, Janelcy Alferes, Frédéric Cloutier, Mansour Talebizadeh, Ruyi Wang, Queralt Plana and all the other members at modelEAU team who offered their generous help to my studies and life.

Unforgettably, I also had a joyful time with the members of the BIOMATH team at the Ghent University in Belgium. Giacomo Barni fully participated in the two measurement campaigns carried out at the Eindhoven WWTP in the Netherlands. Thanks to his expertise and experience of field measurements we could solve all difficulties occurring during the experiments. He is such a kind man and did most of the strenuous work at the plant. Besides, Tinne De Boeck helped analyze the component concentrations. Youri Amerlinck shared with me his modelling experience of the Eindhoven WWTP. He and Thomas Maere organized the BIOMATH days, during which some members from the BIOMATH team came to the Eindhoven plant to help in sampling and lab experiments. Other persons from the BIOMATH team who were involved in the BIOMATH days include Katrijn Cierkens, Wouter Naessens, Usman Ur Rehman and Hannu Poutiainen. Without them, the measurement campaigns would not have been so successful, especially for the sampling task on August 26th 2012, which was a day of heavy rain.

Moreover, I also appreciate the staff at Waterschap De Dommel (the Eindhoven WWTP). During the measurement campaigns at the plant, they gave me so much help, e.g. transporting and moving the big hood. Also, from them, especially from Mr. Peter van Dijk, I learnt how the plant is operated and how the control strategies are adjusted.

Furthermore, Jose Porro is the Chair of the IWA Task Group on Greenhouse Gases. We had a good cooperation in terms of measurement and modelling of GHGs. His research on the integrated modelling of GHGs improved my understanding of GHG emissions from an overall perspective. I also want to thank Matthijs Daelman who has good knowledge about the N₂O measurement equipment (Emerson). I'm also thankful to the staff from DHI, i.e. Enrico Ulisse Remigi and Filip Hector André Claeys, who answered my questions on the WEST software. Dr. Xavier Flores-Alsina and Dr. Lluís Corominas work on the benchmark simulation models. Their previous work provided me with a good basis.

In addition, I acknowledge the financial support obtained through the TECC project funded jointly by the Québec Ministry of Economic Development, Innovation and Exports (MDEIE), the Flemish Fund for Scientific Research (FWO - G.A051.10) and the Canada Research Chair on Water Quality Modelling.

Finally, I would like to express the greatest thanks to my parents. They gave me birth, raised me in a home which is not rich but full of happiness, and stayed with me in any situations. Without them I could not have made such achievements. Their love is the footstone for me to stand up and the motive for me to go further. Thank you.

Foreword

This PhD thesis was composed based on 6 papers as follows:

1. **Guo L.^a** and Vanrolleghem P.A.^a (2014) Calibration and validation of an Activated Sludge Model for Greenhouse gases No. 1 (ASMG1) - Prediction of temperature dependent N₂O emission dynamics. *Bioprocess and Biosystems Engineering*, 37, 151-163.
2. **Guo L.^a**, Porro J.^{b,c}, Sharma K.^d, Amerlinck Y.^c, Benedetti L.^e, Nopens I.^c, Shaw A.^{f,g}, Van Hulle S.W.H.^{c,h}, Yuan Z.^d and Vanrolleghem P.A.^a (2012) Towards a benchmarking tool for minimizing wastewater utility greenhouse gas footprints. *Water Science and Technology*, 66, 2483-2495.
3. **Guo L.^a**, Martin C.^{a,i}, Nopens I.^c and Vanrolleghem P.A.^a (2012) Climate change and WWTPs: Controlling greenhouse gas (GHG) emissions and impacts of increased wet weather disturbances. In proceedings of IWA Nutrient Removal and Recovery 2012: Trends in NRR, Harbin, China, September 23-25 2012.
4. **Guo L.^a**, Lamaille-Chad C.^a, Bellandi G.^c, Daelman M.^{j,k}, Amerlinck Y.^c, Maere T.^c, Nous J.^l, Flameling T.^l, Weijers S.^l, van Loosdrecht M.C.M.^k, Volcke E.I.P.^j, Nopens I.^c and Vanrolleghem P.A.^a (2014) Full-scale field measurement of nitrous oxide (N₂O) gas emissions and its relationship with other nitrogen species under dry and wet weather conditions. Submitted.
5. **Guo L.^a** and Vanrolleghem P.A.^a (2014) Interaction of weather conditions and ammonia-based feedforward and feedback control strategies on N₂O emissions at full-scale wastewater treatment plants. In preparation.
6. **Guo L.^a** and Vanrolleghem P.A.^a (2013) Full-scale simulation of N₂O emissions with ASMG2d and elucidation of its different production and emission sources in nitrogen (N) and phosphorus (P) removal systems. Submitted.

The institutions of the co-authors are given below:

^a modelEAU, Département de génie civil et de génie des eaux, Université Laval, 1065 av. de la Médecine, Québec, QC, Canada G1V 0A6.

^b Malcolm Pirnie, TheWater Division of ARCADIS, 27-01 Queens Plaza North, Ste. 800, Long Island City, NY 11101, USA.

^c BIOMATH, Department of Mathematical Modelling, Statistics and Bioinformatics, Ghent University, Coupure Links 653, 9000 Gent, Belgium.

^d Advanced Water Management Center (AWMC), The University of Queensland, Brisbane QLD 4072, Australia.

^e WATERWAYS srl, Via del Ferrone 88, 50023 Impruneta (FI), Italy

^f Black & Veatch, 8400 Ward Parkway, Kansas City, MO 64114, USA.

^g Department of Civil, Architectural, and Environmental Engineering, Illinois Institute of Technology, Chicago, IL 60616, USA.

^h EnBiChem, University College West Flanders, Graaf Karel de Goedelaan 5, 8500 Kortrijk, Belgium.

ⁱ Deustotech, avenida de las Universidades, 24, 48007 Bilbao, Spain

^j Department of Biosystems Engineering, Ghent University, Coupure links 653, 9000 Ghent, Belgium.

^k Department of Biotechnology, Delft University of Technology, Julianalaan 67, 2628 BC Delft, The Netherlands.

^l Waterschap de Dommel, Postbus 10.001, Boxtel NL-5280 DA, The Netherlands.

The author of this PhD thesis (Lisha Guo) is the first author and corresponding author of all these papers. For paper 1, 5 and 6, the author of this thesis did most of the research and writing work under the supervision of PhD supervisor Prof. Peter A. Vanrolleghem, modelEAU, Université Laval. Paper 2, 3 and 4 involved a lot of cooperation with other persons and groups. In paper 2, the author of this PhD thesis did all simulation work related to BSM2, which is the major part of this paper, and compiled the manuscript by integrating the work from other groups. In paper 3, the author of this PhD thesis did most of the simulation work except the generation of the future influent file, and wrote the manuscript. Paper 2 and paper 3 were finished before paper 1 that carried out the calibration work. Therefore, the results in paper 2 and paper 3 were updated using the calibrated parameters of paper 1. In paper 4, the author of this PhD thesis took charge of the field measurement, performed the data analysis and wrote the manuscript. However, this field measurement campaign required a large effort that cannot be accomplished by only one or two persons. Therefore, a lot of people participated in the measurement campaign. Note that although the author of this thesis wrote all the manuscripts for these papers, the co-authors also contributed with extensive review comments.

1 Introduction

Wastewater treatment plants (WWTPs) are large human engineering constructions used to treat wastewater produced by municipalities and industries. They are developed and designed to have a positive impact on the aquatic environment. Indeed, the treated wastewater that is discharged to the receiving natural water body is much higher in quality than raw sewage and, hence, preserves its quality. However, recent studies investigated the relation between WWTPs and climate change more closely. The latter is found to be a bidirectional effect. On the one hand, WWTPs produce greenhouse gases (GHGs), mainly including carbon dioxide (CO_2), nitrous oxide (N_2O) and methane (CH_4). GHGs are regarded as contributing to global warming or climate change, although the specific relationship is still under research and debate. On the other hand, climate change causes an increasing number of extreme weather events, e.g. storms, which bring (hydraulic) shock loads to WWTPs and affect plant operation and performance.

Among the aforementioned GHGs, N_2O is more powerful compared to CH_4 and CO_2 . According to the report of Intergovernmental Panel on Climate Change (IPCC, 2013), the global warming potential (GWP) value for N_2O is 298 in CO_2 equivalents for a 100-year time horizon, i.e. 1 kilogram (kg) of N_2O has the same global warming effect as 298 kg of CO_2 . Hence, full-scale measurement campaigns of N_2O is necessary and urgent for proper evaluation of N_2O emissions from WWTPs and, hence, to quantify the local and global contribution of WWTPs to climate change. Moreover, in view of mitigation, the N_2O generation mechanism, especially through autotrophic pathways, should be understood, which is not the case to date. This would allow for control strategies for emission mitigation to be developed, with special considerations for N_2O emissions but also trading off between GHG emissions, energy consumption and effluent quality standards instead of

only focusing on the latter two criteria. Such a complex interplay of processes calls for a model-based approach.

Based on such studies, the general process models, e.g. Activated Sludge Model No.1 (ASM1)-ASM3 (Henze et al., 2000), should be extended with pathways for N₂O production by both heterotrophs and autotrophs. The integrated model can then be applied to full-scale plants to provide a comprehensive understanding on the N₂O emissions over the whole process.

Climate change on the other hand may have negative effects on WWTPs performance. Extreme rain events bring a sudden hydraulic shock to WWTPs which usually exceeds the capacity of WWTPs. Meanwhile, in combined sewer systems, after a long period of drought, a large amount of deposits are flushed with stormwater and transported to WWTPs. This further impairs the solids removal performance of primary and secondary clarifiers (Henze et al., 2008). Moreover, rain events may also have effects on N₂O emissions and total GHG emissions but no literature is available on this topic as far as the author is aware. It thus deserves to be further studied through experiments and plant-wide simulations.

The scope of this study is limited to the N₂O production and emission for biological nutrient removal processes in WWTPs. Instead of process mechanism studies run in lab-scale experiments, this research was carried out on full-scale plants to investigate N₂O emissions and production by different processes in a whole treatment plant, especially from the activated sludge reactor, and under complex and less controlled conditions, e.g. different weather conditions.

2 Literature review

2.1 GHGs emissions from WWTPs

2.1.1 WWTPs borne GHGs: classification and evaluation framework

Generally, in a WWTP there are fossil CO₂, biogenic CO₂ and biogenic non-CO₂ GHG emissions. The fossil CO₂ and the biogenic CO₂ is related to the long-term and the short-term carbon cycle in the biosphere respectively. The atmosphere gaseous CO₂ is taken up by plants or autotrophic bacteria, like ammonia-oxidizing bacteria (AOB) and nitrite-oxidizing bacteria (NOB), to produce carbohydrates through photosynthesis or chemosynthesis. The plants are the food for animals which means the carbon assimilated in plants is transferred to animals. However, the carbohydrates are also decomposed into CO₂ that is released again to the atmosphere through respiration by the organisms. Such a carbon cycle is called the short-term carbon cycle and the gaseous CO₂ in this cycle is called biogenic CO₂. After the organisms die, their dead cells sink to the rocks under the earth and after millions of years become fuels such as coal or oil. These fuels are explored by mankind to produce energy. CO₂ produced by burning these fossils is called fossil CO₂ and the corresponding carbon cycle is a comparatively long-term process. In the evaluation framework of the Intergovernmental Panel on Climate Change (IPCC, 2006), the fossil CO₂ is included for evaluating the total GHG emissions while the biogenic CO₂ is not included. Besides CO₂, there are also biogenic non-CO₂ GHGs produced in WWTPs, like CH₄ and N₂O. They do not participate in the carbon cycle but have high GWP values. These non-CO₂ GHGs are also included in the evaluation framework of the IPCC (2006). However, U.S. Environmental Protection Agency (U.S. EPA, 2013) suggests that the effect of biogenic CO₂ on climate change should be evaluated in the same framework as N₂O, CH₄ and fossil CO₂.

According to the concept of the Bridle model (Bridle et al., 2008), which was developed starting from the comprehensive model of Monteith et al. (2005), the GHG emissions from the wastewater treatment plants can be divided into five parts: (1) biotreatment, (2) sludge processing and digestion, (3) net power, (4) chemical use and (5) sludge disposal and reuse. However, the Bridle model does not include the GHG emissions due to the construction and decommissioning of the plant and the reaction of the pollutants, e.g. nitrogen (N), remained in effluent. Figure 2.1 shows the CO₂ emission sources of a WWTP based on the Bridle model. In a WWTP context, N₂O is produced in nitrogen removal processes and CH₄ is a product of sludge digestion. N₂O and CH₄ can be expressed in CO₂ equivalents through the GWP index. Energy consumption for aeration, pumping, etc. and chemical use can also be converted into CO₂ equivalents if they are fossil-sourced. However, the WWTP's fossil CO₂ can be reduced by using CH₄ which is produced during sludge treatment. Usually the CO₂ emissions occur through biomass decay, organics degradation and sludge processing, which are considered as biogenic CO₂ and, hence, are excluded from the evaluation (IPCC, 2006). However, an isotope experiment in Australia showed that 4-14% of the influent wastewater contained fossil carbon (e.g. as part of detergents and other chemicals produced in the petrochemical industry). 88-98% of these fossil carbons were removed either through biomass assimilation or through transformation into CO₂ (Law et al., 2013).

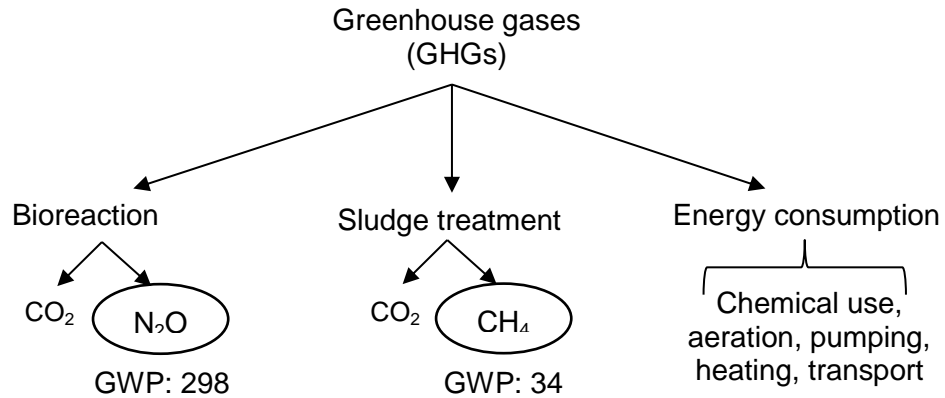


Figure 2.1 GHG emission sources from a WWTP. The GWP values are from the IPCC report (2013).

According to reports of the U.S. EPA (2013) and the Electric Power Research Institute (EPRI, 2002), CH_4 and N_2O emissions from WWTPs account for about 0.4% and the electricity consumption makes up about 1.3% of the total national GHG emissions. According to the 2005 Australian National Greenhouse Gas Inventory (NGGI), CH_4 and N_2O emissions from WWTPs contribute 0.4% of the total national GHG emissions (Foley et al., 2008). However, these numbers should be treated with care as the N_2O emission is calculated following the method proposed by the IPCC (2006), i.e. based on generic emission factors. In IPCC (2006), the default N_2O emission factor is 0.005 kg N_2O -N/kg N discharged as wastewater effluent and it is 2.24 g N_2O -N/person/year for the N_2O emissions during the wastewater treatment at the plant. In other words, these values are not based on specific processes and mechanisms. This has been stated to significantly underestimate N_2O emissions (Ahn et al., 2010; Foley et al., 2010). On the other hand, since CH_4 is a useful source of renewable energy, it only leads to biogenic CO_2 and thus reduces the fossil CO_2 when assuming that all CH_4 can be used as energy supply.

2.1.2 Full-scale N₂O emissions

For comparison purposes of N₂O emission quantities among different conditions, types of WWTPs and plant locations, it would be better to normalize the measurement data rather than using N₂O emission rates directly. Usually, the N₂O emission is normalized to the nitrogen load, i.e. kg N₂O-N per kg of nitrogen where the latter can be either influent or removed load of either total nitrogen (TN) or total Kjeldahl nitrogen (TKN). It is recommended to use the removed nitrogen but it is also dependent on the reactor type (Porro et al., 2014). For example, in a one-stage partial nitritation-anammox system, it is hard to differentiate the amount of NH₄⁺ removed by AOB and by anammox bacteria. Therefore, under such situations, it is suggested to use nitrogen influent load.

A survey of 12 WWTPs of various treatment processes across the USA (Ahn et al., 2010) reported N₂O emission factors of 0.01-1.8% or 0.01-3.3 % which were normalized respectively by influent TKN load and removed TN load. The measurements compared N₂O emissions between the aerated zone and the non-aerated zone and stated that generally the aerated zone emitted more N₂O. Another full-scale experimental campaign was carried out at 7 WWTPs in Australia (Foley et al., 2010) which to a large extent covered the typical full-scale biological nutrient removal processes in use, and N₂O generation was 0.6-25.3% of influent TN removed. Full-scale measurements also showed that the process technologies, in which the dissolved oxygen (DO) was evenly distributed to encourage simultaneous nitrification and denitrification (e.g. an oxidation ditch) emits low N₂O (Ahn et al., 2010; Foley et al., 2010). Ye et al. (2013) proposed a method for measuring the N₂O emissions from open oxidation ditches equipped with surface aerators. This method calculated the N₂O emissions from the gas transfer coefficient and dissolved N₂O measurements, resulting in an emission factor of 0.16-0.52% of influent TKN load for the Australian WWTP.

One year dynamic N₂O emissions were calculated using the on-line data of dissolved N₂O concentration and the off-gas gas flow rate at a WWTP in the Netherlands (Daelman et al., 2013a). The results from the different measurement strategies suggested that long-term on-line sampling better estimated the N₂O emissions and better captured the N₂O variation dynamics. Given the cost of such a one-year campaign, the experiment can be designed as a set of short-term sampling periods randomly distributed over the year (Daelman et al., 2013a).

2.2 N₂O production pathways

The production of N₂O in wastewater treatment processes can be related to different mechanisms which are either chemical or biochemical in nature.

2.2.1 Biochemical pathways

Figure 2.2 shows the mechanisms involved in the biochemical N removal process. In the traditional theory, biological N-removal is described by 2-step autotrophic nitrification, ammonia (NH₄⁺) → nitrite (NO₂⁻) → nitrate (NO₃⁻), and 4-step heterotrophic denitrification, NO₃⁻ → NO₂⁻ → nitric oxide (NO) → N₂O → dinitrogen (N₂). Therefore, N₂O is only considered to be an intermediate product of the heterotrophic denitrification.

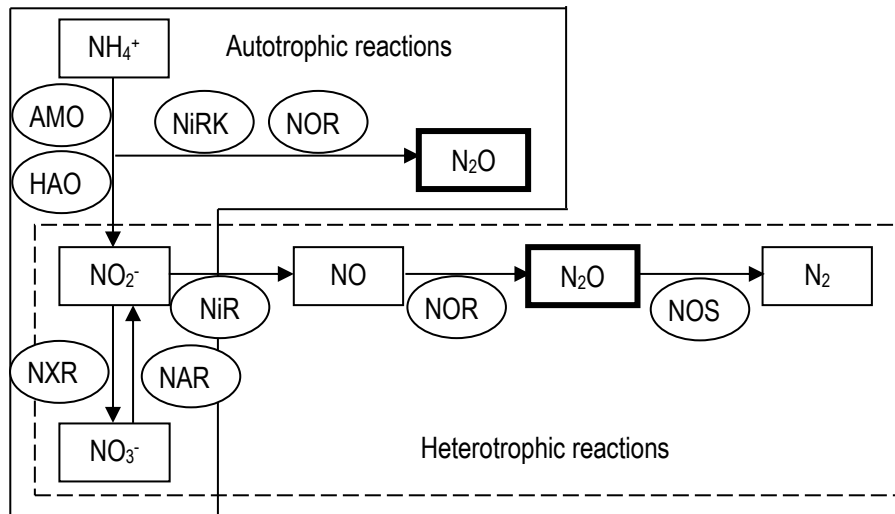


Figure 2.2 Scheme of biochemical N removal and N₂O productions (AMO: ammonia monooxygenase; HAO: hydroxylamine oxidoreductase; NAR: nitrate reductase; NiRK: nitrite reductase used by AOB; NiR: nitrite reductase; NOR: nitric-oxide reductase; NOS: nitrous oxide reductase; NXR: nitrite oxidoreductase).

Besides the heterotrophic denitrification, N₂O may also be the result of the autotrophic metabolisms. This pathway is still under debate but the general view attributes the autotrophic N₂O to the AOB (Bock et al., 1995; Colliver and Stephenson, 2000; Remde and Conrad, 1990; Schmidt and Bock, 1997). The denitrification enzymes NO₂⁻ reductase and nitric oxide reductase are found to exist in *N. europaea*, an AOB, but N₂O reductase converting N₂O to N₂ was not reported yet (Chain et al., 2003; Hooper, 1968).

I. Heterotrophic pathways

In engineering practice, denitrification reaction zones are usually put in front of nitrification zones in order to provide readily biodegradable carbon sources for heterotrophic denitrification. This is usually referred to as the pre-denitrification configuration or the modified Ludzack-Ettinger (MLE) process (Figure 2.3). Sometimes external carbon sources (e.g. methanol or ethanol) are required because the influent ratio between organic carbon and nitrogen (C/N) is low. Another consideration for this reactor configuration is the fact that denitrification produces alkalinity which is destroyed by nitrification. Denitrification

thus reduces the cost of alkalinity dosage. Moreover, nitrification bacteria prefer a somewhat alkaline environment with an optimal pH value of 7.5-8.0 and nitrification rates decrease sharply when the pH drops below 6.8 (Metcalf & Eddy, 2003).

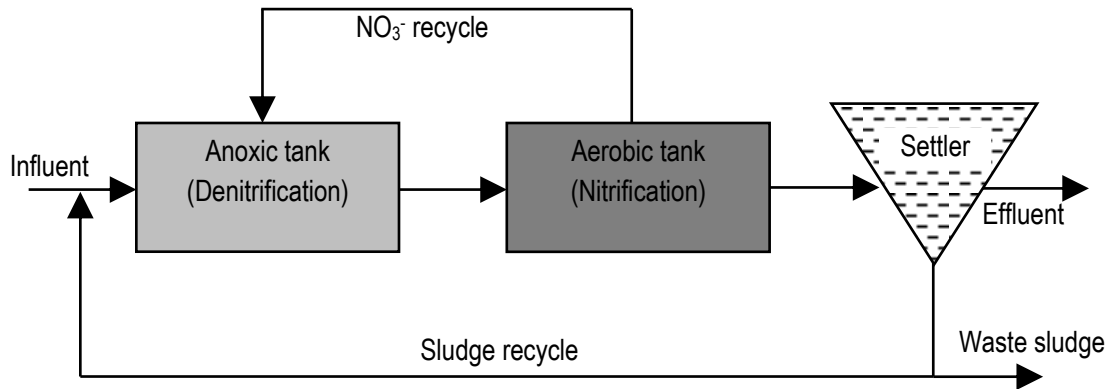


Figure 2.3 Illustration of the MLE process configuration for nitrogen removal.

There are many factors affecting heterotrophic denitrification and related N_2O production as discussed below.

– Organic substrates

In heterotrophic denitrification, the carbon substrate is used as electron donor. When the C/N is low, denitrification will be limited by lack of electron donors. The competition among different nitrogen oxides on the limited electrons results in either increasing or decreasing N_2O production rates (Pan et al., 2012). Those phenomena were observed experimentally (Itokawa et al. 2001; Alinsafi et al., 2008).

The type and properties of the carbon source also affect N_2O emissions. Simple and easily biodegradable substrates like volatile fatty acids (VFAs) are usually preferred by denitrifiers (Elefsiniotis and Wareham, 2007), while the complex organics have to be decomposed into simple organics by hydrolysis for heterotrophic consumption. Adouania

et al. (2010) compared N_2O and NO emission by using three types of carbon sources and reported that acetate produced more N_2O and NO per N denitrified than the other two kinds, and ethanol generated the lowest, while the mixture of short and long chain carbon sources caused quite low N_2O and NO emissions.

- NO_2^-

NO_2^- is an intermediate product of denitrification. Accumulation of NO_2^- changes N_2O generation and emission because of the higher abundance of NO_2^- potentially producing NO and N_2O as well as the well-known inhibition effect of NO_2^- or NO on heterotrophs to reduce N_2O (Alinsafi et al., 2008; Stein and Yung, 2003; Stouthamer et al., 1997).

- DO

N_2O reductase is more sensitive to oxygen compared to other reductases of denitrification, and, consequently, a low concentration of DO around 0.4-2 mg O_2/l may cause N_2O accumulation and emission (Otte et al., 1996; von Schulthess et al., 1994).

- pH

Heterotrophs have been shown to be more sensitive to pH during the reduction of N_2O compared to the reduction of other nitrogen oxides. It is reported that under low pH conditions more N_2O is produced by heterotrophic denitrification (Hanaki et al., 1992; Thörn and Sörensson, 1996; Van Den Heuvel et al., 2011). This could also be due to competition for electrons among different nitrogen oxides (Pan et al., 2012).

II. AOB pathway

Two biochemical AOB pathways exist. In the first one N_2O is generated as an intermediate product during NH_4^+ oxidation to NO_2^- via hydroxylamine (NH_2OH). The second pathway is the so-called the AOB denitrification, i.e. NO_2^- reduction (Ni et al., 2013a; Kampschreur et

al., 2007; Wunderlin et al., 2012). N_2O can also be produced from the chemical cission of the hyponitrous acid (NOH) which is formed during NH_2OH oxidation (Law et al., 2012).

The scientific discussions regarding the AOB pathways of N_2O production concern the effects of NH_4^+ , NO_2^- , NH_2OH and DO on the process rates.

- NH_4^+ , NO_2^- and NH_2OH

It is generally agreed that an increase of NH_4^+ , NH_2OH and NO_2^- leads to an increase of N_2O formation (Kampschreur et al., 2008; Kim et al., 2010; Law et al., 2012; Wunderlin et al., 2012; Yu et al., 2010). No matter which pathway dominates, NH_4^+ is source for all N components, including N_2O . Therefore, an increase of NH_4^+ increases the N pool and results in higher N_2O production potential. The debate on different pathways of N_2O production by AOB is caused by experimental data that showed an increase of N_2O by either increasing NO_2^- or increasing NH_2OH . In the NH_2OH oxidation pathway, NH_2OH serves as electron donor and, hence, adding more NH_2OH supplies more electrons. In the NO_2^- reduction pathway, NO_2^- is first reduced to NO and subsequently to N_2O and, hence, adding more NO_2^- leads to higher N_2O production. The observation of both phenomena indicates that both pathways possibly coexist in the system. Which of the two is dominating depends, according to current understanding, on the system's operational conditions (Wunderlin et al., 2012). However, these authors also mention that in real WWTPs the NH_2OH concentration is usually found to be lower than under experimental conditions in the laboratory and the NO_2^- reduction pathway might then be the main contributor.

Regarding the NO_2^- reduction pathway, another study showed that free nitrous acid (FNA), instead of NO_2^- , is the real electron acceptor (Shiskowski and Mavinic, 2006). Therefore, the pH value would affect N_2O production. The sequencing batch reactor (SBR)

experiments carried out by these authors indicate an increase of N_2O production through the AOB pathway as pH decreases. Wrage et al. (2001) conclude the same from thermodynamic calculations.

- DO

DO is another important factor for N_2O formation through the AOB pathway. Some literature reports that AOB N_2O production happens under oxygen-limited conditions (Kampschreur et al., 2008) or increases with decreasing DO concentrations (Aboobakar et al., 2013). Other researchers observed that AOB N_2O production is occurring during the recovery from an anoxic shock, which in this study consists of a transient anoxic period of 48 hours imposed to the AOB cultivated under chemostat conditions (Yu et al., 2010). According to this finding, an anoxic shock may be created in a MLE process at the place where the wastewater is recycled from the aerobic zone to the anoxic zone, which could thus lead to AOB N_2O production. However, there would be little N_2O production expected from this mechanism, because the anoxic condition is not “transient” in the anoxic zone of a MLE process. There also appears to be a threshold value of DO at which N_2O production by AOB is maximized (Tallec et al., 2006; Law et al., 2012). The different opinions on the DO effect are also due to different experimental observations. However, there seems to be a dual effect by either increasing or decreasing DO. On the one hand, AOB, as aerobic bacteria, prefer aerobic conditions and, hence, higher DO concentrations benefit AOB growth and thus potentially lead to more N_2O production. However, higher DO concentrations can also increase NO_2^- oxidation by NOB, leaving less NO_2^- for N_2O production. The same reasoning can be applied to DO limiting conditions. On the one hand, AOB growth might be hampered by low DO conditions. On the other hand, NO_2^- may accumulate when the DO is insufficient for NO_2^- oxidation to NO_3^- and the large amount of NO_2^- will potentially cause high N_2O production. Changes in DO usually lead to

simultaneous dynamics of other components, like NH_4^+ , NO_2^- and NO_3^- , making the understanding of the different impacts difficult. It is thus important to take into account other components to achieve a comprehensive understanding of AOB N_2O production under different DO conditions.

III. PAO pathway

Under anoxic conditions, it has been observed that some phosphorous accumulating organisms (PAOs) can denitrify NO_3^- and NO_2^- , while storing phosphorous (P) as polyphosphate (Kuba et al., 1993; Ahn et al., 2001). Similar to the ordinary PAOs, denitrifying PAOs (DPAOs) store external carbon sources as internal polyhydroxyalkanoates (PHA) under anaerobic conditions and use the internally stored PHA as energy source for bacterial activities. However, instead of using DO as electron acceptors, DPAOs utilize NO_3^- and NO_2^- under anoxic conditions. The presence of DPAOs in WWTPs brings advantages of saving energy due to reduced aeration demand, lower chemical oxygen demand (COD) requirement and lower sludge production (Kuba et al., 1996).

However, PAOs are in competition with yet another kind of organisms, i.e. glycogen accumulating organisms (GAOs). They also store internal carbon sources, PHA, by uptake of external organic substrate under anaerobic conditions (Cech and Hartman, 1993; Liu et al., 1994). Just like DPAOs, denitrifying GAOs (DGAOs) also denitrify NO_3^- and NO_2^- by using internally stored PHA as electron donors. Obviously, the very similar metabolism between PAOs (or DPAOs) and GAOs (or DGAOs) triggers competition.

Zeng et al. (2003a, 2003b) ran two sets of experiments with a SBR. The first one was run in aerobic-anoxic cycles. The second one was operated in anaerobic-aerobic cycles but the aerobic periods had low DO concentrations to promote simultaneous nitrification and

denitrification. Both experiments show that the major end product of denitrification was N_2O and not N_2 . However, it were the DGAOs playing the major role in the denitrification. P-uptake by PAO is more likely to happen under aerobic conditions. Similar results were obtained by Lemaire et al. (2006) who also ran an anaerobic-aerobic SBR with low DO concentrations in aerobic periods. By comparing the performance of PAOs and ordinary heterotrophic organisms on denitrification, Hu et al. (2002) found that the DPAOs participated in denitrification only when the NO_3^- load was in excess. These studies indicate that DPAOs play a minor role in denitrification when competing with GAOs and ordinary heterotrophs. In this PhD thesis GAOs are not differentiated from other heterotrophs.

2.2.2 Chemical pathway

In the wastewater treatment industry the chemical pathway of N_2O formation was thought to have little or no effect on N_2O production compared to the biochemical pathways. However, under certain conditions it can contribute significantly to N_2O production (Kampschreur et al., 2011). Under anoxic conditions, it was found that when pH was approximately neutral N_2O was produced chemically through the reduction of NO_2^- with simultaneously oxidation of ferrous iron (Fe^{2+}) to ferric iron (Fe^{3+}) as shown in Figure 2.4 (Kampschreur et al., 2011; Tai and Dempsey, 2009; van Cleemput, 1998). Kampschreur et al. (2011) suggested that the chemical NO_2^- reduction should be considered when iron is dosed and a large amount of NO_2^- is present.

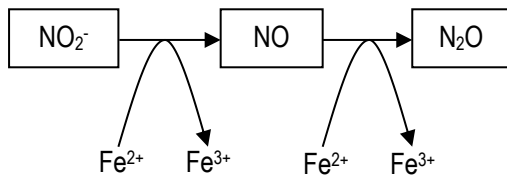


Figure 2.4 Scheme of the chemical NO_2^- reduction (Kampschreur et al., 2011).

Finally, stated before in Section 2.2.1 “II. AOB pathway”, NOH may also be formed during NH_2OH oxidation and be further broken down chemically to N_2O by AOB.

2.3 Modelling of N_2O emissions

This section only discusses the modelling of the biochemical pathways, excluding the chemical pathway. However, the structure of the text is similar as that of Section 2.2.1. Traditional ASMs, i.e. ASM1-ASM3, simply model the nitrification process as a one-step process of ammonia oxidation to NO_3^- and autotrophs are taken as one species without discrimination between AOB and NOB. A similar situation occurs for the heterotrophic denitrification which is described as one step of NO_3^- denitrification to N_2 . Therefore, in order to simulate the dynamics of N_2O produced during heterotrophic denitrification, the single processes of denitrification must be replaced by a multistep process. Moreover, if the N_2O production by AOB is to be taken into consideration, the autotrophic biomass and the nitrification process must be split into separate bacterial consortia and processes.

Table 2.1 summarizes the general information of all models discussed below.

Table 2.1 Structures of models

Models Page 16	Extension on IWA ASMs	Nitrification	N ₂ O (or NO) production by AOB pathways	Heterotrophic denitrification	PAO denitrification	N ₂ O production			Calibration and application
						Heterotrophs	AOB	PAO	
Iacopozzi et al. (2007)	ASM3	2 steps	No	2 steps	No	No	No	No	BSM1
Kaelin et al. (2009)	ASM3	2 steps	No	2 steps	No	No	No	No	Lab-scale batch tests and pilot DN-N plant
von Schulthess and Gujer (1996)	ASM1	2 steps	No	3 steps	No	Yes	No	No	Real DN-N plant
Hiatt and Grady (2008)	ASM1	2 steps	No	4 steps	No	Yes	No	No	Virtual CSTR and MLE processes
Flores-Alsina et al. (2011)	ASM1	2 steps	No	4 steps	No	Yes	No	No	BSM2
Samie et al. (2011)	ASM1	1 step	No	4 steps	No	Yes	No	No	Real denitrifying biofilter
Pan et al. (2013)	-	-	-	4 steps	-	Yes	-	-	Lab-scale SBR
Ni et al. (2011)	ASM1	2 steps	NH ₂ OH pathway	4 steps	No	Yes	Yes	No	Lab-scale batch tests, lab-scale SBRs and pilot aeration tank
Ni et al. (2013a)	ASM1	3 steps	NH ₂ OH pathway	4 steps	No	Yes	Yes	No	Real oxidation ditch
Law et al. (2012)	-	-	NH ₂ OH pathway	-	-	Yes	-	-	Lab-scale batch tests and lab-scale SBR

Note: “-” means not mentioned in the reference paper; “DN-D” stands for denitrification-nitrification; “SBR” stands for sequencing batch reactor; “BSM” stands for benchmark simulation model.

Table 2.1 Structures of models (continued)

Models	Extension on IWA ASMs	Nitrification	N ₂ O (or NO) production by AOB pathways	Heterotrophic denitrification	PAO denitrification	N ₂ O production			Calibration and application
						Heterotrophs	AOB	PAO	
Mampaey et al. (2013)	-	2 steps	NO ₂ ⁻ pathways	-	-	Yes	-	-	Virtual SHARON reactor
Kampschreur et al. (2007)	ASM2d	2 steps	NH ₂ OH pathway and NO ₂ ⁻ pathway	2 steps	1 step	No	No	No	Lab-scale SBR
Ni et al. (2014)	-	3 step	NH ₂ OH pathway and NO ₂ ⁻ pathway	-	-	No	Yes	No	Lab-scale batch tests and lab-scale SBR
Houweling et al. (2011)	-	-	Empirical method	-	-	-	Yes	-	Lab-scale SBR and pilot-scale MLE process
Ali et al. (2013)	-	-	Empirical method	-	-	-	Yes	-	Lab-scale SBR
Sin and Vanrolleghem (2006)	ASM2d	2 steps	No	2 steps	1 step	No	No	No	Pilot-scale SBR
Oehmen et al. (2010)	-	-	-	4 steps	4 steps	Yes	-	Yes	Lab-scale SBRs
Rodriguez-Garcia et al. (2012)	ASM1	2 steps	NO ₂ ⁻ pathways	4 steps	No	Yes	Yes	No	Virtual MLE processes
Pocquet et al. (2012)	ASM3	2 steps	NO ₂ ⁻ pathways NH ₂ OH pathway Empirical method	4 steps	-	Yes	Yes	No	Lab-scale SBRs

Note: “-” means not mentioned in the reference paper; “DN-D” stands for denitrification-nitrification; “SBR” stands for sequencing batch reactor; “BSM” stands for benchmark simulation model; in the combined model of Pocquet et al. (2012) which is based on ASM3, only the empirical method (Houweling et al., 2011) is used to describe the AOB N₂O production, although all three AOB N₂O production models are tested in the aerobic phase of the SBR.

2.3.1 Model structures

In the sequel the different model structures will be presented in the following order: I. heterotrophic N₂O production; II. autotrophic N₂O production; III. N₂O production by PAO; IV. production of N₂O by heterotrophs and autotrophs combined; V. comprehensive N₂O production, including other GHG emissions.

I. Heterotrophic production of N₂O

Biokinetic models with 2-step nitrification and 2-step denitrification existed for some time prior to this PhD study (Iacopozzi et al., 2007; Kaelin et al., 2009; Sin et al., 2008b), i.e. the nitrification had two steps as $\text{NH}_4^+ \rightarrow \text{NO}_2^- \rightarrow \text{NO}_3^-$ and the denitrification also had two steps mainly as $\text{NO}_3^- \rightarrow \text{NO}_2^- \rightarrow \text{N}_2$ or $\text{NO}_3^- (\text{NO}_2^-) \rightarrow \text{N}_2$. The main objective of those models was NO₂⁻ simulation and the primary reasons for describing denitrification in only two steps without consideration of NO and N₂O were the minor contributions of NO and N₂O to the total nitrogen mass flow and the difficulties of predicting NO/N₂O (Sin et al., 2008b). However, the 2-step denitrification models do not allow modelling the N₂O production and thus cannot be used for GHG studies.

von Schulthess et al. (1994) extended the denitrification process of ASM1 into three steps, i.e. $\text{NO}_3^- \rightarrow \text{NO}_2^- \rightarrow \text{N}_2\text{O} \rightarrow \text{N}_2$. The inhibition effect of NO₂⁻ was considered by an inhibition term in the kinetic equation of each step. Later, this model was further modified by (i) adding an organic substrate Monod term in the three denitrification process steps, (ii) separating the nitrification process into two steps by AOB and NOB respectively and (iii) integrating an anoxic hydrolysis process (von Schulthess and Gujer, 1996).

The big change came when Hiatt and Grady (2008) proposed the Activated Sludge Model for Nitrogen (ASMN) which was also based on ASM1 and describes 2-step nitrification and 4-step denitrification. In ASMN, instead of NH₄⁺ and NO₂⁻, free ammonia (FA) and FNA

were considered as true substrates for nitrification of AOB and NOB respectively. The concentrations of FA and FNA are calculated as Eq. (2.1) and Eq. (2.2).

$$S_{\text{FA}} = S_{\text{NH}} \cdot \frac{10^{\text{pH}}}{e^{6344/(273.15 + T)} + 10^{\text{pH}}} \quad \text{Eq. (2.1)}$$

$$S_{\text{FNA}} = S_{\text{NO}_2} \cdot \frac{1}{1 + e^{-2300/(273.15 + T)} \cdot 10^{\text{pH}}} \quad \text{Eq. (2.2)}$$

where S_{NH} and S_{NO_2} are the concentrations of NH_4^+ and NO_2^- and T is the Celsius temperature.

FA inhibition of AOB growth, FNA inhibition of NOB growth and NO inhibition of NO reduction by heterotrophs were described as competitive inhibition terms, Eq. (2.3).

$$\text{Competitive Term} = \frac{S}{K_s + S + K_i / S} \quad \text{Eq. (2.3)}$$

where S is the concentration of FA (for NH_4^+ oxidation) or FNA (for NO_2^- oxidation), K_s is the half-saturation coefficient and K_i is the inhibition coefficient.

Instead of the Arrhenius equation which is usually used in ASM1-ASM3, the temperature dependence of the maximum specific growth rates of AOB, NOB and heterotrophs were described by the Ratkowsky equation in which the maximum specific growth rate first increases and then decreases with increasing temperature (Ratkowsky et al., 1983), Eq. (2.4).

$$\mu_{\text{R,bacteria}} = \left\{ b_{\mu\text{bacteria}} \cdot (T - T_{\text{Min,bacteria}}) \cdot \left[1 - e^{c_{\mu\text{bacteria}} \cdot (T - T_{\text{Max,bacteria}})} \right] \right\}^2 \quad \text{Eq. (2.4)}$$

where $b_{\mu\text{bacteria}}$ and $c_{\mu\text{bacteria}}$ are coefficients, and $T_{\text{Max,bacteria}}$ and $T_{\text{Min,bacteria}}$ are the maximum and minimum temperatures. Figure 2.5 illustrates the difference between the Arrhenius

and Ratkowsky equations on the maximum specific growth rate of heterotrophs with temperature dependency. The parameters of the Arrhenius equations were taken from Henze et al. (2000) and the parameters of the Ratkowsky equations from Hiatt (2006). The two equations give similar kinetics between 5 °C and 25 °C, the typical activated sludge operating range. However, there are cases requiring the model to be applicable for temperatures higher than this boundary. For example, in the SHARON (Single reactor system for High activity Ammonia Removal Over Nitrite) processes, which are used to treat wastewater with high NH_4^+ concentration, a high temperature is usually applied, i.e. between 30-40 °C (Hellings et al., 1999; Volcke et al., 2007). Therefore, for such reactors, the Ratkowsky equation has advantages over the Arrhenius equation.

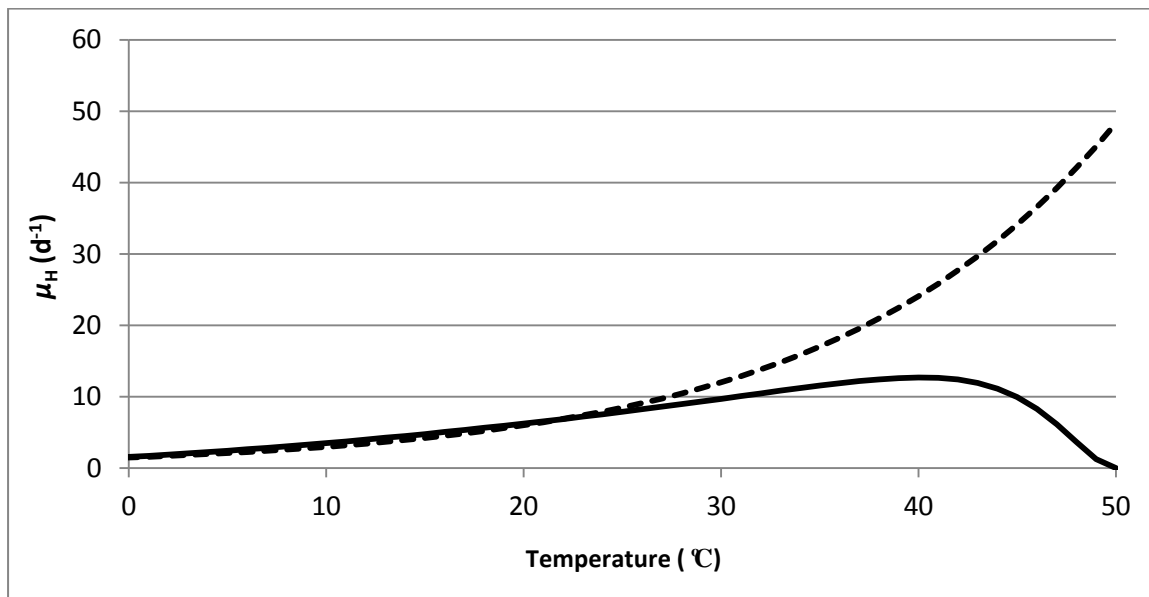


Figure 2.5 Maximum specific growth rate of heterotrophs expressed by the Arrhenius equation (dashed) and the Ratkowsky equation (solid).

Besides the nitrification-denitrification process ASM1N also modelled mixotrophic growth of NOB, i.e. also using organic carbon for growth next to CO_2 , assimilative NO_3^- reduction to ammonia (ANRA), and biodegradation of nitrification inhibitors and priority pollutants. All

these features make ASMN applicable to high-nitrogen load and industrial wastewater treatment. Hiatt and Grady (2008) compared the simulation results of ASMN with ASM1 using the same influent loads. The biomass concentration of nitrifiers was substantially higher for ASMN than the autotrophs in ASM1, because of the mixotrophic growth of NOB in ASMN.

Based on the nitrification and denitrification processes in ASMN of Hiatt and Grady (2008), Flores-Alsina et al. (2011) proposed a model which is suitable for municipal wastewater treatment. ASM1 was used as the basic biokinetic model to model hydrolysis, ammonification, and aerobic growth and decay of heterotrophs. The aerobic growth and decay of autotrophs, AOB and NOB, and the anoxic growth of heterotrophs was modelled as in ASMN (Hiatt and Grady, 2008), and the substance N_2 was added as the product of N_2O reduction. Allowing to make the model's N mass balance, following Henry's law, an aeration equation was included for the oxygen transfer and gas stripping equations modelled the gas emitted flux of NO, N_2O and N_2 . Samie et al. (2011) also extended the denitrification of ASM1 into four steps as in ASMN (Hiatt and Grady, 2008), but the nitrification was still simulated as one step, since their simulation study was focused on denitrifying biofilters.

Instead of using kinetic parameter tuning, Pan et al. (2013) recently proposed a novel model to describe the competition among the four steps of the heterotrophic denitrification on the electrons originating from the organics (Figure 2.6). Two new state variables were added, i.e. S_{Mox} standing for the oxidized mediator and S_{Mred} standing for reduced mediator. The sum of S_{Mox} and S_{Mred} is a constant, i.e. the total concentration of the electron carriers. Instead of directly using the organic substrate as the electron donor, an oxidized mediator is reduced in carbon oxidation processes and subsequently the reduced mediator is used as electron donor for the heterotrophic denitrification. With such a model, the observations

regarding N_2O accumulation can be explained more easily and it proves that the electron competition also happens under carbon-abundant conditions.

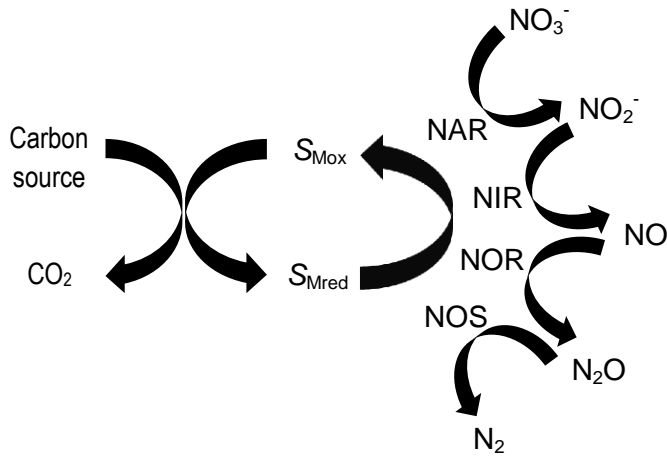


Figure 2.6 Scheme of the model proposed by Pan et al. (2013) (The nomenclature of the enzymes is explained in Figure 2.2).

II. AOB production N_2O

Since the N_2O production through the AOB pathways has not obtained consensus yet, there is no widely accepted corresponding model. Based on various pathways and influencing factors, different biokinetic models have been proposed (Law et al., 2012; Ni et al., 2011; Ni et al., 2013a; Mampaey et al., 2013). These models can be roughly divided into two groups, i.e. models that simulate N_2O production during NH_2OH oxidation and models that simulate N_2O as a product of NO_2^- reduction (also called AOB denitrification).

The two models of Ni et al. (2013a) and Law et al. (2012) belong to the first group. They all assume that first NH_4^+ is oxidized to NH_2OH which then serves as electron donor.

According to the model of Ni et al. (2013a), NH_2OH is first oxidized to NO which is then further oxidized to NO_2^- where N_2O is directly produced from NO denitrification (Figure 2.7 b). The model of Law et al. (2012) further includes NOH , besides NH_2OH . It follows the sequence: $\text{NH}_4^+ \rightarrow \text{NH}_2\text{OH} \rightarrow \text{NOH} \rightarrow \text{NO}_2^-$. N_2O is formed from the chemical breakdown of NOH (Figure 2.8).

In the model of Ni et al. (2011) NH_2OH is also firstly produced from NH_4^+ oxidation but then it is directly oxidized into NO_2^- which is further reduced to NO and N_2O (Figure 2.7 a). The models of Mampaey et al. (2013) do not consider NH_2OH and focus on the NO_2^- reduction pathways. Two model hypotheses were presented, i.e. scenario A and scenario B. They both assume that NH_4^+ is oxidized into NO_2^- which is further reduced to NO and N_2O . The difference between the models is the dependence on DO and electron donor. Scenario A assumes that AOB denitrification is preferred over aerobic conditions and NH_4^+ is used as electron donor whereas in Scenario B the AOB biomass acts as the electron donor and the process occurs under either aerobic or anoxic conditions (Figure 2.9). The effect of pH was considered in Scenario A which assumed FNA, instead of NO_2^- , as the real substrate. Actually, Scenario A of Mampaey et al. (2013) is quite similar to the model of Ni et al. (2011). They both denitrify in steps of $\text{NO}_2^- \rightarrow \text{NO} \rightarrow \text{N}_2\text{O}$, but they use different electron donors, i.e. NH_4^+ (Mampaey et al., 2013) or NH_2OH (Ni et al., 2011). However, NH_2OH is essentially an oxidation product of NH_4^+ . Therefore, the model of Ni et al. (2011) and the models of Mampaey et al. (2013) belong to the group of NO_2^- reduction pathway models.

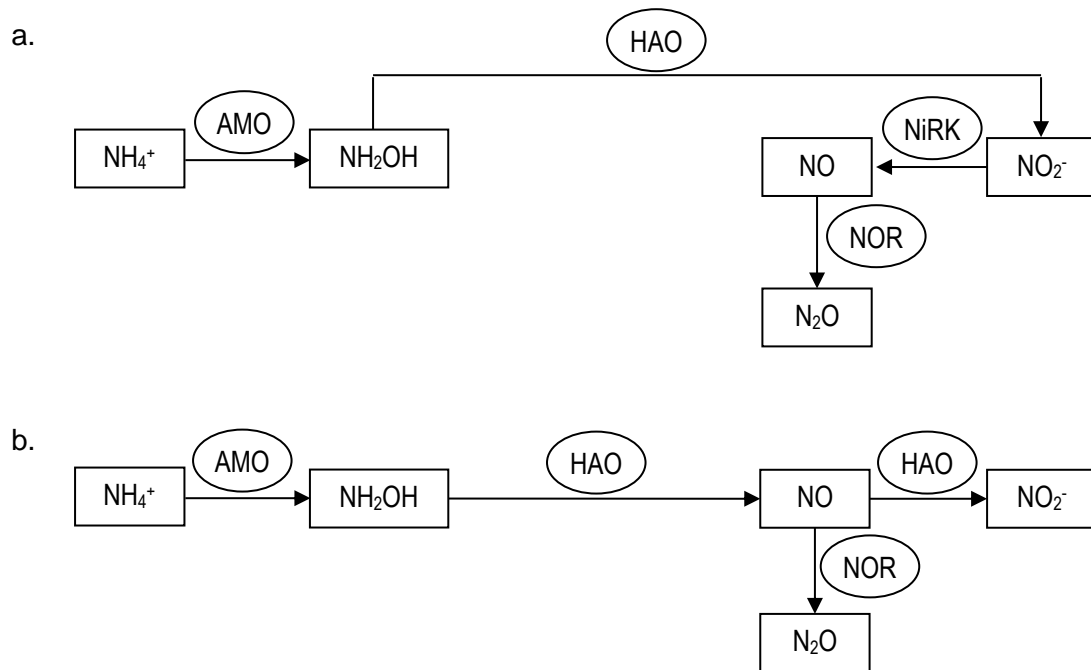


Figure 2.7 Scheme of the model proposed by Ni et al. (2011) (a) and the model proposed by Ni et al. (2013a) (b) (The nomenclature of the enzymes is explained in Figure 2.2).

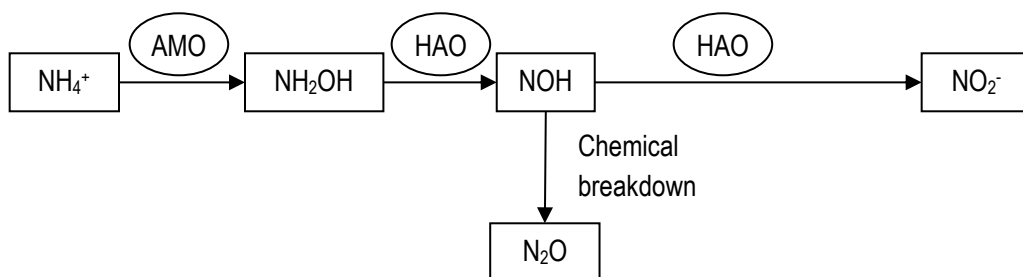


Figure 2.8 Scheme of the model proposed by Law et al. (2012) (The nomenclature of the enzymes is explained in Figure 2.2).

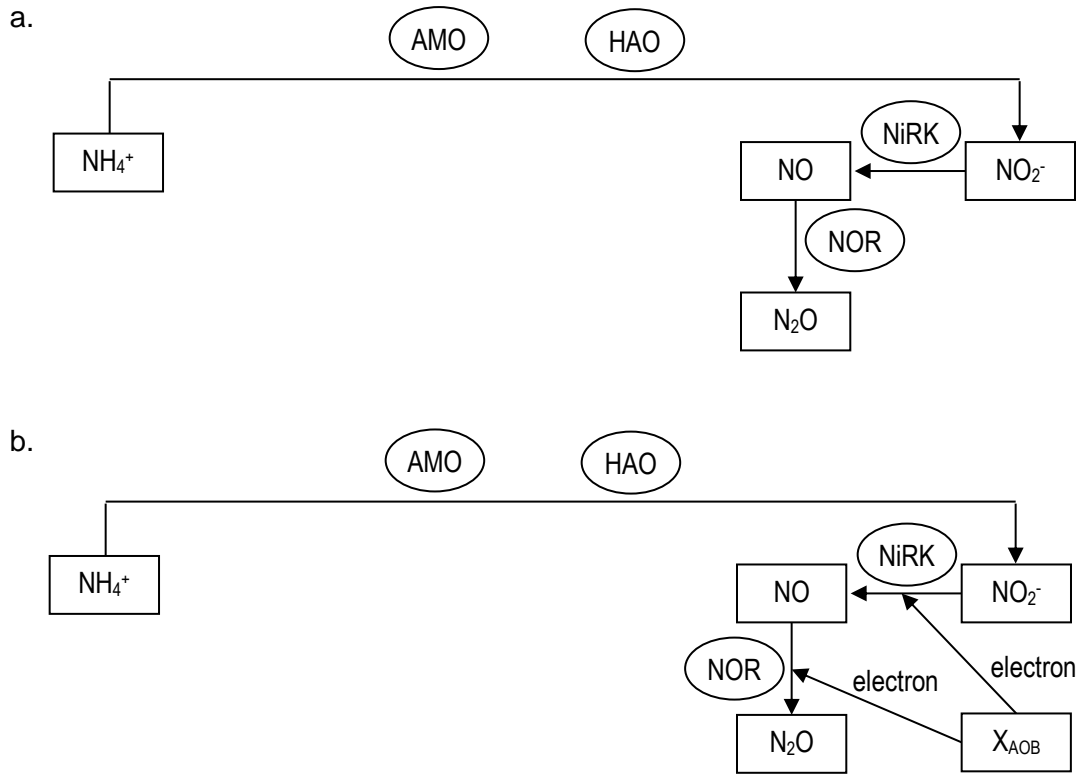


Figure 2.9 Scheme of the models proposed by Mampaey et al. (2013) (The nomenclature of the enzymes is explained in Figure 2.2).

Kampschreur et al. (2007) extended the ASM2d model with three possible pathways for NO production under nitrifying conditions, i.e. escaping as nitrification intermediate, AOB denitrification and heterotrophic denitrification. The model was applied to a lab-scale SBR and the second pathway was suggested to be dominant. However, the model suggested a preference of aerobic over anoxic conditions for NO production from NO_2^- which contradicts with other publications from the same author. Through the measurement of N_2O and NO Kampschreur et al. (2008) concluded that more NO was produced by nitrifiers under anoxic conditions than under aerobic conditions as observed in a full-scale nitrification–anammox process and in lab-scale reactors.

Ni et al. (2013b) compared four models of N_2O production by AOB, i.e. the models of Ni et al. (2011 and 2013), the model of Law et al. (2012) and the Scenario A of Mampaey et al.

(2013). Their performance was evaluated by simulating the batch experimental data from three case studies. However, none of the four models was able to satisfactorily describe all experimental data. Therefore, Ni et al. (2013b) suggest to include both the NH_2OH pathway and NO_2^- denitrification pathway in future models.

Table 2.2 gives the stoichiometric matrices of each AOB N_2O production model discussed above.

Given the various types of AOB N_2O production models, a unified model has very recently been proposed. Ni et al. (2014) built a model combining the two AOB pathways of N_2O production, i.e. NH_2OH oxidation and NO_2^- denitrification. This combined model defines two types of electron carriers, one in reduced form (S_{Mred}) and the other in oxidized form (S_{Mox}), and simulates the bioreactions through electron transfer between the electron carriers that permits to describe the competition between the two pathways, similar to the heterotrophic denitrification model of Pan et al. (2013). However, it is hard to calculate or measure in reality the electron carriers defined in this model and it must be considered that this concept is quite different from the traditional concept of ASM. In the traditional ASM concept, the electron transfer happens directly between the pollutant components and the kinetic terms only consider these pollutant components next to environmental conditions such as pH and temperature. Furthermore, there is an algebraic equation summing the S_{Mred} and S_{Mox} that is that the total amount of carriers is assumed constant C_{tot} . Generally speaking, at this step more validation and application is needed for this new model.

Table 2.2 Stoichiometric matrices of the different AOB N₂O production models

Model	S _o	S _{NH4}	S _{NH2OH}	S _{NOH}	S _{NO}	S _{N2O}	S _{NO2}	X _{AOB}	S _{Mox}	S _{Mred}
Model 1 and 2	-8/7	-1	1							
Model 1 and 2			-1		-4	4	1			
Model 1	$-(16/7 - Y_{AOB})/Y_{AOB}$	$-i_{N, AOB}$	$-1/Y_{AOB}$				$1/Y_{AOB}$	1		
Model 1			-1		4		-3			
Model 2	$-(16/7 - Y_{AOB})/Y_{AOB}$	$-i_{N, AOB}$	$-1/Y_{AOB}$		$1/Y_{AOB}$			1		
Model 2	-4/7				-1		1			
Model 3	-1	-1	1							
Model 3			-1		1					
Model 3				-1			1			
Model 3				-1		1/2				
Model 3	-1									
Model 4 and 5	$-(24/7 - Y_{AOB})/Y_{AOB}$	$-1/Y_{AOB} - i_{N, AOB}$	$1/Y_{AOB}$					1		
Model 4	$-(16/7 - Y_{AOB})/Y_{AOB}$	$-1/Y_{AOB} - i_{N, AOB}$	$-1/Y_{AOB}$				$2/Y_{AOB}$	1		
Model 4	$-(16/7 - Y_{AOB})/Y_{AOB}$	$-1/Y_{AOB} - i_{N, AOB}$	$1/Y_{AOB}$		$-2/Y_{AOB}$	$2/Y_{AOB}$		1		
Model 5		$i_{N, AOB}$			1.75		-1.75	-1		
Model 5		$i_{N, AOB}$			-1.75	1.75		-1		
Model 6	-1	-1	1					1	1	-1
Model 6			-1		1			-3/2	3/2	
Model 6				-1			1	-1/2	1/2	
Model 6				-1		1/2		1/2	-1/2	
Model 6	-1/2							1	1	-1
Model 6						1/2	-1	1	1	-1

Note: Model 1 – Ni et al. (2011), Model 2 – Ni et al. (2013a), Model 3 – Law et al. (2012), Model 4 – Scenario A of Mampaey et al. (2013), Model 5 – Scenario B of Mampaey et al. (2013), Model 6 – Ni et al. (2014).

Besides the mechanistic biokinetic models, empirical methods have been proposed. Houweling et al. (2011) estimated the N_2O production by AOB as a fraction of NH_4^+ oxidation through a correlation function. In other words, the NH_4^+ converted by AOB is separated into two parts, i.e. a part is converted to NO_2^- and another part leads to N_2O . N_2O generation is found to be linked with NH_4^+ and NO_2^- accumulation and low DO conditions. The advantage of such a model is that it avoided the discussion on AOB pathways of producing N_2O , i.e. NH_2OH oxidation or NO_2^- reduction. However, due to this, its applicability is limited. The parameters of the correlation function have to be calibrated based on experimental data. However, the parameter values, i.e. the calculated fraction of NH_4^+ converted to N_2O , may not be suitable when the experimental conditions change.

Ali et al. (2013) performed regression analysis on N_2O emissions from wastewater nitrification in a lab-scale reactor. The N_2O emission was empirically correlated with NH_4^+ and NO_2^- concentrations. The authors found that the N_2O emission increased linearly with the logarithmic increase of NH_4^+ concentration, $\ln(NH_4^+)$, or exponentially with the NO_2^- concentration, $\exp(NO_2^-)$. However, like the model of Houweling et al. (2011), such black-box models may not be applicable when the plants are run outside the experimental boundaries. In other words, the relationship between N_2O emissions and $\ln(NH_4^+)$ or $\exp(NO_2^-)$ may no longer be linear when the NH_4^+ or NO_2^- concentrations are beyond the experimental ranges. This is because the N_2O emission is also related to other factors, e.g. DO, and not only to NH_4^+ and NO_2^- (Aboobakar et al., 2013; Kampschreur et al., 2008; Tallec et al., 2006; Law et al., 2012; Yu et al., 2010).

III. PAO production of N_2O

ASM2d and ASM3P incorporate the denitrification performed by PAOs, but similar to the heterotrophic denitrification in ASMs, the PAO denitrification was modelled as one single process. Sin and Vanrolleghem (2006) expanded ASM2d by describing the nitrification as

a two-step process and the denitrification by PAO and heterotrophs as well. Sin et al. (2008c) further added the effects of NO_2^- on P-uptake under aerobic and anoxic conditions. However, the PAO denitrification process was not modified. Given this two-step nature, these models cannot simulate the N_2O production by PAO.

Oehmen et al. (2010) considered two groups of PAOs, named PAO I and PAO II. PAO I perform denitrification in four steps, i.e. $\text{NO}_3^- \rightarrow \text{NO}_2^- \rightarrow \text{NO} \rightarrow \text{N}_2\text{O} \rightarrow \text{N}_2$, but are not able to utilize DO as electron acceptors under aerobic conditions. In their model Aerobic P uptake is accomplished by PAO II but these organisms are only able to reduce NO_2^- and N_2O . GAOs and DGAOs were also split into different groups with different capabilities under aerobic and anoxic conditions. Therefore, the N_2O production by PAOs can be simulated by the model and the model was calibrated and validated by literature data (Oehmen et al., 2010).

IV. Combined heterotrophic and autotrophic model

In order to simulate N_2O emissions from heterotrophic and AOB pathways, Rodriguez-Garcia et al. (2012) built two models based on ASM1, ASMN (Hiatt and Grady, 2008) and the models of Mampaey et al. (2013). They replaced the 1-step nitrification and 1-step denitrification processes of ASM1 by 2-step nitrification and 4-step denitrification processes as in ASMN (Hiatt and Grady, 2008), similar to the efforts by Flores-Alsina et al. (2011). Then the model was incorporated respectively with the two AOB denitrification models, Scenario A and Scenario B, of Mampaey et al. (2013). In other words, the two integrated models differed in the AOB pathways included for N_2O production.

The models of Ni et al. (2011 and 2013a) included, next to the N_2O production through the NH_2OH pathway in AOBs, the 4-step heterotrophic N_2O -production according to Hiatt and

Grady (2008). The kinetic equations for all steps were also extended with the ones of ASMN (Hiatt and Grady, 2008) with Monod terms of NH_4^+ .

Pocquet et al. (2012) compared the simulation results of three AOB N_2O production models, i.e. (i) the scenario A model proposed by Mampaey et al. (2013), (ii) Ni et al. (2011) and (iii) Houweling et al. (2011). The three models were used to simulate a SBR under aerobic conditions. However, the first two models were found not to give a good prediction on N_2O production. The model of Houweling et al. (2011) simulates the N_2O observed dynamic trend well, but it is limited in its application range of NO_2^- concentration because it is an empirical model. Pocquet et al. (2012) further combined the model of Houweling et al. (2011) with a modified ASM3 in which the one-step heterotrophic denitrification processes were extended into four-step denitrification processes, similar to the ASMN approach (Hiatt and Grady, 2008). This combined model was used to simulate the anoxic-aerobic process of the SBR. Although the simulation results can follow the general trend of the measurement data, the simulation results are considered to be too different from the experimental data and it was thus concluded that the model of Houweling et al. (2011) is not a good choice to simulate the bioreaction kinetics.

Finally, the literature review has shown that, as far as known, no model has at present been proposed that combines N_2O production from heterotrophs, AOB and PAO.

V. Comprehensive model

Next to mechanistic biokinetic models of the bioreactor conversions, empirical models have been developed to estimate N_2O and other GHG emissions from WWTPs. As mentioned earlier, the Bridle model (Bridle et al., 2008), which was developed based on the model of Monteith et al. (2005), estimates the N_2O and other GHG from five sectors by a set of empirical functions. The N_2O emission is estimated by multiplying the amount of N

removed with an empirical fraction factor. Ashrafi et al. (2013) followed a similar approach for pulp and paper industrial wastewater treatment. They also included CO₂ emissions from the primary clarifier which was not taken into account by Bridle et al. (2008). Their reasoning is that the influent of pulp and paper industrial wastewater contains more carbonaceous contaminants compared to typical municipal wastewater. These high-concentration carbonaceous contaminants could already be oxidized biochemically in the primary settlers. Although Rodriguez-Garcia et al. (2012) calculated the N₂O emissions by the bioreaction kinetic models, they used the Activated Sludge/Anaerobic Digester model (AS/AD) (BioWin®, www.envirosim.com) to estimate the non-N₂O GHG emissions. The latter is different from the Bridle model which calculates the CO₂ emissions from biomass decay as a 1-step process, i.e. biomass → CO₂. The method used by Rodriguez-Garcia et al. (2012) treats it as three steps, i.e. biomass → slowly biodegradable substrate → readily biodegradable substrate → CO₂. This allows for more complex dynamics to be simulated under dynamic conditions.

2.3.2 Model applications in full-scale plants

I. Real WWTPs

Samie et al. (2011) applied their modified ASM1 model to a full-scale denitrifying biofilter. The simulation was run for one year and the dynamic simulation results were compared with the denitrifying biofilter effluent measurements in terms of COD, NO₃⁻ and NO₂⁻. However, no detected dynamic measurement data were available for the liquid N₂O concentration. Moreover, there was no dynamic measurement data for N₂O gas emission either, which could be due to the fact that their focus was on the denitrification process which has little gas stripping.

Modelling of N_2O emissions has already been done for real WWTPs. In the same paper where Ni et al. (2013a) developed the model, a dynamic simulation was run for an oxidation ditch with surface aerators as well as an SBR located in Perth, Western Australia. The model was calibrated using data measured at the oxidation ditch during three days and then validated for one-day 24 hour measurement data at the same oxidation ditch. The model was also validated for 2 days, each with a 9-hour measurement record, for the SBR. The model reproduced the dynamics of N-component concentrations and N_2O emissions well but poorly predicted the DO in the oxidation ditch.

von Schulthess and Gujer (1996) simulated the N_2O emissions from the full-scale WWTP in Opfikon, Switzerland, by using and modifying their own model (von Schulthess et al., 1994). This plant had an anoxic tank followed by three aerobic tanks. The anoxic tank could be aerated if required. Generally, the model predicted the measured NO_2^- and NO_3^- concentrations well but predictions of N_2O were not satisfactory. The reason possibly resides in the fact that their model did not consider N_2O production by AOBs.

These two case studies (Ni et al., 2013a; von Schulthess and Gujer, 1996) cannot be treated as long-term dynamic modelling. Firstly, the simulation was run only for one to three days. Secondly, although the simulation was run for 24 hours, the measurement data which were used for calibration or validation were not continuous for 24 hours. Moreover, the measured N_2O emissions differ significantly from those reported in the long-term monitoring work by Daelman et al. (2013a). This suggests that more data collection is needed and that thorough calibration and validation of models on long-term measurement data are required.

II. Benchmark models

WWTPs do not operate in steady state but are subjected to disturbances of influent quantity and quality as well as operating conditions. Control strategies are designed to minimize the impact of disturbances on system performance. The influent conditions are highly dynamic and are different for every WWTP, which makes it difficult to compare control strategies objectively. In review of this, benchmark simulation models (BSMs) have been proposed with define configurations and influent conditions, allowing perfectly reproducible results, as well as objective comparison between different strategies. Since the issue of GHGs has come to the forefront, the original benchmarks have been extended in order to allow evaluation of GHG-focused control strategies, hereby still accounting for operational cost and effluent quality.

BSM2 (Nopens et al., 2010), Figure 2.10, is a plant-wide WWTP layout which extends BSM1 that only focused on the activated sludge system (Alex et al., 2008). It is composed of a primary settler, a bioreactor composed of five completely stirred tank reactors (CSTRs) connected in series, a secondary settler, a sludge thickener, an anaerobic digester, a sludge dewatering unit, a storage tank and two interfaces between the activated sludge and anaerobic digestion models. The first two CSTRs, activated sludge unit 1 (ASU1) and ASU2, are anoxic tanks for denitrification and the following three, ASU3, ASU4 and ASU5, are aerobic tanks for nitrification. An internal NO_3^- recycle and an external sludge recycle line are included. Considering the influent dynamics, three influent bypass routes are added to deal with high hydraulic loads (Figure 2.10). ASM1 with temperature effect included is used for modeling the activated sludge process, ADM1 is used for modeling the anaerobic digester (AD) and the interfaces between ASM1 and ADM1 follow the approach proposed by Nopens et al. (2009). Nopens et al. (2010) illustrated the usage of BSM2 through three control strategies (Figure 2.11). In the 1-DO control strategy, the DO

concentration of the 2nd aerobic zone (ASU4) is maintained by manipulating the oxygen transfer coefficients (k_La) of all three aerobic zones. In the 2-DO control strategy, the 3rd aerobic zone (ASU5) is controlled by a separate DO controller, while the aeration in the two other reactors (ASU3 and ASU4) is controlled on the basis of the DO concentration of ASU4. In the cascade control system, the first two aerobic zones use the same strategy as in the 2-DO control strategy, but the DO setpoint of the aeration controller of ASU5 is controlled by an NH_4^+ controller, yielding a so-called NH_4^+ -DO cascade control set-up.

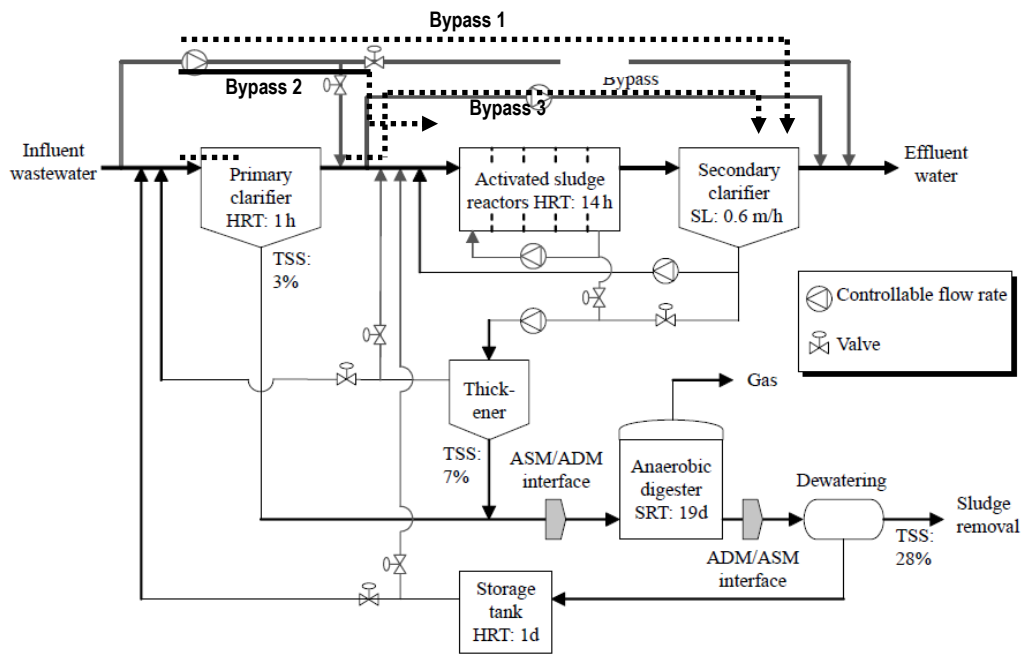
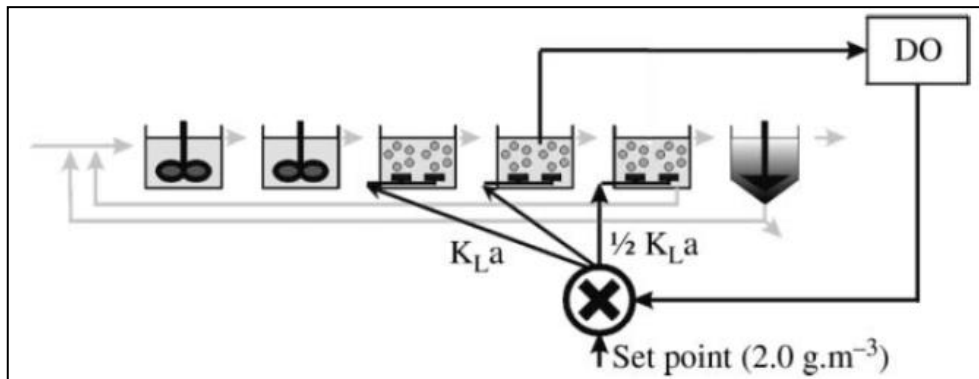
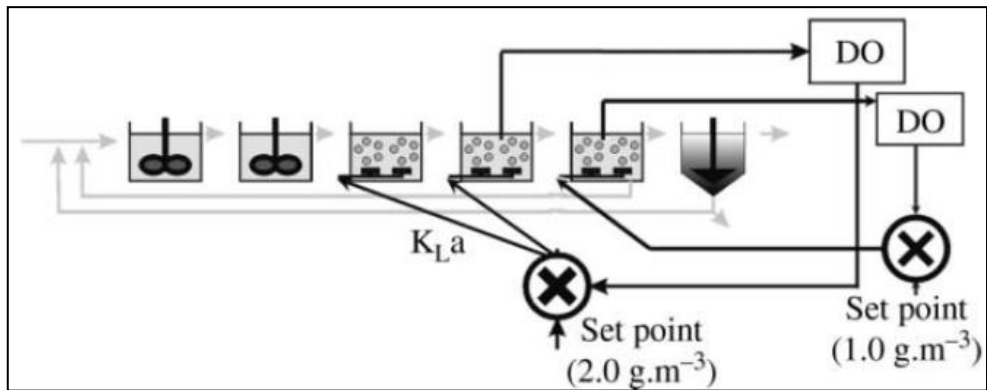


Figure 2.10 BSM2 plant layout (Nopens et al., 2010).

(a) Scenario 1-default scenario



(b) Scenario 2



(c) Scenario 3

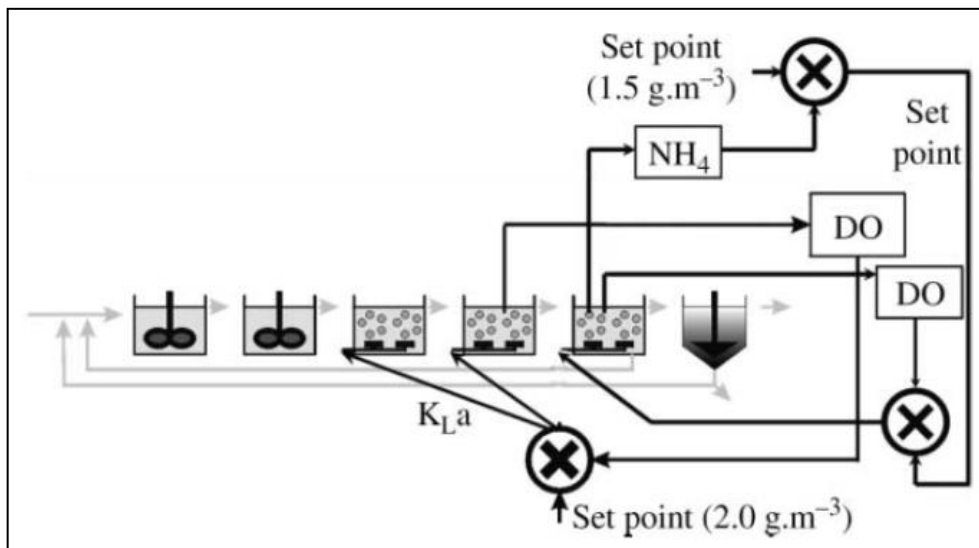


Figure 2.11 BSM2 default control strategies (Nopens et al., 2010).

Criteria for plant performance, mainly including effluent quality and operational cost, and controller performance evaluation were proposed for comparison of control strategies. The effluent quality was judged by the effluent quality index (EQI), an average of the sum of weighted pollutant loads over the evaluated period, and the effluent pollutant violations. The weighting factors of EQI were mainly deduced from Vanrolleghem et al. (1996) and further modified based on the finding of Jeppsson et al. (2007) in order to improve the control of effluent NH_4^+ violation. The operational cost index (OCI) was composed of energy consumption, sludge production and carbon source dosing. For BSM2, the dynamic simulation to be performed is 609 days long in total and the evaluation starts from day 245 to day 609, day 245 corresponding to the 1st of July.

Flores-Alsina et al. (2011) integrated their GHG emission models with the BSM2 and named the modified model BSM2G. The interfaces between ASM and ADM and the definition of EQI were extended since new nitrogen containing substances and autotrophic organisms were defined. The general concept was based on ASM1-ADM1 conversions as described in Nopens et al. (2009). The interfaces now include NO_3^- , NO_2^- , NO and N_2O for the nitrogen balance, NO_3^- , NO_2^- , NO, N_2O , AOB and NOB for the COD mapping, and NO_3^- and NO_2^- for the charge balance, whereas in the ASM1-ADM1 interfaces only the NO_3^- and a single group of autotrophs were considered (Corominas et al., 2012). OCI and effluent violations of BSM2G were calculated in the same way as BSM2. The N_2O emission is directly simulated with the biokinetic model and then converted to CO_2 equivalents through the GWP factor. Other GHG emissions were evaluated using the Bridle model, including CO_2 emission from the bioreactors, CO_2 and CH_4 emissions from the AD, and GHG emissions related to net power consumption, chemical use and sludge disposal and reuse. Similar to BSM2 (Nopens et al., 2010), BSM2G was run for 609 days and evaluated for day 245-609 in terms of effluent quality, operational cost and GHG emissions. The findings

regarding different strategies and scenarios carried out in this BSM2G will be given in Section 2.4 “Control of N₂O emissions”.

III. Other virtual applications

Besides the BSMs, there are other model applications for virtual plants. Rodriguez-Garcia et al. (2012) applied their two integrated models to two virtual case studies with MLE processes. The first one is a MLE process designed by BioWin®. The second one was proposed by Vidal et al. (2002), which was also a MLE process but had sludge thickening and centrifuge blocks. The difference of the simulation results between the two integrated models was mainly shown on the first MLE process. The model using Scenario A of Mampaey et al. (2013) had higher effluent concentrations of NH₄⁺, NO₃⁻, NO₂⁻ and NO but much lower N₂O and total GHG emissions than the model using Scenario B of Mampaey et al. (2013). The difference was basically due to the different preference on DO and different electron donors used by AOB denitrification in the two integrated models. The AOB denitrification model of Scenario B had no preference for aerobic or anoxic conditions, i.e. it happened under both conditions. Therefore, it had the potential to produce more N₂O. The higher conversion rate from NH₄⁺ to N₂O caused lower NH₄⁺ concentrations in effluent. Moreover, in Scenario B the AOB biomass was consumed as electron donor, leading to more CO₂ production because biomass is composed of organics and oxidation of more organics leads to more CO₂ production. However, no clear conclusion could be drawn from this work. In the simulation work of Mampaey et al. (2003) Scenario A had higher N₂O emissions than Scenario B. This is possibly because the higher endogenous respiration of biomass under both aerobic and anoxic conditions might reduce the biomass quantity and the decrease of AOB biomass prevents N₂O production.

2.4 Control of N₂O emissions

2.4.1 Control in BSM2

Flores-Alsina et al. (2011) implemented three control strategies, A1-A3, in BSM2 and compared their plant effluent quality, operational cost and GHG emissions. A1 controlled the DO concentration in the second aerobic tank, ASU4, by manipulating the k_{La} of ASU3-ASU5. Based on A1, A2 added a NO_3^- controller in ASU2 by manipulating the internal recycling rate. A3 further upgraded A2 by manipulating the DO set point through NH_4^+ control, i.e. a NH_4^+ -DO cascade control. All three strategies exhibited improvements on effluent quality and operational cost compared to the open-loop scenario. Especially, the effluent NH_4^+ violation is cut considerably in A3 as the purpose of cascade control is to keep the NH_4^+ concentration under a certain level leading to aeration energy savings. However, the N_2O emission of A3 (0.202 kg $\text{CO}_{2e}/\text{m}^3$) is larger than that of A1 (0.146 kg $\text{CO}_{2e}/\text{m}^3$) and A2 (0.158 kg $\text{CO}_{2e}/\text{m}^3$). This high emission of N_2O is mainly due to the aeration energy saving purpose of the cascade control, which caused low DO conditions most of the time. The low DO concentrations lead to NO_2^- accumulation and increases N_2O production. The overall GHG emission of A3 (1.100 kg $\text{CO}_{2e}/\text{m}^3$) is also higher than that of A1 (1.032 kg $\text{CO}_{2e}/\text{m}^3$) and A2 (1.044 kg $\text{CO}_{2e}/\text{m}^3$).

Based on A2 Flores-Alsina et al. (2011) further examined the effect of changing three operational parameters, i.e. the DO control set point in the aerobic section, the sludge retention time (SRT) and the COD/N ratio. It was found that the DO concentration is best controlled at a moderate level. Both high and low DO concentrations lead to elevated GHG emissions. Reducing the SRT leads to more GHG credits by producing more CH_4 , because more sludge goes into the sludge digester. However, it should be noticed that in their case even under the lower SRT the N is still efficiently removed, which avoids the

huge increase of N_2O production. Increasing the COD/N by adding more external carbon helps N_2O mitigation but increases GHG emissions in other sectors like CO_2 equivalents due to chemical dosing etc.

Generally speaking, the work of Flores-Alsina et al. (2011) proved that there is a trade-off among different GHG emission contributors as well as among different performance objectives, i.e. effluent quality, operational cost and GHG emissions. It also illustrated the usefulness of the benchmarking model in control strategy analysis. However, the BSM2G is not calibrated or validated for a WWTP and the N_2O production by AOB is not included, which limits the reliability of final conclusions that were drawn from the simulation results.

2.4.1 Alternative N_2O mitigation strategies

Desloover et al. (2012) proposed several N_2O mitigation strategies. The major idea was on the one hand to minimize the N_2O produced by AOB and on the other hand to maximize the N_2O consumed by heterotrophs. The N_2O production by AOB could be minimized by preventing the accumulation of NH_2OH and NO_2^- , high sludge specific activity, fluctuation of NH_4^+ and high nitrification activity. Practical approaches were suggested, like adjusting aeration, ensuring complete mixing, bio-augmentation with AOB and NOB, etc. In order to achieve maximum N_2O consumption by heterotrophs it was aimed to improve the complete denitrification or increase the N_2O reduction. To realize these objectives, it was sought to control aeration and COD/N ratio, choose carbon sources for external dosage, lower the removal of COD by aerobic oxidation and pre-settling, bio-augment with denitrifying heterotrophs, etc. Besides these major aspects, the authors also proposed that N_2O emissions in the aerated zone could be minimized through physical methods, i.e. to reduce the N_2O gas emitted into the air. Several approaches were suggested to reduce the mass transfer coefficient of N_2O for different types of aerated bioreactors, for example, limiting the turbulence for passive aeration systems (like rotating biological contactors) and

lowering the aeration rate for active aeration systems (like activated sludge aeration tanks). For plants equipped with capped bioreactors, the gases could be collected and treated at the end of the pipe, which reduces the N_2O emitted into the atmosphere.

2.5 Controlling under rain events

Although the effect of climate change on future rainfall distribution is still not clear, it is suggested that in the future there may be more intense rainfall events over many areas (Giorgi et al., 2001; Hulme et al., 2002; Solomon et al., 2007). This is consistent with recent increases in rainfall intensity (Frich et al., 2002; Ekström et al., 2005; Fowler et al., 2005; Van Steenbergen and Willems, 2012). For instance, in the UK it seems that the climate will become warmer and more humid leading to increases in annual precipitation by up to 10 % by the end of the century (Hulme et al., 2002; Butler and Davies, 2004).

Rain events disturb the typical influent pattern but forecasts of rainfall or influent shocks caused by rainfall can be obtained by weather forecasts or rain intensity measurements so that the plants can adjust their operation to prepare for dealing with rain events. For example, the sludge recycling may be increased to lower the sludge blanket before receiving the influent shock since it is reported that hydraulic shock loadings may exceed the capacities of the settlers resulting in poor effluent quality (Henze et al., 2008).

Generally, storm control is done by feedforward control strategies. The sewers, WWTPs and receiving water are sometimes connected as a whole to study the effects of storms on water quality (Durchschlag et al., 1992; Harremoës et al., 1993; Seggelke et al., 2005). The bypass as well as the storage tank are commonly used methods to deal with influent shocks during storms. Lessard and Beck (1990) discussed several bypass and storage tank filling strategies. Step feeding is also often used as a control strategy during storms. It

distributes the influent between the bioreactors to temporarily decrease the loading to the settlers. This strategy was discussed with respect to plant performance, e.g. energy saving, effluent variability and solids loss (Copp et al., 2002; Thompson et al., 1989). Besides the inclusion of a storm tank and step feed, Bauwens et al. (1996), who used a virtual WWTP model which received wastewater from a sewer model, also discussed a proportional controller to the sludge recycling ratio and the results showed a stable biomass concentration in the aeration tank but a poorer settler performance with more fluctuations of the underflow concentration. Risholt et al. (2002) studied pollution-based real time control which improved the performance stability and reduced effluent variability during storms.

However, these wet-weather control strategies were not evaluated in terms of N₂O emissions or GHG emissions. There were also no strategies proposed in view of making a trade-off between GHG emissions and other plant performance criteria.

2.6 Problem statement

2.6.1 Insufficient full-scale measurement data

Literature describes the diversity of N₂O emissions from different treatment processes and plant locations, but the spatio-temporal variation of N₂O emissions in treatment plants is not described adequately. Better, high time-frequency measurements of the spatial distribution will help understand N₂O emission from full-scale WWTPs and allow better design of control strategies. More long-term on-line continuous measurements at full-scale WWTPs are required to better understand the dynamics of the N₂O emissions changing with the influent load. No literature was found on the effect of rain events or hydraulic shocks on N₂O or GHG emissions in general.

2.6.2 Insufficient model development

The main bottleneck of developing an overall biokinetic model regarding GHG emissions is the existing doubts regarding the pathways of N₂O production by AOB. Detailed biochemical mechanisms, such as transfer of electrons and nitrogen components, and related DO consumption as well as its effect on relevant process rates, are still under debate. The existing models have mostly been derived from lab-scale experiments. Moreover, the difference between different lab-scale experimental methods and results may explain the observed variations in AOB denitrification models. Therefore, it is not only necessary to build a model including N₂O production by both heterotrophs and AOB, but also to propose a method on how to accept or reject such a model. Moreover, for a plant with P removal, the denitrification and the N₂O production by PAOs should be included in the model.

Although the GHG models have been implemented in existing configurations, there remains a lack of calibrations leading to doubts on the reliability of benchmark simulations. For the modelling of real plants, model calibration based on long-term dynamic measurement data is required, for example, by using a dataset of 1 month. The modelling should be extended to estimate the GHG emissions from the whole plant, i.e. to estimate the non-measurable emissions. Moreover, although a lot of GHG models have been proposed and applied in different case studies, insufficient efforts have been spent in terms of model differentiation or selection.

2.6.3 Lack of control strategy studies including GHGs models

Most traditional control strategies and performance evaluations do not take GHGs into account, except for Flores-Alsina et al. (2011) who suggested an evaluation method for GHG emissions and compared a limited number of strategies and scenarios from the point

of N₂O or GHG productions. However, the model used in Flores-Alsina et al. (2011) does not include the autotrophic pathway for N₂O production. Therefore, more work is required for strategy and scenario comparisons when the AOB denitrification pathway is modelled as well. Moreover, the literature does not contain reports on control evaluation for the effects of storm events on GHG emissions nor on dedicated controller development considering both storm event effects and GHG emissions.

In fact, very few control strategies were discussed in the frame of BSM2 that focus on the effects of storm events on the classical performance criteria, e.g. effluent quality and operating costs, and the subject of this thesis, N₂O emissions of WWTPs. Several scenarios were inspected focusing on storm tanks and bypasses in simple layouts, but not in a plant-wide context. Although the storm impacts on WWTPs were discussed over 20 years ago (Durchschlag et al., 1992; Harremoës et al., 1993) and control strategies, like bypassing, storage tank filling and step feeding, are widely discussed, those strategies have not been evaluated in BSM2, the plant-wide benchmarking layout. Moreover, results on strategies focused on the GHG emissions during storms do not yet exist.

2.7 Objectives

The objectives of this work can be defined as follows:

I. Experimentally characterize the spatio-temporal variations of N₂O emissions in full-scale WWTPs

- Record the magnitude and spatio-temporal variation of N₂O emissions
- Study the effect of rain events on GHG emissions

- Analyze N₂O emission with respect to other plant dynamic data, e.g. influent loads and aeration flow rates

II. Modelling of N₂O and other GHG emissions from full-scale plants

- Build activated sludge models for GHGs (ASMG) which integrate the N₂O production by heterotrophic, AOB and PAO pathways using the common ASM submodels as a basis
- Implement the ASMG models in benchmarking systems and real plants
- Estimate the parameter values of the ASMG models on the basis of full-scale measurement data or other suggested values using a long-term dataset
- Estimate the GHG emissions which are not measured at a full-scale plant
- Give suggestions on how to differentiate ASMG models based on qualitative reasoning

III. Develop control strategies for reduction of GHG emissions and wet-weather impacts on GHG emissions

- Include GHG emissions into the plant performance evaluations
- Suggest and benchmark control strategies with the consideration of reducing N₂O production and total GHG emissions
- Investigate the effects of shocks due to the influent flow rate, the component loads and the temperature on the performance of WWTPs, especially with a focus on N₂O emissions
- Propose and benchmark control strategies for storm event handling with consideration of GHG mitigation

3 Benchmark GHG modelling and controlling

3.1 Introduction

In this section, the Activated Sludge Model for GHG No. 1 (ASMG1) is built by combining ASMN (Hiatt and Grady, 2008) and the aerobic AOB denitrification model proposed by Mampaey et al. (2013), which is referred to as “original ASMG1”. In addition, a modification is made to the DO kinetics term of this aerobic AOB denitrification model resulting in the model version referred to as “modified ASMG1”. Calibration and validation is done for both original and modified ASMG1 models. Calibration and validation is intended to agree with, on the one hand, the regular BSM2 simulation results, i.e. effluent quality and operation cost, obtained with the existing BSM2 model which implements ASM1 (Nopens et al., 2010), and, on the other hand, to match overall N₂O emission data reported in the literature (Ahn et al., 2010; Foley et al., 2010).

Following the calibration and the validation, different control strategies are discussed regarding the GHG emissions and other plant performance criteria in the framework of BSM2. The simulations are first run with the current BSM2 influent file and then with a new influent file which contains an increased number of intense rain events in order to analyze the plant performance under hypothetical future climate conditions.

Section 3.2 is redrafted from the paper “Guo L. and Vanrolleghem P.A. (2014) Calibration and validation of an Activated Sludge Model for Greenhouse gases No. 1 (ASMG1) - Prediction of temperature dependent N₂O emission dynamics. *Bioprocess and Biosystems Engineering*, 37, 151-163.”. Section 3.3 is redrafted from the paper “Guo L., Porro J., Sharma K., Amerlinck Y., Benedetti L., Nopens I., Shaw A., Van Hulle S.W.H., Yuan Z. and Vanrolleghem P.A. (2012) Towards a benchmarking tool for minimizing wastewater utility greenhouse gas footprints. *Water Science and Technology*, 66, 2483-2495.” and

“Guo L., Martin C., Nopens I. and Vanrolleghem P.A. (2012) Climate change and WWTPs: Controlling greenhouse gas (GHG) emissions and impacts of increased wet weather disturbances. In proceedings of IWA Nutrient Removal and Recovery 2012: Trends in NRR, Harbin, China, September 23-25 2012.”. These two papers were finished before the completion of the calibration work. Hence, in this thesis the results were updated using the calibrated parameters.

3.2 ASMG1 model calibration and validation using BSM2

3.2.1 Implementation and calibration/validation approaches

I. ASMG1 models and implementation

Two ASMG1 models (Table 3.1) are discussed. The original ASMG1 consists of ASMN (Hiatt and Grady, 2008) which extends ASM1 by including 2-step nitrification, 4-step denitrification, and an aerobic AOB denitrification model proposed by Mampaey et al. (2013) which assumes that a higher DO concentration leads to higher N₂O production and NH₄⁺ donates electrons for NO₂⁻ and NO reductions.

Table 3.1 Summary of the two ASMG1-BSM2 models

	Original ASMG1-BSM2	Modified ASMG1-BSM2
ASMN	Hiatt & Grady	Hiatt & Grady
AOB denitrification	Mampaey A	Modified Mampaey
Reduction factor on NO ₂ ⁻ reduction	Yes	Yes
Reduction factor on NO reduction to N ₂ O	No	Yes
DO kinetics	Monod	Haldane

The concept of the AOB denitrification model of Mampaey et al. (2013) agreed with general ideas in terms of NH_4^+ being used as electron donor (Kampschreur et al., 2007; Yu et al., 2010), and by using this model no components (such as NH_2OH) need to be added to the basis provided by ASMN. One of the most debated aspects regarding the AOB denitrification model is the role of DO (Aboobakar et al., 2013; Kampschreur et al., 2008; Law et al., 2012; Tallec et al., 2006; Yu et al., 2010). Therefore, in the modified ASMG1, a modification was made to the DO kinetics term of the original ASMG1. Some recent research suggests that for N_2O production by AOB denitrification a maximum rate occurs at relatively low DO conditions (Tallec et al., 2006; Law et al., 2012). This behaviour may be explained by the hypothesis that a low DO stimulates N_2O production while high DO inhibits it, meaning that the influence of DO can be expressed by Haldane (1930) kinetics. In this work the intermediate NH_2OH is not considered to keep the model simple and not introduce a component that is hard to measure at full-scale. The overall effect of DO was described by the DO kinetic term defined in Eq. (3.1), which is a modified Haldane kinetic term:

$$\text{DO}_{\text{Haldane}} = \frac{S_{\text{O}}}{K_{\text{SO_AOB den.}} + \eta_{\text{Haldane}} \cdot S_{\text{O}} + S_{\text{O}}^2 / K_{\text{IO_AOB den.}}} \quad \text{Eq. (3.1)}$$

where $K_{\text{SO_AOB den.}}$ and $K_{\text{IO_AOB den.}}$ are the kinetic parameters and η_{Haldane} is calculated from $K_{\text{SO_AOB den.}}$ and $K_{\text{IO_AOB den.}}$ as Eq. (3.2)

$$\eta_{\text{Haldane}} = 1 - 2 \cdot \sqrt{K_{\text{SO_AOB den.}} / K_{\text{IO_AOB den.}}} \quad \text{Eq. (3.2)}$$

The form of the $\text{DO}_{\text{Haldane}}$ is presented in Figure 3.1.

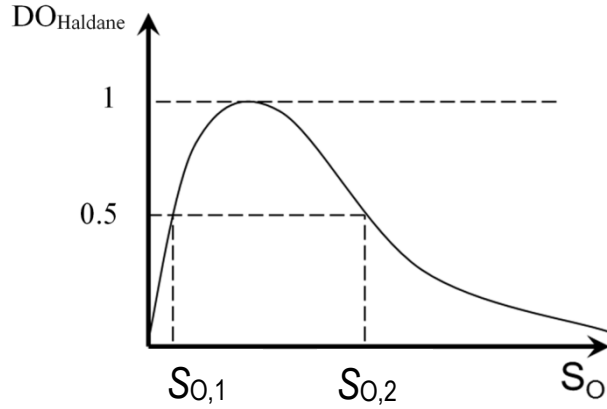


Figure 3.1 Illustration of kinetic relationship between S_O and $DO_{Haldane}$ in the modified Haldane term.

The mathematical structure of the modified Haldane kinetics used here is a little different from the original structure (Haldane, 1930). The original Haldane kinetics never reaches 1 as its maximum, which is different from the Monod kinetics which approaches 1. The proposed modified Haldane kinetics, i.e. Eq. (3.1), sets 1 as its maximum value in order to agree with the Monod term. Therefore, in Eq. (3.1), the parameters can be calculated from the half-saturation DO concentrations, $S_{O,1}$ and $S_{O,2}$, as usually done for Monod kinetics, while this is not possible for the traditional term. $K_{SO_AOB\ den.}$ and $K_{IO_AOB\ den.}$ are calculated respectively by Eq. (3.3) and Eq. (3.4).

$$K_{SO_AOB\ den.} = \frac{S_{O,1} \cdot S_{O,2}}{K_{IO_AOB\ den.}} \quad \text{Eq. (3.3)}$$

$$K_{IO_AOB\ den.} = \left(\sqrt{S_{O,1}} - \sqrt{S_{O,2}} \right)^2 \quad \text{Eq. (3.4)}$$

where $S_{O,1}$ and $S_{O,2}$ are the half-saturation DO concentrations ($\text{mg O}_2/\text{l}$).

Besides the modification of the DO kinetic term, two different growth reduction factors, $\eta_{AOB,1}$ and $\eta_{AOB,2}$, were multiplied respectively with the kinetic equations of the two AOB

denitrification steps, i.e. NO_2^- reduction to NO (step 1) and NO reduction to N_2O (step 2), while in the original aerobic AOB denitrification model (Mampaey et al., 2013) only the step of NO_2^- reduction to NO uses the growth reduction factor. The use of the growth reduction factor for both steps is based on the consideration that the maximum growth rate of AOB can be different for denitrification and nitrification reactions.

In summary, the AOB denitrification model was modified as in Eq. (3.5), Eq. (3.1) replacing the Monod DO limitation term and multiplying the whole kinetic term by growth correction factors for the first and second step of AOB denitrification, $\eta_{\text{AOB}1}$ and $\eta_{\text{AOB}2}$.

$$r_{\text{AOB den.}} = \mu_{\text{AOB}} \cdot (\eta_{\text{AOB}1} \text{ OR } \eta_{\text{AOB}2}) \cdot \text{DO}_{\text{Haldane}} \cdot \left\{ \left(\frac{S_{\text{NH}}}{S_{\text{NH}} + K_{\text{NH_AOB den.}}} \right) \cdot \left(\frac{S_{\text{FNA}}}{S_{\text{FNA}} + K_{\text{FNA_AOB den.}}} \text{ OR } \frac{S_{\text{NO}}}{S_{\text{NO}} + K_{\text{NO_AOB den.}}} \right) \cdot X_{\text{AOB}} \right\}$$

Eq. (3.5)

where $\text{DO}_{\text{Haldane}}$ is the DO kinetics term as defined in Eq. (3.1), η_{AOB} is the growth correction factor, and the multiplication term in curly brace is exactly the term suggested by Mampaey et al. (2013). The details of ASMG1 are given in Appendix D-F.

The modeling and simulation software used is WEST (MIKEbyDHI.com). All ASMG1 models were implemented in the BSM2 whole plant configuration, Figure 2.10, called original or modified ASMG1-BSM2 respectively, and were run under the same conditions as described in the finalized BSM2 paper which uses ASM1 (Nopens et al., 2010), named ASM1-BSM2.

The paper describing ASM1-BSM2 (Nopens et al., 2010) compares the plant performance in open loop, i.e. without any controller active, Figure 2.10, with the performance obtained for three control strategies, i.e. the 1-DO control strategy, the 2-DO control strategy and the cascade control strategy, Figure 2.11. These ASM1-BSM2 reference results of the

open loop and the three control strategies were used to calibrate and validate both ASMG1-BSM2 models. The simulation results in terms of indices of effluent quality and operational cost for the ASMG1s-BSM2 were evaluated by exactly the same method as used for evaluating the ASM1-BSM2 with the extensions for the new oxidized nitrogen components according to Flores-Alsina et al. (2011).

II. Calibration and validation objectives

The ASMG1-BSM2 models were calibrated in open loop and on literature data of yearly N_2O emissions. They were then validated with the data of the three control strategies of ASM1-BSM2 (Nopens et al., 2010). The objectives of model calibration thus include fitting the N_2O emission factor, the effluent quality and the operational cost. Given the fact that BSM2 is a virtual plant, no real N_2O data are available, but a realistic value of N_2O emission can be obtained from literature. For plants with a modified MLE process the N_2O emission factor is in the range of 0.1-1% of the influent TN load (Ahn et al., 2010; Foley et al., 2010). Therefore, for BSM2 which is also a MLE plant, 0.5% was chosen as the N_2O emission factor to be reached after model calibration. Effluent quality, including the EQI and the yearly averaged effluent concentrations, and the OCI should agree with the results given in the finalized ASM1-BSM2 (Nopens et al., 2010). The weight factors used in EQI and OCI were the same as in the finalized ASM1-BSM2. In the EQI, only NO_3^- was included, although there are other oxidized N-species (NO_x), i.e. NO_2^- , NO and N_2O . The reason is that in real WWTPs, usually only effluent NO_3^- is monitored and the concentrations of NO_2^- , NO and N_2O are negligible compared to NO_3^- . The validation only considered the effluent quality and OCI criteria because no N_2O emission factor values are currently available for plants running with such controllers.

The difference between the original and modified AOB denitrification models was further explored in terms of N_2O by comparing their sludge production rates and dynamic N_2O

emissions. Finally, in open loop, the results of implementing only ASMN into BSM2, termed ASMN-BSM2, were compared with those of the ASMG1s-BSM2 to further evaluate the contribution of the AOB denitrification model in the integrated ASMG1 models.

III. Calibration procedure

Firstly, the simulation was run using the default parameter values suggested in the papers of Hiatt and Grady (2008) and Mampaey et al. (2013) to clarify the gaps with the calibration targets. Then the calibration was done following the procedure illustrated in Figure 3.2. This procedure gives the calibration approach and the targets of each step, denoted with “T”. The parameters were tuned under steady state conditions to make the steady state results of ASMG1-BSM2 similar to those of ASM1-BSM2 (Nopens et al., 2010); then the parameter set was used in simulations under dynamic conditions to see whether the results agreed as well. If the dynamic simulation yielded good results, the model was subjected to validation; otherwise, the calibration had to be repeated.

The calibration first focuses on adjusting the ASMN parameters and then moves on to the AOB denitrification parameters, because ASMN includes most processes (nitrification, denitrification, etc.). In terms of N_2O emissions the objective is to obtain a N_2O emission of ASMN-BSM2 lower than 0.5% of the influent TN-load because it can be expected that some of the overall N_2O emission will be produced by AOB denitrification. Also, the bioreactor mixed liquor nitrite concentrations of the calibrated ASMN-BSM2 should be low because nitrite is a reactant for N_2O production through the AOB pathway that will only be evaluated in the next step of the calibration.

The concentrations of particulate biodegradable organic nitrogen (X_{ND}), slowly biodegradable substrate (X_S) and soluble biodegradable organic nitrogen (S_{ND}) were targeted first because they are the sources of readily biodegradable substrate (S_S) and

ammonia which serve in other process steps. Then the parameter tuning was taken to simulate the nitrogen removal process well, i.e. following Corominas et al. (2011) first the ammonia oxidation and nitrite oxidation processes and then the denitrification processes, so as to satisfy the nitrate and nitrite concentrations and ultimately the N_2O gas flux.

The selection of parameters for calibration was based on expert knowledge (Sin et al., 2008a). Some parameter values were initialized based on ASM1-BSM2 (Gernaey et al., 2014), since some processes in ASMG1 have the same kinetic equations as in ASM1, including hydrolysis, ammonification and heterotrophic aerobic organic degradation. It is important to acknowledge that ASMN was proposed for high-strength wastewater in terms of nitrogen load (Hiatt and Grady, 2008), while the BSM2 plant treats typical, less strong municipal wastewater. Hence, some of the parameters in ASMG1-BSM2 should use the commonly accepted values, i.e. the default ASM1 (Henze et al., 2008), instead of the ASMN defaults. Besides absolute values, for some parameters a fixed ratio relationship was adopted, e.g. the half-saturation coefficients for oxygen and substrate (K_{OH} and K_S) in the aerobic heterotrophic growth and anoxic denitrification, and the growth factor of each denitrification step. The nitrogen conversion in each step can then be adjusted through manipulation of the ratios.

Although the calibration procedure described above was only applied to the BSM2 virtual plant, it has a general application potential which is believed to be useful for real plant calibration.

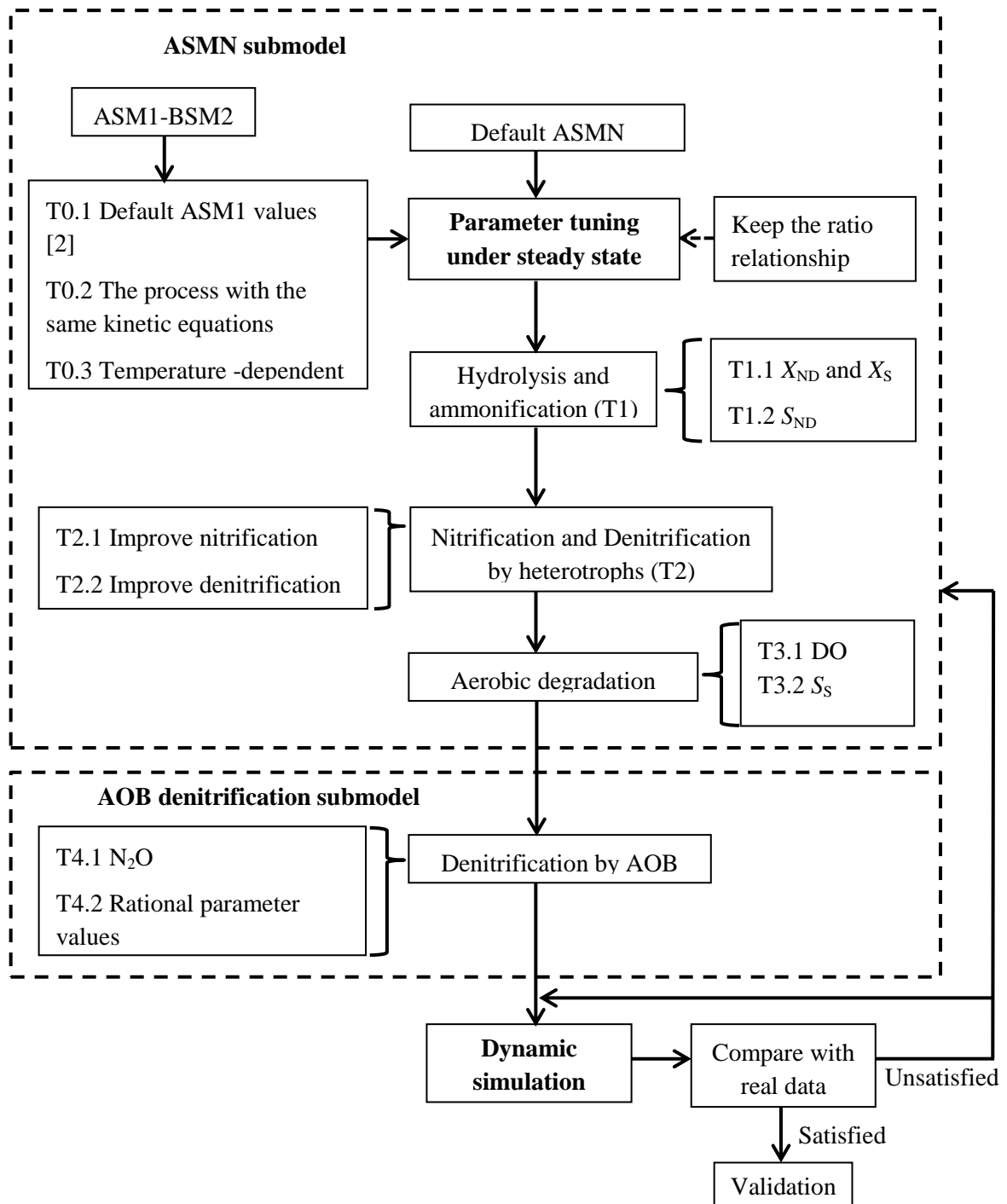


Figure 3.2 The calibration procedure and the sub-targets of each step.

3.2.2 Results

I. Calibration results

Table 3.2 gives the results of ASMN-BSM2 before and after calibration. Compared to the results obtained when using default ASMN parameters the N_2O emission factor of the calibrated ASMN-BSM2 was significantly reduced to below 0.5%. This thus gave the possibility of achieving the pursued N_2O emission factor around 0.5% by adding AOB denitrification (either original or modified ASMG1-BSM2). Also, the NO_2^- concentrations were reduced by the calibration (Table 3.2) and this will also reduce the N_2O production potential by AOB when using the ASMG1-BSM2 models.

Table 3.3 lists the values of the ASMN submodel parameters that were changed from their defaults and states the calibration target that was used to tune each parameter. Table 3.4 lists the parameters of the AOB denitrification models used in the subsequent calibration step. The calibration results of the original and modified ASMG1-BSM2 are given in Table 3.5. Similar results as ASM1-BSM2 in terms of effluent quality and operational costs are obtained and their N_2O emission factors are around 0.5%, indicating that both models thus pass the calibration.

Before validation is started (Figure 3.2) the next step consists of evaluating the models' performance by comparing the results obtained by dynamic simulation with observed data (in our case, from the finalized ASM1-BSM2). Figure 3.3a compares the DO, NO_3^- and NH_4^+ concentrations in ASU4, i.e. the second aerobic tank in the BSM2 configuration, in open loop simulated by the original ASMG1-BSM2, the modified ASMG1-BSM2 with the finalized ASM1-BSM2. The results show that the three models behave very similarly, except for NO_3^- probably because ASM1 has only one type of NO_x while the ASMG1 models include several NO_x components. This result demonstrates that the ASMG1

models are also adequate for dynamic simulation in open loop despite the fact that the model calibration objectives only considered yearly averaged values. It also allows moving on to the validation step.

Table 3.2 Open loop BSM2 results obtained with ASMN with default and calibrated parameters

	Default ASMN-BSM2 ^a	Calibrated ASMN-BSM2
N₂O emission factor^b	6.42%	0.36%
Effluent quality		
Av. S _{NO3} (gN/m ³)	7.62	8.40
Av. S _{NH} (gN/m ³)	3.78	1.82
Av. TN (gN/m ³)	13.01	12.05
Av. TSS (gCOD/m ³)	14.73	14.93
Av. COD (gCOD/m ³)	48.48	48.55
Av. BOD5 (gCOD/m ³)	2.97	2.86
EQI	6649	5737
OCI	8729	9116
Average NO₂⁻ concentration in each ASU		
ASU1	1.07	0.15
ASU2	0.79	0.11
ASU3	1.52	0.24
ASU4	1.77	0.22
ASU5	1.92	0.17

Note: a. Results are calculated by using default parameters given in Hiatt and Grady (2008); b. N₂O emission factor is expressed as the percentage of influent TN load emitted as N₂O-N.

Table 3.3 Tuned parameters of the ASMN submodel and corresponding target of each parameter tuning

Parameter	Unit	Default parameters of ASMN ^a	Calibrated parameters of ASMN	Sub-target
b_{AOB}	d^{-1}	0.055	0.028	T0.3
b_{NOB}	d^{-1}	0.055	0.028	T0.3
b_H	d^{-1}	0.232	0.3	T0.3
k_a	$l/(mg \text{ biomass COD} \cdot d)$	0.1136	0.07	T0.3, T1.1, T1.2
K_{FA}	mg N/l	0.0075	0.004	T2.1
K_{FNA}	mg N/l	0.0001	10^{-6}	T2.1
k_h	mg COD/(mg biomass COD · d)	1.275	2.89	T0.3
K_{10FA}	mg N/l	0.2	0.5	T2.1
K_{10FNA}	mg N/l	0.04	0.1	T2.1
K_{15NO}	mg N/l	0.075	0.2	T2.2
K_{N2O}	mg N/l	0.05	0.02	T2.2
K_{NO}	mg N/l	0.05	0.04	T2.2
K_{NO2}	mg N/l	0.2	0.3	T2.2
K_{NO3}	mg N/l	0.2	1.5	T2.2
K_{OH}	mg O ₂ /l	0.1	0.2	T0.1, T0.2, T5
K_{OH1}	mg O ₂ /l	0.1	0.2	T0.1, T0.2, T5
K_{OH2}	mg O ₂ /l	0.1	0.2	T2.2, T5
K_{OH3}	mg O ₂ /l	0.1	0.2	T2.2, T5
K_{OH4}	mg O ₂ /l	0.1	0.2	T2.2, T5
K_{OH5}	mg O ₂ /l	0.1	0.2	T2.2, T5
K_{S1}	mg COD/l	20	15	T3.1, T3.2
K_{S5}	mg COD/l	40	30	T2.5
K_X	mg COD/mg biomass COD	0.15	0.1	T0.2, T1.1
η_{q2}	-	0.28	0.3	T2.2
η_{q3}	-	0.16	0.3	T2.2
η_{q4}	-	0.35	0.6	T2.2
η_{q5}	-	0.35	0.8	T2.2
η_h	-	0.4	0.8	T0.2, T1.1
Y_H	mg biomass COD formed/ mg COD removed	0.6	0.67	T0.1, T3.1, T3.2

Note: a. Reference temperature is 15 °C and the parameter values are from Hiatt and Grady (2008).

Table 3.4 Tuned parameters of the two AOB denitrification submodels and corresponding target of each parameter tuning

Parameter	Unit	Default parameters of original AOB den. model ^a	Calibrated parameters of original AOB den. model	Calibrated parameters of modified AOB den. model	Sub-target
$K_{FNA_AOB\ den.}$	mg N/l	0.002	0.0006	0.0006	T4.2
$K_{SO_AOB\ den.}$	mg O ₂ /l	0.5	1	-	T4.1
$K_{SO_mod.\ AOB\ den.}$	mg O ₂ /l	-	-	11.40	T4.1
$K_{IO_mod.\ AOB\ den.}$	mg O ₂ /l	-	-	0.035	T4.1
η_{AOB1}	-	0.028	0.5	0.5	T4.1
η_{AOB2}	-	1	0.5	0.5	T4.1

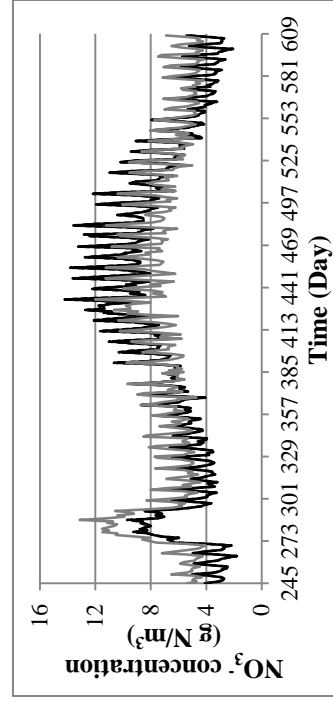
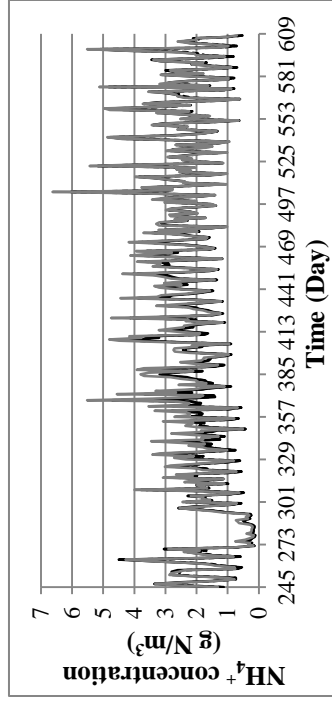
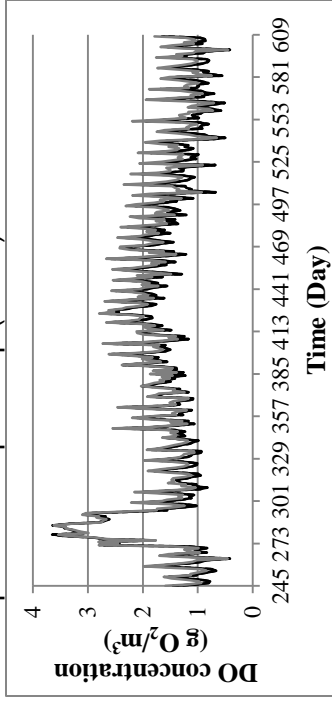
Note: a. Parameter values are from (Mampaey et al., 2013) and “den.” stands for “denitrification”.

Table 3.5 Calibration results of ASMG1 BSM2 in open loop

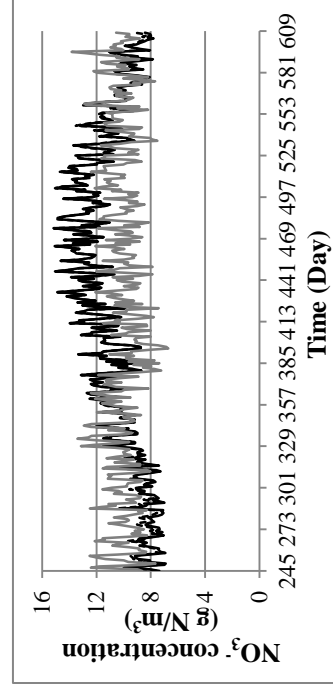
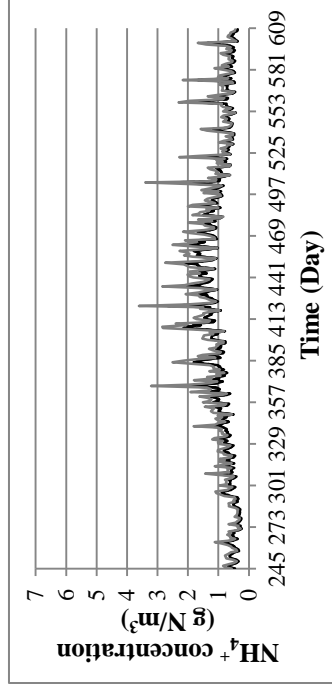
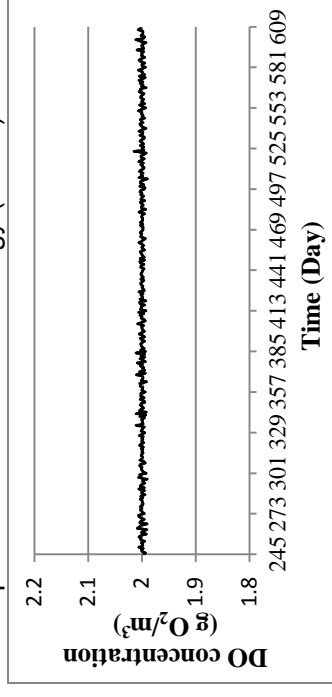
	Finalized ASM1-BSM2 ^a	Calibrated original ASMG1-BSM2	Calibrated modified ASMG1-BSM2
N₂O emission factor^b	-	0.49%	0.50%
Effluent quality			
Av. S _{NO3} (gN/m ³)	7.47	7.32	7.30
Av. S _{NH} (gN/m ³)	1.65	1.51	1.55
Av. TN (gN/m ³)	11.20	10.71	10.74
Av. TSS (gCOD/m ³)	15.90	15.63	15.63
Av. COD (gCOD/m ³)	50.06	49.51	49.51
Av. BOD5 (gCOD/m ³)	2.77	2.82	2.82
EQI	5661	5400	5422
OCI	9208	9104	9104

Note: a. Results are from the BSM2 finalization paper of Nopens et al. (2010); b. Calibration objective of the N₂O emission factor (% of influent TN load emitted as N₂O-N) is 0.5%.

a. Comparison in open loop (ASU4)



b. Comparison under 1-DO strategy (ASU4)



Modified ASMG1-BSM2
 Original ASMG1-BSM2
 Finalized ASMG1-BSM2

Figure 3.3 Comparison of daily averaged dynamic results of ASU4 obtained with the original, the modified ASMG1-BSM2 and the finalized ASMG1-BSM2 in open loop (a) and with 1-DO strategy (b).

II. Validation and model discrimination

The validation was done for the three control strategies proposed in the finalized ASM1-BSM2. Table 3.6 gives the validation results of the calibrated original and modified ASMG1-BSM2. According to Table 3.6, the two ASMG1 models pass validation, indicating good model transferability of the indices listed in Table 3.6. These results thus suggest that the extrapolation power of the models in terms of traditional performance criteria is quite important, especially given the important change these controllers make to the DO dynamics that significantly affect the nitrification/denitrification processes.

In order to better reveal the actual differences between the two models, Table 3.7 compares the average N_2O production rates by the different bacterial groups and the average N_2O emission rates. Under each scenario, little difference was observed between both models for the average total net production rate and the average N_2O emission rate. However, under 1-DO and 2-DO control strategies, the modified ASMG1-BSM2 simulated significantly more AOB-produced N_2O but at the same time also a higher N_2O removal by heterotrophs leading to the same net production rate as the original ASMG1-BSM2. In theory, this significant difference could be used to discriminate between the two models. A recently proposed method based on the isotope signature of N_2O could, for instance, be used to assess the N_2O production by the different pathways, but there still remains difficulties to partition N_2O sources, e.g. under low DO conditions (Wunderlin et al., 2013).

Dynamic results can be considered as an alternative source of information for model discrimination. Indeed, Figure 3.4 compares the sum of dynamic N_2O emissions from the three aerobic tanks during the two warmest weeks and the two coldest weeks for the two models. The dynamic data show that the two calibrated models present little difference in open loop while for the controlled systems during the coldest weeks significantly lower N_2O emissions are obtained when using the modified ASMG1-BSM2 compared to the original

ASMG1-BSM2. According to Table 3.6, the yearly averaged N_2O emission factors of the modified ASMG1-BSM2 and the original ASMG1-BSM2 are similar, which means that during the intermediate temperature periods, more N_2O is emitted by the modified ASMG1-BSM2 than the original ASMG1-BSM2. Generally, the models differ a lot in terms of dynamic N_2O emissions under different control strategies, which suggests that observations under dynamic conditions could be exploited for model discrimination.

As in the calibration step with dynamic model evaluation, Figure 3.3b compares the DO, NO_3^- and NH_4^+ concentrations in ASU4 under the 1-DO control strategy simulated by the original ASMG1-BSM2, the modified ASMG1-BSM2 and the finalized ASM1-BSM2. Again, the three models show very similar dynamics except for NO_3^- , as discussed above.

Table 3.6 Validation of calibrated ASMG1 in BSM2 control strategies

	1-DO control strategy		2-DO control strategy		Cascade control strategy	
	Finalized ASM1-BSM2 ^a	Original ASMG1-BSM2	Finalized ASM1-BSM2 ^a	Modified ASMG1-BSM2	Finalized ASM1-BSM2 ^a	Modified ASMG1-BSM2
N₂O emission factor^b	-	0.48%	-	0.43%	-	0.67%
Effluent quality						
Av. S _{NO3} (gN/m ³)	11.05	12.01	10.40	11.69	7.85	6.30
Av. S _{NH} (gN/m ³)	0.47	0.35	0.48	0.39	1.11	1.76
Av. TN (gN/m ³)	13.53	14.17	12.89	13.90	10.94	9.82
Av. TSS (gCOD/m ³)	15.17	14.96	15.17	14.95	14.92	14.66
Av. COD (gCOD/m ³)	49.02	48.38	49.03	48.42	48.78	48.56
Av. BOD5 (gCOD/m ³)	2.79	2.82	2.79	2.83	2.74	2.87
EQI	5577	5557	5447	5517	5274	5250
OCI	9450	9467	9348	9353	8052	8043

Note: a. Results are from the BSM2 finalization paper (Nopens et al., 2010); b. N₂O emission factor is expressed as % of influent TN load emitted as N₂O-N.

Table 3.7 Comparison of average heterotrophic and autotrophic N₂O production rates and the emission rate for the two AOB models

Averaged process rate (g N/d)	Open loop		1-DO control		2-DO control		Cascade control	
	Original ASMG1-BSM2	Modified ASMG1-BSM2						
Net N₂O produced	5717	5825	5441	5609	4879	4973	7739	6919
by heterotrophs	-2763	-2159	-2086	-3661	-2070	-3575	-2521	-3469
by AOB	8480	7984	7526	9270	6949	8547	10260	10388
N₂O emission	-5639	-5753	-5435	-5605	-4874	-4969	-7631	-6812

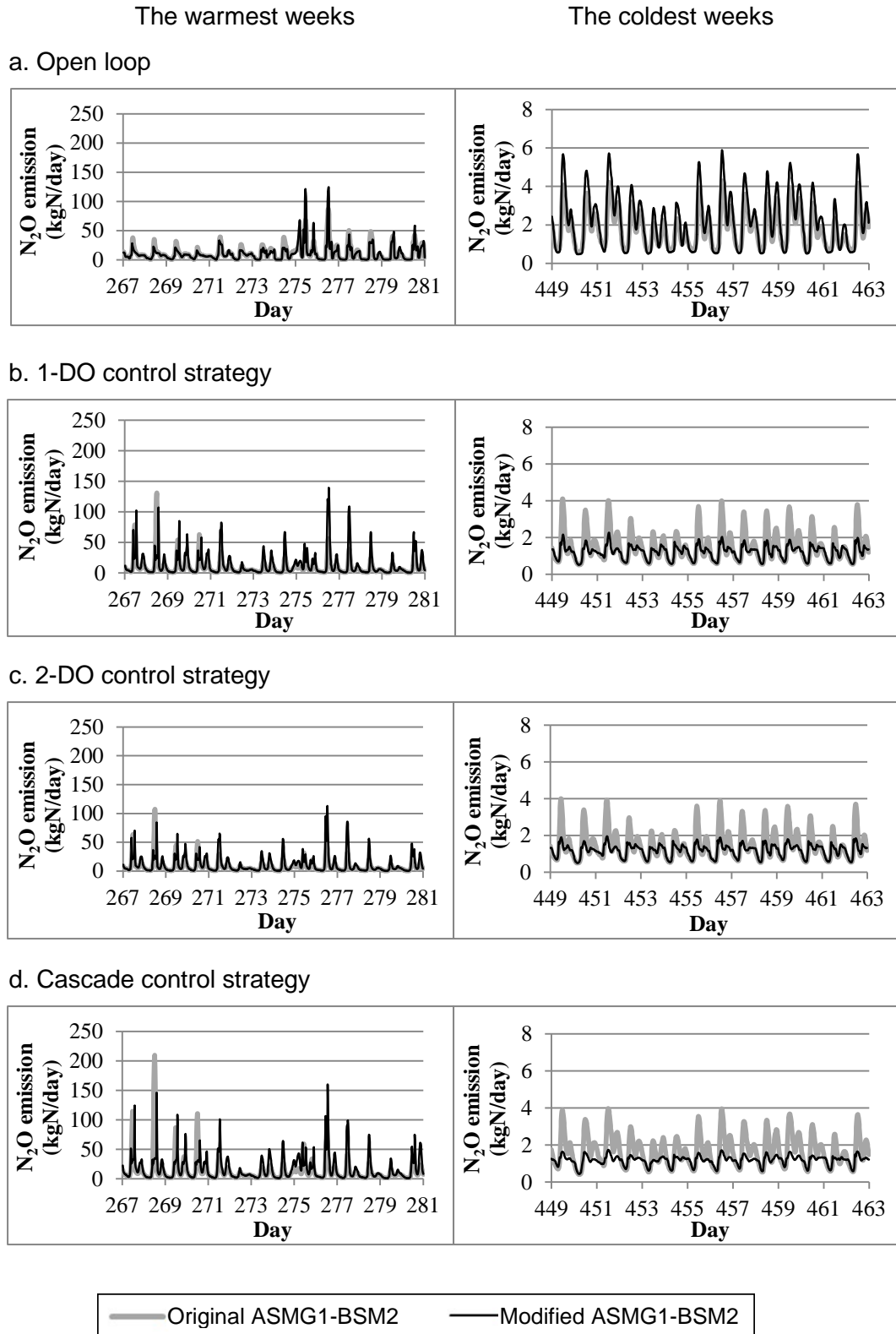


Figure 3.4 Comparison of total dynamic N_2O emissions in the two warmest (a) and the two coldest weeks (b) in open loop and under the three tested control strategies.

3.2.3 Discussion

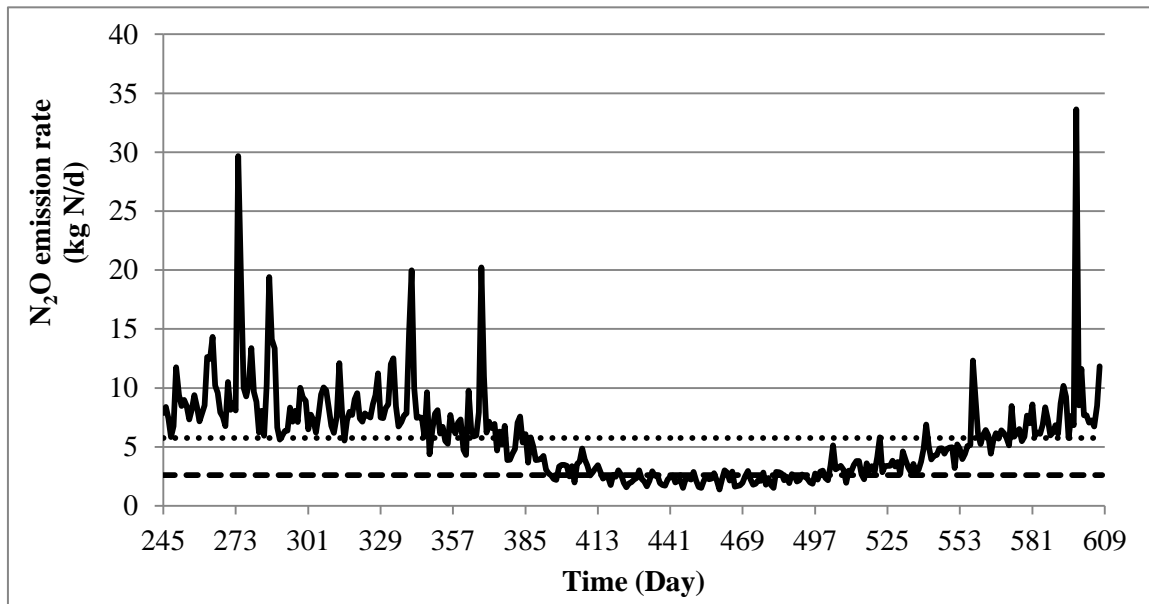
I. Calibration and validation method

The calibration and validation procedure proposed in this section was applied to fit a model using the virtual data provided by the BSM2 benchmark model, but the procedure can generally be applied to calibrate/validate full-scale plants. The particularity of the approach to calibrate/validate a new model is that it took advantage of the knowledge consolidated in a widely accepted model. Such a model is used to generate data that represent reality in such a way that it is acceptable for a new model to be calibrated/validated using these virtual data. In fact this calibration/validation concept exploits the fact that when different models are used for the same system (plant or reactor), they should give similar results. In this case these are the traditional plant performance indices, i.e. the effluent quality and the operational cost.

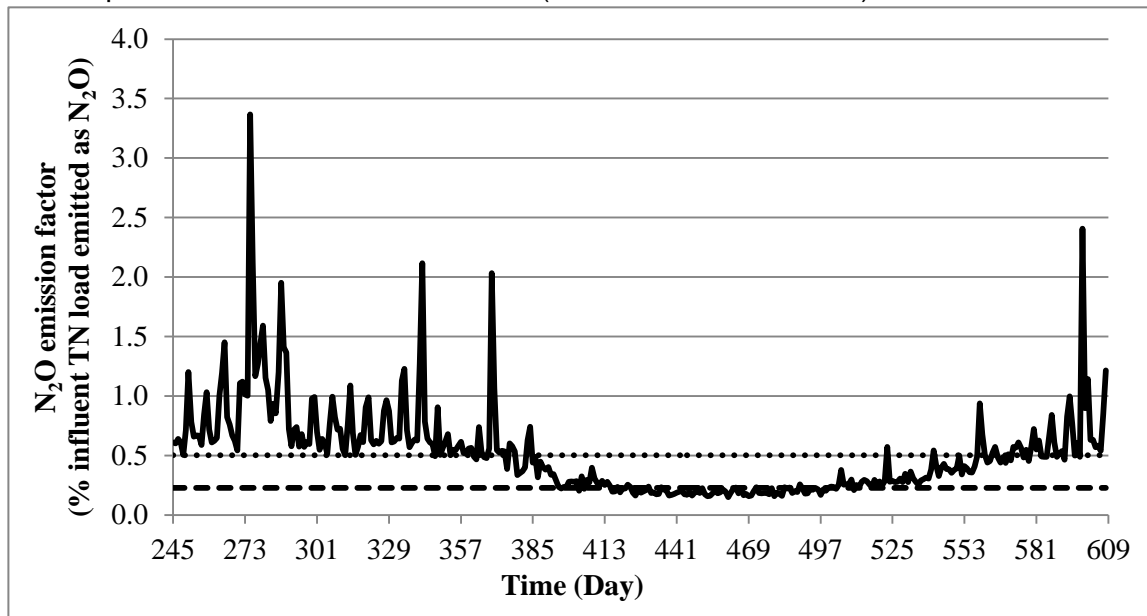
Importantly, it is believed that the proposed calibration procedure provides expert guidance on how an ASMG1 model could be calibrated for a real plant. This calibration method is applied to an actual plant in Chapter 4.

Comparing the N₂O emissions from a steady-state simulation with those for a dynamic simulation (Figure 3.5a) confirms that the steady-state N₂O emissions can be quite different from the average of N₂O emissions calculated under dynamic conditions. Dividing the emission rates with the influent TN load did not reduce the variation (Figure 3.5b). This indicated the importance of dynamic simulation rather than by steady-state simulation. In other words, the model should be run dynamically to get the proper value to compare with.

a. Comparison of N₂O emissions (modified ASMG1-BSM2)



b. Comparison of N₂O emissions factors (modified ASMG1-BSM2)



— Dynamic - - - - Steady state ····· Average of dynamic

Figure 3.5 Comparison of daily averaged N₂O emissions in open loop under steady-state simulation and dynamic simulation with the modified ASMG1-BSM2.

In this section, the averaged dynamic simulation results are used as objectives of the new model's calibration and validation. However, model calibration and validation objectives reflect the purpose of the model (Gernaey et al., 2004b). In most applications of the benchmark models, different scenarios are evaluated and compared in terms of these yearly averaged index values (Flores-Alsina et al., 2011; Nopens et al., 2010) and this was the underlying reason for the objectives adopted in this section. Moreover, Figure 3.3 demonstrates that the ASMG1 models calibrated using the yearly averaged values satisfactorily pass the comparison with the finalized ASM1-BSM2 model under dynamic conditions. However, while this holds for this case study calibration and validation under dynamic conditions may be needed in other cases, e.g. when applying the model for more detailed process optimization or peak performance (Gernaey et al., 2004b).

II. Contribution from the AOB denitrification models

The N_2O production by AOB is still under study and no model has been agreed upon yet. This section illustrates how this still unclear part of the N_2O model may affect simulation results and may therefore help directing experimental work. Comparing the calibration results under open loop in Table 3.2 and Table 3.5, once the ASMN parameters are set, the effluent quality index and operational cost index of using only the ASMN submodel can give similar results as using the whole ASMG1, but the N_2O emission factor obtained by using ASMG1 was obviously larger than by using ASMN. The results also show that compared to ASMN, adding the AOB denitrification submodel has only little influence on the average simulation values of effluent quality and OCl. This is quite different for its contribution to N_2O production.

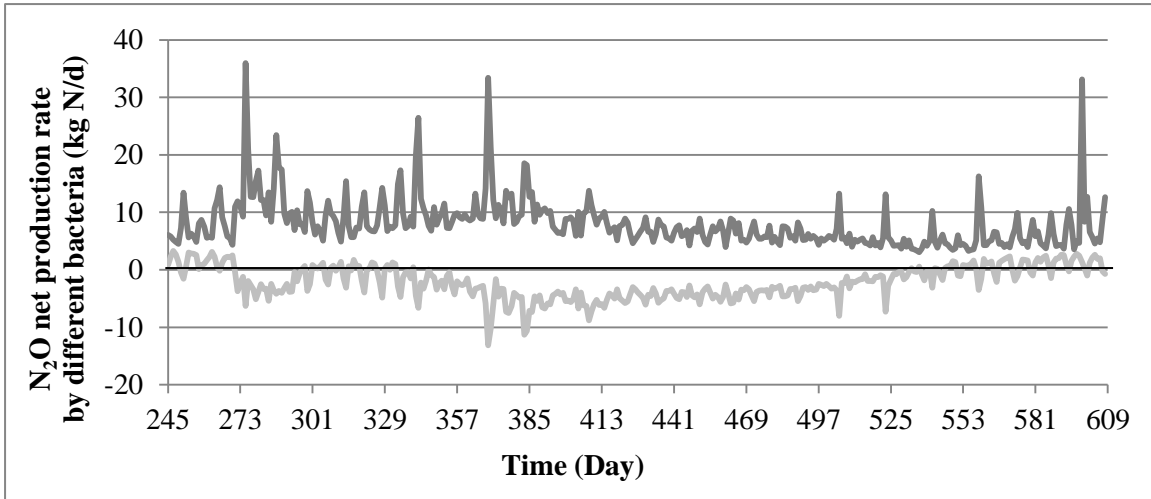
A new mathematical formulation of the Haldane kinetics term, Eq. (3.1), was proposed and used to describe the influence of DO in the modified ASMG1-BSM2. Using this kinetics model structure has two advantages: its parameters can easily be obtained from half-

saturation concentrations, and the maximum is kept at 1 as for Monod kinetics. This modified Haldane kinetics term has not been applied to the FNA, FA and NO inhibition terms in this section, since the calibration and validation objectives are already satisfied. Moreover, compared to DO whose concentration has a significant effect on the model simulation results, the FNA, FA and NO concentrations are usually low making that their inhibition terms approximate 1. However, for the future it is suggested to use this new kinetics term to also describe substrate inhibition given its two advantages compared to the original Haldane term.

III. N₂O emissions under different process conditions

The relationship between N₂O production and different process conditions has already been discussed (Lotito et al., 2012). Figure 3.4 presents the effect of temperature variation on the model's response. Although the two ASMG1 models show different dynamic patterns of N₂O emission under particular conditions (Figure 3.4), they both simulated higher N₂O emissions under warm conditions. The fact that this seasonality is what is generally observed in practice, e.g. Daelman et al. (2013a), can be considered an important independent validation of these two models. The models allowed suggesting the following explanation. Increasing temperatures increase bioreaction rates, e.g. heterotrophic denitrification rates and AOB denitrification rates. Heterotrophs reduce NO to N₂O, but more importantly, they also reduce N₂O to N₂. Since the rates of both reactions increase with temperature, the net production rate by heterotrophs, equal to the difference of the two reaction rates, does not change too much over the year (Figure 3.6a). However, AOB can only reduce NO to N₂O and are unable to further reduce N₂O to N₂. Hence, the increasing rate of AOB denitrifying NO to N₂O results in a pure increase in accumulation of N₂O in warmer conditions. As a result, the total net N₂O production rate, the sum of net production rates by heterotrophs and AOB, is higher during warm periods (Figure 3.6b).

a. Comparison of N_2O net production rate by AOB and heterotrophs (modified ASMG1-BSM2)



b. N_2O total net production rate (modified ASMG1-BSM2)

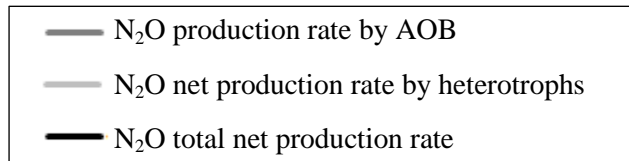
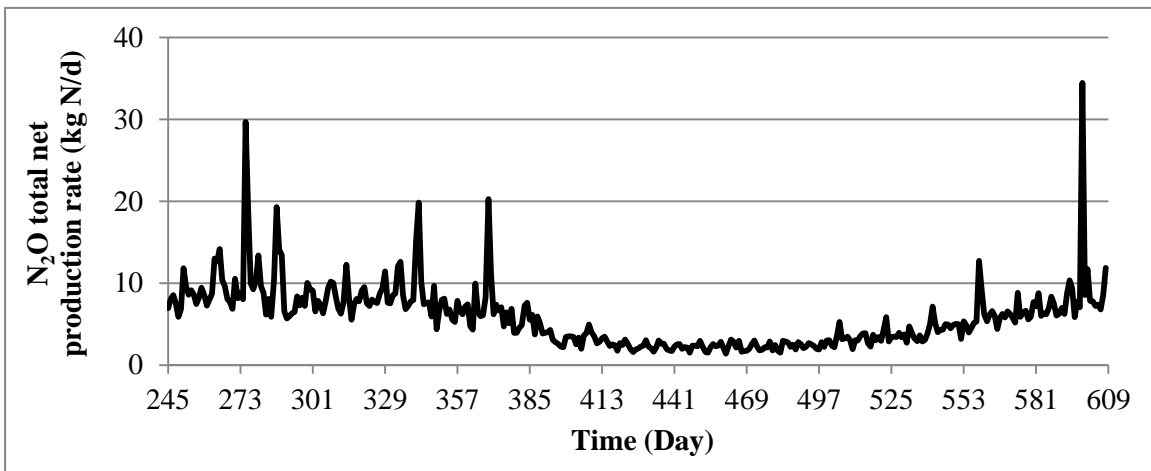


Figure 3.6 Comparison of daily averaged dynamic N_2O production rates by different bacteria groups simulated with the modified ASMG1-BSM2 in open loop.

Besides temperature dependency, the different control system scenarios discussed below exhibit different N₂O emissions. The cascade control strategy has clearly higher N₂O emissions than the other two control strategies and the open loop system. The cascade control has a tendency to decrease the DO concentrations to enhance energy saving (Flores-Alsina et al., 2011). According to the description in Section 3.2.1 “I. ASMG1 models and implementation”, this low DO level will directly stimulate AOB-produced N₂O through the Haldane term of the modified ASMG1. It may also induce a high NO₂⁻ concentration which indirectly promotes AOB-produced N₂O. Both modified and original ASMG1 models predict such behavior. The way the models describe the relationship between N₂O production and DO concentrations agrees with experimental observation (Yu et al., 2010; Lotito et al., 2012).

IV. Future N₂O measurement strategies

While the ASMG1 models do not show differences in terms of averaged measurement values, even for the different control strategies that bring the models in more extreme situations, the detailed dynamic results suggest that several short-term on-line measurements of N₂O emissions should be carried out to help discriminate the models. This conclusion has practical consequences and is in an agreement with Daelman et al. (2013a) who demonstrated the usefulness of on-line high-frequency data for studying the process. Considering financial and other limitations, measurement campaigns for N₂O emissions could be designed to be spread over several short-term campaigns, e.g. every one or two weeks, over a whole year to cover different seasons. Then, by comparing the measurement data with the simulation results, the models can be further validated or falsified.

3.3 Control of GHG emissions in BSM2

3.3.1 Methods

I. Models and control strategies

In order to find the strategies which can achieve a good balance between EQI, OCI and GHG emissions under different weather conditions, six scenarios or control strategies were studied in this section (Table 3.8). It must be noticed that the evaluation of GHG emissions follows the approach of Flores-Alsina et al. (2011), that is the N₂O emissions are calculated from the modified ASMG1 while other contributions to total net GHG emissions, like CO₂ emissions due to energy consumption, CO₂ emissions from bioreaction, are evaluated by the Bridle model.

In order to maintain the controlled variables (e.g. DO and NH₄⁺ concentrations) around the setpoints, the proportional-integral (PI) algorithm, Eq. 3.6, is used to adjust the values of the manipulated variables.

$$u_{PI} = u_0 + K_P \cdot \left(e + \frac{1}{T_I} \cdot \int e \cdot dt \right) \quad \text{Eq. (3.6)}$$

where u_{PI} is the manipulated variable calculated by the PI algorithm, e is the error between the measurement and the setpoint of the controlled variable, and u_0 , K_P and T_I are the coefficients of the PI controller. Moreover, for some PI controllers, there are limits for the manipulated variable. When $u_{PI} < u_{Min}$, the final value of the manipulated variable, u , is u_{Min} ; when $u_{PI} > u_{Max}$, $u = u_{Max}$.

The parameters of the PI controllers are given in Table 3.9. The bioreaction model used in this section is the modified ASMG1-BSM2 after calibration.

The open-loop Scenario 1 is different from the one used in the BSM2 calibration, Section 3.2. The bypasses were removed in Scenario 1, in order to better compare the plant performance when the wet weather control strategies were added. The NH_4^+ -DO control strategy adds a minimal DO concentration requirement for the first aerobic tank ASU3, Figure 3.7. As mentioned in Section 3.2, the purpose of the cascade control is to limit the NH_4^+ violation with minimal aeration energy consumption. Hence, in some cases when the effluent NH_4^+ concentration is low, the controller will allow the DO to drop to low values. The resulting low DO concentrations can result in high NO_2^- concentrations and then promote the N_2O production by AOB. In order to make the N_2O production not substantially exceed the ones obtained by other control strategies, the DO of ASU3 is kept above 1 mg/l in the cascade control. In other words, the DO controller of ASU3 receives two signals for $k_{\text{La}3}$: one being a ratio to the $k_{\text{La}5}$ and the other imposing a minimal DO concentration. The controller picks the larger value for $k_{\text{La}3}$. A separate DO control strategy was tested. It controls the DO concentration of each aerobic ASU individually. A 3 DO control strategy was also studied by Vanrolleghem and Gillot (2002) inspired by the constant aeration intensity of BSM1 causing insufficient DO in the aerobic tanks at daytime and excessive DO at night. This simple 3 DO strategy proved to give acceptable performance in terms of effluent quality, energy cost and investment cost in the case of BSM1 (Vanrolleghem and Gillot, 2002). In this section, this strategy is proposed and studied with particular consideration on N_2O and GHG emissions. A NH_4^+ -DO cascade control strategy in which the NH_4^+ controller sets the DO setpoint has the advantage of limiting NH_4^+ violations whereas controlling the spatial DO distribution is meaningful for the N_2O production. Consequently, a combination strategy, i.e. Scenario 2, was studied, as presented in Figure 3.8.

Table 3.8 Control strategies tested in the thesis

Scenario #	Description	Controlling parameters ^a		
Scenario 1	Open loop	$k_{La3}=1.5 \cdot k_{La4}=3 \cdot k_{La5}=180 \text{ d}^{-1}$		
Scenario 2	Cascade	$\text{NH}_4^+_{\text{SP5}}=1.0 \text{ mg/l}$ $\text{DO}_{\text{Min}3}=1.0 \text{ mg/l}$	$\text{DO}_{\text{SP5}}=\text{NH}_4^+_{\text{u5}}$ $k_{La3}=1.5 \cdot k_{La4}=3 \cdot k_{La5}$	
Scenario 3	Separate DO	$\text{DO}_{\text{SP3}} = 2$	$\text{DO}_{\text{SP4}} = 2$	$\text{DO}_{\text{SP5}} = 1$
Scenario 4	Cascade + 1 DO	$\text{DO}_{\text{SP3}} = 2$ $\text{DO}_{\text{SP5}}=\text{NH}_4^+_{\text{u5}}$	$\text{NH}_4^+_{\text{SP5}} = 1.5$ $k_{La4}=2 \cdot k_{La5}$	
Scenario 5	Step feeding + Scenario 4	$\text{DO}_{\text{SP3}} = 2$ $k_{La4}=2 \cdot k_{La5}$ $Q_T = 60000$	$\text{NH}_4^+_{\text{SP5}} = 1.5$ $f3=f4=f5=1/3$	
Scenario 6	Sludge recycling + Scenario 4	$\text{DO}_{\text{SP3}} = 2$ $k_{La4}=2 \cdot k_{La5}$	$\text{NH}_4^+_{\text{SP5}} = 1.5$ $r_{\text{under}} = 0.5$	

Note: a. DO_{SP3} , DO_{SP4} and DO_{SP5} are the DO set points (mg/l) of ASU3-ASU5 respectively; $\text{NH}_4^+_{\text{SP5}}$ is the NH_4^+ concentration setpoint (mg/l) of ASU5; $\text{NH}_4^+_{\text{u5}}$ is the controller output (mg/l) of the NH_4^+ controller in ASU5; k_{La4} and k_{La5} are the oxygen transfer coefficients (d^{-1}) of ASU4 and ASU5 respectively; $f3$, $f4$ and $f5$ are the setpoints for the inflow distribution fractions to ASU3-ASU5; Q_T (m^3/d) is the threshold of the plant inflow at which step feeding begins; r_{under} is the ratio of the settler underflow rate to the inflow rate of the secondary settler.

Table 3.9 Parameters of the PI controllers

Controlled variable	Applied in ASU # of Scenario #	u_0^a	K_P^b	T_I^c	u_{Max}^d	u_{Min}^d
NH_4^+	ASU5 of Scenario 2, 4-6	0.1	-10	1	N/A	N/A
	ASU5 of Scenario 2, 4-6	60	1000	500	300	0
DO	ASU1-3 of Scenario 3; ASU3 of Scenario 2, 4-6	135	400	0.1	300	0

Note: a. unit of u_0 , K_P and T_I is $\text{mg O}_2/\text{l}$ for NH_4^+ controller and is d^{-1} for DO controller; b. unit of K_P is $\frac{\text{mg O}_2/\text{l}}{\text{mg NH}_4^+-\text{N/l}}$ for NH_4^+ controller and is $\frac{\text{d}^{-1}}{\text{mg NH}_4^+-\text{N/l}}$ for DO controller; c. unit of T_I is d^{-1} for both NH_4^+ controller and DO controller; d. u_{Max} and u_{Min} is the name as u_0 .

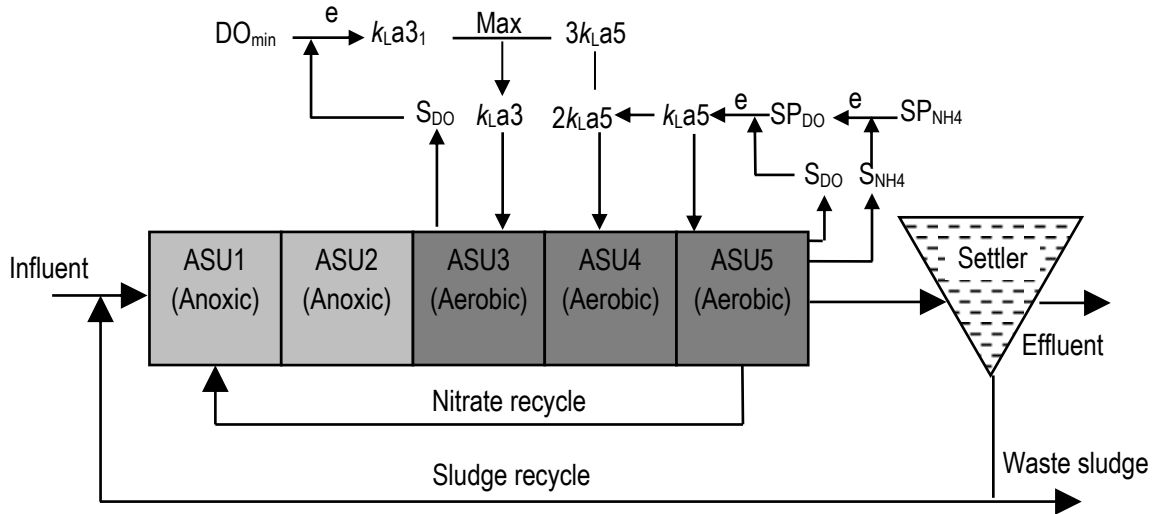


Figure 3.7 NH_4^+ -DO cascade with minimal DO requirement strategy. S_{DO} (mg/l) is the measured DO concentration; S_{NH_4} (mg/l) is the measured NH_4^+ concentration; DO_{min} (mg/l) is the minimal DO requirement; SP_{NH_4} (mg/l) is the NH_4^+ setpoint; e (mg/l) is the error between measured value and setpoint; $k_{\text{La}3_1}$ is the oxygen transfer coefficient based on minimal DO requirement; Max means to take the larger value between $k_{\text{La}3_1}$ and $3k_{\text{La}5}$ as the final $k_{\text{La}3}$.

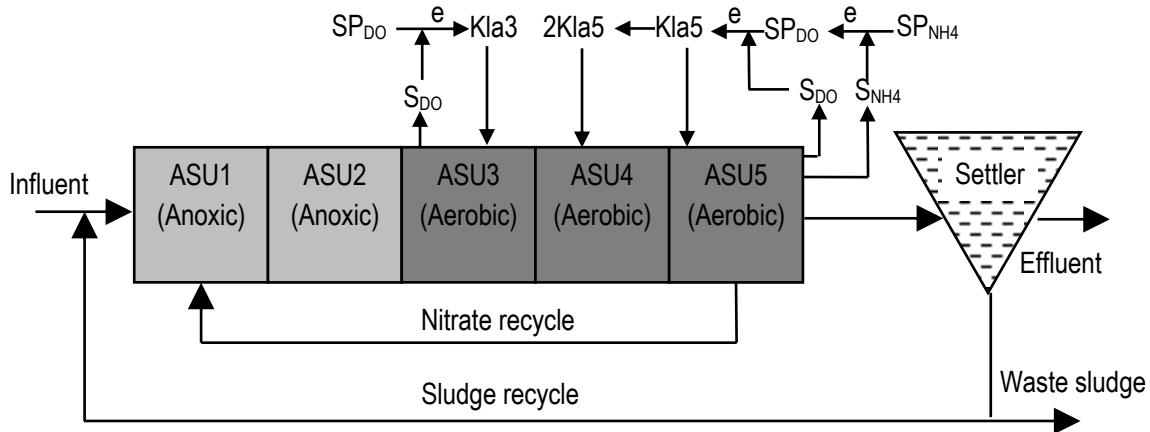


Figure 3.8 NH_4^+ -DO cascade plus 1 DO controller strategy. SP_{NH_4} (mg/l) is the NH_4^+ setpoint; other denotations have the same meaning as in Figure 3.7.

To deal with hydraulic shocks two control strategies were tested, a step feeding strategy and a sludge recycling control strategy. The step feeding strategy equally distributes the influent over the three aerobic tanks. The sludge recycling strategy uses a ratio controller,

i.e. the underflow rate of the secondary settler is proportional to its inflow rate. Olsson and Stephenson (1985) made it clear that it is much better to use the inflow to the settler as input to the controller than the influent flow rate of the WWTP. This is because of the hydraulic propagation that leads to a time delay between flow rate increases in the influent and the increase in the inflow to the settler. If this delay is not considered properly this may disturb the settler hydraulics. Even though the BSM2 model does not describe such hydraulic propagation, it was decided for didactical reasons that the sludge recycling controller uses the inflow rate of the secondary settler and multiplies it with a ratio to calculate the sludge recycling flow rate. The two rain event control strategies were combined with the Scenario 2 controller. All scenarios were evaluated in terms of GHG emissions, effluent quality and operational cost, with the same criteria as in Section 3.2.

II. New influent file

In order to further study the effect of rain events on plant performance, a new 609-day input file was generated using the influent disturbance scenario generator of Gernaey et al. (2011). This generator is a phenomenological model that represents the main characteristics of a catchment area (rainfall, household and industry discharges, soil infiltration, sewer network, etc.) to describe the typical dynamic characteristics observed in a full scale WWTP influent such as: diurnal phenomena, weekend effect, seasonal phenomena (e.g. increased infiltration in the wet season compared to the dry season), holiday periods, and rain events. The output is the influent flow rate and temperature profile and the pollutant concentrations in terms of the ASM1, ASM2d or ASM3 state variables.

In view of the effect that climate change might have on the intensity and frequency of rain events (Giorgi et al., 2001; Hulme et al., 2002; Solomon et al., 2007) a new influent profile

was generated by modifying the parameters in the rainfall generator (Gernaey et al., 2011). The generation of the rain intensity in the influent generator depends on 2 parameters: the constant converting the output of the random number generator to a value representing rainfall intensities, *LLrain*, and flow rate per mm rain, *Qpermm*. A sensitivity analysis of the model (Flores-Alsina et al., 2012) showed that *LLrain* is related to the number of rain events and a lower value corresponds to more rain events, and *Qpermm* is related to the intensity of the rains where a larger value results in a higher intensity. In order to generate an influent file with more rain events and higher rain intensity, *LLrain* was set at 3.4 mm/d and *Qpermm* at 1600 m³/mm. The influent generator also considers the effect of the sewer system and includes a simple model to describe the first flush effect (Gernaey et al., 2011).

Although the number of rain events did not increase significantly (324 against 318), the new rain profile exhibits higher intensity rain events (maximum intensity of 85687 m³/day against 78800 m³/day of the original file), indicating that in the future there will be more intense storm events. Overall, a total rainfall increment of 16% was considered (from 1.43×10⁶ to 1.67×10⁶ m³). However, the effect on the final flow rate entering the WWTP is not so important since the contribution from the household and industries (around 60 % of the flow) was not modified. The influent quality does not change too much either since the same influent composition was used. The Influent Quality Index (IQI) for the last 364 days is 74785 pollution units/d for the current influent file compared to 75301 pollutions units/d for the adapted influent file.

3.3.2 Results and discussion

Figures 3.9 and 3.10 compare the performance of the different control strategies for 8 criteria using the current influent file and the future influent file respectively.

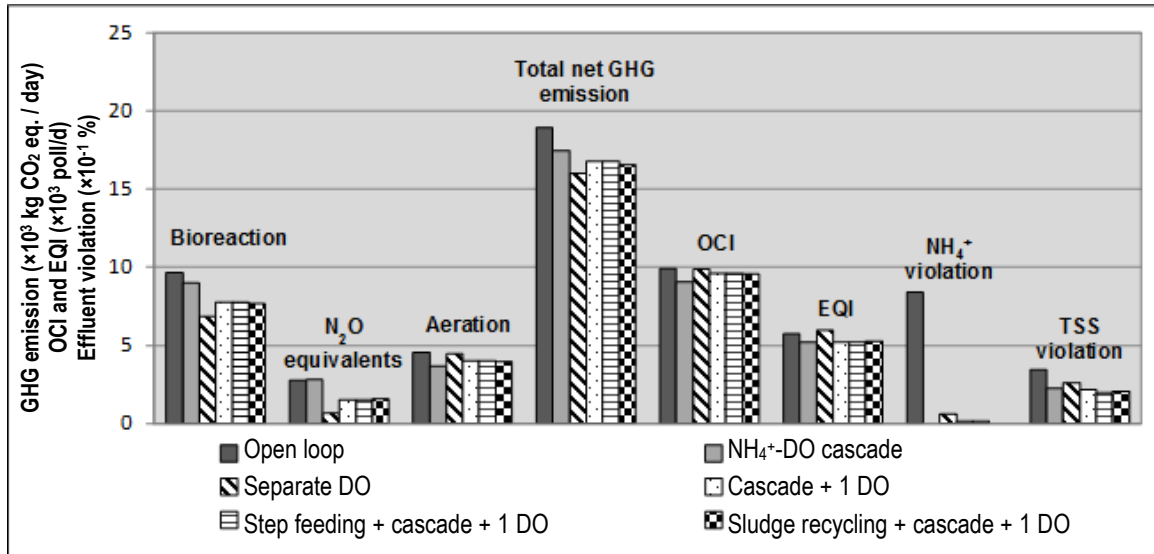


Figure 3.9 Comparison of different control strategies using the current influent file. OCI: Operation Cost Index; EQI: Effluent Quality Index. First 4 criteria relate to GHG; next 4 to traditional BSM2 criteria.

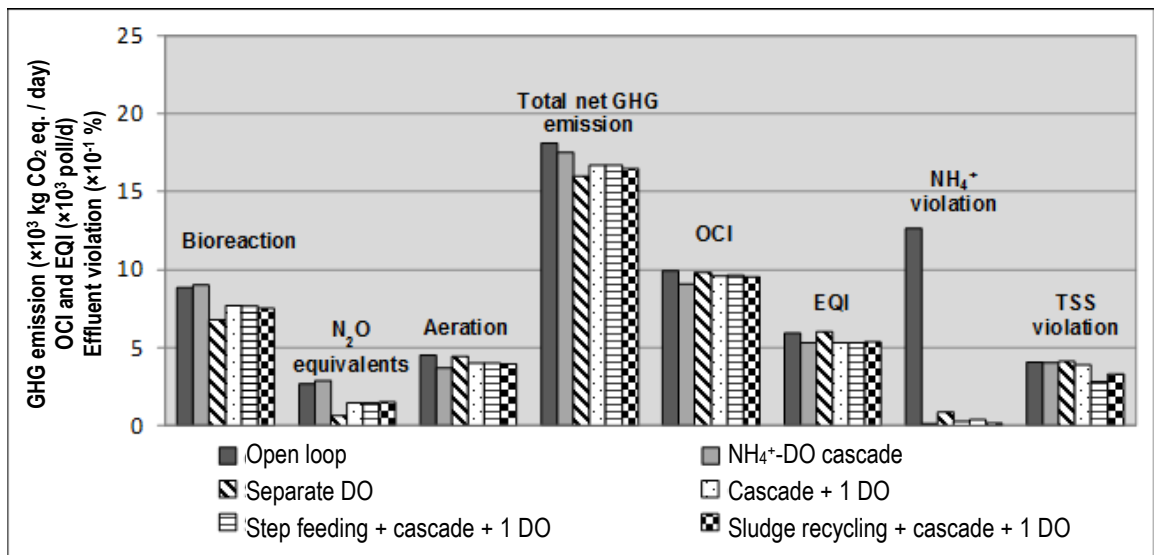


Figure 3.10 Comparison of different control strategies using the future influent file.

I. Current conditions

When comparing the different controllers under current climate conditions, the open loop generally has the largest or the second largest value in all evaluation criteria compared to those of the control strategies (Figure 3.9). Especially, the NH_4^+ violation in open loop is much higher than the values for the control strategies. It means that using control strategies can improve plant performance in at least one aspect of EQI, OCI and GHG emissions.

The separate DO control shows the largest reduction in N_2O emissions, which is 76.2% compared to the open loop. However, all the scenarios, including the open-loop scenario and the control strategies, do not show a big difference in the total net GHG emission, because in the total net GHG emission the GHG emission from the biodegradation of the wastewater takes the largest proportion and this does not change significantly among all scenarios. However, it must be noticed that according to the IPCC (2006), the bioreaction- CO_2 belongs to biogenic CO_2 and it is to be excluded from the evaluation. The lowest total net GHG emission is still observed for the separate DO control strategy, which is 15.3% compared to the open loop. The cascade strategy does not reduce N_2O as much as the separate DO strategy, but it showed no NH_4^+ violation and a low EQI combined with low aeration energy consumption and low OCI. Compared to the open loop, the EQI and the OCI are reduced by 8.8% and 9.4% respectively under cascade control. Although the separate DO control strategy also reduced NH_4^+ violations a lot compared to the open loop, the value is still larger than the cascade control, and it comes as well with higher OCI and EQI. Compared to the open loop, the decrease of OCI is almost negligible (0.8%) under separate DO control and the EQI is even increased slightly by 3.0%. Actually the cascade control focuses on limiting the NH_4^+ effluent violation with low aeration energy consumption. Therefore, it tends to set a low DO setpoint which may lead to more N_2O

production by AOB denitrification. On the other hand, although the 3 DO control strategy proved to have good performance on making balance among different criteria in terms of energy cost, effluent quality and investment cost (Vanrolleghem and Gillot, 2002), the original motivation for designing the separate DO control strategy was not focused only on effluent quality, but e.g. either aiming at N₂O control as in the current paper or optimizing aeration as in Vanrolleghem and Gillot (2002). Therefore, such a kind of control strategy is not reliable for effluent quality control, i.e. the effluent quality is unpredictable when only focusing on DO control. Actually, the separate DO strategy presented the highest NH₄⁺ violations among all control strategies, i.e. 0.06% under current conditions, and this violation was further increased to 0.09% under future conditions, although such violations are also quite small compared to the values in open loop. Therefore, in order to optimize for objectives on both N₂O emission reduction and NH₄⁺ violation control, the cascade plus 1 DO control strategy was proposed. Figure 3.9 shows that this strategy reduces N₂O emission by 44.1% compared to the open loop. This N₂O emission amount is lower than that under cascade control. Meanwhile, the cascade plus 1 DO control strategy has lower NH₄⁺ violation, which is a negligible violation, and lower EQI and OCI than the separate DO control. It suggests that this coupled strategy makes a balance between N₂O mitigation and effluent quality control.

With these promising results, the step feeding and the sludge recycling control were added to the cascade plus 1 DO control strategy. The two strategies present very similar performance. The sludge recycling control emitted slightly less GHG (16.5×10^3 kg CO₂ eq./day against 16.7 kg CO₂ eq./day), but its violation total suspended solids (TSS) is a little higher (0.21% against 0.19%). Such differences are negligible under current conditions, but the differences on effluent violations are amplified a little under future

conditions, i.e. 0.33% with sludge recycling control against 0.28% with step feeding for TSS violations.

II. Future conditions

Figure 3.10 clearly shows that although the rain events are predicted to increase by 16%, not too much difference is found in the evaluation results, probably because of their similar IQI values. However, some differences are still present in the NH_4^+ and TSS violations. One thing that must be kept in mind though is that in BSM2 the primary settler is simulated by the Otterpohl-Freund model (Otterpohl and Freund, 1992; Otterpohl et al., 1994), the secondary settler is modelled by a Takács 10-layer model (Takács et al., 1991) and the sludge thickener is described by point settler model. It is generally accepted that such kind of state-of-the-art models is not really applicable to describe settlers under storm conditions and further development is required in terms of better simulating the effluent solids concentration and modelling the continuous sedimentation (Plósz et al., 2007; Plósz et al., 2009; Bürger et al., 2011).

Based on the studies in this thesis, it is shown in Figure 3.10 that without any control strategy, i.e. in open loop, the effluent NH_4^+ exceeds the effluent limits more under future climate conditions, while the N_2O and GHG emissions remain essentially the same. All strategies still have good performance on limiting the NH_4^+ violation but the effluent TSS is better controlled by the step feeding strategy and the sludge recycling control strategy. The step feeding shows the smallest TSS violation, reducing the TSS violation by 30.3% compared to that of open loop, and the sludge recycling control reduced the TSS violation by 19.0%. The results tell that these extended strategies handle the hydraulic shocks well and maintain a good balance between the N_2O emissions and the effluent quality.

3.4 Conclusion

- A modified Haldane term was proposed to describe the DO effect on N_2O production by AOB. It reflects that the N_2O production by AOB first increases and then decreases with increasing DO concentrations. The parameters of this modified Haldane term can be calculated from DO half-saturation concentrations, which is an important improvement compared to the original Haldane formulation.
- The ASMG1 models were calibrated and validated using the framework of BSM2 by comparing the plant effluent quality and operating costs simulated by ASMG1 with the values simulated by the finalized ASM1-BSM2 model (Nopens et al., 2010), together with a consideration of reasonable N_2O emission factors (0.5% of the influent TN-load). The calibration procedure for the calibration of ASMG1-BSM2 is also applicable to real plants, e.g., the Eindhoven plant in Chapter 4.
- The two ASMG1 models showed little difference for the average values, but the big difference of N_2O dynamic emissions using different control strategies under cold weather conditions suggested that the models can be discriminated by carrying out more experimental studies in dynamic conditions, asking for high-frequency N_2O data collection, and under different weather conditions.
- The N_2O emissions exhibited a relationship with the weather conditions and the operating conditions. N_2O emissions are higher in summer than in winter. This result was shown to be related to the temperature dependency of bacterial activity. The accumulation of N_2O in summer is mainly due to the increased AOB pathway activity, while the net N_2O production by heterotrophs does not change too much all year round. The tested NH_4^+ -based cascade control has a disadvantage in terms of N_2O emissions, although it has an advantage in terms of limiting the NH_4^+ violations. On the other hand, spatially distributing the DO concentrations in the aerated zone,

especially increasing the DO concentration at the entrance of the aerated zone, e.g. ASU3 in BSM2, will significantly reduce N_2O emissions, but it does not aim to limit NH_4^+ violation.

- Combining two simple strategies usually can improve the balance between the advantages of the two individual strategies. For instance, the cascade plus 1 DO strategy can appropriately limit the NH_4^+ violation and the N_2O emissions.
- The strategies which extend the cascade plus 1 DO strategy with two wet weather control strategies, i.e. step feeding and sludge recycling control, allowed for good reduction in terms of TSS violations under future climate change affected conditions which may include more intense wet weather conditions. Again, these combined strategies inherited the advantages of the cascade plus 1 DO strategy.

4 Measuring and modelling N₂O emissions from a real WWTP

4.1 Introduction

In this chapter, N₂O emissions were studied on a real full-scale WWTP, i.e. the Eindhoven WWTP (The Netherlands). A one-month comprehensive measurement campaign was carried out at the plant to measure the dynamic N₂O gaseous emission from the aeration zone of the bioreactor (Section 4.2). A detailed analysis was performed on these measurement data to investigate the relationship between the N₂O emissions and the aeration flow rate and DO, NH₄⁺ and NO₃⁻ concentrations. Specifically, knowledge was expanded regarding the DO effect on N₂O production by AOB. Furthermore, considering that in the future there may be more extreme rain events caused by climate change (Giorgi et al., 2001; Hulme et al., 2002; Solomon et al., 2007), this measurement study also focused on the N₂O emissions under wet weather conditions.

In Section 4.3, an ASM model was built to simulate the N₂O emission from this biological N and P removal plant. The model was developed on the basis of ASM2d and was named activated sludge model for GHG No. 2d (ASMG2d). This model was calibrated using the data collected during the one-month measurement campaign carried out at the Eindhoven WWTP. Model simulations allow for a better understanding of the complex interactions of processes contributing to N₂O emissions compared to a pure measurement data analysis.

Section 4.2 is based on the papers “Guo L., Lamaire-Chad C., Bellandi G., Daelman M., Amerlinck Y., Maere T., Nous J., Flameling T., Weijers S., van Loosdrecht M.C.M., Volcke E.I.P., Nopens I. and Vanrolleghem P.A. (2014) Full-scale field measurement of nitrous oxide (N₂O) gas emissions and its relationship with other nitrogen species under dry and wet weather conditions. Submitted.” and “Guo L. and Vanrolleghem P.A. (2014) Interaction

of weather conditions and ammonia-based feedforward and feedback control strategies on N₂O emissions at full-scale wastewater treatment plants. In preparation.”. Section 4.3 is redrafted from the paper “Guo L. and Vanrolleghem P.A. (2013) Full-scale simulation of N₂O emissions with ASMG2d and elucidation of its different production and emission sources in nitrogen (N) and phosphorus (P) removal systems. Submitted.”

4.2 Measuring N₂O emissions from a real WWTP

4.2.1 Materials and methods

I. Plant operation and control strategy

The 750,000 PE WWTP of Eindhoven (The Netherlands) receives wastewater from a catchment whose surface area is about 600 km² and covers 10 municipalities. The data of rain gauges distributed over the catchment include the gauges installed by the Waterschap De Dommel (WDD rain gauges), the municipality of Eindhoven (NM rain gauges) and the Royal Netherlands Meteorological Institute (KNMI rain gauges).

The Eindhoven WWTP has three parallel treatment lines. Each line has one primary settler, one bioreactor and four secondary settlers. Using the University Cape Town (UCT) process, each bioreactor consists of an inner ring serving as a plug flow anaerobic tank, a carousel type middle ring as anoxic tank and a carousel type outer ring as aerobic/anoxic tank (Figure 4.1). Aeration is provided by a main continuously active, but air flow rate controllable, “summer package”, and by a backup “winter package”. Both summer and winter packages are equipped with plate aerators to generate fine bubbles. The aeration intensity at the summer aeration package is controlled by proportional-integral-derivative (PID) controllers while the winter aeration package uses an on-off controller.

A NH_4^+ -DO cascade control system is applied to manipulate the aeration flow rate of the summer aeration package (Figure 4.1a). Both NH_4^+ and DO sensors are installed near the outlet of the bioreactor. Once the NH_4^+ sensor detects that the NH_4^+ concentration is higher than the setpoint of 1 mg N/l, the DO setpoint is increased and the PID controller takes care of increasing the air flow rate of the summer aeration package in order to provide more DO for NH_4^+ oxidation. The purpose of the NH_4^+ -DO cascade control is to maintain the effluent NH_4^+ concentration below the limit at minimum consumption of aeration energy. In addition to this NH_4^+ -DO cascade feedback control, there is a feedforward control of the aeration based on the plant inflow rate. This controller is utilized to adjust the aeration flow rate under hydraulic shocks, i.e. wet weather conditions. When the plant inflow rate exceeds $26.4 \times 10^4 \text{ m}^3/\text{day}$ for 10 minutes, the DO setpoint of the summer aeration package, instead of depending on the NH_4^+ concentration, is adjusted to 3.5 mg O_2/l . When the plant inflow rate decreases to be below $20.4 \times 10^4 \text{ m}^3/\text{day}$ for a certain period, the feedforward control stops acting and the NH_4^+ -DO cascade control again takes over the aeration. However, the maximum time of feedforward control is 4 hours, i.e. after 4 hours the feedforward control is switched to the NH_4^+ -DO cascade control even if the inflow rate has not dropped below $20.4 \times 10^4 \text{ m}^3/\text{day}$. Note that (1) the duration of the high inflow rate ($26.4 \times 10^4 \text{ m}^3/\text{day}$) required to switch on the feedforward control, (2) the DO setpoint under feedforward control and (3) the maximum time of the feedforward control, are all adjustable in the SCADA system.

Next to overruling the summer package cascade controller, the inflow-based feedforward control also activates the winter aeration package. Note that the winter aeration package is also manipulated when a certain time of maximal aeration in the summer package is exceeded. During this particular measurement campaign, the winter package was activated to its maximum capacity which is about $10 \times 10^4 \text{ Nm}^3/\text{day}$ when the summer

package was operated at its maximum capacity for 5 min. When the summer package is operated at a capacity lower than 60% for 2 min, the winter package will again be turned off.

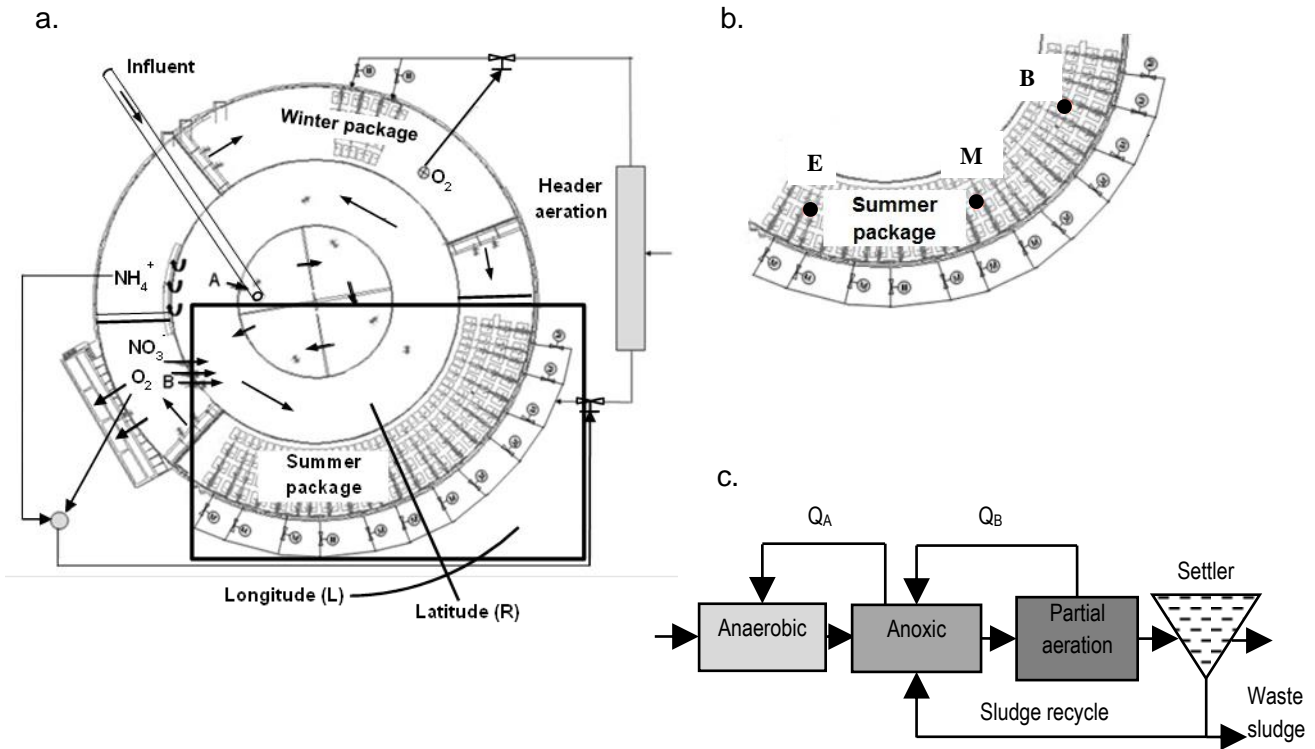


Figure 4.1 Bird view of bioreactor (a), location of N_2O sampling points (B: beginning, M: middle, E: end) (b) and scheme of UCT process (c).

II. On-line measurements

Three sampling points for N_2O gaseous measurements were distributed longitudinally, respectively at the beginning, middle and end of the summer package aeration zone in the bioreactor of the second treatment line (Figure 4.1b). Each sampling point was monitored for about 1 week. Off-gas was collected by a floating hood and was conducted to the on-line N_2O measurement equipment (Emerson), which measured the volume percentage of N_2O in the total emitted gas (ppm) at a measurement interval of 1 minute by a X-STREAM enhanced general purpose process gas analyzer (XEGP).

The air temperature was generally between 10-30 °C during the measurement campaign except for the sampling week for the middle section when the daytime maximum air temperature was above 35 °C. This elevated air temperature caused the on-line N₂O measurement equipment (Emerson) to stop sampling and led to a gap in the results for the middle section. Therefore, before using the recorded data in the analysis, the log file of the equipment was rigorously checked to delete those data from the dataset.

The water temperature was stable during dry weather days, around 20-21 °C. According to the temperature dependency of the biomass growth rate equations (Ratkowsky et al., 1983), the maximum specific growth rate is 6.25-6.56 d⁻¹ for heterotrophs, 0.78-0.82 d⁻¹ for AOB and 0.79-0.81 d⁻¹ for NOB. Therefore, not too much influence of temperature on kinetic rates should be expected during the dry weather days. However, the water temperature dropped from 20.8 °C to 18.7 °C around 9:30 am on August 26th, which was a rainy day. Such a decrease of water temperature may have an effect on kinetic rates.

The plant is equipped with several sensors for process monitoring and control. The influent concentration of total and soluble COD (COD_t and COD_s) was measured by a spectrophotometric sensor (S::CAN, Austria), and the influent NH₄⁺ concentration was monitored with an Anasense sensor (Hach Lange, Germany) (Cierkens et al., 2012). Sensors for DO, NH₄⁺, NO₃⁻ and TSS were also installed at the outlet of the bioreactor, close to the N₂O sampling point at the end of the summer package (Figure 4.1a). The aeration flow rate data were used to support the process calculations and discussions regarding the N₂O emissions.

The measured volume percentage of N₂O emission (ppm) was converted to N₂O emission rate (kg N₂O-N/d) using the aeration flow rate. Figures 4.2-4.4 illustrate the N₂O emission rate (kg N₂O-N/d) and provide a comparison with different process variables. The N₂O emission factor was calculated by expressing the N₂O emission rate as a fraction of

influent TKN load with consideration of the delay time taken for the wastewater to flow from the plant inlet to the summer package. The detailed calculation of N₂O emission rates and N₂O emission factors are given in Appendix A.

III. Off-line measurement

In order to provide for a more comprehensive mapping of N components, the NO₂⁻ concentration was measured off-line in the lab. Mixed liquor was sampled near the end of the summer package and under 3 dry-weather days and 2 rainy days during the whole measurement campaign. For each sampling day, the sampling lasted from the morning around 8:30 till the evening around 18:30 with a sampling interval of 1 hour. Analyses of NO₂⁻ concentration were done by using Hack kits.

IV. Rain events

The whole measurement campaign included rain events at midnight of August 16th and on August 25th-26th. However, no N₂O emission data can be used in the analysis of the rain event on August 16th due to an equipment failure that night. Fortunately, rain events on August 25th-26th provided information on N₂O emissions under wet weather conditions.

The rain gauges distributed over the catchment of the Eindhoven WWTP show that the precipitation on the 25th was around 2mm and was more than 10mm on the 26th. These precipitation values were not quite big, but had contributed a significant increase to the plant inflow rate, see Section 4.2.3.

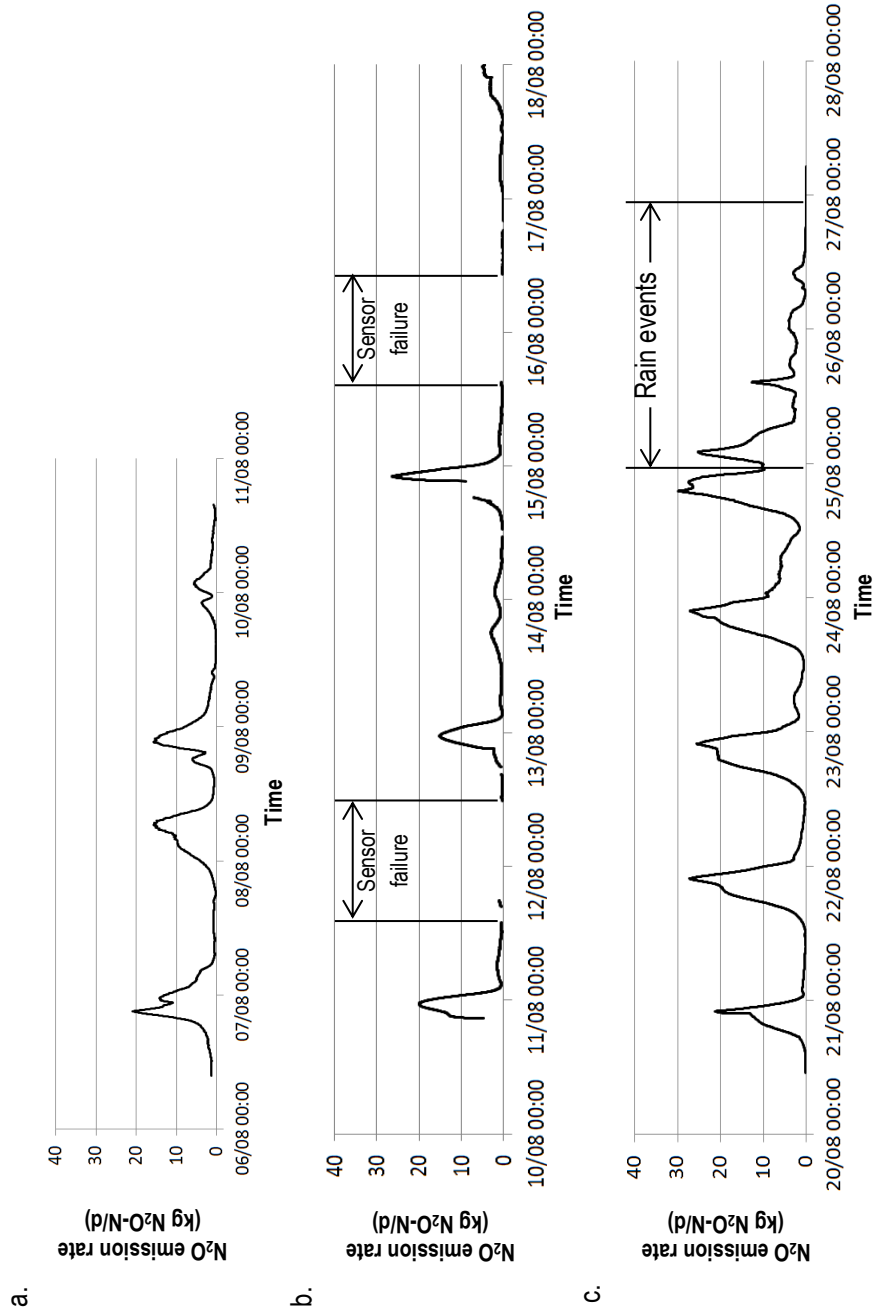


Figure 4.2 Temporal variation of N₂O emission rate at the beginning (a), the middle (b) and the end section (c) of the summer package.

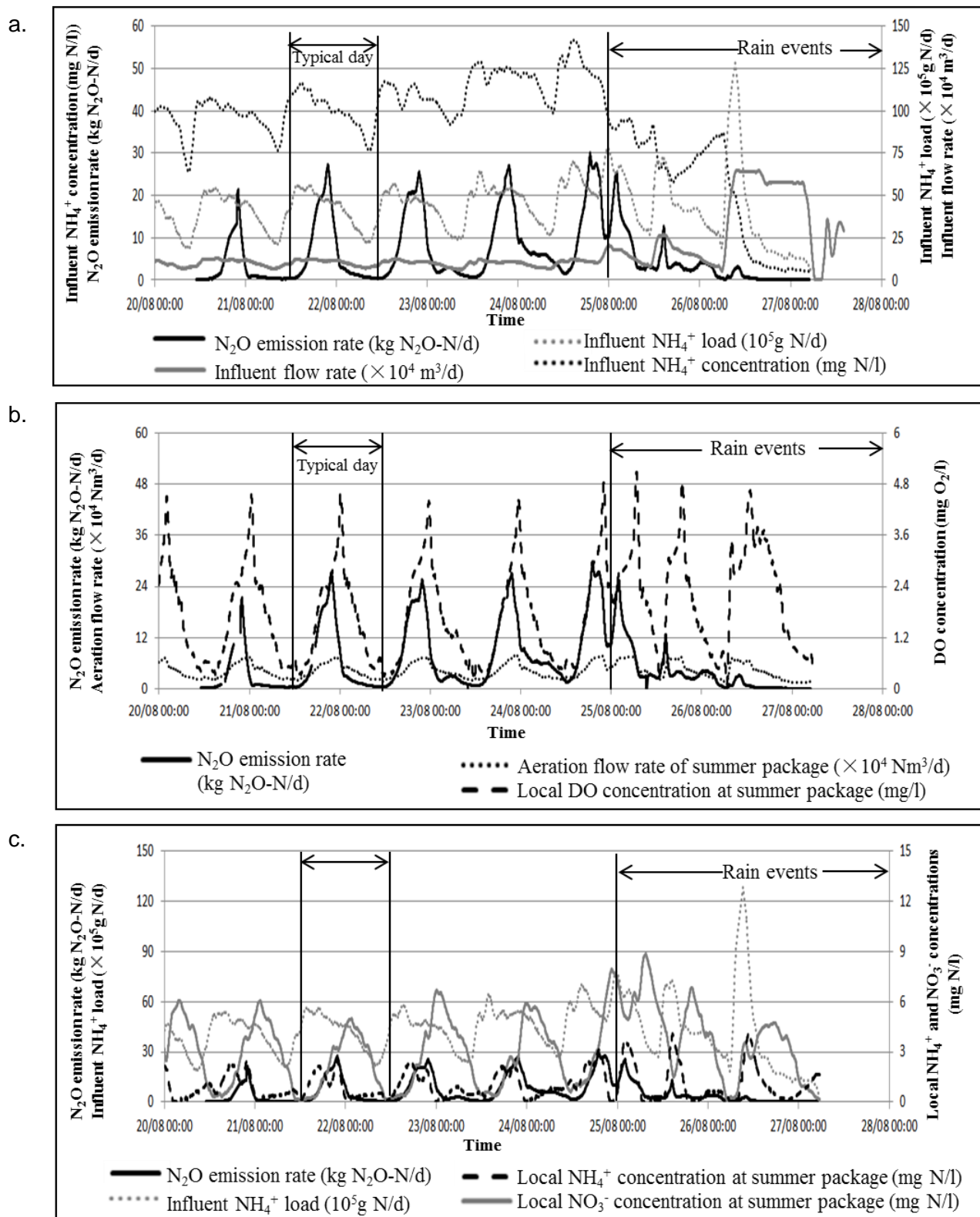


Figure 4.3 Comparison of N_2O emission rates at the end section of the summer package with influent flow rate and influent NH_4^+ concentrations and loads (a), local aeration flow rate and DO concentration (b), and N component concentrations at the end of the summer package (c).

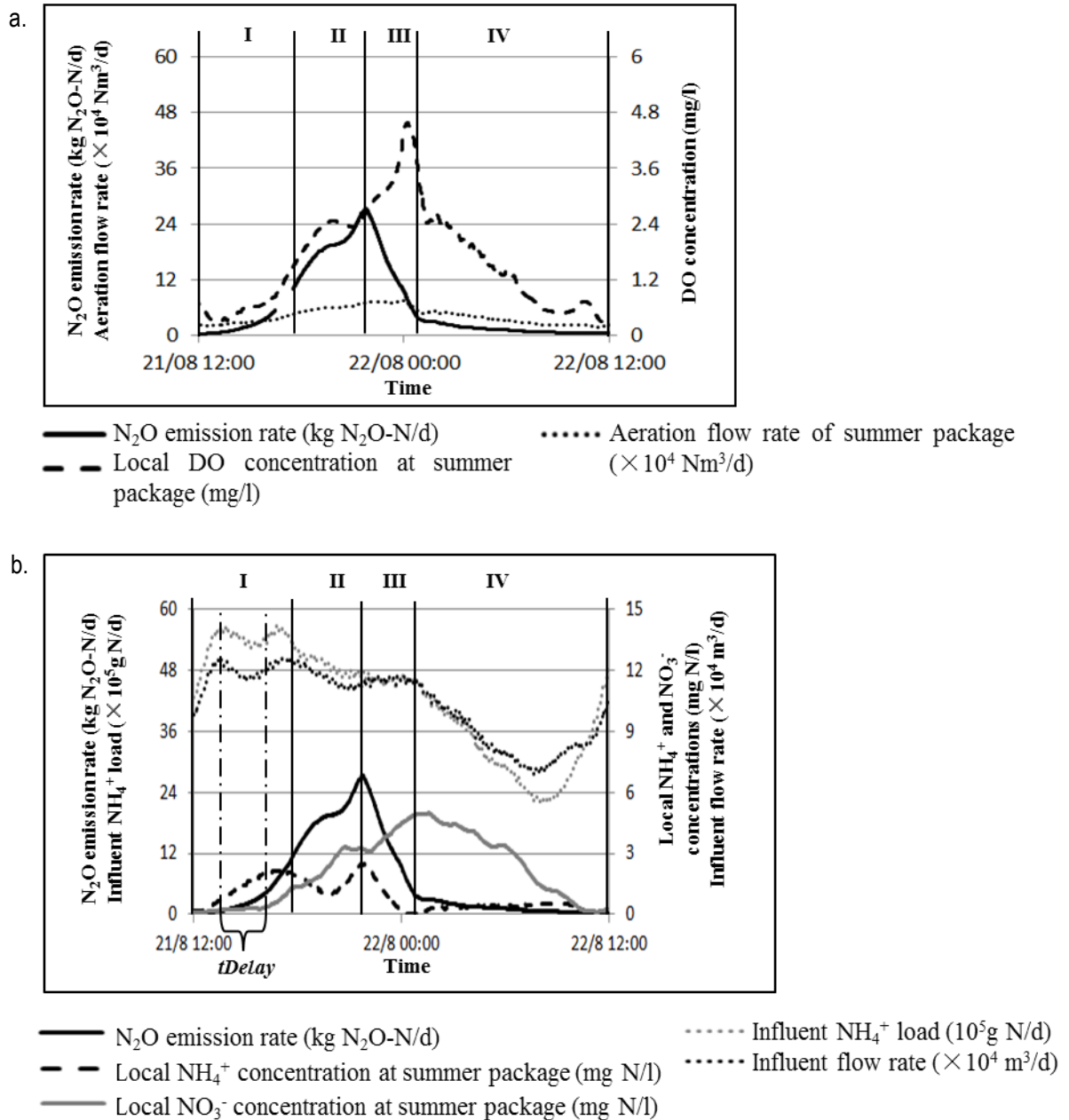


Figure 4.4 Comparison of N₂O emission rates at the end section of the summer package with the local aeration flow rate and the DO concentration (a), and with N components concentrations at the end of the summer package and influent NH₄⁺ concentrations and loads (b) for one typical dry day (Note the delay time *t*Delay is denoted by line - · -).

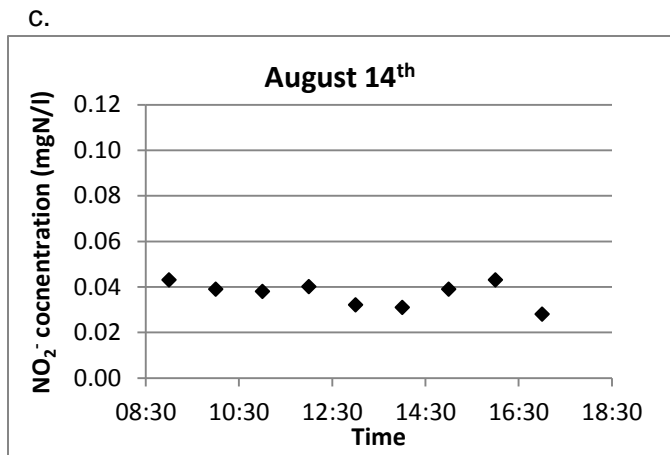
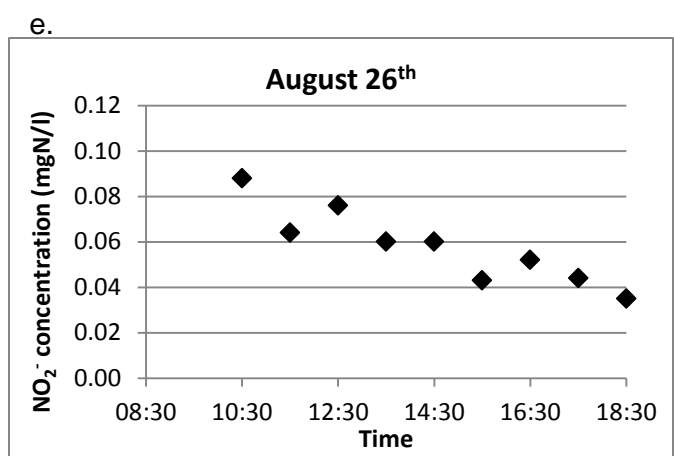
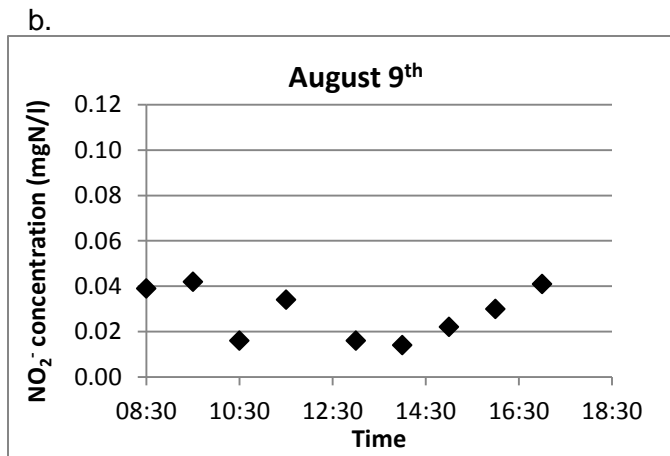
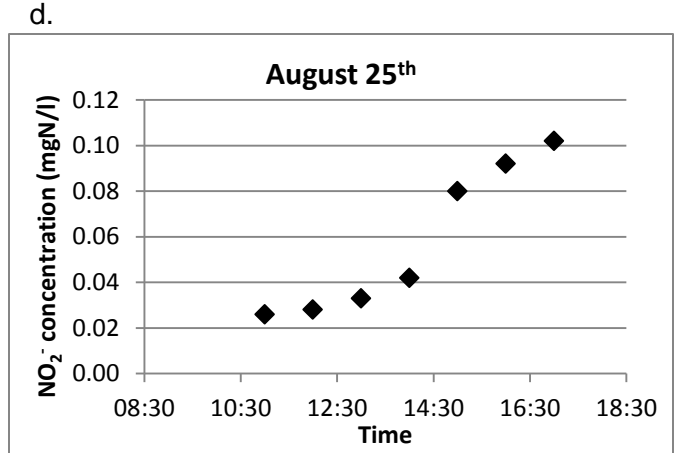
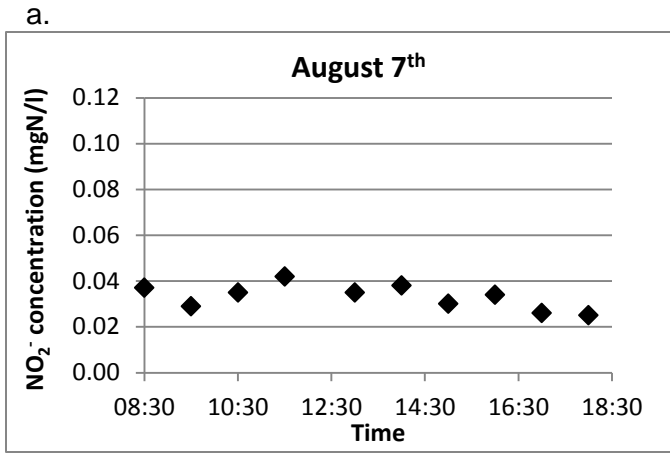


Figure 4.5 Off-line measurement of NO₂⁻ concentration under three dry-weather days (a-c) and two wet-weather days (d-e).

4.2.2 N₂O emissions under dry weather conditions

I. Overall assessment

Under dry weather conditions, the end section of the summer package showed more repeatable dynamics of the variables than the other two sections of the summer package (Figure 4.2). It also showed a higher average N₂O emission rate and a higher average emission factor compared to the beginning section and the middle section (Table 4.1).

Table 4.1 Average N₂O emission rates and emission factors

	Beginning section	Middle section	End section
N ₂ O emission rate (kg N ₂ O-N/d)	10.7 (0.5-47.4)	7.7 (0.8-79.3)	20.3 (0.3-82.2)
N ₂ O emission factor (% of influent TKN load)	0.20 (0.01-1.10)	0.11 (0.02-0.98)	0.28 (0.02-1.11)

The N₂O emissions show significant temporal variations (Figure 4.2). In general, the lowest emissions occur at night or early morning when the influent loads are small, whereas peak emissions begin from noon and continue till the evening after the peak load hits the plant (Figure 4.3.a). For each dry weather day, the influent flow rate exhibited similar dynamics, and the same pattern was observed in the influent NH₄⁺ load and the aeration flow rate. Moreover, the impacts of temperature on the kinetic rates can be neglected given the small variation of the water temperature, which was around 20-21 °C, during the dry weather days of the measurement campaign. Therefore, although the N₂O emission at the different sections of the summer package were not measured in the same week, it can be assumed that the N₂O emission exhibits a similar longitudinal spatial distribution for every dry weather day, which means that the emissions at the beginning, middle and end section of the summer package followed the same pattern. Under these assumptions, the total emission factor of the summer package can be calculated to be 0.59% of the influent TKN load over the dry days during the measurement campaign in August 2012, following the

procedure of Appendix A. The emission factors obtained in this measurement campaign are comparable to the ones reported in other full-scale measurements (Ahn et al., 2010; Daelman et al., 2013a; Foley et al., 2010). However, the difference with those measured N_2O emission factors are due to the different sampling strategies used (Daelman et al., 2013a).

II. N_2O emission through the AOB pathway

The measured emitted N_2O could have been produced in the area of the summer package, i.e. an aerobic zone, where autotrophic activity and heterotrophic aerobic activity dominate. Alternatively, it could have been produced in the upstream anoxic zone where heterotrophic denitrification happens. Indeed, the N_2O produced in the anoxic zone will also be stripped out at the beginning of the summer package. Appendix B calculates and discusses the contribution of the anoxically produced N_2O to the stripped N_2O gas and evaluates how much of the emitted N_2O is coming from the bioreactions in the summer aeration package (AOB pathways). It was concluded that at least 12.9 kg N_2O -N/d out of the 20.3 kg N_2O -N/d N_2O emissions at the end section of the summer package is produced by the AOB pathways, that is more than 33.3% of total N_2O emissions, meaning that the contribution of AOB to the N_2O emissions is significant.

III. Four-phase dynamics of N_2O emissions during dry weather

The N_2O measurements at the end of the summer package, August 20th-24th were done during a dry weather period. During this period, not only the N_2O emissions showed a clear regular pattern (Figure 4.3a), the influent conditions and the local concentrations of NH_4^+ and NO_3^- near the outlet of the summer package also presented regular cycles (Figure 4.3b and 4.3c). Therefore, given the observed dynamics it is proposed to divide each dry

day into 4 phases. Figure 4.4 shows the different variables considered for one typical dry day taken from Figure 4.3, starting at noon when the influent peak hits the plant.

In Phase I, the NH_4^+ peak arrives at the plant inlet around noon and the NH_4^+ peak load hits the summer package about three hours later, as observed by the increase of the local NH_4^+ concentration at the end of the summer package. This increase in local NH_4^+ concentration leads to an increase of the aeration intensity through the NH_4^+ -DO cascade control. When aeration starts increasing, a concomitant rise in N_2O emissions is observed. This increase of N_2O emissions (kg N/d) is mainly due to a higher N_2O production (kg N/d) by AOB biochemical activity (Appendix C). Other studies also observed that an increase of the NH_4^+ concentration usually leads to an increase of the N_2O production (Kampschreur et al., 2008; Wunderlin et al., 2012; Yu et al., 2010).

In Phase II, as aeration keeps increasing due to the cascade controller, NH_4^+ is increasingly removed by oxidation, resulting in a short-term decrease of the local NH_4^+ concentration. However, the load dynamics is such that the NH_4^+ concentration resumes its increasing trend. Nonetheless, during the period with decreasing NH_4^+ concentration, the N_2O emission is not decreasing. Instead, it keeps increasing, but for a short term, likely due to the dip in local NH_4^+ concentration, the increasing rate of N_2O emission is slowed down.

At the beginning of Phase III, when the DO reaches even higher concentrations compared to those in Phase I and II (around 2.5 mg O_2 /l in Figure 4.4a), N_2O emissions drop suddenly, coinciding with the drop in NH_4^+ concentration, while the NO_3^- concentration keeps increasing (Figure 4.4b). Note that although during this phase and Phase II the influent NH_4^+ load decreases a little, it still remains high and such a decrease of influent NH_4^+ load is quite small compared to the decrease of the local NH_4^+ concentrations measured at the summer package (Figure 4.4b). Therefore, it means that the decrease of

the NH_4^+ concentration at the summer package is quite possibly due to the increased conversion resulting from the increased DO.

Literature agrees that there are 2 major AOB bioreaction pathways to produce N_2O (Wunderlin et al., 2012): one occurs during NH_4^+ oxidation to NO_2^- while the other occurs through reduction of NO_2^- to N_2O . For both pathways, NH_4^+ is the N source of N_2O . On the other hand, NO_3^- also sources its N from NH_4^+ . If the fractions of NH_4^+ converted to N_2O and NO_3^- keep increasing with increasing DO, the NO_3^- concentration and the N_2O emission rate will also increase. However, in Phase III, the local NH_4^+ concentration and N_2O emission rate decrease and only the NO_3^- concentration increases. Therefore, it is deduced that a possible explanation for the turning point (around 2.5 mg O_2/l) of N_2O emission in this phase is that under high DO conditions the fraction of NH_4^+ converted to N_2O is reduced compared to that under lower DO conditions while the fraction converted to NO_3^- is increased. This suggests that under these conditions the reaction rate of N_2O production reduces compared to that of NO_3^- production. The metabolic explanation of the phenomenon is not clear yet, since there are two AOB pathways producing N_2O . However, it appears that the NH_4^+ is increasingly converted to NO_3^- rather than to N_2O at the turning point.

However, it must be noticed that according to the off-line NO_2^- measurement data, the NO_2^- concentration under dry-weather days was generally around 0.03 mgN/l (Figure 4.5a-c) but it does not show an evident trend as other components. By sampling only every hour some variation details may be lost. Moreover, the off-line sampling finished around 18:30 in the evening, while the turning point happened around 21:30 in the evening. Therefore, the off-line NO_2^- measurement data cannot be used to further investigate the N_2O emissions and its relationship with NO_2^- . It is suggested to carry out on-line NO_2^- measurement with high temporal-resolution similar to the other components.

In Phase IV, as the influent NH_4^+ load peak reduces to very low levels, the NH_4^+ concentration, the N_2O emissions and the NO_3^- concentration decrease. This behaviour coincides with the reduction of aeration and local DO concentrations governed by the cascade control strategy.

Overall, the on-line measurement results at the end of the summer package suggest that AOB-produced N_2O emission reaches its maximum in conjunction with both high NH_4^+ concentrations and intermediate DO concentrations (2.5 mg O_2/l in this case study). Compared to the N_2O production, the NO_3^- production is not inhibited by high DO levels and it is increased as DO increases. This finding is in agreement with other studies (Colliver and Stephenson, 2000; Zhu et al., 2013).

4.2.3 N_2O emissions under wet weather conditions

The data collected on August 25th-26th can be used to better understand the impacts of wet weather conditions on N_2O emissions. However, one must recognize that these parts of the N_2O emission data were only collected at the end section of the summer package aeration zone. In fact, in order to obtain the total N_2O emissions from the whole summer package under rain events, also the beginning and middle sections of the summer package aeration zone should be monitored.

I. Influent loads

Figure 4.3a indicates that hydraulic shocks hit the plant early in the morning of the 25th, in the mid-afternoon of the 25th and in the morning of the 26th. Compared to dry weather days, the influent flow rates were almost doubled on the 25th and were quintupled on the 26th (Figure 4.3a). The higher influent flow rate results in a shorter hydraulic retention time (HRT). A zoom-in on Figure 4.3c shows that under storm conditions it took about one hour

for the influent NH_4^+ peak to arrive at the location of the summer package, which was about two hours faster than under dry weather conditions.

Such hydraulic shocks also cause dilution of the influent components. Figure 4.3a shows that the influent NH_4^+ concentrations under wet weather days dropped compared to that of dry weather days. However, as expected, the daily averaged NH_4^+ load was similar regardless of the weather conditions. The averaged NH_4^+ load for dry days (August 20th-24th) was 4385 kgN/d, and it was 5033 kgN/d on the 25th and 4059 kgN/d on the 26th.

Conversely, the temporal variation of the NH_4^+ loads was different for August 25th and 26th. On the 25th the NH_4^+ peak load was similar to that of the dry days but on the 26th the NH_4^+ peak load was much higher (Figure 4.3a). This difference in NH_4^+ peak loads was related to the different influent flow peaks. Although the influent flow peaks on both the 25th and 26th were increased compared to the dry weather days, the increase on the 26th was much more pronounced than that on the 25th, indicating that the rain event happening on the 26th was more intense (10mm versus 2mm). Wastewater that moves at such high-speed in the sewer system makes that the arrival of the sewage with dry weather concentrations present in the sewer was compressed in time, causing a sudden increase of the NH_4^+ load (Krebs et al., 1999). Another explanation about this NH_4^+ load peak is that during dry-weather days the organic N that is contained in the settled sludge may be released as NH_4^+ and then flows into the plant together with the first flash at the start of the rain event. After this transient peak, the NH_4^+ load became quickly diluted, resulting in a similar daily averaged load compared to that of August 25th and dry weather days.

II. Relationship between N_2O emissions and other variables

The temporal variation of N_2O emissions during dry days showed that the N_2O emission rates increased with the increasing local NH_4^+ concentrations (Figure 4.4b). However,

Figure 4.3c showed that although during rainy days (August 25th-26th) the maximum NH_4^+ concentration at the end of the summer package was significantly higher compared to the dry weather days, this increasing local NH_4^+ concentration did not lead to a higher N_2O emission. The NO_2^- concentration measured off-line also showed an increase on August 25th and 26th, around 0.6 mgN/l on average (Figure 4.5d-e). However, this increase of NO_2^- did not cause an increase of N_2O as observed by other research (Kampschreur et al., 2008; Kim et al., 2010; Yu et al., 2010). Instead, both the average N_2O emission rate and emission factor under rainy days were reduced by about half compared to the dry weather days. The average emission rate at the end of the summer aeration package was 11.9 kg N_2O -N/d (ranging between 0.3-75.9 kg N_2O -N/d) and its emission factor calculated on an hourly basis (see Appendix A) was 0.15% on average (ranging between 0.00-0.67%).

This decrease of N_2O emissions could be due to the lower biochemical NH_4^+ oxidation rate (kg N/d) under wet weather conditions. The daily averaged NH_4^+ effluent load of the bioreactor was about 102 kgN/d for dry days (August 20th-24th), while it was 254 kgN/d on the 25th and 541 kgN/d on the 26th. Assuming that the influent NH_4^+ concentration of the bioreactor was the same as the plant influent NH_4^+ concentration, therefore, on average, the NH_4^+ removed in the bioreactor was 4283 kgN/d with a removal percentage of 98% during dry days. The value was 4779 kgN/d (95%) for the 25th and 3518 kgN/d (86.7%) for the 26th. It can thus be concluded that on the 26th, in which a considerable hydraulic shock loaded the plant, the NH_4^+ removal decreased in terms of both amount and percentage. The smaller NH_4^+ removal on August 26th could thus result in smaller N_2O emissions.

The water temperature dropped from 20.8 °C to 18.7 °C, contributing to the reduced NH_4^+ oxidation rate. However, the reduced NH_4^+ oxidation rate is also caused by other factors, such as the shorter HRT under rainy days. The shorter HRT reduces the reaction time to produce N_2O . It also changes the flow regime and mixing conditions in the bioreactor,

which also affect the bioreactions. Moreover, the concentrations of the different components are lowered during rain events. Importantly, the measured TSS concentration at the summer package was generally around 3-3.5 g/l under dry weather conditions but it dropped to around 2-2.7g/l under wet weather conditions, indicating the AOB biomass concentration in the bioreactors was reduced and therefore the oxidation rate as well. The lower concentrations of components may also lower the bioreaction rates (Henze et al., 2000), resulting in lower NH_4^+ oxidation rate and N_2O production rate.

However, the lower NH_4^+ removal rate cannot fully explain the low N_2O emissions under wet weather conditions, especially for the one occurring during the mid-afternoon on the 25th, since the NH_4^+ removal rate on August 25th (4779 kgN/d) was not decreased compared to that during dry weather days (4283 kgN/d). To answer this question, the control strategy used by the Eindhoven WWTP has to be investigated. The plant adjusts its operation and control strategy corresponding to different weather conditions and therefore influences the concentrations of the components. On the other hand, the component concentration also influences the operation of the controllers, e.g. in the NH_4^+ -DO cascade control the DO controller changing its setpoint with NH_4^+ concentration. The control strategy that is activated under different weather conditions is shown to be an important reason for the low N_2O emission under rain events, see Section 4.2.4 and Section 4.2.5.

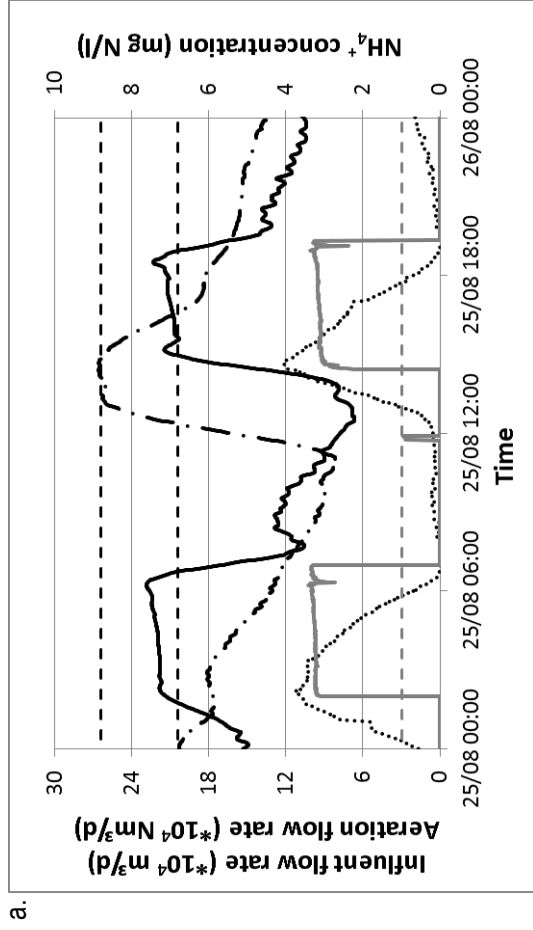
4.2.4 Relationship between N_2O emissions and control strategies

Generally speaking, the NH_4^+ -DO cascade control is in charge of the aeration control under dry weather days, but the inflow-based feedforward control is activated under wet weather conditions. Below, the functioning of these controllers is analyzed, their interactions clarified and improvements proposed.

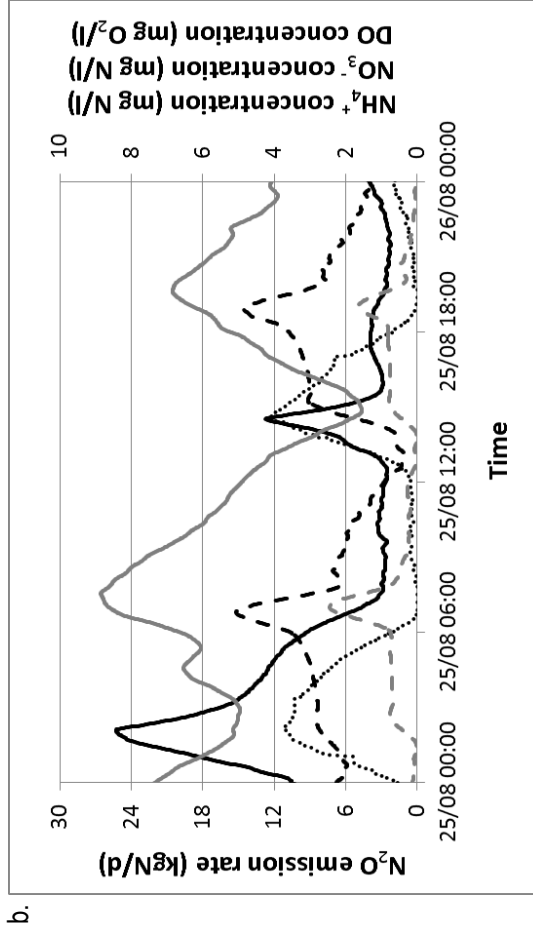
I. NH₄⁺-DO cascade control

For dry weather conditions, the influent flow rate remains below the switch-on value ($26.4 \times 10^4 \text{ m}^3/\text{day}$) for feedforward control (Figure 4.6). Therefore, the aeration air flow rate of the summer package is only manipulated by the NH₄⁺-DO cascade control. The on/off switch of the winter package depends on the operation time of the summer package under its maximum capacity or 60% capacity.

August 25th was a wet weather day and received two peaks of inflow, in the morning and in the afternoon respectively. Figure 4.6 reveals how the control is performed and describes the relationship between the N₂O emissions and the other component concentrations.



- Aeration flow rate of summer package
- Aeration flow rate of winter package
- · - Influent flow rate
- - - Inflow rate switch-on/off value for feedforward control
- Local NH₄⁺ concentration at summer package
- - - NH₄⁺ setpoint



- N₂O emission rate
- - - Summer package DO
- · - Winter package DO
- NH₄⁺ concentration
- NO₃⁻ concentration

Figure 4.6 Comparison of aeration flow rate, NH₄⁺ concentration and influent flow rate for the wet weather day August 25th (a) and comparison of N₂O emission rate, NH₄⁺ concentration, DO concentration and NO₃⁻ concentration for the same wet weather day (b).

However, although both peak inflow rates on August 25th were larger than the flows on dry weather days, the maximum value of the first peak did not hit the switch-on value of the inflow-based feedforward control, meaning that the NH_4^+ -DO cascade control was still in charge of the aeration control during the first peak on August 25th, that is when the NH_4^+ concentration was above 1 mg N/l, the aeration flow rate is increased to enhance NH_4^+ oxidation. The operation of the winter package is decided by the operation of the summer package as under normal dry-weather days.

Therefore, the dynamic profile during the first peak on August 25th had similar properties as dry weather profile. The N_2O emissions first increased as the NH_4^+ concentration increased which was brought about by the influent peak load and then they decreased as the DO at the summer package bioreactor section was increased above 2.5 mg O_2 /l (Figure 4.6b). In contrast, the NO_3^- concentration always followed the DO concentration. When the DO exceeded 2.5 mg O_2 /l, the NH_4^+ decreased but the NO_3^- kept increasing. This finding was in agreement with the observations under dry weather conditions.

The transient period with low DO and high NH_4^+ concentrations which leads to N_2O emission peaks is caused by the operational strategy of the NH_4^+ -DO cascade control. The NH_4^+ -DO cascade control is a feedback control, which makes that the system only takes action after it observes a deviation of the setpoint. Given that this is a low gain controller (Åmand et al., 2013), the increase in aeration is rather slow. The delay between increasing aeration and observing NH_4^+ increase is shown in Figure 4.6b, i.e. the periods with increasing or peak values of DO, as well as NO_3^- concentrations, occurred later than the periods with increasing or peak values of the NH_4^+ concentration.

During the second peak of August 25th, the inflow rate exceeded the switch-on boundary for a short while, about 40 minutes, at the end of this peak. This short period of high inflow rate was long enough (longer than 10 min) to trigger the inflow-based feedforward control

and thus both winter and summer aeration packages were operated at their maximum capacity. However, the inflow rate dropped quickly back $20.4 \times 10^4 \text{ m}^3/\text{day}$, so the NH_4^+ -DO cascade control took back the charge of the aeration control. The combination of the two strategies leads to a mixed behavior during the second peak on August 25th, e.g. its N_2O emission peak is lower than that during the first peak on August 25th but is higher than that on August 26th. Further information regarding the second peak on August 25th is given in Section 4.2.5-II “a. Feedforward control switched on after the peak arrived”.

II. Inflow-based feedforward control

The inflow-based feedforward control was activated shortly at the end of the peak load in the afternoon of August 25th and was active from the very beginning of the storm event on August 26th.

a. Feedforward control switched on after the peak arrived

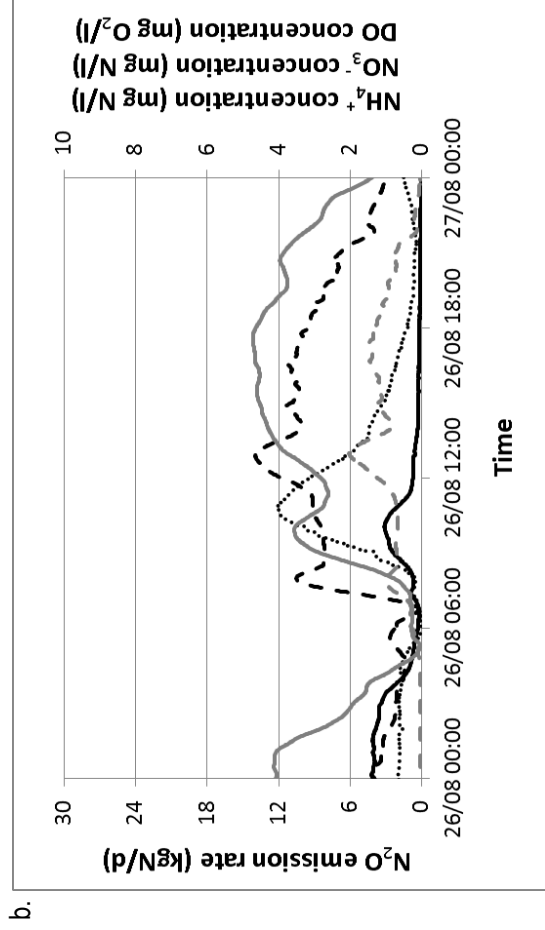
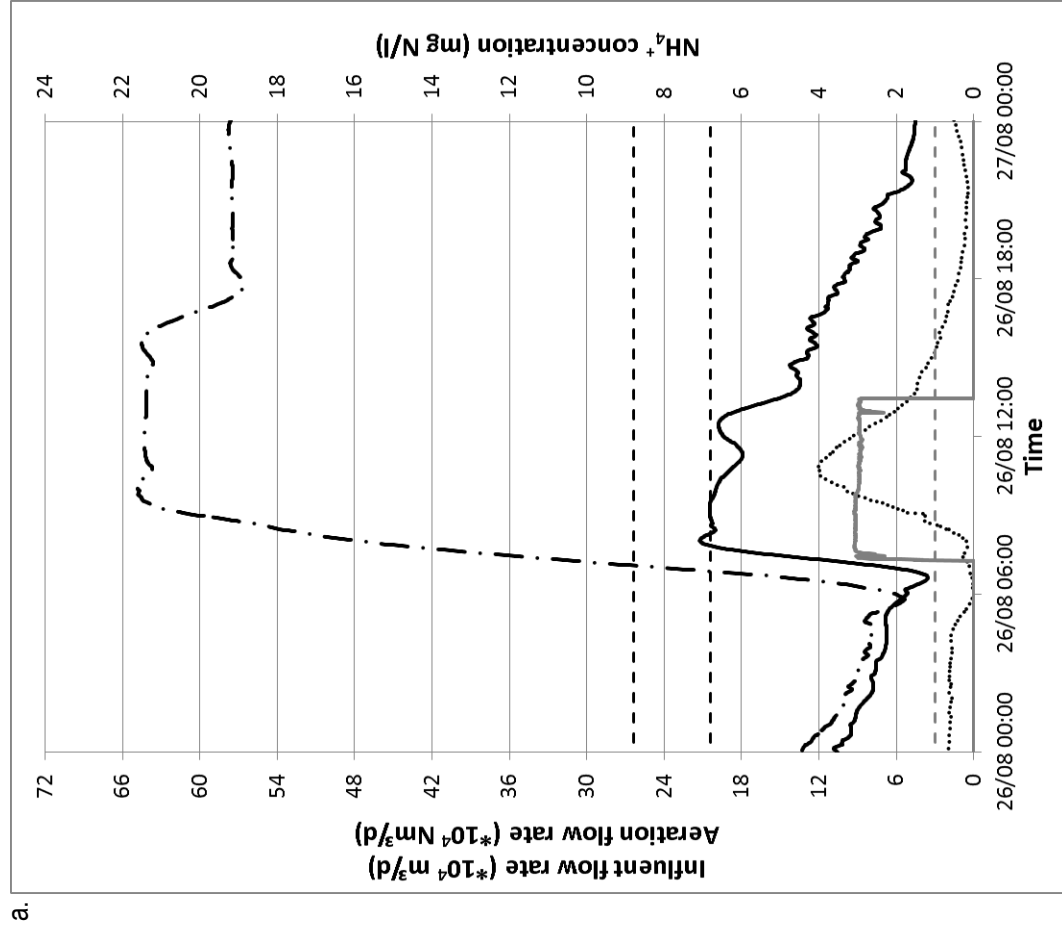
The aeration flow rate was increased twice on August 25th, in the morning and the afternoon respectively. However, the increase of the aeration flow rate in the afternoon was steeper than that in the morning. This was because the inflow-based feedforward control directly adjusted the DO setpoint to $3.5 \text{ mg O}_2/\text{l}$. The winter aeration package was also fully switched on twice to its full capacity, around $10 \times 10^4 \text{ Nm}^3/\text{day}$, because the summer package was operated at its maximum capacity longer than 5 min.

The N_2O emission peak which occurred in the afternoon of August 25th was much smaller than the one in the morning (Figure 4.6b). This was because, as mentioned before, the inflow-based feedforward control which was opened instantly in the afternoon caused a steeper increase of the aeration flow (Figure 4.6a), which resulted in a faster increase of the DO concentration than that in the morning (Figure 4.6b). In other words, the DO concentration in the afternoon reached $2.5 \text{ mg O}_2/\text{l}$ in a shorter time, meaning that the N_2O

emissions started to decrease sooner, never leading the high levels observed in the morning.

b. Feedforward control switched on when the peak arrived

Figure 4.7 reveals how the control is performed and how the relationship is between the N_2O emissions and the other component concentrations on August 26th when the plant experienced an even bigger storm event than on August 25th. The maximum flow rate increased up to $65 \times 10^4 \text{ m}^3/\text{day}$ around 7:00 am. Soon, both summer and winter aeration packages were operated at their maximal capacities, although the NH_4^+ concentration measured near the outlet of bioreactor was still below 1 mg N/l, i.e. the inflow-based feedforward control took over the aeration system from the NH_4^+ -DO cascade control. Thus, the aeration during the feedforward control is increased before the influent peak load strikes the bioreactor, while in the case the NH_4^+ -DO cascade controller, which is a feedback controller, was in charge the aeration is only increased after the influent peak load has upset the bioreactor. After 4 hours the inflow-based feedforward control gave back the charge to the NH_4^+ -DO cascade controller even though the inflow rate was still high. The winter package kept at its maximum capacity until the aeration of the summer package dropped below its 60% capacity, around $17 \times 10^4 \text{ Nm}^3/\text{day}$.



Legend of (a):

- Aeration flow rate of summer package
- Aeration flow rate of winter package
- · - Influent flow rate
- - - Inflow rate switch-on/off value for feedforward control
- Local NH_4^+ concentration at summer package
- - - NH_4^+ setpoint

Legend of (b):

- N_2O emission rate
- - - Summer package DO
- - - Winter package DO
- NH_4^+ concentration
- NO_3^- concentration

Figure 4.7 Comparison of aeration flow rate, NH_4^+ concentration and influent flow rate for the wet weather day August 26th (a) and comparison of N_2O emission rate, NH_4^+ concentration, DO concentration and NO_3^- concentration for the same wet weather day (b).

On August 26th the N₂O emissions were very low compared to the other days (Figure 4.7b). Only a small increase was observed around 9:00 am when the NH₄⁺ concentration peak arrived. The low N₂O emission was mainly due to the fact that on August 26th the inflow-based feedforward control was active from the beginning of the storm event, which is a situation different from that in the afternoon of August 25th when the inflow-based feedforward control was only switched on for a short while after the inflow peak had already impacted the bioreactor.

Therefore, on August 26th the DO concentration was proactively increased before the influent NH₄⁺ peak arrived at the summer aeration package. On the one hand, the high DO concentration at the summer package, which was increased above 2.5 mg O₂/l in advance, was not beneficial for N₂O production, similar to the conditions on dry days and the low intensity wet day (August 25th). On the other hand, independent of the weather conditions, the DO concentrations increased as the aeration flow rate increased, resulting in an increased NO₃⁻ concentration (Figure 4.6b and Figure 4.7b). Therefore, this increase of the DO prior to the arrival of the NH₄⁺ peak under the storm event on August 26th directly caused the increase of the NO₃⁻ concentration. As shown in Figure 4.7b, the increase or peak of NO₃⁻ occurred almost at the same time as NH₄⁺. This means that before the NH₄⁺ peak load hits the summer package, most of the NH₄⁺ has been converted to NO₃⁻ thanks to the high DO conditions in the summer package, above 2.5 mg O₂/l near the outlet of the bioreactor.

4.2.5 Control improvement

To sum up, the high N₂O emissions on dry weather days are a result of the way the NH₄⁺-DO cascade control causes the DO concentration to increase after detecting the NH₄⁺ peak. Besides this delay which is one factor causing the transient high N₂O emission, the NH₄⁺-DO cascade control is disadvantageous in view of N₂O mitigation, because its

energy saving objective causes low DO concentrations which stimulate the N_2O production by both AOB and denitrifiers as stated in Chapter 3 and by Flores-Alsina et al. (2011). Interestingly, the low N_2O emissions on wet weather days could be attributed to the inflow-based feedforward control which increased the DO concentration before the arrival of the NH_4^+ peak which allowed the NH_4^+ to be converted into NO_3^- rather than to N_2O . Therefore, the comparison between N_2O emissions under different control strategies showed that in order to avoid high N_2O emissions, the DO at the entering part of the aerobic zones should not be too low when NH_4^+ concentrations increase. This is exactly what a NH_4^+ -DO cascade controller should be doing too, but its feedback nature and low gain prevent it from reaching that timely.

Although the NH_4^+ -DO cascade control can cause high N_2O emissions, it retains its advantage of aeration energy saving. Therefore, there is an appeal to find strategies which can reduce the N_2O emissions and at the same time maintain the energy saving advantage. In the framework of BSM2, the traditional NH_4^+ -DO control strategy has been improved by adding an independent DO controller to the first aerobic tank (Chapter 3). However, those approaches did not consider the temporal variation of N_2O emissions. In this case study, during dry weather days the high N_2O emissions occurred only during NH_4^+ peaks, while during the rest of the day they were low. Therefore, it is necessary to take into account the temporal variation when designing the control strategy.

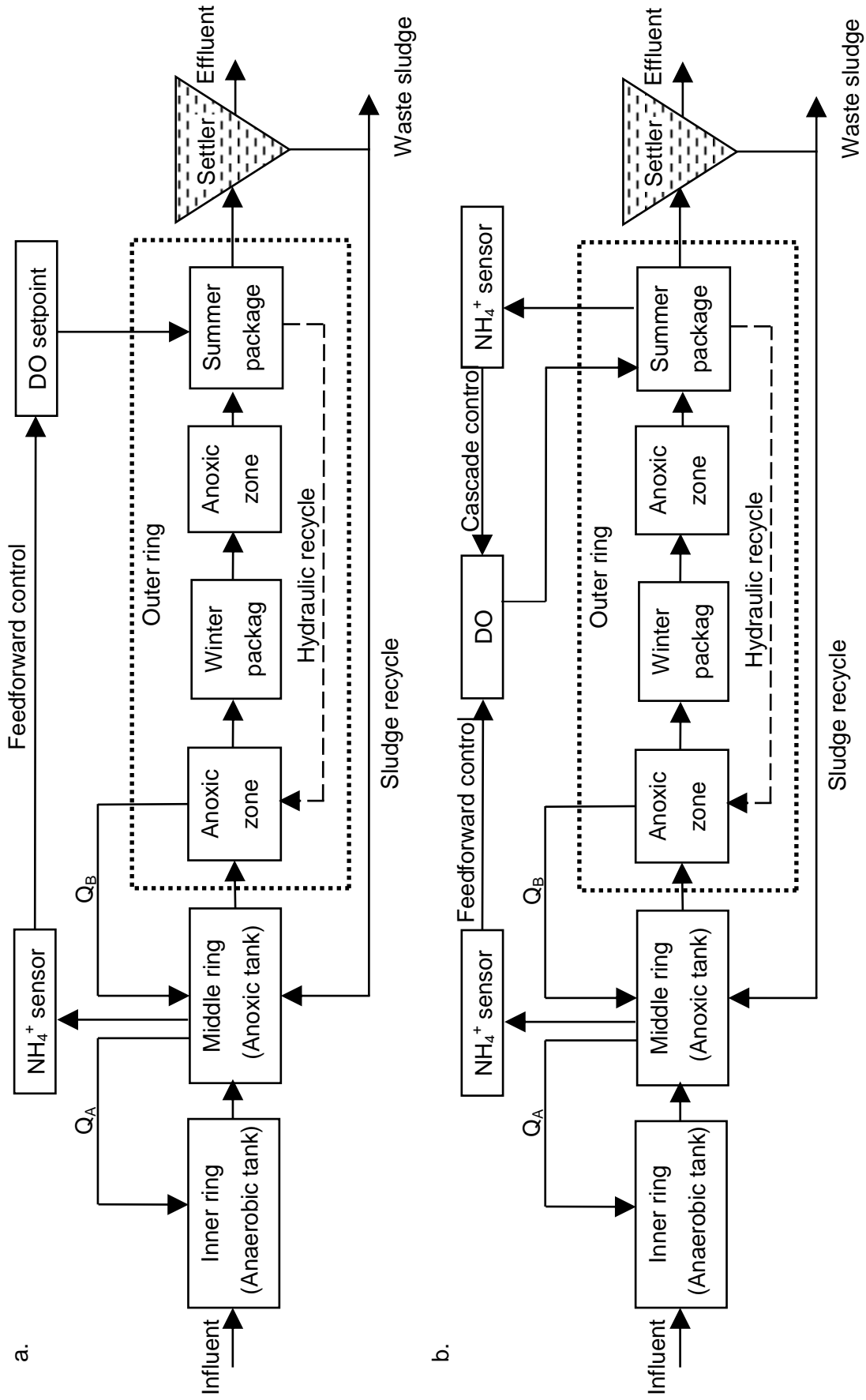


Figure 4.8 Scheme of control strategies.

One proposed solution is to install a NH_4^+ sensor upstream the aeration zone, i.e. in the anoxic tank. This NH_4^+ sensor can work with the DO sensor as a NH_4^+ -DO feedforward control system, Figure 4.8a. When the NH_4^+ sensor detects the NH_4^+ peak, the aeration can be increased to reach 2.5 mg O_2/l as above. In another strategy which is a bit more complex, Figure 4.8b, two NH_4^+ sensors are applied, one at the anoxic tank (upstream) to measure the NH_4^+ peak and the other remaining near the outlet of the bioreactor (downstream) for the effluent quality control. When there is no peak, the system uses the NH_4^+ -DO cascade control, i.e. it manipulates the DO setpoint according to the downstream NH_4^+ sensor. When the upstream NH_4^+ sensor detects a peak, the control system will switch to the NH_4^+ -DO feedforward control, i.e. the DO setpoint will be increased before the summer aeration package receives the NH_4^+ peak.

One simple method can be used as an alternative for these control strategies that use an upstream NH_4^+ sensor. The strategies in Figure 4.8 were proposed to deal with the huge N_2O emission peaks under dry-weather days, since under wet-weather conditions the N_2O emission is comparatively low. Note that under dry-weather days the operation and performance of the plant show a regular daily pattern. The NH_4^+ peaks arrive at the plant around noon (12:00 pm.) every dry-weather day (Figure 4.4b). Therefore, the DO setpoint of the summer package can be increased to 2.5 mg O_2/l around 2:30 pm., taking into account the 3 hours necessary for the wastewater to flow from the plant inlet to the summer package.

These ideas for new control strategies for wet weather days have not been tried out on the Eindhoven WWTP in this thesis, but will be the subject of future research.

4.3 Modelling N₂O emissions from a real WWTP

4.3.1 ASMG2d model and implementation of a real WWTP

I. General model structure

ASM2d is a published and well-known model that describes the removal of organics and nutrients, i.e. N and P (Henze et al., 1999). Gernaey and Jørgensen (2004a) modified the biomass lysis processes proposed by Henze et al. (1999) to take into account the difference in rates under anaerobic, anoxic and aerobic conditions. ASMG2d is basically developed from the modified ASM2d of Gernaey and Jørgensen (2004a). The extension of ASMG2d compared to ASM2d is that, in the same way as for ASMG1 (Chapter 3), the N-related processes are described in more detail. New components, i.e. NO₃⁻, NO₂⁻, NO, N₂O and N₂, were used in ASMG2d to replace the single N component of ASM2d. All PAO mediated denitrification processes were modelled in four steps instead of one, in the same way as the heterotrophic denitrification i.e. NO₃⁻→NO₂⁻, NO₂⁻→NO, NO→N₂O, and N₂O→N₂ (Hiatt and Grady, 2008). N₂O production through the AOB pathway was also included in ASMG2d and was modelled in the same way as in ASMG1. The AOB denitrification model proposed by Mampaey et al. (2013) was chosen as the basic model for the AOB pathway to produce N₂O but a Haldane term was used to modify the DO effect. This model agreed with the general ideas that the NH₄⁺ is used as electron donor and it describes the high DO inhibiting the AOB mediated NO₂⁻ denitrification to N₂O without adding more components (see Chapter 3). Details about the model are given in Appendix G-I.

II. PAO denitrification

In ASM2d (Henze et al., 1999), the storage of poly-phosphate particulate material (X_{PP}) and the growth of PAO biomass (X_{PAO}) are separated as two processes and the denitrification happens during both anoxic storage of X_{PP} and anoxic growth of X_{PAO} . In ASMG2d, the two denitrification processes were extended into four steps respectively, which means that both X_{PP} storage and X_{PAO} growth can produce N_2O under anoxic conditions (Oehmen et al., 2010).

III. Temperature dependence of bacterial growth rate

The Arrhenius equation is a common method of describing the temperature dependency of the maximum growth rates, Eq. (4.1).

$$\mu_{A,T,bacteria} = \mu_{A,T_{Ref20},bacteria} \cdot \theta_{A,bacteria}^{T-T_{A,Ref20}} \quad \text{Eq. (4.1)}$$

where the subscript “bacteria” stands for the bacteria species, i.e. heterotrophs (H), AOB, NOB and PAO, $T_{A,Ref20}$ represents the reference temperature of 20 °C used in the Arrhenius equation, T is the actual temperature, $\mu_{A,T,bacteria}$ is the growth rate of bacteria at temperature T , $\mu_{A,T_{Ref20},bacteria}$ is the growth rate at the reference temperature 20 °C and $\theta_{A,bacteria}$ is a coefficient. According to ASM2d (Henze et al., 1999), for heterotrophs $\mu_{A,T_{Ref20},H}=6d^{-1}$ and for PAO $\mu_{A,T_{Ref20},PAO}=1d^{-1}$. ASM2d also provides the growth rate at 10 °C, i.e. for heterotrophs $\mu_{A,10,H}=3d^{-1}$ and for PAO $\mu_{A,10,PAO}=0.67d^{-1}$. Therefore, $\theta_{A,bacteria}$ can be calculated for heterotrophs and PAO: $\theta_{A,H}=1.072$ and $\theta_{A,PAO}=1.041$. However, the Arrhenius equation is not suitable for the growth rate at high temperature (above 35 °C). It is always good to provide a model for a wider application range. Therefore, the Ratkowsky equation, Eq. (4.2), can be

used to describe the biomass growth rates with temperature dependency (Hiatt and Grady, 2008).

$$\mu_{R,bacteria} = \left\{ b_{\mu_{bacteria}} \cdot (T - T_{Min,bacteria}) \cdot \left[1 - e^{c_{\mu_{bacteria}} \cdot (T - T_{Max,bacteria})} \right] \right\}^2 \quad \text{Eq. (4.2)}$$

In this equation, the growth rates, $\mu_{R,bacteria}$, are first increasing and then decreasing with temperature. In ASMG1 (Chapter 3), all growth rates were calculated by the Ratkowsky equation, Eq. (4.2). Therefore, in ASMG2d the calculations of the maximum growth rates of heterotrophs, AOB and NOB, use the same equations as those of ASMG1, i.e. $\mu_{R,H}$, $\mu_{R,AOB}$ and $\mu_{R,NOB}$. However, so far the Ratkowsky equation has not been used for PAO, i.e. no suggested parameter values are available for $\mu_{R,PAO}$. Therefore, parameters of $\mu_{R,PAO}$ had to be estimated. There are four parameters in the Ratkowsky equation, i.e. $b_{\mu_{bacteria}}$, $c_{\mu_{bacteria}}$, $T_{Max,bacteria}$ and $T_{Min,bacteria}$. It is assumed that $T_{Max,PAO}$ and $T_{Min,PAO}$, which are the maximum and minimum tolerant temperatures, of PAO are the same as those of the other heterotrophs, considering that PAO are just a special group of ordinary heterotrophs.

The next step was to estimate $b_{\mu_{PAO}}$ and $c_{\mu_{PAO}}$ values. Further assuming that $\mu_{R,PAO}$ should be similar to $\mu_{A,T,PAO}$ for the temperature range 0-35 °C, the best $b_{\mu_{PAO}}$ value was pursued in the range of 0.05-0.5 and the best $c_{\mu_{PAO}}$ in the range of 0.05-0.5. The best $b_{\mu_{PAO}}$ and $c_{\mu_{PAO}}$ values were obtained at the smallest mean squared error between $\mu_{R,PAO}$ and $\mu_{A,PAO}$ for the temperature range 0-35 °C. In Figure 4.9, the $\mu_{R,PAO}$, which was calculated from the Ratkowsky equation with the estimated parameters, is compared with the original $\mu_{A,T,PAO}$ of ASMG2d. It shows that $\mu_{R,PAO}$ inherits the trend of $\mu_{A,PAO}$ for the temperature range 0-35 °C.

Note that the water temperature of the plant was stable around 20-21 °C under dry weather conditions but under wet weather conditions it dropped from 20.8 °C to 18.7 °C which contributed to the reduction of the NH_4^+ conversion rate, see Section 4.2.3.

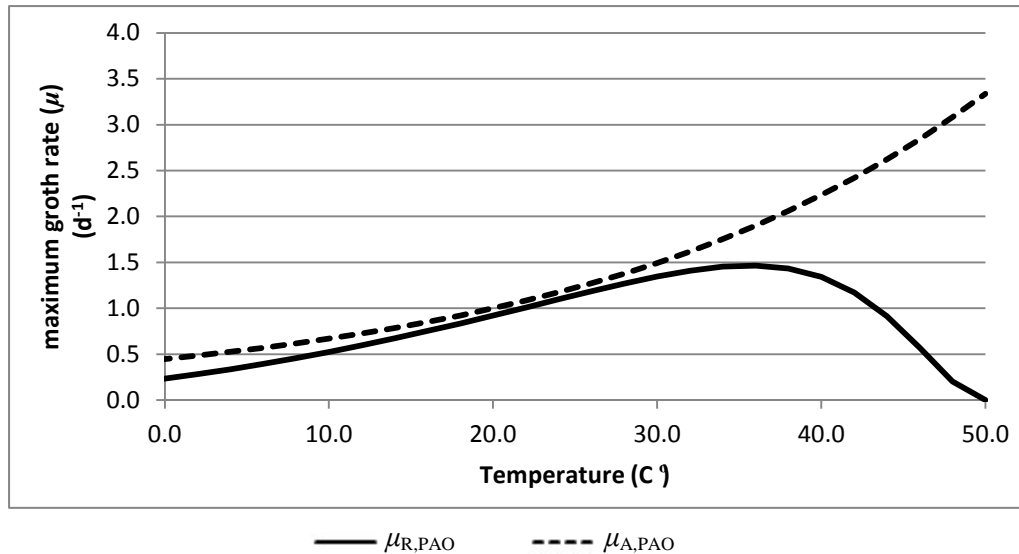


Figure 4.9 Comparison of different μ_{PAO} values in ASM2d based on the Arrhenius temperature dependency ($\mu_{A,T,PAO}$) and in ASMG2d based on the Ratkowsky temperature dependency ($\mu_{R,PAO}$).

IV. Implementation in Eindhoven WWTP

An ASM2d-based dynamic model was already applied to the Eindhoven WWTP (Amerlinck et al., 2013). Compared to the ASM2d of Gernaey and Jørgensen (2004), it has added two new components, i.e. the soluble aluminium (S_{Al}) and inert inorganic particulate material (X_{ii}), because the Eindhoven WWTP also doses Al, besides iron, to remove phosphorus. These two components were also added to the ASMG2d model that was implemented to the same configuration as that of Amerlinck et al. (2013).

After steady-state simulation for 100 days, the dynamic simulation was carried out from mid-night of August 1st till mid-night August 27th, the same period for which the intensive N_2O measurement campaign was done. The whole period included two important rain events, one around mid-night on August 16th and one on August 25th-27th.

The plant has spectrophotometric sensors (S::CAN, Austria) to measure influent concentrations of COD_t, COD_s and TSS and flow sensors to measure inflow rate. There is

no sensor at the plant inlet to measure influent phosphate (PO_4^-). Therefore, the PO_4^- concentration measured by the on-line sensor installed at the outlet of the primary clarifier was used as the influent PO_4^- concentration, assuming that the P removal in the primary clarifier is negligible. The operation files, e.g. the chemical dosing rate, the recycling flow rate, the air flow rate and the sludge flow rate, during this period were also obtained from the plant's on-line sensors. The original sensor data had a lot of noise, so a Savitzky-Golay filter (Press et al., 2007) was used to smooth the original signals before applying them to the model.

Although the plant sensor data provide information about influent flow rate and concentrations of COD_t , COD_s , TSS, NH_4^+ and phosphate (PO_4^-), these influent data are not suitable for ASMG2d. Therefore, a fractionation model was used, Figure 4.10. The fraction parameters and certain assumed values of influent component concentrations were the same as in the original Eindhoven plant model (Amerlinck et al., 2013). The concentration of S_{N_2} is assumed to be saturated, i.e. 13.32 mg/l.

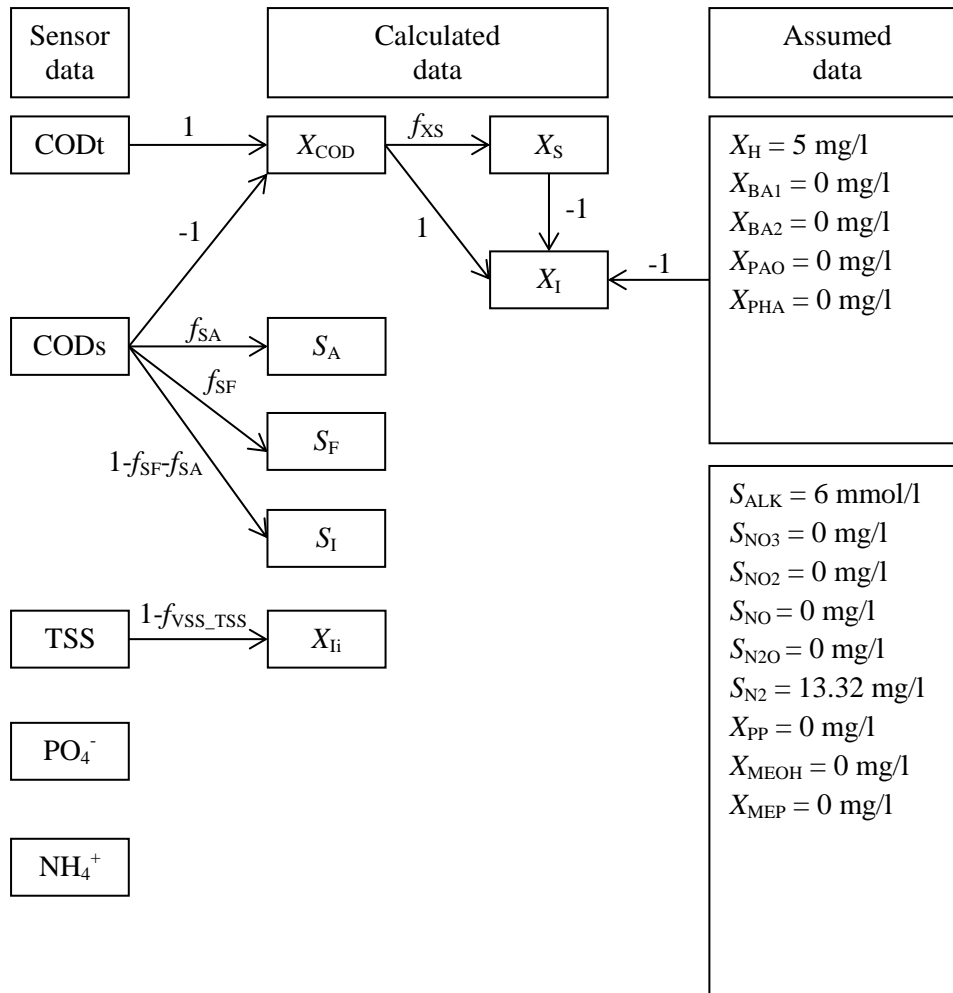


Figure 4.10 ASMG2d influent fractionation model.

The Eindhoven WWTP has three parallel bioreactor lines and each bioreactor uses a UCT process which consists of three rings, i.e. an anaerobic tank of 11,196 m³, an anoxic tank of 28,750 m³ and a partially aerated tank of 50,310 m³. In the outer ring, two aeration packages are installed, a so-called summer package with a volume of 16,099 m³, a winter package of 5,950 m³ and non-aerated zones of 28,261 m³. In the model, each ring of the bioreactor was divided into several CSTRs. Considering the ring shape of the bioreactor, the circumfluence of the outer ring was simulated by using a recycling flow from the last CSTR to the first CSTR of the outer ring. The same concept was applied for the middle ring. However, the inner ring is divided directly into four CSTRs without circumfluence (Figure 4.1a). The outlet of the bioreactor is a weir, so the flow at the outlet is a waterfall with considerable oxygen transfer and it is modelled as a 100 m³ aerobic tank. The plant utilizes control strategies to manipulate its chemical dosage for P-removal, recycling, aeration and sludge disposal. However, in this section, instead of implementing these control strategies, the actuator settings recorded by the plant, i.e. the chemical dosing rate, the recycling flow rate, the air flow rate and the sludge flow rate, were directly used as inputs to the model. The calibration with implemented control strategies requires more time and efforts, because it is quite difficult to extract the details of the control algorithms from the supervisory control and data acquisition (SCADA) system. Also, imperfect sensor signals make that deviations will occur between the modelled and real system, leading to problems to correctly simulate the observed behaviour with control loops active.

The oxygen transfer coefficient ($k_L a$) was calculated by an aeration model which took into account the air flow rate (Q_{air}), the sludge age (θ_{Sludge}) and the temperature (T). The original aeration model used by (Amerlinck et al., 2013) was modified as Eq. (4.3).

$$k_L a = \left[f(Q_{air}, \theta_{Sludge}, T) \right] \cdot \left(1 - e^{-\beta \cdot Q_{air}} \right)^\alpha \quad \text{Eq. (4.3)}$$

where $f(Q_{\text{air}}, \theta_{\text{Sludge}}, T)$ is the function of the original aeration model and β and α are coefficients. This empirical modification was aimed at achieving smaller $k_L a$ values and therefore better description of the DO and N_2O data under low air flow rate (Q_{air}) conditions compared to the original aeration model (see Section 4.3.1 “V. Calibration”). Figure 4.11 compares the $k_L a$ calculated by the modified model with the original model when θ_{Sludge} is 5.74 d and T is 20.26 °C. The plant operational range of aeration flow rate was 150,000-700,000 m^3/d .

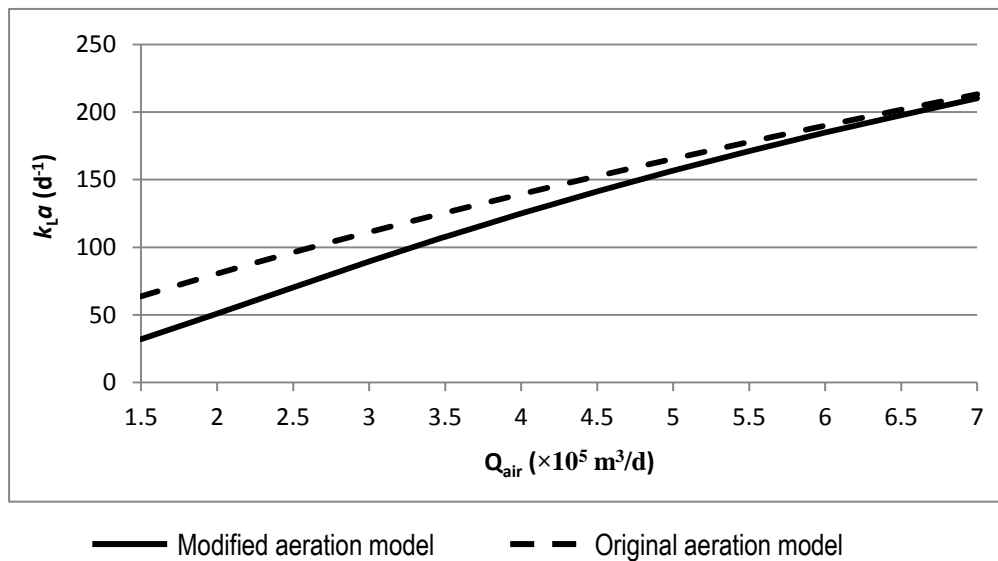


Figure 4.11 Comparison of $k_L a$ calculated by original aeration model and the modified model at 20.26 °C with sludge age of 5.74 d.

V. Calibration

The model calibration followed the same procedure as proposed for ASMG1 calibration in Chapter 3. First, the calibration was done under steady state and then the model was further tuned under dynamic conditions. During steady state calibration, first TSS in the reactors was calibrated to be around 3500mg/l which was the normal value according to the plant on-line data. Second, the calibration focused on the hydrolysis and fermentation process, because these two processes provide the substrates for the heterotrophs and the PAO. If the

simulated substrate concentrations are wrong, the heterotrophs and the PAO will not grow properly. Then, the nitrification by autotrophs, the denitrification and the aerobic degradation by heterotrophs, and the PAO-related processes were calibrated. This step also included the calibration of the N_2O production during denitrification. Finally, the parameters of N_2O production by the AOB were adjusted. It must be noticed that the procedure introduced above just provides the general idea about how to start and carry on calibration. In practice the calibration is often not a one-way procedure. There is interaction among the calibration steps and iteration is necessary: the calibration steps in later stages affect the results obtained in former steps of the calibration. For example, N_2O is produced by both heterotrophs and AOB and it is affected by the NO_2^- concentration. When the N_2O emissions are made to meet the calibration data, the NO_2^- concentration may have turned to be wrong and under this situation, the nitrification and the heterotrophic denitrification must be re-calibrated. Therefore, it is often required to repeat the calibration several times.

The model calibrated under steady state was subsequently subjected to dynamic tests. The field measurement campaign and the measurement results were previously described in details in Section 4.2. It was found to be difficult to satisfy all available sensor data. Only the N-related components, i.e. the concentrations of NH_4^+ , NO_3^- and NO_2^- near the outlet of the bioreactor and the N_2O emissions at the beginning, middle and end of the summer aeration package, and the DO concentrations near the outlet of the bioreactor were selected as calibration targets. The NH_4^+ , NO_3^- and DO concentrations were recorded by plant on-line sensors and the N_2O emissions were measured by an on-line analyser, but the NO_2^- concentration was measured by an off-line method at an interval of 1 hour during day time for 3 dry weather days and 2 wet weather days. The plant sensor data, i.e. NH_4^+ , NO_3^- and DO were also filtered by the Savitzky-Golay algorithm. The parameter values obtained after calibration are given in Table 4.2.

Table 4.2 Parameters of ASMG2d^a

Parameter	Description	Unit	Value in ASMG1 ^b	Value in ASMG2d
Conversion factors				
f_{S_i}	Production of S_i in hydrolysis	-	-	0
f_{X_i}	Fraction of X_i generated in biomass lysis	-	-	0.1
$i_{N,BM}$	N content of biomass	mg N/mg COD	0.086	0.07
i_{N,S_F}	N content of S_F	mg N/mg COD	-	0.03
i_{N,S_i}	N content of S_i	mg N/mg COD	-	0.033 ^c
i_{N,X_i}	N content of X_i	mg N/mg COD	-	0.02
i_{N,X_S}	N content of X_S	mg N/mg COD	-	0.04
$i_{P,BM}$	P content of biomass	mg P/mg COD	-	0.02
i_{P,S_F}	P content of S_F	mg P/mg COD	-	0.01
i_{P,S_i}	P content of S_i	mg P/mg COD	-	0
i_{P,X_i}	P content of X_i	mg P/mg COD	-	0.01
i_{P,X_S}	P content of X_S	mg P/mg COD	-	0.01
$i_{TSS,BM}$	TSS to COD ratio for biomass	mg TSS/mg COD	-	0.9
i_{TSS,X_i}	TSS to COD ratio for X_i	mg TSS/mg COD	-	0.75
i_{TSS,X_S}	TSS to COD ratio for X_S	mg TSS/mg COD	-	0.75
Precipitation and Redissolution				
k_{PRE}	P precipitation rate	l/[mg Fe(OH) ₃ xd]	-	1
k_{RED}	P redissolution rate	d ⁻¹	-	0.6
$K_{Alk,RED}$	Saturation coefficient for alkalinity	mmol HCO ₃ ⁻ /l	-	0.1 ^d
Heterotrophic processes				
$K_{Alk,H}$	Saturation coefficient for alkalinity (HCO ₃ ⁻)	mmol HCO ₃ ⁻ /l	-	0.1
$K_{NH_4,H}$	Saturation coefficient for ammonia (nutrient)	mg N/l	-	0.05
$K_{P,H}$	Saturation coefficient for phosphorus (nutrient)	mg P/l	-	0.01
$b_{\mu H}$	Coefficient b for Ratkowsky equation	-	0.0625	0.031 ^e
$c_{\mu H}$	Coefficient c for Ratkowsky equation	-	0.3	0.3 ^e
$T_{Max,H}$	Maximum temperature for Ratkowsky equation	°C	50	50 ^e
$T_{Min,H}$	Minimum temperature for Ratkowsky equation	°C	-20	-20 ^e
Y_H	Yield coefficient	mg COD/mg COD	0.67	0.625
η_{YH}	Anoxic reduction factor for yield	-	0.9	0.5 ^e
b_H	Maximum lysis rate	d ⁻¹	0.3	0.3 ^d
θ_{bH}	Coefficient θ for lysis rate equation	-	1.072	1.072
$K_{NO_x,H,b}$	Saturation coefficient for nitrate in lysis	mg N/l	-	0.5
$K_{O,H,b}$	Saturation/Inhibition coefficient for oxygen in lysis	mg O ₂ /l	-	0.2
$\eta_{H,b}$	Anoxic reduction factor for lysis	-	-	0.33

Note: a. Reference temperature is 15 °C; b. the parameter values are from Chapter 3; c. these ASM2d (Gernaey and Jørgensen, 2004a) parameters were calibrated by Amerlinck et al. (2013); d. these ASM2d (Gernaey and Jørgensen, 2004a) parameters are calibrated in this section; e. these are new ASMG2d parameters that are calibrated in this section.

Table 4.2 Parameters of ASMG2d^a (continued)

Parameter	Description	Unit	Value in ASMG1 ^b	Value in ASMG2d
Heterotrophic processes				
k_h	Maximum hydrolysis rate	d ⁻¹	2.89	5 ^d
θ_{kh}	Coefficient θ for hydrolysis rate equation	-	1.041	1.041
K_X	Maximum saturation coefficient for X_S	mg COD/mg COD	0.1	10 ^d
θ_{KX}	Coefficient θ for K_X temperature-dependency equation	-	0.896	0.896 ^c
$K_{NO_x,Hyd}$	Saturation/Inhibition coefficient for nitrate in hydrolysis	mg N/l	-	2 ^d
$K_{O,Hyd}$	Saturation/Inhibition coefficient for oxygen in hydrolysis	mg O ₂ /l	-	0.2
η_{Hyd}	Anoxic reduction factor for hydrolysis	-	0.4	0.8 ^d
η_{fe}	Anaerobic reduction factor for hydrolysis	-	-	0.2 ^d
q_{fe}	Maximum fermentation rate	d ⁻¹	-	2.12
θ_{qfe}	Coefficient θ for fermentation rate equation	-	-	1.072
K_{fe}	Saturation coefficient for fermentation of S_F	mg COD/l	-	20 ^d
$K_{NO_x,Ferm}$	Inhibition coefficient for nitrate in fermentation	mg N/l	-	0.1 ^d
$K_{O,Ferm}$	Inhibition coefficient for oxygen in fermentation	mg O ₂ /l	-	0.2
K_{A1}	Saturation coefficient for S_A in aerobic growth	mg COD/l	15 ^f	20 ^d
K_{F1}	Saturation coefficient for S_F in aerobic growth	mg COD/l	15 ^f	20 ^d
K_{OH1}	Saturation coefficient for oxygen in aerobic growth	mg O ₂ /l	0.2	1 ^d
K_{A2}	Saturation coefficient for S_A in denitrification of $NO_3^- \rightarrow NO_2^-$	mg COD/l	20 ^f	10 ^e
K_{A3}	Saturation coefficient for S_A in denitrification of $NO_2^- \rightarrow NO$	mg COD/l	20 ^f	10 ^e
K_{A4}	Saturation coefficient for S_A in denitrification of $NO \rightarrow N_2O$	mg COD/l	20 ^f	10 ^e
K_{A5}	Saturation coefficient for S_A in denitrification of $N_2O \rightarrow N_2$	mg COD/l	30 ^f	10 ^e
K_{F2}	Saturation coefficient for S_F in denitrification of $NO_3^- \rightarrow NO_2^-$	mg COD/l	20 ^e	10 ^e
K_{F3}	Saturation coefficient for S_F in denitrification of $NO_2^- \rightarrow NO$	mg COD/l	20 ^e	10 ^e
K_{F4}	Saturation coefficient for S_F in denitrification of $NO \rightarrow N_2O$	mg COD/l	20 ^e	10 ^e
K_{F5}	Saturation coefficient for S_F in denitrification of $N_2O \rightarrow N_2$	mg COD/l	30 ^e	10 ^e

Note: a. Reference temperature is 15 °C; b. the parameter values are from Chapter 3; c. these ASM2d (Gernaey and Jørgensen, 2004a) parameters were calibrated by Amerlinck et al. (2013); d. these ASM2d (Gernaey and Jørgensen, 2004a) parameters are calibrated in this section; e. these are new ASMG2d parameters that are calibrated in this section; f. these values are for K_S in ASMG1.

Table 4.2 Parameters of ASMG2d^a (continued)

Parameter	Description	Unit	Value in ASMG1 ^b	Value in ASMG2d
Heterotrophic processes				
$K_{N3NO,H}$	Inhibition coefficient for NO in denitrification of $NO_2^- \rightarrow NO$	mg N/l	0.5	0.5 ^e
$K_{N4NO,H}$	Inhibition coefficient for NO in denitrification of $NO \rightarrow N_2O$	mg N/l	0.3	0.3 ^e
$K_{N5NO,H}$	Inhibition coefficient for NO in denitrification of $N_2O \rightarrow N_2$	mg N/l	0.075	0.2 ^e
$K_{N2O,H}$	Saturation coefficient for N_2O in denitrification of $N_2O \rightarrow N_2$	mg N/l	0.05	0.3 ^e
$K_{NO,H}$	Saturation coefficient for NO in denitrification of $NO \rightarrow N_2O$	mg N/l	0.05	0.1 ^e
$K_{NO2,H}$	Saturation coefficient for nitrite in denitrification of $NO_2^- \rightarrow NO$	mg N/l	0.2	1 ^e
$K_{NO3,H}$	Saturation coefficient for nitrate in denitrification of $NO_3^- \rightarrow NO_2^-$	mg N/l	0.2	3 ^e
K_{OH2}	Inhibition coefficient for oxygen in denitrification of $NO_3^- \rightarrow NO_2^-$	mg O ₂ /l	0.2	1 ^e
K_{OH3}	Inhibition coefficient for oxygen in denitrification of $NO_2^- \rightarrow NO$	mg O ₂ /l	0.2	1 ^e
K_{OH4}	Inhibition coefficient for oxygen in denitrification of $NO \rightarrow N_2O$	mg O ₂ /l	0.2	1 ^e
K_{OH5}	Inhibition coefficient for oxygen in denitrification of $N_2O \rightarrow N_2$	mg O ₂ /l	0.2	1 ^e
η_{H2}	Anoxic reduction factor for denitrification of $NO_3^- \rightarrow NO_2^-$	-	0.3	0.3 ^e
η_{H3}	Anoxic reduction factor for denitrification of $NO_2^- \rightarrow NO$	-	0.6	0.3 ^e
η_{H4}	Anoxic reduction factor for denitrification of $NO \rightarrow N_2O$	-	0.8	0.5 ^e
η_{H5}	Anoxic reduction factor for denitrification of $N_2O \rightarrow N_2$	-	0.8	0.7 ^e
Autotrophic processes				
$K_{Alk,Aut}$	Saturation coefficient for alkalinity (HCO_3^-)	mmol HCO_3^- /l	-	0.1 ^d
$K_{P,Aut}$	Saturation coefficient for phosphorus (nutrient)	mg P/l	-	0.01
$b_{\mu AOB}$	Coefficient <i>b</i> for Ratkowsky equation of AOB growth	-	0.0255	0.0255 ^e
$b_{\mu NOB}$	Coefficient <i>b</i> for Ratkowsky equation of NOB growth	-	0.0235	0.0235 ^e
$c_{\mu AOB}$	Coefficient <i>c</i> for Ratkowsky equation of AOB growth	-	0.15	0.15 ^e
$c_{\mu NOB}$	Coefficient <i>c</i> for Ratkowsky equation of NOB growth	-	0.05	0.05 ^e

Note: a. Reference temperature is 15 °C; b. the parameter values are from Chapter 3; c. these ASM2d (Gernaey and Jørgensen, 2004a) parameters were calibrated by Amerlinck et al. (2013); d. these ASM2d (Gernaey and Jørgensen, 2004a) parameters are calibrated in this section; e. these are new ASMG2d parameters that are calibrated in this section.

Table 4.2 Parameters of ASMG2d^a (continued)

Parameter	Description	Unit	Value in ASMG1 ^b	Value in ASMG2d
Autotrophic processes				
$T_{Max,AOB}$	Maximum temperature for Ratkowsky equation of AOB growth	°C	50	50 ^e
$T_{Max,NOB}$	Maximum temperature for Ratkowsky equation of NOB growth	°C	57	57 ^e
$T_{Main,AOB}$	Minimum temperature for Ratkowsky equation of AOB growth	°C	-15	-15 ^e
$T_{Main,NOB}$	Minimum temperature for Ratkowsky equation of NOB growth	°C	-25	-25 ^e
Y_{AOB}	Yield coefficient for AOB	mg COD/mg N	0.18	0.18 ^e
Y_{NOB}	Yield coefficient for NOB	mg COD/mg N	0.06	0.1 ^e
η_{YAOB}	Anoxic yield factor for AOB	-	0.83	0.83 ^e
b_{AOB}	Maximum AOB lysis rate	d ⁻¹	0.028	0.028 ^e
b_{NOB}	Maximum NOB lysis rate	d ⁻¹	0.028	0.028 ^e
θ_{bAOB}	Coefficient θ for AOB lysis rate equation	-	1.116	1.116
θ_{bNOB}	Coefficient θ for NOB lysis rate equation	-	1.116	1.116
$\eta_{AOB,b}$	Anoxic reduction factor for AOB lysis	-	-	0.33
$\eta_{NOB,b}$	Anoxic reduction factor for NOB lysis	-	-	0.33
$K_{NOx,AOB,b}$	Saturation coefficient for nitrate in AOB lysis	mg N/l	-	0.5
$K_{NOx,NOB,b}$	Saturation coefficient for nitrate in NOB lysis	mg N/l	-	0.5
$K_{O,AOB,b}$	Saturation/Inhibition coefficient for oxygen in AOB lysis	mg O ₂ /l	-	0.2
$K_{O,NOB,b}$	Saturation/Inhibition coefficient for oxygen in NOB lysis	mg O ₂ /l	-	0.2
K_{FA}	Saturation coefficient for free ammonia (FA) in nitrification of NH ₄ ⁺ → NO ₂ ⁻	mg N/l	0.004	0.005 ^e
$K_{IFA,1}$	Inhibition coefficient for FA in nitrification of NH ₄ ⁺ → NO ₂ ⁻	mg N/l	1	0.1 ^e
$K_{IFNA,1}$	Inhibition coefficient for FNA in nitrification of NH ₄ ⁺ → NO ₂ ⁻	mg N/l	0.1	0.001 ^e
K_{FNA}	Saturation coefficient for free nitrous acid (FNA) in nitrification of NO ₂ ⁻ → NO ₃ ⁻	mg N/l	10 ⁻⁶	1×10 ⁻⁶ (e)
$K_{IFA,2}$	Inhibition coefficient for FA in nitrification of NO ₂ ⁻ → NO ₃ ⁻	mg N/l	0.5	1 ^e
$K_{IFNA,2}$	Inhibition coefficient for FNA in nitrification of NO ₂ ⁻ → NO ₃ ⁻	mg N/l	0.1	0.1 ^e
K_{OA1}	Saturation coefficient for oxygen in nitrification of NH ₄ ⁺ → NO ₂ ⁻	mg O ₂ /l	0.6	0.4 ^e
K_{OA2}	Saturation coefficient for oxygen in nitrification of NO ₂ ⁻ → NO ₃ ⁻	mg O ₂ /l	1.2	1 ^e

Note: a. Reference temperature is 15 °C; b. the parameter values are from Chapter 3; c. these ASM2d (Gernaey and Jørgensen, 2004a) parameters were calibrated by Amerlinck et al. (2013); d. these ASM2d (Gernaey and Jørgensen, 2004a) parameters are calibrated in this section; e. these are new ASMG2d parameters that are calibrated in this section.

Table 4.2 Parameters of ASMG2d^a (continued)

Parameter	Description	Unit	Value in ASMG1 ^b	Value in ASMG2 ^d
Autotrophic processes				
$K_{FNA,AOBden}$	Saturation coefficient for FNA in AOB denitrification	mg N/l	0.0006	1×10^{-6e}
$K_{FA,AOBden}$	Saturation coefficient for FA in AOB denitrification	mg N/l	0.0027	0.0021 ^e
$K_{NO,AOBden}$	Saturation coefficient for NO in AOB denitrification	mg N/l	1	0.1 ^e
$K_{O,AOBden}$	Saturation coefficient for oxygen in AOB denitrification	mg O ₂ /l	11.40	3.59 ^e
$K_{IO,AOBden}$	Inhibition coefficient for oxygen in AOB denitrification	mg O ₂ /l	0.035	5.01 ^e
$\eta_{AOBden1}$	Reduction factor for AOB denitrification of NO ₂ ⁻ → NO	-	0.5	0.3 ^e
$\eta_{AOBden2}$	Reduction factor for AOB denitrification of NO → N ₂ O	-	0.5	0.3 ^e
PAO processes				
$K_{Alk,PAO}$	Saturation coefficient for alkalinity (HCO ₃ ⁻)	mmol HCO ₃ ⁻ /l	-	0.1
$K_{NH4,PAO}$	Saturation coefficient for ammonia (nutrient)	mg N/l	-	0.05
$K_{P,PAO}$	Saturation coefficient for phosphorus (nutrient)	mg P/l	-	0.01
$b_{\mu PAO}$	Coefficient <i>b</i> for Ratkowsky equation	-	-	0.0256 ^e
$c_{\mu PAO}$	Coefficient <i>c</i> for Ratkowsky equation	-	-	0.17 ^e
$T_{Max,PAO}$	Maximum temperature for Ratkowsky equation	°C	-	50 ^e
$T_{Min,PAO}$	Minimum temperature for Ratkowsky equation	°C	-	-20 ^e
Y_{PAO}	Yield coefficient	mg COD/mg COD	-	0.625
Y_{PHA}	PHA requirement for X _{PP} storage	mg COD/mg P	-	0.2
η_{YPAO}	Anoxic reduction factor for yield	-	-	0.5 ^e
η_{YPHA}	Anoxic reduction factor for X _{PP} storage	-	-	0.5 ^e
b_{PAO}	Maximum X _{PAO} lysis rate	d ⁻¹	-	0.14
b_{PHA}	Maximum X _{PHA} lysis rate	d ⁻¹	-	0.14
b_{PP}	Maximum X _{PP} lysis rate	d ⁻¹	-	0.14
θ_{bPAO}	Coefficient θ for X _{PAO} lysis rate equation	-	-	1.072
θ_{bPHA}	Coefficient θ for X _{PHA} lysis rate equation	-	-	1.072
θ_{bPP}	Coefficient θ for X _{PP} lysis rate equation	-	-	1.072
$K_{NOx,PAO,b}$	Saturation coefficient for nitrate in lysis	mg N/l	-	0.5
$K_{O,PAO,b}$	Saturation/Inhibition coefficient for oxygen in lysis	mg O ₂ /l	-	0.2
$\eta_{PAO,b}$	Anoxic reduction factor for lysis	-	-	0.33

Note: a. Reference temperature is 15 °C; b. the parameter values are from Chapter 3; c. these ASM2d (Gernaey and Jørgensen, 2004a) parameters were calibrated by Amerlinck et al. (2013); d. these ASM2d (Gernaey and Jørgensen, 2004a) parameters are calibrated in this section; e. these are new ASMG2d parameters that are calibrated in this section.

Table 4.2 Parameters of ASMG2d^a (continued)

Parameter	Description	Unit	Value in ASMG1 ^b	Value in ASMG2d
PAO processes				
q_{PHA}	Maximum X_{PHA} storage rate	d^{-1}	-	2.45
θ_{qPHA}	Coefficient θ for X_{PHA} storage rate equation	-	-	1.041
$K_{A,PHAstor}$	Saturation coefficient for S_A in X_{PHA} storage	mg COD/l	-	5 ^d
K_{PP}	Saturation coefficient for X_{PP}/X_{PAO} ratio in X_{PHA} storage	mg P/mg COD	-	0.01
Y_{PO}	S_{PO4} released per X_{PHA} stored	mg P/mg COD	-	0.4
q_{PP}	Maximum X_{PP} storage rate	d^{-1}	-	1.23
θ_{qPP}	Coefficient θ for X_{PP} storage rate equation	-	-	1.041
$K_{P,PPstor}$	Saturation coefficient for S_{PO4} in X_{PP} storage	mg P/l	-	0.2
K_{IPP}	Inhibition coefficient for X_{PP}/X_{PAO} ratio in X_{PP} storage	mg P/mg COD	-	0.02
K_{MAX}	Maximum limit for X_{PP}/X_{PAO} ratio in X_{PP} storage	mg P/mg COD	-	0.34
$K_{O,PAO}$	Saturation coefficient for oxygen	mg O ₂ /l	-	0.2
K_{PHA}	Saturation coefficient for X_{PHA}	mg COD/l	-	2 ^d
$K_{I3NO,PAO}$	Inhibition coefficient for NO in denitrification of NO ₂ ⁻ → NO	mg N/l	-	0.5 ^e
$K_{I4NO,PAO}$	Inhibition coefficient for NO in denitrification of NO → N ₂ O	mg N/l	-	0.3 ^e
$K_{I5NO,PAO}$	Inhibition coefficient for NO in denitrification of N ₂ O → N ₂	mg N/l	-	0.2 ^e
$K_{N2O,PAO}$	Saturation coefficient for N ₂ O in denitrification of N ₂ O → N ₂	mg N/l	-	0.3 ^e
$K_{NO,PAO}$	Saturation coefficient for NO in denitrification of NO → N ₂ O	mg N/l	-	0.1 ^e
$K_{NO2,PAO}$	Saturation coefficient for nitrite in denitrification of NO ₂ ⁻ → NO	mg N/l	-	1 ^e
$K_{NO3,PAO}$	Saturation coefficient for nitrate in denitrification of NO ₃ ⁻ → NO ₂ ⁻	mg N/l	-	3 ^e
η_{PAO2}	Anoxic reduction factor for denitrification of NO ₃ ⁻ → NO ₂ ⁻	-	-	0.1 ^e
η_{PAO3}	Anoxic reduction factor for denitrification of NO ₂ ⁻ → NO	-	-	0.1 ^e
η_{PAO4}	Anoxic reduction factor for denitrification of NO → N ₂ O	-	-	0.2 ^e
η_{PAO5}	Anoxic reduction factor for denitrification of N ₂ O → N ₂	-	-	0.2 ^e

Note: a. Reference temperature is 15 °C; b. the parameter values are from Chapter 3; c. these ASM2d (Gernaey and Jørgensen, 2004a) parameters were calibrated by Amerlinck et al. (2013); d. these ASM2d (Gernaey and Jørgensen, 2004a) parameters are calibrated in this section; e. these are new ASMG2d parameters that are calibrated in this section.

The empirical modification of the aeration model allowed a significantly better fit of the DO and N₂O data, as shown in Figure 4.12.

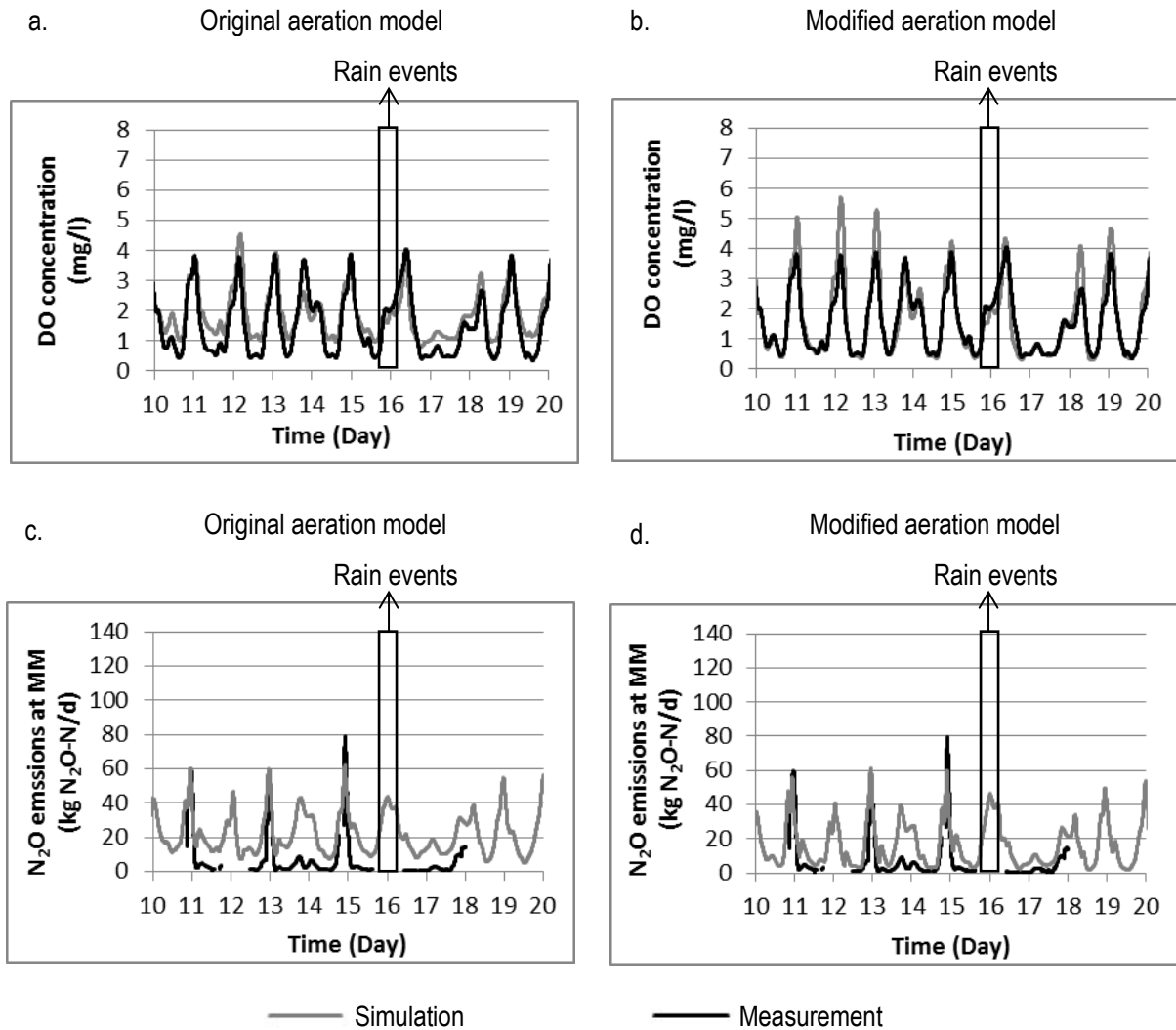


Figure 4.12 Comparison in terms of DO and N₂O simulation results between using original aeration model (a and c) and modified aeration model (b and d) (MM: the middle section of the summer aeration package).

4.3.2 Simulation results of a real WWTP

The simulated DO concentration near the outlet of the bioreactor is compared with the measurement data in Figure 4.13, showing good agreement. It is noteworthy that the aeration intensity used in these simulations is given by the air flow data of the plant. Figure 4.14 compares the dynamic simulation results of the NH_4^+ , NO_3^- and NO_2^- concentrations with their on-line measurements. Figure 4.15 compares the simulated and measured total N_2O emissions from different sections of the summer aeration package. In each section the off-gas N_2O measurement hood was installed for about one week (Section 4.2).

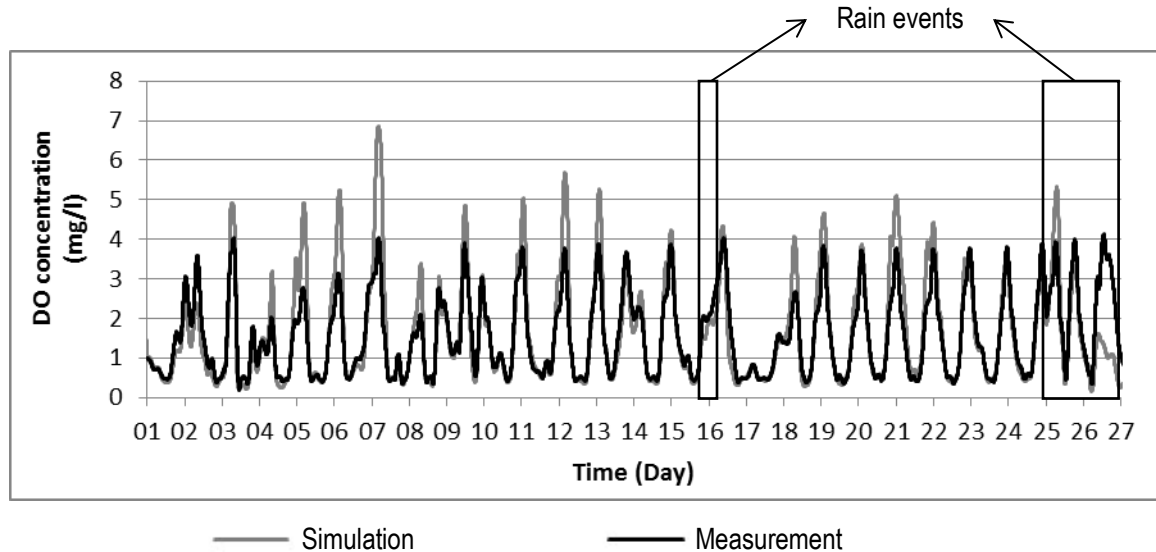


Figure 4.13 Comparison of the measured DO concentrations near the outlet of the bioreactor with the simulation results.

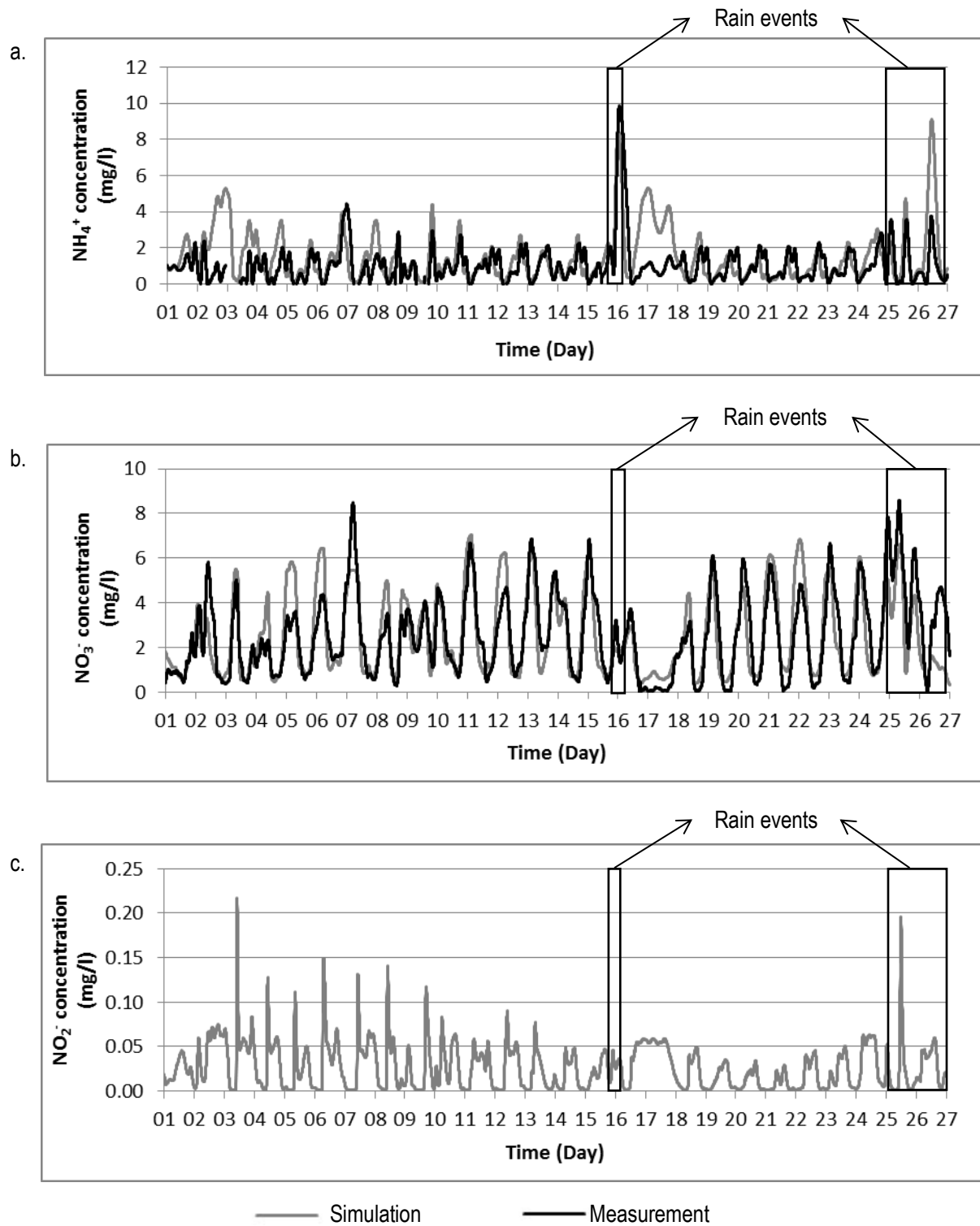
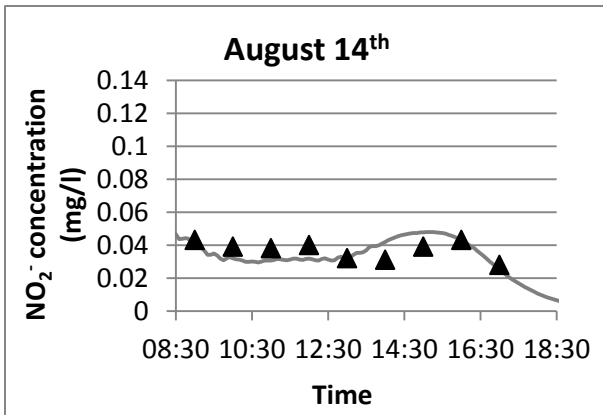
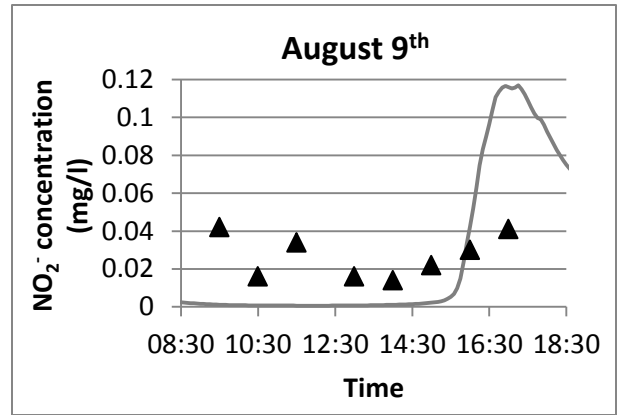
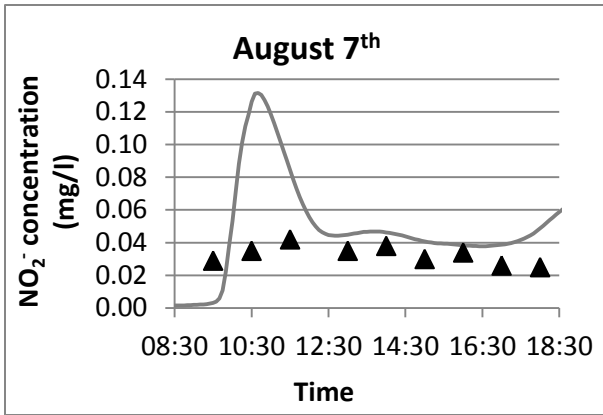


Figure 4.14 Comparison of the measurement results with the simulation results of NH_4^+ (a), NO_3^- (b) and NO_2^- (c).



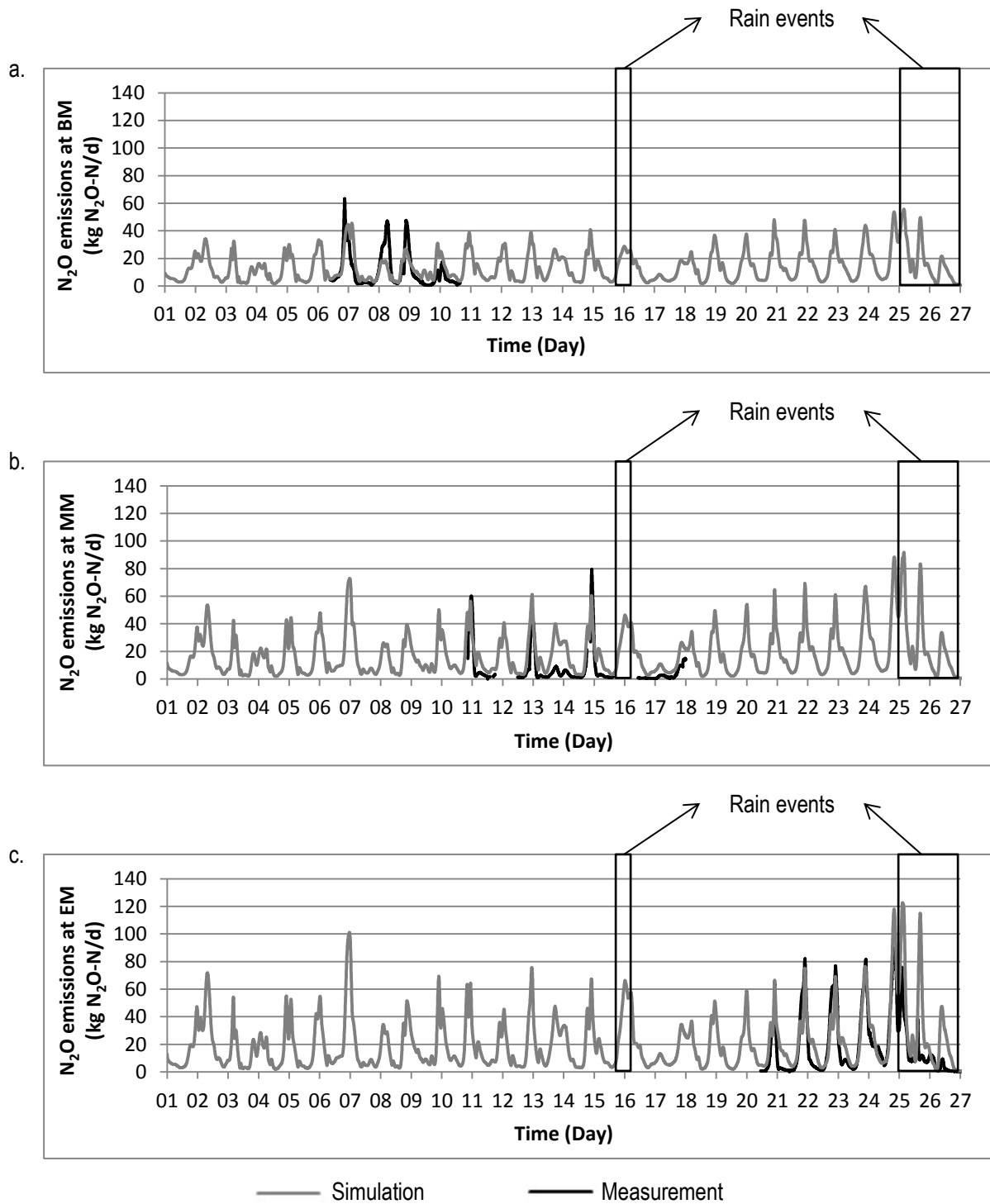


Figure 4.15 Comparison of simulated and measured N_2O emissions at the beginning (BM) (a), the middle (MM) (b) and the end section (EM) (c) of the summer aeration package.

I. Dry weather days

a. DO and liquid N-component concentrations

Under dry weather conditions, generally, the simulation of the DO, NH_4^+ and NO_3^- concentrations follows the dynamic trends of the measurement data really well. Occasionally, the simulation values showed large differences with the measurements. Regarding the NO_2^- simulation, August 14th shows good agreement with the measurement. However, the simulation results of August 9th differ a lot from the measurements.

b. N_2O emissions

The general dynamic profiles for N_2O emissions were captured by the model. By comparing the three graphs in Figure 4.15, the N_2O emissions from the end section of the summer aeration package are always higher than those from the middle and beginning sections of the summer package. Taking the same evaluation period of dry days as in Section 4.2, the simulated average N_2O emission rate is 12.4 kg N_2O -N/d at the beginning section, 17.9 kg N_2O -N/d at the middle section and 22.8 kg N_2O -N/d at the end section, while the corresponding measurement data are 10.7, 7.7 and 20.3 kg N_2O -N/d (Section 4.2). The main differences are found for the middle section due to the obviously higher simulation value on August 13th-14th. However, it is unclear whether this is due to modelling or measurement errors. The modelling error may come from the bioreaction model or the mixing model. One should note, however, that the simulation results on DO, NH_4^+ and NO_3^- agree well with the measurement data on August 13th-14th, indicating that the difference for the N_2O emission data is possibly caused by measurement errors. Indeed, during that measurement week the air temperature was considerably higher than during the other periods. The high air temperature caused the N_2O measurement

equipment to fail occasionally, e.g. on 12th August (Figure 4.15b). Therefore, such high air temperature may have introduced measurement errors also on August 13th-14th.

c. Errors

The errors could be due to either measurement or simulation errors. The model errors may originate from the fractionation model, the bioreaction kinetic model or the hydraulic mixing model (i.e. CSTRs). Measurement errors on N₂O emissions may be due to the high temperature, which affected the N₂O measurement equipment. Also, the measurement values of the plant on-line sensors and the off-line sampling may not reflect the real concentration in the bioreactor, because the flow in the ditch-type reactor is not completely mixed. For example, the locations where the sensors are placed or the wastewater was sampled may be dead zones resulting in different concentrations compared to the entire section (Rehman et al., 2013).

On August 5th and 6th, the simulated DO and NO₃⁻ concentrations are lower than the sensor data, although the NH₄⁺ concentrations are similar between the simulation and the measurement. This difference may be due to model deficiencies because among the three variables (DO, NO₃⁻ and NH₄⁺) there are two simulated variables (DO and NO₃⁻) that diverge from the measurements. As mentioned before, the reason could be related to the fractionation model, the bioreaction kinetic model or the hydraulic mixing model. Compared to the other dry days, the influent may contain less S₅ for these two days, which results in less DO consumption by aerobic substrate degradation and less NO₃⁻ reduction by heterotrophic denitrification. Another reason could be that the hydrolysis rate is decreased and aeration is possibly increased for these two days compared to other days.

However, for August 2nd, 16th and 17th, the DO and NO₃⁻ simulation concentrations are similar to the sensor data, while the simulated NH₄⁺ concentration fails. The differences

could again come from the simulation in terms of hydrolysis and aeration, but measurement errors could also be considered because among the three variables (DO, NO_3^- and NH_4^+) only one simulated variable (NH_4^+) diverges from the measurements. Moreover, the plant suffered from abnormal operational conditions on August 16th - 17th, causing difficulties to fit the measurements. Figure 8 compares the bioreactor internal recycling flows on August 16th-17th with the values of two normal dry days. The internal recycling from the middle ring to the inner ring (Q_A) was kept at its maximum value 60,000 m^3/d for the entire day of August 16th, while the internal recycling from the outer ring to the middle ring (Q_B) jumped to its lowest value 26,000 m^3/d for the entire day of August 17th. Such extreme operational conditions probably are outside the operational range of the model. Also, the flow regime may be changed under such conditions, so the mixing model, including the number and the size of the CSTRs, may have to be reconsidered for these days.

The NO_2^- simulation shows more peaks, compared to the off-line measurements. Actually, it is quite doubtful for the NO_2^- measurement to exhibit so little dynamics compared to the measurements of NH_4^+ and NO_3^- (Figure 5). The sampling interval may have missed the peaks or the sampling location may not reflect the concentration of the entire section due to the mixing problems (Rehman et al., 2013). Therefore, it is highly recommended to carry out on-line NO_2^- monitoring in future studies in order to better capture the temporal variation.

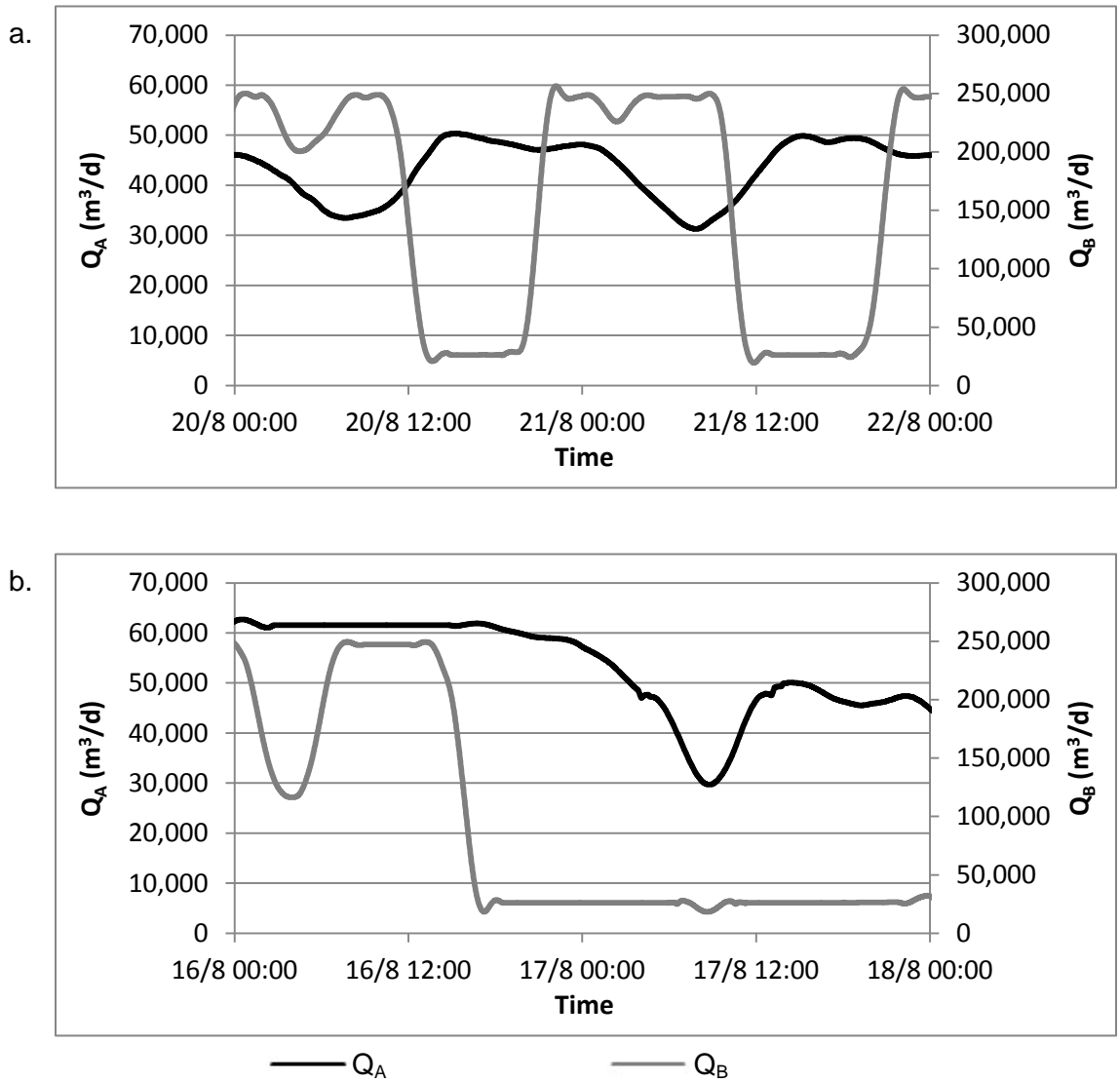


Figure 4.16 Comparison of the internal recycle flow rate from the middle ring to the inner ring (Q_A) and the internal recycling flow rate from the outer ring to the middle ring (Q_B) on August 16th-17th (b) with the values under two normal dry days (a).

II. Wet weather days

Two big rain events occurred during the measurement period. Unfortunately no N_2O measurement data could be collected for the first rain event happening on August 16th due to an equipment failure that night. However, the simulated DO , NH_4^+ and NO_3^-

concentrations agree well with the measurement data, which increases the credibility of the simulated N₂O emissions for the first rain event.

However, the N₂O emission during the second rain event was successfully recorded. The simulated N₂O emission rates show a decrease on August 26th, in agreement with the measurement which showed that the N₂O emission rate was lower under wet weather conditions than under dry weather conditions. However, generally speaking, compared to the simulation performance under dry weather conditions, the model does not demonstrate as good a simulation performance under wet weather conditions. The simulated N₂O emission rates are not as low as the measured values, while the simulated NO₃⁻ and DO concentrations are lower than the measured ones (Figure 4.13-4.15). The NO₂⁻ simulation was also not satisfying. With a higher DO level, more NO₃⁻ would be produced, with a concomitant reduction in the N₂O emission rate. Therefore, a larger *k_La* value was tried for the aeration packages under wet weather conditions. However, no improvement could be achieved. The reasons underlying the difference between the simulation and measurement data under rain events was further discussed in Section 4.3.3 “IV. Modelling under wet weather conditions”.

4.3.3 Discussion

I. Simulation of P removal

P removal is done in two ways at the plant: through both the biological and chemical pathways. The biological removal is further split into accumulation by PAO, which plays the dominant role in biological P removal, and assimilation as nutrient by the different bacterial species. By the chemical pathway P precipitates by additions of aluminium or iron. During the simulation of the Eindhoven WWTP, in order to make the simulated plant effluent PO₄⁻ concentration to resemble the plant on-line measurement data which was

around 0.5 mg/l, chemical dosage was used as the major approach to remove P, following Amerlinck et al. (2013).

It was found difficult to remove P biologically in the model (Amerlinck et al., 2014). There is competition for organics between heterotrophs and PAO. In ASM2d as modified by Gernaey and Jørgensen (2004), PAO store Polyhydroxyalkanoates (PHA) by assimilating S_A and there is no inhibition kinetic term of DO or NO_3^- , indicating that in the model the storage of PHA is feasible under aerobic, anoxic and anaerobic conditions. However, S_A is produced only from the fermentation of S_F under anaerobic conditions. Therefore, in order to guarantee that sufficient PHA is available for P accumulation, the fermentation of S_F and the hydrolysis of X_S have to be intensive under anaerobic conditions. However, heterotrophs can easily utilize S_F under aerobic and anoxic conditions, leading to a shortage of S_F and X_S to be transformed to S_A under anaerobic conditions. One possible solution is to measure the influent volatile fatty acids (VFA) in order to check whether S_A is correctly predicted by the influent fractionation model. Moreover, the initial concentration of X_{PAO} was also found to have influence on biological P removal (Zhang et al, 2010). Therefore, it is also necessary to analyze the bacterial composition in the bioreactor to better simulate the P removal. However, in this chapter the focus is on N_2O production, instead of P removal. The P-removal part is still kept as it was modelled by Amerlinck et al. (2013). This is aimed to provide a fundament for future studies and other applications.

Regarding the N-removal part, the model also showed a negligible contribution by PAO to N_2O production (< 0.01%). Although the models, i.e. ASM2d or ASMG2d, show difficulties to simulate of biological P removal, a sensitivity analysis on ASM2d showed that the P-related parameters had only a weak influence on the COD and N removal processes (Cosenza et al., 2014). On the other hand, research also found that the major contribution to denitrification is from heterotrophs instead of DPAO (Lemaire et al., 2006; Zeng et al.,

2003a; Zeng et al., 2003b). Therefore, little N₂O production should be expected from DPAO pathways.

II. N₂O sources

Table 4.3 compares the average contributions (%) of heterotrophs and AOB to the overall N₂O production in the different sections of the bioreactor. Positive values mean that N₂O has been produced while negative values represent consumption. Among the different N₂O production pathways, it is important to realize that the AOB can produce N₂O by NO₂⁻ reduction but they cannot remove N₂O by reduction to N₂, which means they always contribute to production, i.e. a positive value, of N₂O. Conversely, the heterotrophs can both reduce NO to N₂O and reduce N₂O to N₂. When the N₂O reduction rate is higher than the NO reduction, N₂O will be consumed, resulting in a negative value.

Table 4.3 Average contribution to N₂O production (%)

Location	Heterotrophs	AOB	Net production
Inner ring (Anaerobic tank)	-0.17	0.14	0.31
Middle ring (Anoxic tank)	-9.80	2.16	-7.64
Outer ring (Partial aeration tank)	-189.23	291.80	102.57
Summer package	50.74	173.25	223.98
Winter package	-25.45	12.35	-13.10
Non-aerated zones	-214.52	106.20	-108.32
Waterfall	1.75	3.01	4.76
Total	-197.11	297.11	100.00

The total N₂O production by AOB is 297.11% of the net production while the heterotrophs contribute by -197.11% which is two thirds of the N₂O production by AOB. These large values indicate that both AOB and heterotrophs are quite active in N₂O production or consumption. Generally, N₂O is produced through the AOB pathway but is consumed by heterotrophic denitrification. This finding is applicable to each section of the bioreactor except for the summer package aeration zone, the waterfall and the inner ring where the

heterotrophs' N₂O contribution exhibits near-zero or positive values, meaning that N₂O is produced or is little affected by heterotrophs here.

Among the different sections of the bioreactor, almost all N₂O is produced in the outer ring, 102.57%, while the waterfall and the inner ring make a very small contribution, 4.76% and 0.31% respectively. The middle ring shows a negative value which means that in this section more N₂O is consumed than produced. In the outer ring, the summer package is the only section with N₂O accumulation (223.98%), while the winter package, which is not aerated most of time, and the non-aerated zones show negative N₂O contributions. The large production of N₂O in the summer aeration package is mainly because of the AOB pathway that is contributing with 173.25%. This is the largest N₂O source among all sections and all bacteria species. The heterotrophs in the summer package also produce 50.74% of N₂O by denitrification. While this is small compared to the AOB pathway, it is the largest heterotrophic source for N₂O among all sections. According to the simulations the DO concentration in the summer package drops to around 1mg/l at night which may stimulate the heterotrophic production of N₂O. The N₂O produced by heterotrophs is almost all produced in the beginning section of the summer package, because here the DO drops to its lowest values, around 0.5 mg O₂/l at night compared to the middle and end sections. The non-aerated zone shows the second largest contribution to N₂O production, also by AOB, but the N₂O consumption by heterotrophs is much bigger, resulting in a negative percentage.

III. N₂O emissions

In this part of the discussion the focus is no longer on the production or consumption but on the transfer into the gas phase, i.e. the N₂O emission. About 93.29% of the total N₂O emissions happen in the outer ring. Based on the modelling results, the total on-site N₂O emission is 58.8 kgN/d on average, that in equivalent of CO₂ is 28 ton CO_{2,e}/d,

corresponding to an emission factor of 0.88% of the influent TKN load. IPCC (2013) assumes that the on-site N₂O emission is 3.2 g N₂O/person/year. The capacity of the Eindhoven WWTP is 750,000 PE. Therefore, using the same unit as IPCC (2013), the on-site N₂O emission is 45 g N₂O/person/year, indicating that the IPCC (2013) guideline may underestimate the N₂O emissions.

The summer package produces 90.70% of the total emissions while the winter package zone emits only 0.57%. The N₂O emitted due to the waterfall at the weir of the bioreactor is 5.94%. Figure 4.15 shows that the end section of the summer aeration package exhibits a higher emission rate than the beginning and middle sections, which could be related to the spatial distribution of the DO concentration. The average DO concentration of the three sections is below 2.5 mgO₂/l, but the end section has a higher average DO concentration (1.87 mgO₂/l) than the beginning and middle parts (0.93 mgO₂/l and 1.44 mgO₂/l), leading to higher N₂O production in the end part.

According to Table 4.3, the majority of N₂O is produced in the summer package by the AOB pathway, so most of the N₂O emissions are expected to come from this source. This finding agrees with the observation in Section 4.2 where, from a pure data analysis, it was proposed that the N₂O emissions measured at the summer package were mostly produced by AOB in the zone of the summer package. The difference with Section 4.2.2 is that the percentage of the AOB contribution is now calculated by a modelling exercise and it is much larger than the value calculated from the data analysis only. This is not unexpected, because the data analysis in Section 4.2.2 can only provide the minimal contribution of AOB to N₂O emissions. This finding suggests that a model-based analysis allows for better elucidation of the process than an analysis of measurement data alone.

Of course, it must be kept in mind that the values given by the model should also be interpreted carefully since no model is without errors. The real on-site N₂O emissions

should be lower than the simulated results, because the simulated N₂O emission is higher than the measurement under wet-weather days (Figure 4.15c). However, no big difference should be expected, because the rain events were only observed on August 15th, 25th and 26th, which are very short periods compared to the entire measurement campaign.

Besides the on-site N₂O emissions, there are also off-site N₂O emissions coming with the plant effluent and the waste sludge disposal. The plant effluent and the waste sludge contain residual N₂O, even after stripping in the bioreactor and the waterfall at the bioreactor outlet. However, compared to the N₂O emitted at the plant (58.8 kgN/d), this amount of off-site N₂O emission is very small, i.e. 3.0 kgN/d for the plant effluent and 0.1 kgN/d for the waste sludge.

There may also be indirect N₂O emissions due to off-site N conversion. The average TN load is 950 kg/d for the plant effluent and 2146 kg/d for the waste sludge. Using the estimation method and the default parameters of IPCC (2006), the indirect N₂O emission due to N conversion may be about 4.8 kgN/d for the plant effluent and about 9.1 kgN/d for the waste sludge disposal. Therefore, the sum of the direct and the indirect off-site N₂O emissions is 17.0 kg N₂O-N/d, which is lower than the on-site N₂O emissions (58.8 kgN/d) but is also non-negligible. The simulation results suggest that in order to mitigate the N₂O emissions, the emphasis should be given to the aeration control of the summer aeration package.

Summing up the on-site N₂O emission and the off-site N₂O emission, the final total N₂O emission is 75.8 kgN/d which is 35 ton CO_{2,e}/d.

IV. Nitrite effect

It is reported that NO₂⁻ affects N₂O production by AOB. Higher NO₂⁻ leads to higher N₂O production by AOB (Kampschreur et al., 2008; Pocquet et al., 2012). However, in this case,

the NO_2^- concentration increased under wet-weather days but the simulated N_2O emissions were still higher compared to the measurements (Figure 4.5d-e). A possible explanation is that it is the NH_2OH pathway, instead of the NO_2^- pathway, that is dominating the AOB N_2O production under wet-weather days. However, ongoing simulation work using the NH_2OH pathway still presents high N_2O emissions, similar to the NO_2^- pathway (Spérandio et al., 2014). Therefore, a possible solution is to combine the two pathways and make them have different N_2O productions under different weather conditions.

V. Modelling under wet weather conditions

A big difference was observed between the simulation and the measurements on August 25th and 26th, as mentioned before, which could be attributed to the fact that perhaps different pathways, i.e. the NH_2OH pathway and NO_2^- pathway, dominate AOB N_2O production under different weather conditions. The other reason could be related to the different influent compositions under wet weather conditions. When a storm starts, the sewer emits a first flush flow carrying a lot of suspended solids which is settled during dry days. Then, as the storm continues, the influent wastewater becomes more diluted compared to the wastewater under dry days, as it contains more rain water and fewer pollutants. Therefore, the wastewater composition under rain events is different compared to the dry weather conditions. The lower simulated DO concentration under rain events may possibly be due to a different wastewater fractionation, for example, higher f_{XI} , should be used (Choubert et al., 2013). The flow regime will be changed under wet weather conditions which will affect the mixing and the aeration in the plant (Vanrolleghem et al., 2014). Therefore, it is suggested to use a different mixing model, e.g. re-designing the number and the size of CSTRs, under wet weather conditions. All this requires however additional experiments to further analyze the composition of organic substrate and extra

tracer tests or computational fluid dynamics (CFD) studies to elucidate the flow regime under rain events. Given the limited data available for wet weather conditions, this should be subject of further research.

4.4 Conclusion

- The intensive dynamic full-scale measurement campaign helps to improve the understanding of N_2O emissions. A one-month measurement campaign carried out at the Eindhoven WWTP (The Netherlands) showed that N_2O emission is high in high NH_4^+ and intermediate DO (2.5 mg O_2/l in this thesis) conditions, while the NO_3^- production is increased with an increase in DO concentration.
- Different control strategies applied under different weather conditions have impacts on N_2O emissions. The NH_4^+ -DO cascade control strategy, which is the dominant strategy under dry weather days, leads to high N_2O emissions, because its feedback and low-gain properties cause a delay between increasing the aeration and detecting the increase of the NH_4^+ concentration. The inflow-based feedforward control, which is switched on during wet weather conditions, leads to lower N_2O emissions, because it increases the aeration before the bioreactor receives the NH_4^+ peak.
- An ASMG2d model was built to include N and P removal and also N_2O productions from the heterotrophic denitrification, the PAO denitrification and the AOB pathway. The simulation results in dry weather conditions agree well with the measurement data, while the simulation results during high-flow conditions are not as satisfactory as those during dry weather days (i.e. normal-flow conditions), indicating that the two pathways of AOB N_2O production, i.e. the NH_2OH oxidation pathway and the NO_2^- reduction pathway, should be integrated in one model, dynamically modelling the contribution of the different AOB pathways to the N_2O production in changing conditions. It also indicates that the flow

regime, i.e. the mixing, during wet weather conditions, may be different from that in dry weather conditions, indicating that a different mixing model may have to be used for wet weather flow situations.

- The process is better elucidated by using a model than by using an analysis purely based on measurements. The model can calculate the N₂O emissions or productions from different groups of bacteria and calculates contributions at all locations of the WWTP. This would be much more difficult for a field measurement.
- Both the analysis based on measurement data and modelling revealed that N₂O is significantly produced by AOB in the aerated zone. The results suggest that the focus should be given to the aeration in the outer ring when aiming at mitigating N₂O emissions. The role of heterotrophs in the net production of N₂O has been highlighted, including that up to two thirds of the produced N₂O is denitrified heterotrophically. This significantly reduces N₂O emissions.
- It is suggested to add the current NH₄⁺-DO cascade control strategy with an extra NH₄⁺ sensor at the upstream of the bioreactor to detect NH₄⁺ peaks and increase the aeration in advance. This idea will be tried out in future work.

5 Conclusions and perspectives

The major focus of this thesis was to investigate N₂O emissions from WWTPs, both within the context of the whole plant Benchmark Simulation Model No.2 (BSM2) and a real large-scale plant i.e. the Eindhoven WWTP in the Netherlands. The thesis also studied the performance of WWTPs, including effluent quality, operational cost and GHG emissions, under different weather conditions.

Both field measurements and mathematical model simulations were used in order to analyze the spatio-temporal variations of N₂O emissions and develop new ASM models to allow modelling N₂O production by both heterotrophs and ammonia oxidizing bacteria (AOB). Based on this experimental and modelling work, control strategies were proposed to better deal with the trade-off among effluent quality, operational cost and GHG emissions.

This thesis was conducted within the framework of the Flanders-Québec TECC project funded by the Québec Ministry of Economic Development, Innovation and Exports (MDEIE) on wastewater treatment and climate change and has also been contributing to the research carried out by the IWA Task group on modelling of GHG emissions.

5.1 Conclusions

5.1.1 Full-scale measurement experience

An on-line one-month intensive measurement campaign regarding N₂O emissions from the aeration zone of bioreactors was carried out at the Eindhoven WWTP, the Netherlands. The whole experimental campaign included dry and wet weather days and under changing

weather conditions the plant adjusted its control strategies to manipulate aeration. Such a variety in plant operation provides an opportunity to perform a delicate analysis of the intensive data set of N_2O emissions and other variables, allowing improving the understanding of N_2O emissions, next to providing data for model calibration.

Usually field measurements carried out at a real plant will suffer from emergent and unexpected situations which may cause measurement failures or untrustable data. Therefore, besides recording the measured data of the studied components, it was found very useful to also record the operation status of the measurement equipment. In this thesis this operation status of the equipment (Emerson) was stored as log files. With the help of these log files, the periods of abnormal operation of the equipment (due to excessive temperatures in summer 2012) could be identified and the untrustable data recorded under those abnormal operations could be deleted.

5.1.2 DO effect on AOB denitrification

Experimental data showed that the N_2O production by AOB is stimulated by high NH_4^+ concentrations and intermediate DO concentrations (2.5 mg O_2/l in this study), while the NO_3^- production keeps increasing as DO is increased. These findings supported the proposal that a modified Haldane term should be used to describe the DO effect in an AOB denitrification model whose original kinetic equation of DO effect was a simple Monod term (Mampaey et al., 2013). The DO effect on NO_3^- production can remain to be expressed as a Monod term. Compared to the original Haldane kinetics the way the modified Haldane term has been written mathematically in this thesis has the advantages that its parameters can be expressed by DO “half-saturation concentrations”, while at the same time getting μ_{max} as its maximum value.

5.1.3 Model calibration and validation

Two types of ASMs were studied in this thesis to describe the N₂O production and emission during the bioreaction. One is the ASMG1 model, including the original extension, called ASMG1, and the subsequently modified ASMG1. These models are mainly based on ASM1 and describe the N and C removal with a special focus on N₂O production by heterotrophs and AOB. The other type of ASM model is the ASMG2d model which is mainly based on the ASM2d model and describes the N, P and C removal with a special consideration of N₂O production by heterotrophs, PAO and AOB. In both ASMG1 and ASMG2d, the N₂O production by AOB follows the NO₂⁻ reduction pathway, i.e. the AOB denitrification model (Mampaey et al., 2013). Both ASMG2d and the modified ASMG1 use the aforementioned modified Haldane term to describe the DO effect in the AOB denitrification model while the original ASMG1 uses the original Monod term of Mampaey et al. (2013).

Both ASMG1 models were calibrated and validated by using the BSM2 whole plant model that is considered to represent realistic plant behavior (so-called ASMG1-BSM2). Both the original and modified ASMG1-BSM2 models were successfully calibrated to meet the fitting requirements of predicting a 0.5% N₂O emission factor. At the same time the calibrated model predicts the effluent quality and operating costs of the original BSM2 whole plant benchmark model, thus allowing to conclude that ASMG1-BSM2 provides realistic simulation of a nitrogen removal plant. The validation of the model run under three control strategies was also successful according to the results of effluent quality and operational cost as published for the finalized ASM1-BSM2 conditions (Nopens et al., 2010). Further evaluation of the two calibrated ASMG1-BSM2 models under dynamic conditions showed that they both can follow well the ASM1-BSM2 dynamics.

Following a calibration procedure similar to the one followed for ASMG1-BSM2, the

ASMG2d model was calibrated based on a 1-month measurement campaign at a full scale WWTP, i.e. the Eindhoven WWTP in the Netherlands. The original aeration model of the ASM2d-based Eindhoven model by Amerlinck et al. (2013) was modified to improve the simulation of DO, in particular to better approximate the low DO concentrations observed under low air flow rates. The calibration result showed that under dry-weather days, the dynamic simulation results meet the calibration requirements on both on-line (NH_4^+ , NO_3^- and DO concentration) and off-line data (NO_2^- concentration) collected near the outlet of the bioreactor. Importantly in view of this thesis' objectives the simulation results also fit the N_2O emissions measurements collected at different sections of the so-called summer aeration package area in the WWTP.

Under wet-weather days, the simulation result was not as satisfactory as that under dry-weather days. The reason could be due to the fact that the alternative pathway, i.e. the NH_2OH oxidation pathway and not the NO_2^- reduction pathway should be used under these weather conditions. The change of the flow regime may also contribute to the simulation errors. Further studies will be needed to confirm these possibilities. Finally, note that although the description of phosphorus dynamics is not the focus of this thesis, the modelling of P removal was still included in the model (i.e. ASMG2d) because the plant is removing P both by chemical but also some biological processes. The calibration effort remained limited to achieving an approximation of the average effluent phosphate concentrations.

Through the calibration of ASMG1 and ASMG2d, useful experience was obtained regarding future N_2O -related ASM model calibrations on full-scale data. The key idea behind the adopted procedure is to first calibrate the aeration and the C submodels and only then move on to the calibration of the N submodels.

5.1.4 Model discrimination

The two ASMG1 models implemented in BSM2 (the original and modified ASMG1-BSM2) showed little difference in average values of effluent quality, operating costs and net N₂O production and emission rates under each scenario. However, a significant difference showed up when studying the N₂O reaction rates by the different bacterial groups and the dynamic N₂O emissions under control strategies and, surprisingly, also under cold weather conditions. It is suggested to take advantage of the reported difference under dynamic conditions to achieve model discrimination. This encourages more dynamic N₂O data collection in view of model discrimination. One feasible plan is to organize several short-term measurement campaigns over a whole year to cover the important seasonal variations in N₂O emissions.

While both traditional and modified ASMG1 could achieve good reproduction of the BSM2 simulations, for the simulation of the Eindhoven WWTP, the modified Haldane term had to be selected to describe the DO effect on AOB denitrification in ASMG2d. This selection was based on experimental observations as mentioned in section 5.1.2, i.e. the N₂O emission suddenly decreases when DO is increased above 2.5 mg O₂/l. This model choice is supported by good simulation results for dry-weather days. However, the poor simulation results related to rain events suggested that perhaps different models or kinetic terms should be used to simulate the N₂O emission under wet-weather conditions. This should be subject of future work.

5.1.5 Contribution from AOB denitrification

Thanks to the calibrated models, the processes could be better elucidated than if only an analysis of the measurement data was conducted. The model gives a more accurate answer on the actual values and can remove the complex interactions with other

processes such as mixing, mass transfer, and the large number of bioprocesses. The model for instance calculates the N_2O emission or production by other bacterial groups, i.e. heterotrophs and PAO, and allows calculating all contributions at all locations of the WWTP, including on-site and off-site emissions. This would be much more difficult for an analysis based on field measurements alone.

In contrast to ASMG1 which models N_2O production by both heterotrophic and AOB pathways, ASMN (Hiatt and Grady, 2008) only includes the N_2O production by heterotrophs. This was the original implementation of N_2O production in BSM2 (the so-called ASMN-BSM2, Flores-Alsina et al., 2011). The comparison between the results of ASMN-BSM2 and ASMG1-BSM2 revealed that little difference occurs at the level of effluent quality and operating cost. On the other hand, the N_2O emission factor is increased significantly when including AOB denitrification (ASMG1). This is because when N_2O is produced by AOB's, they cannot remove it. The only way produced N_2O can be removed is by consumption by heterotrophs, which can reduce N_2O to N_2 , under anoxic conditions.

Both the original and modified ASMG1 models show more N_2O emissions in summer than in winter which is consistent with the full-scale observations of Daelman et al. (2013). This result was shown to be related to the temperature dependency of bacterial activity. The accumulation of N_2O in summer is mainly due to the increased AOB pathway activity, while the net N_2O production by heterotrophs does not change too much all year round. These results indicate that AOB is a major contributor to the N_2O emissions in terms of both quantity and variation, whereas heterotrophs can play an important role to reduce the emission of N_2O produced by AOBs.

This conclusion is further supported by the full-scale measurements and simulation of the Eindhoven WWTP. The phenomena observed from measurements and the analysis of the

modelling results showed that the AOB pathway in the summer package was the main producer of the N_2O while the heterotrophic denitrification of the produced N_2O in the non-aerated zone of the outer ring led to the overall observed net production of N_2O consumption that was 66.7% of the net N_2O production by AOB. At the Eindhoven WWTP the PAO played a negligible role in N removal and N_2O production. N_2O was basically emitted at the summer aeration package. The results suggest that in this plant attention should be focused on the aeration in the outer ring when trying to reduce the N_2O emissions. More discussion regarding control strategies can be found in section 5.1.7.

5.1.6 N_2O emissions under wet-weather conditions

Measurement data at the Eindhoven WWTP showed that under wet-weather conditions the N_2O emission is reduced. It was also found that the fraction of NH_4^+ being removed was lower under rain events.

A delicate analysis on the data set showed that different control strategies applied under different weather conditions had a significant impact on N_2O emissions. For the studied full-scale WWTP of Eindhoven, compared to the NH_4^+ -DO cascade control strategy which is the dominant strategy for aeration manipulation under dry-weather conditions, the inflow-based feedforward control which is switched on under hydraulic shocks led unexpectedly to lower N_2O emissions, especially in terms of lower N_2O emission peaks.

The difference in performance of N_2O emissions under the different control strategies is basically due to timing, i.e. whether the system takes actions, i.e. amplifying the aeration, before or after the aeration zone receives NH_4^+ peaks. The NH_4^+ -DO cascade control is a low-gain feedback controller, and there is thus a delay between detecting the rise of NH_4^+ concentration and increasing the aeration. Such delays cause a transient condition with high NH_4^+ and intermediate DO concentrations, which stimulates N_2O emission.

Conversely, the inflow-based feedforward control makes the DO concentration increase before the NH_4^+ peak hits the bioreactor, resulting in lower N_2O emissions. Other reasons like decreased biomass concentration in the bioreactor and a shorter hydraulic retention time may also contribute to lower N_2O emissions under wet weather conditions.

However, when interpreting the effect of rain events in the virtual case study with ASMG1-BSM2, a different result is obtained. When using a new 609-day influent file with 16% more rain events generated to account for future conditions under climate change, only little changes in N_2O emissions compared to the current influent conditions could be shown. One must realize, however, that these N_2O emission values obtained with ASMG1-BSM2 are yearly average values. When investigating the effect of wet-weather conditions on N_2O emissions specific rain events should be picked up for analysis, instead of just taking an average evaluation.

5.1.7 Control strategies

After model calibration and validation of the modified ASMG1 in the framework of BSM2, different scenarios and strategies were proposed with a combined consideration of GHG emissions, effluent quality, operational cost and hydraulic shocks.

The effect of the spatial distribution of DO on reducing N_2O emissions was confirmed by the separate DO strategy which controls DO concentration in each aerobic tank with an individual DO controller and setpoint. This separate DO strategy achieves the largest reduction in N_2O emissions, i.e. the N_2O emission is reduced by 76.2% compared to the open-loop scenario. On the other hand, it also shows the worst values in terms of OCl, EQI and NH_4^+ violation among all studied control strategies, clearly indicating the compromise that has to be sought.

In contrast, the NH_4^+ -DO cascade control has a poor performance in terms of controlling N_2O emissions (almost equal to those of the open loop), but its OCI value is the lowest (reduced by 9.4% compared to the open loop) and there is almost zero NH_4^+ violation. This is due to the fact that its aeration energy saving purpose has a tendency to cause intermediate DO conditions which are beneficial for N_2O production by AOB.

With this insight, a cascade plus 1 DO control strategy was proposed. It proved to have the advantages of N_2O mitigation, as the separate DO strategy, and effluent quality control and energy saving, as the pure NH_4^+ -DO cascade controller. The N_2O emission of this cascade plus 1 DO control strategy is in between the values of the separate DO strategy and the pure NH_4^+ -DO cascade control strategy, showing a reduction of 44.1% compared to that of the open loop. Its OCI value is also between the values of the separate DO strategy and the pure NH_4^+ -DO cascade control strategy. Its effluent NH_4^+ violation is negligible too.

Subsequently, this cascade plus 1 DO strategy was coupled with two wet weather control strategies, i.e. step feeding and sludge recycling control. The two extended strategies inherit the advantages of the cascade plus 1 DO strategy, showing similar EQI, OCI and GHG emissions as the cascade plus 1 DO strategy. However, compared to the other strategies they also show better controls of the TSS violations caused by hydraulic disturbance of the settling process. With the proposed influent file reflecting climate change impacts such as more intense rainfall, the TSS violations under either the open loop or closed loop strategies are increased. The two extended strategies are, however, able to handle this challenge. The strategy extended with step feeding lowers the TSS violation by 30.3% and the strategy extended with sludge recycling control lowers the TSS violation by 19.0% compared to that of the open-loop scenario.

However, these control strategies did not fully consider the impacts of the timing on the process conditions on the N_2O emissions. Indeed, according to the observations at the Eindhoven WWTP the N_2O emission was not always kept at high levels but was actually only increased under NH_4^+ peaks. The model-based analysis indicated that the slow reaction of the cascade controller led to conditions of high NH_4^+ and intermediate DO concentrations that lead to peak N_2O emissions. Therefore, to counter this timing issue it is suggested to put a NH_4^+ sensor upstream of the aeration zone, i.e. in the anoxic tank, with the objective of detecting an incoming NH_4^+ peak, and can work individually or together with the downstream NH_4^+ sensor which is already used in the current cascade feedback controller of the Eindhoven WWTP. When the upstream NH_4^+ detects an upcoming NH_4^+ peak, the DO setpoint of the aeration zone can be increased prior to the arrival of the NH_4^+ peak in the aeration zone, while under normal NH_4^+ loading the plant can still work under the current cascade feedback controller to realize the purpose of energy saving and effluent quality control.

5.2 Perspectives

5.2.1 A unified model of AOB N_2O production

The current general consensus is that N_2O production by AOB can be attributed to two pathways, i.e. the NH_2OH oxidation pathway and the NO_2^- reduction pathway, possibly concomitantly. Future work should include evaluating the contribution of the two pathways to the total N_2O production through experimental and modelling work.

Regarding the modelling approach, work has already been done to simulate the bioreactor in full-scale WWTP by applying different models which use different pathways, either NH_2OH oxidation pathway or NO_2^- reduction pathway. Two SBR, one UCT process and

one oxidation ditch have been tested, see the paper of Spérandio et al. (2014) in Appendix J. The result showed that none of the proposed models is able to describe all the studied systems, which suggests that the activity of each pathway is dependent on reactor conditions. Considering the simulation results of the Eindhoven WWTP under dry and wet weather conditions, it may be that a switch between the two pathways is the only solution to describe the collected data under all weather conditions. It can thus be concluded that models are required that can integrate the two pathways of AOB N_2O production and the scientific community is about to achieve this. For instance, a model integrating the two pathways has just been proposed by Ni et al. (2014), but it must be stated that the concept of Ni et al. (2014) based on electron carriers is quite different from traditional bioreaction kinetic models and may not be that easy to be accepted by the wastewater modelling community. Also, this new concept needs further validation. Besides, a model integrating the two pathways of AOB N_2O production could also be built following the traditional concept. Such model does not use the competition between electron carriers but expresses the electron transfer directly among the pollutant components with kinetic relations based on component concentrations to describe the switch between pathways (Spérandio, personal communication at WWTmod2014). Later on, these two kinds of integrated models, i.e. using either the electron carriers or traditional concepts, should be compared and evaluated by applying them to full-scale or lab-scale studies. Through such efforts a unified or an almost unified model regarding the AOB N_2O production will be obtained.

5.2.2 Wet-weather studies

In contrast to dry-weather conditions, the plant behavior under wet-weather conditions is more irregular, causing difficulties to simulate plant performance. As mentioned above the unsatisfactory simulation of N_2O emissions under rain events could be due to the fact that

a different AOB pathway dominates the N_2O production under wet-weather conditions. This would require a model that is able to switch among the two AOB pathways, i.e. NH_2OH oxidation pathway and NO_2^- reduction pathway, under dry and wet weather conditions. The underlying mechanism will have to be elucidated but the time evolution of the concentrations of NH_4^+ and DO seem good candidates for this.

The flow regime under hydraulic shocks is different from that under dry-weather conditions which indicates that the mixing model, e.g. the number and the size of the CSTRs, may have to be re-assessed during wet-weather conditions. The effect of different mixing on aeration, N_2O production and other aspects may thus have to be estimated as well.

The variation under rain events is fast and transient demanding experimental studies that focus on fast dynamics. In other words, high-frequency monitoring is required. Given such fast dynamics, the design of control strategies should also take into account the system variation. The strategies for N_2O mitigation proposed for the Eindhoven plant should be tried out.

5.2.3 Sensitivity analysis of ASMG2d

An on-going study in which the ASMG2d model is implemented in the Benchmark Simulation Model No.1 extended with P-removal (ASMG2d-BSM1) showed that the initial values of the ASMG2d components in the bioreactors have an effect on the final results, even under steady-state simulation. This is a special result probably related to nonlinearities in the model that warrants further analysis as this is not often observed with activated sludge models. To this end, a sensitivity analysis on the initial values of ASMG2d components will be of great interest. A set of critical variables should be selected based on simulation experience. The results of the sensitivity analysis will not only explain the initial

value problem but it will also provide important information for the calibration of ASMG2d when applying it to other WWTPs.

5.2.4 Other GHGs besides N₂O

Besides N₂O the gas measurement equipment (Emerson) has also recorded the volume concentration (ppm) of other types of gases, i.e. CO₂, CH₄ and O₂. The full-scale measurements at the Eindhoven WWTP showed that the emission of CH₄ was around 50 ppm, i.e. in a similar magnitude as N₂O. The GWP of CH₄ is 32 (IPCC, 2013). Therefore, it will be interesting to also take these CH₄ emissions into account. The Eindhoven WWTP has no sludge digester where CH₄ is produced and thus, no CH₄ would enter the plant from internal recycles of sludge digestion reject water. The CH₄ may be produced in the plant, e.g. in the primary and the secondary settlers, the sludge recycling line and the anaerobic tank (Czepiel et al., 1993; Daelman et al., 2013b). However, a population of methanogens should be maintained there, which needs further verification. Experiments will thus have to be conducted to clarify these observations.

The emission of CO₂ was approximately 100 times that of the CH₄ and N₂O emissions, i.e. around 35,000 ppm. Of course CO₂ is a much less powerful GHG compared to CH₄ and N₂O, but such a huge amount of emission indicates that the CO₂ emission from the bioreactors should be rethought and examined carefully. Although most of the emitted CO₂ will be considered short-term carbon cycle CO₂ and will thus not be included in the total GHG emission according to the IPCC (2007), it will also contain considerable amounts of fossil CO₂ (Law et al., 2013) that should be accounted for. Also, some researchers also suggest that the biogenetic CO₂ should not be excluded from the GHG evaluation framework (EPA, 2013) as from a global warming perspective no difference should be made between these two types of CO₂.

Another gas which may deserve further studies is NO which can also be a product of heterotrophic denitrification and also occurs in AOB N₂O production. However, NO is unstable and is easily oxidized into NO₂ which is a gas leading to acid rain and photochemical smog. The instability of NO also brings difficulties in measurements. Therefore, one may have to measure both NO and NO₂ in the emitted gas. Spérandio et al. (2014) indicated that measurement of NO can help elucidating which pathway is dominant in AOB N₂O production.

5.2.5 Integrated models

This thesis only focused on GHG emissions from WWTPs, without consideration of GHG emissions from sewers and rivers. However, the sewer, the WWTP and the river constitute an integrated system and there are important interactions among them. For example, the WWTPs receive wastewater from sewer systems, so the design and the operation of a sewer system will change the wastewater composition and thus affect WWTP performance. Besides, there is also GHG production and emission from the sewer system, like CH₄. Studies in a view of the sewer-plant-river integrated system have already been carried out at levels of benchmarks and real plants (Benedetti et al., 2013; Guo et al., 2012). However, there is still a long way to get a good understanding of the GHG emissions from the integrated system. More work needs to be done, including data collection about GHG emissions from the three subsystems (sewers, WWTPs and rivers) and model development to include GHG productions in such a big framework. Work is ongoing within the framework of the IWA Task Group on GHG emissions.

References

- Aboobakar A., Cartmell E., Stephenson T., Jones M., Vale P. and Dotro G. (2013) Nitrous oxide emissions and dissolved oxygen profiling in a full-scale nitrifying activated sludge treatment plant. *Water Research*, 47 (2), 524-534.
- Ahn J.H., Kim S., Park H., Rahm B., Pagilla K. and Chandran K. (2010) N₂O emissions from activated sludge processes, 2008a-2009: Results of a national monitoring survey in the United States. *Environmental Science and Technology*, 44 (12), 4505-4511.
- Ahn J., Daidou T., Tsuneda S. and Hirata A. (2001) Metabolic behavior of denitrifying phosphate-accumulating organisms under nitrate and nitrite electron acceptor conditions. *Journal of bioscience and bioengineering*, 92 (5), 442-446.
- Adouania N., Lendormia T., Limousya L. and Sirea O. (2010) Effect of the carbon source on N₂O emissions during biological denitrification. *Resources, Conservation and Recycling*, 54 (5), 299-302.
- Alex J., Benedetti L., Copp J., Gernaey K.V., Jeppsson U., Nopens I., Pons M.-N., Rieger L., Rosen C., Steyer J.P., Vanrolleghem P.A. and Winkler S. (2008). Benchmark Simulation Model no. 1 (BSM1).
<http://www.iea.lth.se/publications/Reports/LTH-IEA-7229.pdf>.
- Ali T.U., Ahmed Z. and Kim D. (2013) Estimation of N₂O emission during wastewater nitrification with activated sludge: Effect of ammonium and nitrite concentration by regression analysis. *Journal of Industrial and Engineering Chemistry*.
<http://dx.doi.org/10.1016/j.jiec.2013.10.042>.
- Alinsafi A., Adouani N., Béline F., Lendormi T., Limousy L. and Sire O. (2008) Nitrite effect on nitrous oxide emission from denitrifying activated sludge. *Process Biochemistry*, 43 (6), 683-689.

- Åmand L., Olsson G. and Carlsson B. (2013) Aeration control – a review. *Water Science and Technology*, 67 (11), 2374-2398.
- Amerlinck Y., Flameling T., Maere T., Weijers S. and Nopens I. (2013). Practical application of dynamic process models for wastewater treatment plant of optimization: work in progress. In proceedings of the WEFTEC 2013 - 86th Annual Water Environment Federation Technical Exhibition and Conference, Chicago, USA, October 5-9 2013.
- Ashrafi O., Yerushalmi L. and Haghghat F. (2013) Greenhouse gas emission by wastewater treatment plants of the pulp and paper industry – Modeling and simulation. *International Journal of Greenhouse Gas Control*, 17, 462-472.
- Bauwens W., Vanrolleghem P.A. and Smeets M. (1996) An evaluation of the efficiency of the combined sewer - wastewater treatment system under transient conditions. *Water Science and Technology*, 33 (2), 199-208.
- Bock E., Schmidt I., Stuvén R. and Zart D. (1995) Nitrogen loss caused by nitrifying *Nitrosomonas* cells using ammonia or hydrogen as electron donors and nitrite as electron acceptor. *Archives of Microbiology*, 163 (1), 16-20.
- Bridle T., Shaw A., Cooper S., Yap K.C., Third K. and Domurad M. (2008) Estimation of greenhouse gas emissions from wastewater treatment plants. In proceedings of the IWA World Water Congress 2008, Vienna, Austria, September 7-12 2008.
- Bürger R., Diehl S. and Nopens I. (2011). A consistent modelling methodology for secondary settling tanks in wastewater treatment. *Water Research*, 45 (6), 2247-2260.
- Butler D. and Davies J. (2004). *Urban Drainage*, 2nd Edition, E & FN Spon. London, UK.
- Cech J. and Hartman P. (1993) Competition between polyphosphate and polysaccharide accumulating bacteria in enhanced biological phosphate removal systems. *Water Research*, 27 (7), 1219-1225.

- Chain P., Lamerdin J., Larimer F., Regala W., Lao V., Land M., Hauser L., Hooper A., Klotz M., Norton J., Sayavedra-Soto L., Arciero D., Hommes N., Whittaker M. and Arp D. (2003). Complete genome sequence of the ammonia-oxidizing bacterium and obligate chemolithoautotroph *Nitrosomonas europaea*. *Journal of Bacteriology*, 185 (9), 2759-2773.
- Choubert J.-M., Rieger L., Shaw A., Copp J., Spérandio M., Sørensen K., Rønner-Holm S., Morgenroth E., Melcer H. and Gillot S. (2013) Rethinking wastewater characterisation methods for activated sludge systems - a position paper. *Water Science and Technology* 67 (11), 2363-2373.
- Cierkens K., Plano S., Benedetti L., Weijers S., de Jonge J. and Nopens I. (2012) Impact of influent data frequency and model structure on the quality of WWTP model calibration and uncertainty. *Water Science and Technology*, 65 (2), 233-242.
- Colliver B.B. and Stephenson T. (2000) Production of nitrogen oxide and dinitrogen oxide by autotrophic nitrifiers. *Biotechnology Advances*, 18 (3), 219-232.
- Copp J.B., Spanjers H. and Vanrolleghem P.A. (2002) *Respirometry in control of the activated sludge process: benchmarking control strategies*. IWA Publishing, London, UK.
- Corominas Ll., Flores-Alsina X., Snip L. and Vanrolleghem P.A. (2012) Comparison of different modeling approaches to better evaluate greenhouse gas emissions from whole wastewater treatment plants. *Biotechnology and Bioengineering*, 109 (11), 2854-2863.
- Corominas Ll., Sin G., Puig S., Balaguer M., Vanrolleghem P.A. and Colprim J. (2011) Modified calibration protocol evaluated in a model-based testing of SBR flexibility. *Bioprocess and Biosystems Engineering*, 34 (2), 205-214.
- Cosenza A., Mannina G., Vanrolleghem P.A. and Neumann M.B. (2014) Variance-based sensitivity analysis for wastewater treatment plant modelling. *Science of the Total*

Environment, 470-471, 1068-1077. Czepiel P.M., Crill P.M. and Harriss R.C. (1993) Methane emissions from municipal wastewater treatment processes. *Environmental Science and Technology*, 27, 2472-2477.

Daelman M.R.J., De Baets B., van Loosdrecht M.C.M. and Volcke E.I.P. (2013a) Influence of sampling strategies on the estimated nitrous oxide emission from wastewater treatment plants. *Water Research*, 47 (9), 3120-3130.

Daelman M.R.J., van Voorthuizen E.M., van Dongen L.G., Volcke E.I. and van Loosdrecht M.C. (2013b) Methane and nitrous oxide emissions from municipal wastewater treatment - results from a long-term study. *Water Science and Technology*, 67 (10), 2350-2355.

Desloover J., Vlaeminck S.E., Clauwaert P., Verstraete W. and Boon N. (2012) Strategies to mitigate N₂O emissions from biological nitrogen removal systems. *Current Opinion in Biotechnology*, 23 (3), 474-482.

Durchschlag A., Hartel L., Hartwig P., Kaselow M., Kollatsch D., Otterpohl R. and Schwentner O. (1992) Joint consideration of combined sewerage and wastewater treatment plants. *Water Science and Technology*, 26 (5-6), 1125-1134.

Ekström M., Fowler H.J., Kilsby C.G. and Jones P.D. (2005). New estimates of future changes in extreme rainfall across the UK using regional climate model integrations. 2. Future estimates and use in impact studies. *Journal of Hydrology*, 300 (1-4), 234-251.

Elefsiniotis P. and Wareham D.G. (2007) Utilization patterns of volatile fatty acids in the denitrification reaction. *Enzyme and Microbial Technology*, 41 (1-2), 92-97.

Flores-Alsina X., Corominas L., Snip L. and Vanrolleghem P.A. (2011) Including greenhouse gas emissions during benchmarking of wastewater treatment plant control strategies. *Water Research*, 45 (16), 4700-4710.

- Flores-Alsina X., Gernaey K.V. and Jeppsson U. (2012) Global sensitivity analysis of the BSM2 dynamic influent disturbance scenario generator. *Water Science and Technology*, 65 (11), 1912-1922.
- Foley J., de Haas D., Yuan Z. and Lant P. (2010) Nitrous oxide generation in full-scale biological nutrient removal wastewater treatment plants. *Water Research*, 44 (3), 831-844.
- Foley J., Lant P. and Donlon P. (2008) Fugitive greenhouse gas emissions from wastewater system. *Water Journal of the Australian Water Association*, 38 (2), 18-23.
- Fowler H.J., Ekström M., Kilsby C.G. and Jones P.D. (2005). New estimates of future changes in extreme rainfall across the UK using regional climate model integrations. 1. Assessment of control climate. *Journal of Hydrology*, 300 (1-4), 212-233.
- Frich P., Alexander L.V., Della-Marta P., Gleason B., Haylock M., Tank A.M.G.K. and Peterson T. (2002). Observed coherent changes in climatic extremes during the second half of the twentieth century. *Climate Research*, 19 (3), 193–212.
- Gernaey K.V., Flores-Alsina X., Rosen C., Benedetti L. and Jeppsson U. (2011). Dynamic influent pollutant disturbance scenario generation using a phenomenological modelling approach. *Environmental Modelling and Software*, 26 (11), 1255-1267.
- Gernaey K.V., Jeppsson U., Vanrolleghem P.A., Copp J.B. and Steyer J.-P. (ed) (2014). *Benchmarking of Control Strategies for Wastewater Treatment Plants*. IWA Scientific and Technical Report. IWA Publishing, London, UK.
- Gernaey K.V. and Jørgensen S.B. (2004a) Benchmarking combined biological phosphorus and nitrogen removal wastewater treatment processes. *Control Engineering Practice*, 12 (3), 357-373.
- Gernaey K.V., van Loosdrecht M.C.M., Henze M., Lind M. and Jørgensen S.B. (2004b) Activated sludge wastewater treatment plant modelling and simulation: state of the art. *Environmental Modelling and Software*, 19 (9), 763-783.

Giorgi F., Hewitson B., Christensen J., Hulme M., Von Storch H., Whetton P., Jones R., Mearns L. and Fu C. (2001). Chapter 10. Regional climate information—evaluation and projections, In: J.T. Houghton, Y. Ding, D.J. Griggs, M. Noguer, P. van der Linden, X. Dai, K. Maskell, C.I. Johnson (Eds.), *Climate Change 2001: The Scientific Basis, Contribution of Working Group I to the Third Assessment Report of the Intergovernmental Panel on Climate Change*, Cambridge University Press, Cambridge, 583–638.

Gujer W. (2008) *Systems Analysis for Water Technology*. Springer, Heidelberg, Germany.

Haldane J.B.S. (1930) *Enzymes*. Longmans, Green and Company, Ltd., London, UK.

Hanaki K., Hong Z. and Matsuo T. (1992) Production of nitrous oxide gas during denitrification of wastewater. *Water Science and Technology*, 26 (5-6), 1027-1036.

Harremoës P., Capodaglio A.G., Hellstrom B.G., Henze M., Jensen K.N., Lynggaard-Jensen A., Otterpohl R. and Sørensen H. (1993) Wastewater treatment plants under transient loading – performance, modelling and control. *Water Science and Technology*, 27 (12), 71-115.

Hellinga C., van Loosdrecht M.C.M. and Heijnen J.J. (1999) Model based design of a novel process for nitrogen removal from concentrated flows. *Mathematical and Computer Modelling of Dynamical Systems*, 5 (4), 351-371.

Henze M., Gujer W., Mino T. and van Loosdrecht M.C.M (2000). *Activated sludge models ASM1, ASM2, ASM2d and ASM3*. IWA publishing.

Henze M., Gujer W., Mino T., Matsuo T., Wentzel M., Marais G.v.R. and van Loosdrecht M.C.M. (1999) Activated sludge model No. 2d, ASM2d. *Water Science and Technology*, 39 (1), 165-182.

Henze M., van Loosdrecht M.C.M. and Ekama G.A. (2008) *Biological wastewater treatment: principles, modeling, and design*. IWA Publishing, London, UK.

- Hiatt W.C. (2006) Activated sludge modeling for elevated nitrogen conditions. PhD thesis. Clemson University, CA, U.S.
- Hiatt W.C. and Grady C.P.L.Jr (2008) An updated process model for carbon oxidation, nitrification, and denitrification. *Water Environmental Research*, 80 (11), 2145-2156.
- Hooper A.B. (1968). A nitrite-reducing enzyme from *Nitrosomonas europaea*. Preliminary characterization with hydroxylamine as electron donor. *Biochimica et Biophysica Acta (BBA) - Bioenergetics*, 162 (1), 49-65.
- Houweling D., Wunderlin P., Dold P., Bye C., Joss A. and Siegrist H. (2011) N₂O emissions: modeling the effect of process configuration and diurnal loading. *Water Environment Research*, 83 (12), 2131-2139.
- Hu Z., Wentzel M.C. and Ekama G.A. (2002) Anoxic growth of phosphate-accumulating organisms (PAOs) in biological nutrient removal activated sludge systems. *Water Research*, 36 (19), 4927-4937.
- Hulme M., Jenkins G.J., Lu X., Turnpenny J.R., Mitchell T.D., Jones R.G., Lowe J., Murphy J.M., Hassell D., Boorman, P., McDonald R. and Hill S. (2002). *Climate Change Scenarios for the United Kingdom: The UKCIP02 Scientific Report*, Tyndall Centre for Climate Change Research, UK.
- Electric Power Research Institute (EPRI). (2002) *Water & Sustainability (Volume 4): U.S. Electricity Consumption for Water Supply & Treatment - The Next Half Century*. Goldstein R. and Smith W. Palo Alto, CA, USA
- Iacopozzi I., Innocenti V., Marsili-Libelli S. and Giusti E. (2007) A modified Activated Sludge Model No. 3 (ASM3) with two-step nitrification-denitrification. *Environmental Modelling and Software*, 22 (6), 847-861.
- Intergovernmental Panel on Climate Change (IPCC). (2006) *IPCC Guidelines for National Greenhouse Gas Inventories*, Prepared by the National Greenhouse Gas Inventories

Programme. Eggleston H.S., Buendia L., Miwa K., Ngara T. and Tanabe K. (eds.).
IGES, Japan.

Intergovernmental Panel on Climate Change (IPCC). (2013) Fifth Assessment Report:
Climate Change 2013 (AR5). Cambridge University Press.

Itokawa H., Hanaki K. and Matsuo T. (2001) Nitrous oxide production in high-loading
biological nitrogen removal process under low COD/N ratio condition. *Water Research*,
35 (3), 657-64.

Jeppsson U., Pons M.-N., Nopens I., Alex, J., Copp J., Gernaey K.V., Rosen C., Steyer J.-
P. and Vanrolleghem P.A. (2007) Benchmark simulation model no 2-general protocol
and exploratory case studies. *Water Science and Technology*, 56 (8), 67-78.

Kaelin D., Manser R., Rieger L., Eugster J., Rottermann K. and Siegrist H. (2009)
Extension of ASM3 for two-step nitrification and denitrification and its calibration and
validation with batch tests and pilot scale data. *Water Research*, 43 (6), 1680-1692.

Kampschreur M.J., Kleerebezem R., de Vet W.W.J.M. and van Loosdrecht M.C.M. (2011)
Reduced iron induced nitric oxide and nitrous oxide emission. *Water Research*, 45 (18),
5945-5952.

Kampschreur M.J., Picioreanu C., Tan N., Kleerebezem R., Jetten M.S.M. and Van
Loosdrecht M.C.M. (2007) Unraveling the source of nitric oxide emission during
nitrification. *Water Environment Research*, 79 (13), 2499-2509.

Kampschreur M.J., Tan N.G., Kleerebezem R., Picioreanu C., Jetten M.S.M. and van
Loosdrecht M.C.M. (2008) Effect of dynamic process conditions on nitrogen oxides
emission from a nitrifying culture. *Environmental Science and Technology*, 42 (2), 429-
435.

Kim S.-W., Miyahara M., Fushinobu S., Wakagi T., Shoun H. (2010) Nitrous oxide
emission from nitrifying activated sludge dependent on denitrification by ammonia-
oxidizing bacteria. *Bioresource Technology*, 101 (11), 3958-3963.

- Krebs P., Holzer P., Huisman J.L. and Rauch W. (1999) First flush of dissolved compounds. *Water Science and Technology*, 39 (9), 55-62.
- Kuba T., Smolders G., van Loosdrecht M.C.M and Heijnen J.J. (1993) Biological phosphorus removal from wastewater by anaerobic-anoxic sequencing batch reactor. *Water Science and Technology*, 27 (5-6), 241-252.
- Kuba T., van Loosdrecht M.C.M. and Heijnen J.J. (1996) Phosphorus and nitrogen removal with minimal cod requirement by integration of denitrifying dephosphatation and nitrification in a two-sludge system. *Water Research*, 30 (7), 1702-1710.
- Law Y., Jacobsen G. E., Smith A. M., Yuan Z. and Lant P. (2013) Fossil organic carbon in wastewater and its fate in treatment plants. *Water Research*, 47 (14), 5270-5281.
- Law Y., Ni B.-J., Lant P. and Yuan Z. (2012) N₂O production rate of an enriched ammonia-oxidising bacteria culture exponentially correlates to its ammonia oxidation rate. *Water Research*, 46 (10), 3409-3419.
- Lemaire R., Meyer R., Taske A., Crocetti G.R., Keller J. and Yuan Z. (2006) Identifying causes for N₂O accumulation in a lab-scale sequencing batch reactor performing simultaneous nitrification, denitrification and phosphorus removal. *Journal of Biotechnology*, 122 (1), 62-72.
- Lessard P. and Beck M.B. (1990) Operational water quality management: control of storm sewage at a wastewater treatment. *Research Journal of the Water Pollution Control Federation*, 62 (6), 810-819.
- Liu W.-T, Mino T., Nakamura K. and Matsuo T. (1994) Role of glycogen in acetate uptake and polyhydroxyalkanoate synthesis in anaerobic-aerobic activated sludge with a minimized polyphosphate content. *Journal of fermentation and bioengineering*, 77 (5), 535-540.

- Lotito A.M., Wunderlin P., Joss A., Kipf M. and Siegrist H. (2012) Nitrous oxide emissions from the oxidation tank of a pilot activated sludge plant. *Water Research*, 46 (11), 3563-3573.
- Mampaey KE, Beuckels B, Kampschreur MJ, Kleerebezem R, van Loosdrecht MCM, Volcke EIP (2013) Modelling nitrous and nitric oxide emissions by autotrophic ammonia-oxidizing bacteria. *Environmental Technology*, 34 (12), 1555-1566.
- Metcalf & Eddy. (2003) *Wastewater engineering: treatment and reuse*. 4th ed., McGraw-Hill Science Engineering.
- Monteith H.D., Sahely H.R., MacLean H.L. and Bagley D.M. (2005) A rational procedure for estimation of greenhouse-gas emissions from municipal wastewater treatment plants. *Water Environmental Research*, 77 (4), 390-403.
- Ni B.-J., Peng L., Law Y., Guo J. and Yuan Z. (2014) Modeling of nitrous oxide production by autotrophic ammonia-oxidizing bacteria with multiple production pathways. *Environmental Science and Technology*, 48 (7), 3916-3924.
- Ni B.-J., Rusalleda M., Pellicer-Nacher C. and Smets B.F. (2011) Modeling nitrous oxide production during biological nitrogen removal via nitrification and denitrification: Extensions to the general ASM models. *Environmental Science and Technology*, 45 (18), 7768-7776.
- Ni B.-J., Ye L., Law Y., Byers C. and Yuan Z. (2013a) Mathematical modeling of nitrous oxide (N₂O) emissions from full-scale wastewater treatment plants. *Environmental Science and Technology*, 47 (14), 7795-7803.
- Ni B.-J., Yuan Z., Chandran K., Vanrolleghem P.A. and Murthy S. (2013b) Evaluating four mathematical models for nitrous oxide production by autotrophic ammonia-oxidizing bacteria. *Biotechnology and Bioengineering*, 110(1):153-163.

- Nopens I., Batstone D.J., Copp J.B., Jeppsson U., Volcke E., Alex J. and Vanrolleghem P.A. (2009) An ASM/ADM model interface for dynamic plant-wide simulation. *Water Research*, 43 (7), 1913-1923.
- Nopens I., Benedetti L., Jeppsson U., Pons M.-N., Alex J., Copp J.B., Gernaey K.V., Rosen C., Steyer J.-P. and Vanrolleghem P.A. (2010) Benchmark Simulation Model No 2: finalisation of plant layout and default control strategy. *Water Science and Technology*, 62 (9), 1967-1974.
- Oehmen A., Lopez-Vazquez C.M., Carvalho G., Reis M.A.M., van Loosdrecht M.C.M. (2010) Modelling the population dynamics and metabolic diversity of organisms relevant in anaerobic/anoxic/aerobic enhanced biological phosphorus removal processes. *Water Research*, 44 (15), 4473-4486.
- Olsson G. and Stephenson J.P. (1985). The propagation of hydraulic disturbances and flow rate reconstruction in activated sludge plants. *Environmental Technology Letters*, 6 (12), 536-545.
- Otte S., Grobben N.G., Robertson L.A., Jetten M.S.M. and Kuenen J.G. (1996). Nitrous oxide production by *Alcaligenes faecalis* under transient and dynamic aerobic and anaerobic conditions. *Applied and Environmental Microbiology*, 62 (7), 2421-2426.
- Otterpohl R. and Freund M. (1992). Dynamic models for clarifiers of activated sludge plants with dry and wet weather flows. *Water Science and Technology*, 26 (5-6), 1391-1400.
- Otterpohl R., Raak M. and Rolfs T. (1994). A mathematical model for the efficiency of the primary clarification. In proceeding of IAWQ 17th Biennial International Conference, Budapest, Hungary, July 24-29 1994.

- Pan Y., Ye L., Ni B.-J. and Yuan Z. (2012) Effect of pH on N₂O reduction and accumulation during denitrification by methanol utilizing denitrifiers. *Water Research*, 46 (15), 4832-4840.
- Pan Y., Ye L., Ni B.-J. and Yuan Z. (2013) Modeling electron competition among nitrogen oxides reduction and N₂O accumulation in denitrification. *Environmental Science and Technology*, 47 (19), 11083-11091.
- Plósz B.Gy., Liltved H. and Ratnaweera H. (2009) Climate change impacts on activated sludge wastewater treatment: A case study from Norway. *Water Science and Technology*, 60 (2), 533-541.
- Plósz B.Gy., Weiss M., Printemps C., Essemiani K. and Meinhold J. (2007). One-dimensional modelling of the secondary clarifier - Factors affecting simulation in the clarification zone and the assessment of the thickening flow dependence. *Water Research*, 41 (15), 3359-3371.
- Pocquet M., Filali A., Bessiere Y., Guo L., Queinnec I., Vanrolleghem P. A., Sperandio M. (2012) Analysis and modelling of process conditions influencing N₂O emission by aerobic granular sludge processes for N/DN treatment. In proceedings of the IWA Nutrient Removal and Recovery 2012: Trends in NRR, Harbin, China, September 23-25 2012.
- Samie G., Bernier J., Rocher V., Lessard P. (2011) Modeling nitrogen removal for a denitrification biofilter. *Bioprocess and Biosystem Engineering*, 34 (6), 747-755.
- Spérandio M. and Paul E. (1997) Determination of carbon dioxide evolution rate using on-line gas analysis during dynamic biodegradation experiments. *Biotechnology and Bioengineering*, 53 (3), 243-252.
- Spérandio M., Pocquet M., Guo L., Ni B.-J., Vanrolleghem P.A. and Yuan Z. (2014) Calibration of five candidate nitrous oxide production models with four continuous long-term wastewater treatment process data series. In preparation.

- Porro J., Pijuan M., Kampschreur M., Volcke E., Daelman M., Guo L., Nopens I., Vanrolleghem P.A., Chandran K. and Yuan Z. and Murthy S. (2014). In proceedings of IWA Specialist Conference on Global Challenges for Sustainable Wastewater Treatment and Resource Recovery, Kathmandu, Nepal, October 26-30 2014. (Accepted)
- Press W.H., Teukolsky S., Vetterling W.T., Flannery B.P., 2007. Numerical Recipes 3rd Edition: The Art of Scientific Computing. Cambridge University Press. London, England.
- Ratkowsky D.A., Lowry R.K., McMeekin T.A., Stokes A.N., and Chandler R.E. (1983) Model for bacterial culture growth rate throughout the entire biokinetic temperature range. *Journal of Bacteriology*, 154 (3), 1222-1226.
- Rehman U., Vesvikar M., Maere T., Guo L., Vanrolleghem P.A. and Nopens I. (2013) Effect of sensor location on controller performance in a wastewater treatment plant. In proceedings of the 11th IWA conference on instrumentation control and automation, Narbonne, France, September 18-20 2013.
- Remde A. and Conrad R. (1990). Production of nitric oxide in *Nitrosomonas europaea* by reduction of nitrite. *Archives of Microbiology*, 154 (2), 187-91.
- Risholt L.P., Schilling W., Erbe V. and Alex J. (2002) Pollution based real time control of wastewater systems. *Water Science and Technology*, 45 (3), 219-228.
- Rodriguez-Garcia G., Hospido A., Bagley D.M., Moreira M.T. and Feijoo G. (2012) A methodology to estimate greenhouse gases emissions in Life Cycle Inventories of wastewater treatment plants. *Environmental Impact Assessment Review*, 37, 37-46.
- Schmidt I. and Bock E. (1997) Anaerobic ammonia oxidation with nitrogen dioxide by *Nitrosomonas eutropha*. *Archives of Microbiology*, 167 (2-3), 106-111.
- Seggelke K., Rosenwinkel K.-H., Vanrolleghem P.A. and Krebs P. (2005) Integrated operation of sewer system and WWTP by simulation-based control of the WWTP inflow. *Water Science and Technology*, 52 (5), 195-203.

- Shiskowski D.M. and Mavinic D.S. (2006) The influence of nitrite and pH (nitrous acid) on aerobic-phase, autotrophic N₂O generation in a wastewater treatment bioreactor. *Journal of Environmental Engineering and Science*, 5 (4), 273-283.
- Sin G, De Pauw DJW, Weijers S, Vanrolleghem PA (2008a) An efficient approach to automate the manual trial and error calibration of activated sludge models. *Biotechnology and Bioengineering*, 100 (3), 516-528.
- Sin G., Kaelin D., Kampschreur M.J., Takács I., Wett B., Gernaey K.V., Rieger L., Siegrist H. and Van Loosdrecht M.C.M. (2008b). Modelling nitrite in wastewater treatment systems: a discussion of different modelling concepts. *Water Science and Technology*, 58 (6), 1155-1171.
- Sin G., Niville K., Bachis G., Jiang T., Nopens I., van Hulle S. and Vanrolleghem P.A. (2008c) Nitrite effect on the phosphorus uptake activity of phosphate accumulating organisms (PAOs) in pilot-scale SBR and MBR reactors. *Water SA*, 34 (2), 249-260.
- Sin G. and Vanrolleghem P.A. (2006) Evolution of an ASM2d-like model structure due to operational changes of an SBR process. *Water Science and Technology*, 53 (12), 237-245.
- Solomon S., Qin D., Manning M., Chen Z., Marquis M., Averyt K.B., Tignor M. and Miller H.L. (Eds.) (2007) *Climate Change 2007: The Physical Science Basis, Contribution of Working Group I to the Fourth Assessment Report of the Intergovernmental Panel on Climate Change*, Cambridge University Press, Cambridge, United Kingdom and New York, USA.
- Stein L.Y. and Yung Y.L. (2003) Production, isotopic composition, and atmospheric fate of biologically produced nitrous oxide. *Annual Review of Earth and Planetary Sciences*, 31, 329-356.

- Stouthamer A.H., De Boer A.P.N., Van der Oost J. and Van Spanning R.J.M. (1997) Emerging principles of inorganic nitrogen metabolism in *Paracoccus Denitrificans* and related bacteria. *Antonie van Leeuwenhoek*, 71 (1-2), 33-41.
- Takács I., Patry G.G. and Nolasco D. (1991). A dynamic model of the clarification thickening process. *Water Research*, 25 (10), 1263-1271.
- Tai Y.-L. and Dempsey B.A. (2009) Nitrite reduction with hydrous ferric oxide and Fe(II): Stoichiometry, rate, and mechanism. *Water Research*, 43 (2), 546-552.
- Tallec G., Garnier J., Billen G. and Gossailles M. (2006). Nitrous oxide emissions from secondary activated sludge in nitrifying conditions of urban wastewater treatment plants: Effect of oxygenation level. *Water Research*, 40 (15), 2972-2980.
- Thompson D., Chapman D.T. and Murphy K.L. (1989) Step feed control to minimize solids loss during storm flows. *Research Journal WPCF*, 61 (11-12), 1658-1665.
- Thörn M. and Sörensson F. (1996) Variation of nitrous oxide formation in the denitrification basin in a wastewater treatment plant with nitrogen removal. *Water Research*, 30 (6), 1543-1547.
- U.S. Environmental Protection Agency (U.S. EPA). (2013) Inventory of U.S. Greenhouse Gas Emissions and Sinks: 1990 – 2011. EPA 430-R-08-005. Washington, D.C. USA.
- van Cleemput O. (1998) Subsoils: chemo- and biological denitrification, N₂O and N₂ emissions. *Nutrient Cycling in Agroecosystems* 52 (2-3), 187-194.
- Van Den Heuvel R.N., Bakker S.E., Jetten M.S.M. and Hefting M.M. (2011) Decreased N₂O reduction by low soil pH causes high N₂O emissions in a riparian ecosystem. *Geobiology*, 9 (3), 294-300.
- Van Steenberghe N. and Willems P. (2012). Method for testing the accuracy of rainfall–runoff models in predicting peak flow changes due to rainfall changes, in a climate changing context. *Journal of Hydrology*, 414-415, 425-434.

- Vanrolleghem P.A., Benedetti, L.B., Sahni N. and Moisisio S. (2014) Modeling for wet weather. In: Tabor C. and Sandino J. (Eds.) Wet Weather Design and Operation in Water Resource Recovery Facilities. Special Publication of the Water Environment Publications, Alexandria, VA, USA. In press.
- Vanrolleghem P.A. and Gillot S. (2002). Robustness and economic measures as control benchmark performance criteria. *Water Science and Technology*. 45 (4-5), 117-126.
- Vanrolleghem P.A., Jeppsson U., Carstensen J., Carlsson B. and Olsson G. (1996) Integration of WWT plant design and operation - a systematic approach using cost functions. *Water Science and Technology*, 34 (3-4), 159-171.
- Vidal N., Poch M., Martí E. and Rodríguez-Roda I. (2002) Evaluation of the environmental implications to include structural changes in a wastewater treatment plant. *Journal of Chemical Technology and Biotechnology*, 77 (11), 1206-1211.
- Volcke E.I.P., Loccufier M., Noldus E.J.L. and Vanrolleghem P.A. (2007) Operation of a SHARON nitrification reactor: practical implications from a theoretical study. *Water Science and Technology*, 56 (6), 145–154.
- von Schulthess R. and Gujer W. (1996) Release of nitrous oxide (N_2O) from denitrifying activated sludge: verification and application of a mathematical model. *Water Research*, 30 (3), 521-530.
- von Schulthess R., Wild D. and Gujer W. (1994). Nitric and nitrous oxides from denitrifying activated sludge at low oxygen concentration. *Water Science and Technology*, 30 (6), 123-132.
- Wrage W., Velthof G.L., van Beusichem M.L. and Oenema O. (2001) Role of nitrifier denitrification in the production of nitrous oxide. *Soil Biology and Biochemistry*, 33 (12-13), 1723-1732.
- Wunderlin P., Lehmann M.F., Siegrist H., Tuzson B., Joss A., Emmenegger L. and Mohn J. (2013) Isotope signatures of N_2O in a mixed microbial population system: constraints on

- N₂O producing pathways in wastewater treatment. *Environmental Science and Technology*, 47 (3), 1339-1348.
- Wunderlin P., Mohn J., Joss A., Emmenegger L. and Siegrist H. (2012) Mechanisms of N₂O production in biological wastewater treatment under nitrifying and denitrifying conditions. *Water Research*, 46 (4), 1027-1037.
- Ye L., Ni B.-J., Law Y., Byers C. and Yuan Z. (2013) A novel methodology to quantify nitrous oxide emissions from full-scale wastewater treatment systems with surface aerators. *Water Research*, 48, 257-268.
- Yu R., Kampschreur M. J., van Loosdrecht M. C. M. and Chandran K. (2010) Mechanisms and specific directionality of autotrophic nitrous oxide and nitric oxide generation during transient anoxia. *Environmental Science and Technology*, 44 (4), 1313-1319.
- Zeng R.J., Lemaire R., Yuan Z. and Keller J. (2003a) Simultaneous nitrification, denitrification, and phosphorus removal in a lab-scale sequencing batch reactor. *Biotechnology and Bioengineering*, 84 (2), 170-178.
- Zeng R.J., Yuan Z. and Keller J. (2003b) Enrichment of denitrifying glycogen-accumulating organisms in anaerobic/anoxic activated sludge system. *Biotechnology and Bioengineering*, 81 (4), 397-404.
- Zhu X., Burger M., Doane T.A. and Horwath W.R. (2013) Ammonia oxidation pathways and nitrifier denitrification are significant sources of N₂O and NO under low oxygen availability. In proceedings of the National Academy of Sciences, USA, 110 (16), 6328-6333.

Appendix A Calculation of N₂O emissions

For the three sections of the summer aeration package (beginning, middle and end), the collected data set of N₂O emissions is different in terms of the length of the time series for each section. Therefore, when calculating the average N₂O emission rates, the average N₂O emission factors and the total N₂O emission factor under dry weather conditions, three dry-weather days were selected for which complete data were available. They were August 7th-9th for the beginning section, from noon on August 12th to noon of August 15th for the middle section and August 21st-23rd for the end section.

1. N₂O emission rate

Assume that: (I) the surface of the summer package is equally divided into 3 sections (the beginning, middle and end sections) and the N₂O emission is equally distributed over each section's surface; (II) the aeration flow rate of the summer package is equally distributed longitudinally throughout the bioreactor, so that the local aeration flow rate for each section can be calculated as one third of the total aeration flow rate; (III) in the other two lines the bioreactors show similar behaviours as the measured one. Given these assumptions, the N₂O emission rate can be calculated as:

$$N_2O_emission_min_{i,t} = \frac{N_2O_ppm_{i,t}}{10^6} \times Q_{i,t} \times \frac{0.028}{0.0224} \times 3 \quad \text{Eq. (A.1)}$$

where i stands for the different locations of the summer package ($i=1, 2, 3$ meaning the beginning, middle and end section respectively), $N_2O_emission_min_{i,t}$ is the N₂O emission rate (kg N₂O-N/d) on a minute basis for the i th section of the summer package at time t , $N_2O_ppm_{i,t}$ is the raw measurement value of N₂O (ppm) at time t , collected on a minute basis, $Q_{i,t}$ is the aeration flow rate in the i th section of the summer package at time t (m³/d),

0.028 is the N mass contained per mole of N₂O (kg N₂O-N/mol), 0.0224 is the molar volume of N₂O gas (m³/mol), 10⁶ is a coefficient for converting the unit ppm to dimensionless (ppm) and the number 3 refers to the three parallel treatment lines.

Q_{*i,t*} is calculated by:

$$Q_{i,t} = \frac{Q_{Total,t}}{3} \quad \text{Eq. (A.2)}$$

where Q_{Total,t} is the total aeration flow rate of the summer package at time *t* on a minute basis (m³/d).

2. N₂O emission factor

Influent components do not reach the end of a bioreactor immediately after they arrive at the plant inlet. In other words, there is a delay time (*tDelay*) for the components between arriving at the plant inlet and hitting the downstream summer package. Therefore, the N₂O emitted at time *t* is actually the result of the influent N at time *t-tDelay*. When calculating the N₂O emission factors, this delay time was taken into account:

$$f_{N_2O,i,t} = \frac{N_2O_emission_hour_{i,t}}{TKN_load_{t-tDelay}} \quad \text{Eq. (A.3)}$$

where *f*_{N₂O,t} is the hourly averaged N₂O emission factor for the *i* th section of the summer package at time *t*, N₂O_emission_hour_{*i,t*} is the hourly averaged N₂O emission rate (kg N₂O-N/d) for the *i* th section of the summer package at time *t*, *tDelay* is the hydraulic delay time for influent components arriving at the summer package, and TKN_load_{*t-tDelay*} is the influent total Kjeldahl nitrogen (TKN) load at the current time *t* minus *tDelay* (kg N₂O-N/d). In this case study, *tDelay* was estimated from the figures by comparing the arrival time of the

influent NH_4^+ peak loads with the time of occurrence of the maximum local NH_4^+ concentration measured at the summer package. Note that $tDelay$ should change with the plant influent flow rate but it is hard to obtain this dynamic $tDelay$ only from measurement data because there are internal recyclings among different rings and circulation flows in the outer ring. A tracer test in a model simulation can help answer this question, but modelling is not the purpose of this paper.

The influent TKN load is:

$$\text{TKN_load}_{t-tDelay} = S_{\text{TKN},t-tDelay} \cdot Q_{\text{inf},t-tDelay} / 1000 \quad \text{Eq. (A.4)}$$

where $Q_{\text{inf},t-tDelay}$ is the influent flow rate at time $t-tDelay$ (m^3/d), $S_{\text{TKN},t-tDelay}$ is the influent TKN concentration at time $t-tDelay$ (gN/m^3), and the number 1000 is used to convert concentration from gN/d to kgN/d .

Besides the influent flow rate and the ammonia concentrations (S_{NH}), the plant has spectrophotometric sensors for influent CODs and CODt (Cierkens et al., 2012). With this, the influent TKN concentration was calculated as defined:

$$\begin{aligned} S_{\text{TKN},t-tDelay} = & (1 - f_{\text{SA}} - f_{\text{SF}}) \cdot \text{CODs}_{t-tDelay} \cdot i_{\text{N,SI}} + f_{\text{SF}} \cdot \text{CODs}_{t-tDelay} \cdot i_{\text{N,SF}} \\ & + f_{\text{XS}} \cdot (\text{CODt}_{t-tDelay} - \text{CODs}_{t-tDelay}) \cdot i_{\text{N,XS}} \\ & + \left[(\text{CODt}_{t-tDelay} - \text{CODs}_{t-tDelay}) \cdot (1 - f_{\text{XS}}) - X_{\text{BM}} \right] \cdot i_{\text{N,XI}} \\ & + X_{\text{BM},t-tDelay} \cdot i_{\text{N,BM}} + S_{\text{NH},t-tDelay} \end{aligned} \quad \text{Eq. (A.5)}$$

where parameters $f_{\text{SA}}=0.38$, $f_{\text{SF}}=0.39$, $f_{\text{XS}}=0.45$, $i_{\text{N,SI}}=0.033$, $i_{\text{N,SF}}=0.03$, $i_{\text{N,XS}}=0.04$, $i_{\text{N,XI}}=0.02$, $i_{\text{N,BM}}=0.07$ and the concentration of influent biomass is assumed as $X_{\text{BM}}=5$ mg/l .

Note that the N_2O emission rate is calculated every minute as the raw data of the N_2O analyser and other plant sensors are collected every minute, giving more detailed information on the short-term dynamic variations. The emission factor on the other hand is

calculated as an hourly average because the calculation of the emission factor should consider the effect of hydraulic delay time and due to that the *tDelay* was only estimated from visual comparison in figures the result could not be precise if too small time intervals are used. The more precise values need the help of modelling.

Appendix B Contribution of AOB pathway to N₂O emissions

It is hard to precisely calculate the N₂O emissions by the AOB pathways. However, its minimum value can be estimated under the assumption of limit conditions as explained below.

Assume that the N₂O emissions at the summer package are only due to the stripping of N₂O produced anoxically in the upstream anoxic zone. In other words, it is assumed that no bioreaction (including AOB N₂O production) occurs in the aerobic zone. In this limit situation one can calculate how the N₂O emissions would decrease along the aerated zone as the dissolved N₂O is decreasing due to stripping (remember: no N₂O production occurs, so the N₂O concentration can only go down). If the evolution of the calculated N₂O emissions along the aerated zone is not equal to the measured evolution of the N₂O emissions, it means that this assumption is not correct and that the AOB contribute to the N₂O emissions.

Considering a steady-state situation and assuming that the liquid N₂O equilibrium concentration is 0 mg N/l (the aeration air does not contain N₂O), the following equation holds:

$$N_2O_emission_min_i = k_L a_{N_2O} \cdot C_i \cdot V_i \quad \text{Eq. (B.1)}$$

where $N_2O_emission_min_i$ is the N₂O emission rate (kg N₂O-N/d) for the i th section ($i=1, 2, 3$ meaning the beginning, middle and end sections respectively) of the summer packages at time t , C_i is the liquid N₂O concentration (kg N₂O-N/m³) for the i th aeration sections, $k_L a_{N_2O}$ is the N₂O mass transfer coefficient (d⁻¹) and V_i is the liquid volume of the i th section (m³).

Assuming that the summer package in the bioreactor can be described as a series of completely stirred tank reactors (CSTR), the following equation can be used to calculate the outlet concentration of a section with stripping of a component (Gujer, 2008):

$$C_i = C_0 \cdot \left(\frac{1}{k_L a_{N_2O} \cdot \theta_i + 1} \right)^i \quad \text{Eq. (B.2)}$$

where θ_i is the hydraulic retention time (HRT) in the CSTRs of the summer package and C_0 is the liquid N_2O concentration at the entry of the summer package. Substituting Eq. (B.2) into Eq. (B.1) leads to:

$$\begin{aligned} N_2O_emission_min_i &= K l a_{N_2O} \cdot C_0 \cdot \left(\frac{1}{k_L a_{N_2O} \cdot \theta_i + 1} \right)^i \cdot V_i \\ &= N_2O_emission_min_1 \cdot \left(\frac{1}{k_L a_{N_2O} \cdot \theta_i + 1} \right)^{(i-1)} \end{aligned} \quad \text{Eq. (B.3)}$$

$k_L a_{N_2O}$ can be calculated from (Spérandio and Paul, 1997):

$$k_L a_{N_2O} = k_L a \cdot \sqrt{\frac{D_{N_2O}}{D_{O_2}}} \quad \text{Eq. (B.4)}$$

where $k_L a$ is the oxygen transfer coefficient (d^{-1}), D_{O_2} is the diffusion coefficient for oxygen ($2.12 \times 10^{-9} \text{ m}^2/\text{s}$) and D_{N_2O} is the diffusion coefficient for N_2O ($1.77 \times 10^{-9} \text{ m}^2/\text{s}$).

From Cierkens et al. (2012), $k_L a$ is 125 d^{-1} under steady state, and according to Eq.(B.4), $k_L a_{N_2O} = 114.22 \text{ d}^{-1}$.

The total volume of the summer package aeration zones, considering the three parallel lines, is $16,100 \text{ m}^3$, so the volume of each CSTR is $V=16,100/3 \text{ m}^3$, and the flow rate through the summer packages is $55,985,200 \text{ m}^3/\text{d}$. Then for the middle and end sections

of the summer packages, θ_t is about 1.3 minutes and 2.6 minutes. For the beginning section of the summer packages, θ_t is 0.

With this the evolution of the N_2O emissions during the aerated zone can be calculated. According to the assumption, all N_2O emission at the beginning section of the summer package is from upstream anoxic denitrification, i.e. substituting $N_2O_emission_min_1 = 10.7$ kg N_2O -N/d in Eq. (B.3). When the mixed liquor reaches the end section of the summer package, i.e. after 2.6 minutes, the emission of N_2O originating from the upstream anoxic zone is:

$$N_2O_emission_min_3 = 10.7 \times \left(\frac{1}{114.22 \times 2.6/24/60 + 1} \right)^{(3-1)} = 7.4 \text{ kg } N_2O\text{-N/d}$$

Following the calculation of Appendix A, the N_2O emission rate at the end section of the summer package is 20.3 kg N_2O -N/d. Hence, the remainder, $20.3 - 7.4 = 12.9$ kg N_2O -N/d, must be produced in the summer package.

Applying the same calculations for the middle section, 9.7 kg N_2O -N/d is emitted that is the result of the upstream anoxic production. This is higher than the measured value (7.7 kg N_2O -N/d), which indicates that the assumed 10.7 kg N_2O -N/d emitted in the beginning section must already contain some AOB produced N_2O .

It can therefore be concluded that the extreme condition assumed above is not valid and that, in other words, the N_2O emission at the summer package must also be partially produced within the summer package. Considering that AOB activity will dominate the summer package which is aerobic, the N_2O produced in the summer package will be mostly coming from the AOB pathways. Consequently, for the end section of the summer package, the N_2O emission due to the AOB pathway will be higher than 12.9 kg N_2O -N/d. Moreover, considering that the N_2O emissions at the beginning and the middle sections

may also partially come from the AOB pathway, the overall N_2O emissions due to AOB activity will be higher than 12.9 kg $\text{N}_2\text{O-N/d}$. In addition, given the ring configuration of the bioreactor, some of the N_2O in the liquid leaving the aeration package is recycled back to the beginning of the ring. This further supports the hypothesis that the N_2O emission at the summer package cannot originate from the anoxic zones only. In conclusion, it can thus be stated that AOB considerable contributes to the overall N_2O emission.

Appendix C Liquid-gas equilibrium of N₂O

The time needed to reach liquid-gas equilibrium is (Gujer, 2008):

$$\tau = -\ln(1 - 0.99) \frac{H\phi_B}{6k_1} \quad \text{Eq. (C.1)}$$

where H is the Henry coefficient, ϕ_B is the diameter of bubbles, and k_1 is the mass transfer coefficient.

$$k_1 = \sqrt{\frac{4 \cdot D \cdot u}{\pi \cdot \phi_B}} \quad \text{Eq. (C.2)}$$

where D is the molecular diffusion coefficient and u is the rise velocity of bubbles.

For N₂O, $H = 1.614$ and $D = 1.77 \times 10^{-9}$ m²/s. Assuming $\phi_B = 0.003$ m and $u = 0.3$ m/s (Gujer, 2008), $k_1 = 41$ m/d, $\tau = 7.8$ s.

The height of the bioreactor at the Eindhoven WWTP is 7 m. According to the assumption of $u = 0.3$ m/s, it takes at least 23 s for bubbles to rise from the bottom to the top of the bioreactor. It indicates that N₂O in the gas bubbles can get to equilibrium quite fast before they leave the reactor. Therefore, the gas concentration of N₂O (ppm) reflects the liquid concentration of N₂O. Note that it is the emission rate (kg/d) that is given in the figures but a similar trend is observed in the N₂O concentrations in the emitted gas (ppm), which means that the variation of the N₂O emissions shown in the figures is mainly due to variation in the bioreactions, not in variation in the efficiency of the physical stripping.

Appendix D Stoichiometric matrix of ASMG1

	S_1	S_0	S_{NO3}	S_{NO2}	S_{NO}	S_{N2O}	S_{N2}	S_S
P 1								1
P 2								
P 3								
P 4		$1 - \frac{1}{Y_H}$						$-\frac{1}{Y_H}$
P 5			$-\frac{7}{8} \cdot \frac{1 - Y_H \cdot \eta_{YH}}{Y_H \cdot \eta_{YH}}$	$\frac{7}{8} \cdot \frac{1 - Y_H \cdot \eta_{YH}}{Y_H \cdot \eta_{YH}}$				$-\frac{1}{Y_H \cdot \eta_{YH}}$
P 6				$-\frac{7}{4} \cdot \frac{1 - Y_H \cdot \eta_{YH}}{Y_H \cdot \eta_{YH}}$	$\frac{7}{4} \cdot \frac{1 - Y_H \cdot \eta_{YH}}{Y_H \cdot \eta_{YH}}$			$-\frac{1}{Y_H \cdot \eta_{YH}}$
P 7					$-\frac{7}{4} \cdot \frac{1 - Y_H \cdot \eta_{YH}}{Y_H \cdot \eta_{YH}}$	$\frac{7}{4} \cdot \frac{1 - Y_H \cdot \eta_{YH}}{Y_H \cdot \eta_{YH}}$		$-\frac{1}{Y_H \cdot \eta_{YH}}$
P 8						$-\frac{7}{4} \cdot \frac{1 - Y_H \cdot \eta_{YH}}{Y_H \cdot \eta_{YH}}$	$\frac{7}{4} \cdot \frac{1 - Y_H \cdot \eta_{YH}}{Y_H \cdot \eta_{YH}}$	$-\frac{1}{Y_H \cdot \eta_{YH}}$
P 9								
P 10		$1 - \frac{24}{7} \cdot \frac{1}{Y_{AOB}}$		$\frac{1}{Y_{AOB}}$				
P 11		$1 - \frac{8}{7} \cdot \frac{1}{Y_{NOB}}$	$\frac{1}{Y_{NOB}}$	$-\frac{1}{Y_{NOB}}$				
P 12		$1 - \frac{16}{7} \cdot \frac{1}{Y_{AOB} \cdot \eta_{YAOb}}$		$-\frac{1}{Y_{AOB} \cdot \eta_{YAOb}}$	$\frac{2}{Y_{AOB} \cdot \eta_{YAOb}}$			
P 13		$1 - \frac{16}{7} \cdot \frac{1}{Y_{AOB} \cdot \eta_{YAOb}}$		$\frac{1}{Y_{AOB} \cdot \eta_{YAOb}}$	$-\frac{2}{Y_{AOB} \cdot \eta_{YAOb}}$	$\frac{2}{Y_{AOB} \cdot \eta_{YAOb}}$		
P 14								
P 15								

Appendix D Stoichiometric matrix of ASMG1

	S_{NH4}	S_{ND}	S_{AIK}
P 1			
P 2		1	
P 3	1	-1	$\frac{1}{14}$
P 4	$-i_{N,BM}$		$-\frac{1}{14} \cdot i_{N,BM}$
P 5	$-i_{N,BM}$		$-\frac{1}{14} \cdot i_{N,BM}$
P 6	$-i_{N,BM}$		$-\frac{1}{14} \cdot i_{N,BM} + \frac{7}{64} \cdot \frac{1 - Y_H \cdot \eta_{YH}}{Y_H \cdot \eta_{YH}}$
P 7	$-i_{N,BM}$		$-\frac{1}{14} \cdot i_{N,BM}$
P 8	$-i_{N,BM}$		$-\frac{1}{14} \cdot i_{N,BM}$
P 9			
P 10	$-i_{N,BM} - \frac{1}{Y_{AOB}}$		$-\frac{1}{14} \cdot i_{N,BM} - \frac{1}{7} \cdot \frac{1}{Y_{AOB}}$
P 11	$-i_{N,BM}$		$-\frac{1}{14} \cdot i_{N,BM}$
P 12	$-i_{N,BM} - \frac{1}{Y_{AOB} \cdot \eta_{YAOB}}$		$-\frac{1}{14} \cdot i_{N,BM}$
P 13	$-i_{N,BM} - \frac{1}{Y_{AOB} \cdot \eta_{YAOB}}$		$-\frac{1}{14} \cdot i_{N,BM} - \frac{1}{7} \cdot \frac{1}{Y_{AOB} \cdot \eta_{YAOB}}$
P 14			
P 15			

Appendix D Stoichiometric matrix of ASMG1

	X_i	X_s	X_H	X_{AOB}	X_{NOB}	X_P	X_{ND}
P 1		-1					
P 2							-1
P 3							
P 4			1				
P 5			1				
P 6			1				
P 7			1				
P 8			1				
P 9		$1-f_p$	-1			f_p	$i_{N,BM} - f_p \cdot i_{N,XP}$
P 10				1			
P 11					1		
P 12				1			
P 13				1			
P 14		$1-f_p$		-1		f_p	$i_{N,BM} - f_p \cdot i_{N,XP}$
P 15		$1-f_p$			-1	f_p	$i_{N,BM} - f_p \cdot i_{N,XP}$

Appendix E Kinetic equations of ASMG1

Process Number	Description	Kinetic equation (ρ)
Heterotrophic processes		
P 1	Hydrolysis of entrapped organics	$k_{h,Temp} \cdot \frac{X_S / X_H}{K_X + X_S / X_H} \cdot \left(\frac{S_O}{K_{O,Hyd} + S_O} + \eta_{Hyd} \cdot \frac{K_{O,Hyd}}{K_{O,Hyd} + S_O} \cdot \frac{S_{NOx}}{K_{NOx,Hyd} + S_{NOx}} \right) \cdot X_H$
P 2	Hydrolysis of entrapped organic nitrogen	$k_{h,Temp} \cdot \frac{X_{ND} / X_H}{K_X + X_S / X_H} \cdot \left(\frac{S_O}{K_{O,Hyd} + S_O} + \eta_{Hyd} \cdot \frac{K_{O,Hyd}}{K_{O,Hyd} + S_O} \cdot \frac{S_{NOx}}{K_{NOx,Hyd} + S_{NOx}} \right) \cdot X_H$
P 3	Ammonification of soluble organic nitrogen	$k_{a,Temp} \cdot S_{ND} \cdot X_H$
P 4	Heterotrophic aerobic growth	$\mu_{R,H} \cdot \frac{S_O}{K_{OH1} + S_O} \cdot \frac{S_S}{K_{S1} + S_S} \cdot X_H$
P 5	Heterotrophic denitrification of $NO_3^- \rightarrow NO_2^-$	$\rho_{R4} \cdot \eta_{H2} \cdot \frac{K_{OH1} + S_O}{S_O} \cdot \frac{K_{S1} + S_S}{K_{S2} + S_S} \cdot \frac{K_{OH2}}{K_{OH2} + S_O} \cdot \frac{S_{NO3,H}}{K_{NO3,H} + S_{NO3}}$
P 6	Heterotrophic denitrification of $NO_2^- \rightarrow NO$	$\rho_{R4} \cdot \eta_{H3} \cdot \frac{K_{OH1} + S_O}{S_O} \cdot \frac{K_{S1} + S_S}{K_{S3} + S_S} \cdot \frac{K_{OH3}}{K_{OH3} + S_O} \cdot \frac{S_{NO2,H}}{K_{NO2,H} + S_{NO2}} \cdot \frac{K_{I3NO,H}}{K_{I3NO,H} + S_{NO}}$
P 7	Heterotrophic denitrification of $NO \rightarrow N_2O$	$\rho_{R4} \cdot \eta_{H4} \cdot \frac{K_{OH1} + S_O}{S_O} \cdot \frac{K_{S1} + S_S}{K_{S4} + S_S} \cdot \frac{K_{OH4}}{K_{OH4} + S_O} \cdot \frac{S_{NO}}{K_{NOH} + S_{NO} + S_{NO}^2 / K_{I4NO,H}}$
P 8	Heterotrophic denitrification of $N_2O \rightarrow N_2$	$\rho_{P4} \cdot \eta_{H5} \cdot \frac{K_{OH1} + S_O}{S_O} \cdot \frac{K_{F1} + S_F}{K_{F5} + S_F} \cdot \frac{K_{OH5}}{K_{OH5} + S_O} \cdot \frac{S_{N2O,H}}{K_{N2O,H} + S_{N2O}} \cdot \frac{K_{I5NO,H}}{K_{I5NO,H} + S_{NO}}$
P 9	Decay of heterotrophs	$b_{H,Temp} \cdot X_H$

Appendix E Kinetic equations of ASMG1

Process Number	Description	Kinetic equation (ρ)
Heterotrophic processes		
P 10	Growth of X_{AOB} with nitrification of $NH_4^+ \rightarrow NO_2^-$	$\mu_{R, AOB} \cdot \frac{S_{FA}}{K_{FA} + S_{FA} + S_{FA}^2 / K_{IFA,1}} \cdot \frac{K_{IFNA,1}}{K_{IFNA,1} + S_{FNA}} \cdot \frac{S_O}{K_{OA1} + S_O} \cdot X_{AOB}$
P 11	Growth of X_{NOB} with nitrification of $NO_2^- \rightarrow NO_3^-$	$\mu_{R, NOB} \cdot \frac{S_{FNA}}{K_{FNA} + S_{FNA} + S_{FNA}^2 / K_{IFNA,2}} \cdot \frac{K_{IFA,2}}{K_{IFA,2} + S_{FA}} \cdot \frac{S_O}{K_{OA2} + S_O} \cdot X_{NOB}$
P 12	AOB denitrification of $NO_2^- \rightarrow NO$	$\mu_{R, AOB} \cdot \eta_{AOBden1} \cdot \frac{S_{FNA}}{K_{FNA, AOBden1} + S_{FNA}} \cdot \frac{S_{FA}}{K_{FA, AOBden1} + S_O} \cdot DO_{Haldane} \cdot X_{AOB}$
P 13	AOB denitrification of $NO \rightarrow N_2O$	$\mu_{R, AOB} \cdot \eta_{AOBden2} \cdot \frac{S_{NO}}{K_{NO, AOBden2} + S_{FNA}} \cdot \frac{S_{FA}}{K_{FA, AOBden2} + S_O} \cdot DO_{Haldane} \cdot X_{AOB}$
P 14	Decay of X_{AOB}	$b_{AOB, Temp} \cdot X_{AOB}$
P 15	Decay of X_{NOB}	$b_{NOB, Temp} \cdot X_{NOB}$

Note:

- $DO_{Haldane} = \frac{S_O}{K_{SO, AOBden} + \left(1 - 2 \cdot \sqrt{K_{O, AOBden} / K_{IO, AOBden}}\right) \cdot S_O + S_O^2 / K_{IO, AOBden}}$
- $k_{h, Temp} = k_h \cdot \theta_{kh}^{T-T_{reference}}$, $b_{h, Temp} = b_h \cdot \theta_{bh}^{T-T_{reference}}$
- $b_{AOB, Temp} = b_{AOB} \cdot \theta_{bAOB}^{T-T_{reference}}$, $b_{NOB, Temp} = b_{NOB} \cdot \theta_{bNOB}^{T-T_{reference}}$
- $S_{NOx} = S_{NO3} + S_{NO2}$
- $f_{\#}$ stands for the kinetic equation of process P#.

Appendix F Component matrix of ASMG1

Component	Unit	COD (g COD)	N (g N)	Charge (mol)
S_{O_2}	g O ₂	-1	0	0
S_S	g COD	1	0	0
S_{NH_4}	g N	0	1	1/14
S_{NO_3}	g N	64/14	1	-1/14
S_{NO_2}	g N	48/14	1	-1/14
S_{NO}	g N	40/14	1	0
S_{N_2O}	g N	31/14	1	0
S_{N_2}	g N	24/14	1	0
S_I	g COD	1	0	0
S_{Alk}	mol HCO ₃ ⁻	0	0	-1
X_I	g COD	1	0	0
X_S	g COD	1	0	0
X_H	g COD	1	$i_{N,BM}$	0
X_{AOB}	g COD	1	$i_{N,BM}$	0
X_{NOB}	g COD	1	$i_{N,BM}$	0
X_P	g COD	1	$i_{N,XP}$	0
X_{ND}	g N	0	1	0

Appendix G Stoichiometric matrix of ASMG2d

	S_I	S_{O_0}	S_{NO_3}	S_{NO_2}	S_{NO}	S_{N_2O}	S_{N_2}	S_{AI}
P 1	f_{SI}							
P 2	f_{SI}							
P 3	f_{SI}							
P 4		$1 - \frac{1}{Y_H}$						
P 5		$1 - \frac{1}{Y_H}$						
P 6			$-\frac{7}{8} \cdot \frac{1 - Y_H \cdot \eta_{YH}}{Y_H \cdot \eta_{YH}}$	$\frac{7}{8} \cdot \frac{1 - Y_H \cdot \eta_{YH}}{Y_H \cdot \eta_{YH}}$				
P 7			$-\frac{7}{4} \cdot \frac{1 - Y_H \cdot \eta_{YH}}{Y_H \cdot \eta_{YH}}$	$-\frac{7}{4} \cdot \frac{1 - Y_H \cdot \eta_{YH}}{Y_H \cdot \eta_{YH}}$	$\frac{7}{4} \cdot \frac{1 - Y_H \cdot \eta_{YH}}{Y_H \cdot \eta_{YH}}$			
P 8					$-\frac{7}{4} \cdot \frac{1 - Y_H \cdot \eta_{YH}}{Y_H \cdot \eta_{YH}}$	$\frac{7}{4} \cdot \frac{1 - Y_H \cdot \eta_{YH}}{Y_H \cdot \eta_{YH}}$		
P 9						$-\frac{7}{4} \cdot \frac{1 - Y_H \cdot \eta_{YH}}{Y_H \cdot \eta_{YH}}$	$\frac{7}{4} \cdot \frac{1 - Y_H \cdot \eta_{YH}}{Y_H \cdot \eta_{YH}}$	
P 10			$-\frac{7}{8} \cdot \frac{1 - Y_H \cdot \eta_{YH}}{Y_H \cdot \eta_{YH}}$	$\frac{7}{8} \cdot \frac{1 - Y_H \cdot \eta_{YH}}{Y_H \cdot \eta_{YH}}$				
P 11			$-\frac{7}{4} \cdot \frac{1 - Y_H \cdot \eta_{YH}}{Y_H \cdot \eta_{YH}}$	$-\frac{7}{4} \cdot \frac{1 - Y_H \cdot \eta_{YH}}{Y_H \cdot \eta_{YH}}$	$\frac{7}{4} \cdot \frac{1 - Y_H \cdot \eta_{YH}}{Y_H \cdot \eta_{YH}}$			
P 12					$-\frac{7}{4} \cdot \frac{1 - Y_H \cdot \eta_{YH}}{Y_H \cdot \eta_{YH}}$	$\frac{7}{4} \cdot \frac{1 - Y_H \cdot \eta_{YH}}{Y_H \cdot \eta_{YH}}$		
P 13						$-\frac{7}{4} \cdot \frac{1 - Y_H \cdot \eta_{YH}}{Y_H \cdot \eta_{YH}}$	$\frac{7}{4} \cdot \frac{1 - Y_H \cdot \eta_{YH}}{Y_H \cdot \eta_{YH}}$	
P 14								

Appendix G Stoichiometric matrix of ASMG2d (continued)

	S_i	S_{NO3}	S_{NO2}	S_{NO}	S_{N2O}	S_{N2}	S_{AI}
P 15							
P 16							
P 17	$-Y_{PHA}$						
P 18		$-\frac{7}{8} \cdot Y_{PHA} \cdot \eta_{Y_{PHA}}$	$\frac{7}{8} \cdot Y_{PHA} \cdot \eta_{Y_{PHA}}$				
P 19			$-\frac{7}{4} \cdot Y_{PHA} \cdot \eta_{Y_{PHA}}$	$\frac{7}{4} \cdot Y_{PHA} \cdot \eta_{Y_{PHA}}$			
P 20				$-\frac{7}{4} \cdot Y_{PHA} \cdot \eta_{Y_{PHA}}$	$\frac{7}{4} \cdot Y_{PHA} \cdot \eta_{Y_{PHA}}$		
P 21					$-\frac{7}{4} \cdot Y_{PHA} \cdot \eta_{Y_{PHA}}$	$\frac{7}{4} \cdot Y_{PHA} \cdot \eta_{Y_{PHA}}$	
P 22	$1 - \frac{1}{Y_{PAO}}$						
P 23		$-\frac{7}{8} \cdot \frac{1 - Y_{PHA} \cdot \eta_{Y_{PHA}}}{Y_{PHA} \cdot \eta_{Y_{PHA}}}$	$\frac{7}{8} \cdot \frac{1 - Y_{PHA} \cdot \eta_{Y_{PHA}}}{Y_{PHA} \cdot \eta_{Y_{PHA}}}$				
P 24			$-\frac{7}{4} \cdot \frac{1 - Y_{PHA} \cdot \eta_{Y_{PHA}}}{Y_{PHA} \cdot \eta_{Y_{PHA}}}$	$\frac{7}{4} \cdot \frac{1 - Y_{PHA} \cdot \eta_{Y_{PHA}}}{Y_{PHA} \cdot \eta_{Y_{PHA}}}$			
P 25				$-\frac{7}{4} \cdot \frac{1 - Y_{PHA} \cdot \eta_{Y_{PHA}}}{Y_{PHA} \cdot \eta_{Y_{PHA}}}$	$\frac{7}{4} \cdot \frac{1 - Y_{PHA} \cdot \eta_{Y_{PHA}}}{Y_{PHA} \cdot \eta_{Y_{PHA}}}$		
P 26					$-\frac{7}{4} \cdot \frac{1 - Y_{PHA} \cdot \eta_{Y_{PHA}}}{Y_{PHA} \cdot \eta_{Y_{PHA}}}$	$\frac{7}{4} \cdot \frac{1 - Y_{PHA} \cdot \eta_{Y_{PHA}}}{Y_{PHA} \cdot \eta_{Y_{PHA}}}$	
P 27							
P 28							
P 29							

Appendix G Stoichiometric matrix of ASMG2d (continued)

	S_F	S_A	S_{PO4}	S_{NH4}	S_{Alk}
P 1	$1 - f_{SI}$		$i_{p,XS} - f_{SI} \cdot i_{p,SI}$ $-(1 - f_{SI}) \cdot i_{p,SF}$	$i_{N,XS} - f_{SI} \cdot i_{N,SI}$ $-(1 - f_{SI}) \cdot i_{N,SF}$	$\frac{1}{14} \cdot [i_{N,XS} - f_{SI} \cdot i_{N,SI} - (1 - f_{SI}) i_{N,SF}]$ $-\frac{3}{62} \cdot [i_{p,XS} - f_{SI} \cdot i_{p,SI} - (1 - f_{SI}) i_{p,SF}]$
P 2	$1 - f_{SI}$		$i_{p,XS} - f_{SI} \cdot i_{p,SI}$ $-(1 - f_{SI}) \cdot i_{p,SF}$	$i_{N,XS} - f_{SI} \cdot i_{N,SI}$ $-(1 - f_{SI}) \cdot i_{N,SF}$	$\frac{1}{14} \cdot [i_{N,XS} - f_{SI} \cdot i_{N,SI} - (1 - f_{SI}) i_{N,SF}]$ $-\frac{3}{62} \cdot [i_{p,XS} - f_{SI} \cdot i_{p,SI} - (1 - f_{SI}) i_{p,SF}]$
P 3	$1 - f_{SI}$		$i_{p,XS} - f_{SI} \cdot i_{p,SI}$ $-(1 - f_{SI}) \cdot i_{p,SF}$	$i_{N,XS} - f_{SI} \cdot i_{N,SI}$ $-(1 - f_{SI}) \cdot i_{N,SF}$	$\frac{1}{14} \cdot [i_{N,XS} - f_{SI} \cdot i_{N,SI} - (1 - f_{SI}) i_{N,SF}]$ $-\frac{3}{62} \cdot [i_{p,XS} - f_{SI} \cdot i_{p,SI} - (1 - f_{SI}) i_{p,SF}]$
P 4	$-\frac{1}{Y_H}$		$\frac{1}{Y_H} \cdot i_{p,SF} - i_{p,BM}$	$\frac{1}{Y_H} \cdot i_{N,SF} - i_{N,BM}$	$\frac{1}{14} \cdot \left(\frac{1}{Y_H} \cdot i_{N,SF} - i_{N,BM} \right) - \frac{3}{62} \cdot \left(\frac{1}{Y_H} \cdot i_{p,SF} - i_{p,BM} \right)$
P 5		$-\frac{1}{Y_H}$	$-i_{p,BM}$	$-i_{N,BM}$	$-\frac{1}{14} \cdot i_{N,BM} + \frac{3}{62} \cdot i_{p,BM} + \frac{1}{64} \cdot \frac{1}{Y_H}$
P 6	$-\frac{1}{Y_H \cdot \eta_{YH}}$		$\frac{1}{Y_H \cdot \eta_{YH}} \cdot i_{p,SF} - i_{p,BM}$	$\frac{1}{Y_H \cdot \eta_{YH}} \cdot i_{N,SF} - i_{N,BM}$	$\frac{1}{14} \cdot \left(\frac{1}{Y_H \cdot \eta_{YH}} \cdot i_{N,SF} - i_{N,BM} \right) - \frac{3}{62} \cdot \left(\frac{1}{Y_H \cdot \eta_{YH}} \cdot i_{p,SF} - i_{p,BM} \right)$
P 7	$-\frac{1}{Y_H \cdot \eta_{YH}}$		$\frac{1}{Y_H \cdot \eta_{YH}} \cdot i_{p,SF} - i_{p,BM}$	$\frac{1}{Y_H \cdot \eta_{YH}} \cdot i_{N,SF} - i_{N,BM}$	$\frac{1}{14} \cdot \left(\frac{1}{Y_H \cdot \eta_{YH}} \cdot i_{N,SF} - i_{N,BM} + \frac{7}{4} \cdot \frac{1 - Y_H \cdot \eta_{YH}}{Y_H \cdot \eta_{YH}} \right)$ $-\frac{3}{62} \cdot \left(\frac{1}{Y_H \cdot \eta_{YH}} \cdot i_{p,SF} - i_{p,BM} \right)$

Appendix G Stoichiometric matrix of ASMG2d (continued)

	S _F	S _A	S _{PO4}	S _{NH4}	S _{AIK}
P 8	$-\frac{1}{Y_H \cdot \eta_{YH}}$		$\frac{1}{Y_H \cdot \eta_{YH}} \cdot i_{P,SF} - i_{P,BM}$	$\frac{1}{Y_H \cdot \eta_{YH}} \cdot i_{N,SF} - i_{N,BM}$	$\frac{1}{14} \cdot \left(\frac{1}{Y_H \cdot \eta_{YH}} \cdot i_{N,SF} - i_{N,BM} \right) - \frac{3}{62} \cdot \left(\frac{1}{Y_H \cdot \eta_{YH}} \cdot i_{P,SF} - i_{P,BM} \right)$
P 9	$-\frac{1}{Y_H \cdot \eta_{YH}}$		$\frac{1}{Y_H \cdot \eta_{YH}} \cdot i_{P,SF} - i_{P,BM}$	$\frac{1}{Y_H \cdot \eta_{YH}} \cdot i_{N,SF} - i_{N,BM}$	$\frac{1}{14} \cdot \left(\frac{1}{Y_H \cdot \eta_{YH}} \cdot i_{N,SF} - i_{N,BM} \right) - \frac{3}{62} \cdot \left(\frac{1}{Y_H \cdot \eta_{YH}} \cdot i_{P,SF} - i_{P,BM} \right)$
P 10		$-\frac{1}{Y_H \cdot \eta_{YH}}$	$-i_{P,BM}$	$-i_{N,BM}$	$-\frac{1}{14} \cdot i_{N,BM} + \frac{3}{62} \cdot i_{P,BM} + \frac{1}{64} \cdot \frac{1}{Y_H \cdot \eta_{YH}}$
P 11		$-\frac{1}{Y_H \cdot \eta_{YH}}$	$-i_{P,BM}$	$-i_{N,BM}$	$-\frac{1}{14} \cdot \left(i_{N,BM} - \frac{7}{4} \cdot \frac{1 - Y_H \cdot \eta_{YH}}{Y_H \cdot \eta_{YH}} \right) + \frac{3}{62} \cdot i_{P,BM} + \frac{1}{64} \cdot \frac{1}{Y_H \cdot \eta_{YH}}$
P 12		$-\frac{1}{Y_H \cdot \eta_{YH}}$	$-i_{P,BM}$	$-i_{N,BM}$	$-\frac{1}{14} \cdot i_{N,BM} + \frac{3}{62} \cdot i_{P,BM} + \frac{1}{64} \cdot \frac{1}{Y_H \cdot \eta_{YH}}$
P 13		$-\frac{1}{Y_H \cdot \eta_{YH}}$	$-i_{P,BM}$	$-i_{N,BM}$	$-\frac{1}{14} \cdot i_{N,BM} + \frac{3}{62} \cdot i_{P,BM} + \frac{1}{64} \cdot \frac{1}{Y_H \cdot \eta_{YH}}$
P 14	-1	1	$-i_{P,SF}$	$-i_{N,SF}$	$\frac{1}{14} \cdot i_{N,SF} - \frac{3}{62} \cdot i_{P,SF} - \frac{1}{64}$
P 15			$i_{P,BM} - f_{XI} \cdot i_{P,XI} - (1 - f_{XI}) \cdot i_{P,XS}$	$i_{N,BM} - f_{XI} \cdot i_{N,XI} - (1 - f_{XI}) \cdot i_{N,XS}$	$\frac{1}{14} \cdot \left[i_{N,BM} - f_{XI} \cdot i_{N,XI} - (1 - f_{XI}) \cdot i_{N,XS} \right] - \frac{3}{62} \cdot \left[i_{P,BM} - f_{XI} \cdot i_{P,XI} - (1 - f_{XI}) \cdot i_{P,XS} \right]$
P 16		-1	Y_{PO}		$-\frac{1}{62} \cdot Y_{PO} + \frac{1}{64}$

Appendix G Stoichiometric matrix of ASMG2d (continued)

	S_F	S_A	S_{PO4}	S_{NH4}	S_{Alk}
P 17			-1		$\frac{1}{62}$
P 18			-1		$\frac{1}{62}$
P 19			-1		$\frac{1}{62} + \frac{7}{14} \cdot Y_{PHA} \cdot \eta_{YPHA}$
P 20			-1		$\frac{1}{62}$
P 21			-1		$\frac{1}{62}$
P 22			$-i_{P,BM}$	$-i_{N,BM}$	$-\frac{1}{14} \cdot i_{N,BM} + \frac{3}{62} \cdot i_{P,BM}$
P 23			$-i_{P,BM}$	$-i_{N,BM}$	$-\frac{1}{14} \cdot i_{N,BM} + \frac{3}{62} \cdot i_{P,BM}$
P 24			$-i_{P,BM}$	$-i_{N,BM}$	$-\frac{1}{14} \cdot \left(i_{N,BM} - \frac{7}{4} \frac{1 - Y_{PAO} \cdot \eta_{YPAO}}{Y_{PAO} \cdot \eta_{YPAO}} \right) + \frac{3}{62} \cdot i_{P,BM}$
P 25			$-i_{P,BM}$	$-i_{N,BM}$	$-\frac{1}{14} \cdot i_{N,BM} + \frac{3}{62} \cdot i_{P,BM}$
P 26			$-i_{P,BM}$	$-i_{N,BM}$	$-\frac{1}{14} \cdot i_{N,BM} + \frac{3}{62} \cdot i_{P,BM}$
P 27			$i_{P,BM} - f_{XI} \cdot i_{P,XI}$ $-(1 - f_{XI}) \cdot i_{P,XS}$	$i_{N,BM} - f_{XI} \cdot i_{N,XI}$ $-(1 - f_{XI}) \cdot i_{N,XS}$	$\frac{1}{14} \cdot [i_{N,BM} - f_{XI} \cdot i_{N,XI} - (1 - f_{XI}) \cdot i_{N,XS}]$ $-\frac{3}{62} \cdot [i_{P,BM} - f_{XI} \cdot i_{P,XI} - (1 - f_{XI}) \cdot i_{P,XS}]$

Appendix G Stoichiometric matrix of ASMG2d (continued)

	S _F	S _A	S _{PO4}	S _{NH4}	S _{Aik}
P 28			1		$\frac{1}{-62}$
P 29		1			$\frac{1}{-64}$
P 30			$-i_{P,BM}$	$-\frac{1}{Y_{AOB}} \cdot i_{N,BM}$	$-\frac{1}{14} \cdot \left(i_{N,BM} + \frac{2}{Y_{AOB}} \right) + \frac{3}{62} \cdot i_{P,BM}$
P 31			$-i_{P,BM}$	$-i_{N,BM}$	$-\frac{1}{14} \cdot i_{N,BM} + \frac{3}{62} \cdot i_{P,BM}$
P 32			$-i_{P,BM}$	$-\frac{1}{Y_{AOB} \cdot \eta_{YAOB}} \cdot i_{N,BM}$	$-\frac{1}{14} \cdot i_{N,BM} + \frac{3}{62} \cdot i_{P,BM}$
P 33			$-i_{P,BM}$	$-\frac{1}{Y_{AOB} \cdot \eta_{YAOB}} \cdot i_{N,BM}$	$-\frac{1}{14} \cdot \left(i_{N,BM} + \frac{2}{Y_{AOB} \cdot \eta_{YAOB}} \right) + \frac{3}{62} \cdot i_{P,BM}$
P 34			$i_{P,BM} - f_{XI} \cdot i_{P,XI}$ $-(1-f_{XI}) \cdot i_{P,XS}$	$i_{N,BM} - f_{XI} \cdot i_{N,XI}$ $-(1-f_{XI}) \cdot i_{N,XS}$	$\frac{1}{14} \cdot \left[i_{N,BM} - f_{XI} \cdot i_{N,XI} - (1-f_{XI}) \cdot i_{N,XS} \right]$ $-\frac{3}{62} \cdot \left[i_{P,BM} - f_{XI} \cdot i_{P,XI} - (1-f_{XI}) \cdot i_{P,XS} \right]$
P 35			$i_{P,BM} - f_{XI} \cdot i_{P,XI}$ $-(1-f_{XI}) \cdot i_{P,XS}$	$i_{N,BM} - f_{XI} \cdot i_{N,XI}$ $-(1-f_{XI}) \cdot i_{N,XS}$	$\frac{1}{14} \cdot \left[i_{N,BM} - f_{XI} \cdot i_{N,XI} - (1-f_{XI}) \cdot i_{N,XS} \right]$ $-\frac{3}{62} \cdot \left[i_{P,BM} - f_{XI} \cdot i_{P,XI} - (1-f_{XI}) \cdot i_{P,XS} \right]$
P 36			-1		$\frac{3}{62}$
P 37			1		$-\frac{3}{62}$

Appendix G Stoichiometric matrix of ASMG2d (continued)

	X_i	X_S	X_H	X_{PAO}	X_{PP}	X_{PHA}	X_{AOB}	X_{NOB}	X_{ij}	X_{MeOH}	X_{MeP}	X_{TSS}
P 1		-1										$-i_{TSS,XS}$
P 2		-1										$-i_{TSS,XS}$
P 3		-1										$-i_{TSS,XS}$
P 4			1									$-i_{TSS,BM}$
P 5			1									$-i_{TSS,BM}$
P 6			1									$-i_{TSS,BM}$
P 7			1									$-i_{TSS,BM}$
P 8			1									$-i_{TSS,BM}$
P 9			1									$-i_{TSS,BM}$
P 10			1									$-i_{TSS,BM}$
P 11			1									$-i_{TSS,BM}$
P 12			1									$-i_{TSS,BM}$
P 13			1									$-i_{TSS,BM}$
P 14												$-i_{TSS,BM}$

Appendix G Stoichiometric matrix of ASMG2d (continued)

	X_i	X_S	X_H	X_{PAO}	X_{PP}	X_{PHA}	X_{AOB}	X_{NOB}	X_{ij}	X_{MeOH}	X_{MeP}	X_{TSS}
P 15	f_{XI}	$1 - f_{XI}$	-1									$-i_{TSS,BM} + f_{XI} \cdot i_{TSS,XI}$ $+(1 - f_{XI}) \cdot i_{TSS,XS}$
P 16				$-Y_{PO}$	1							$-3.23 \cdot Y_{PO} + 0.6$
P 17					1	$-Y_{PHA}$						$3.23 - 0.6 \cdot Y_{PHA}$
P 18					1	$-Y_{PHA} \cdot \eta_{YPHA}$						$3.23 - 0.6 \cdot Y_{PHA} \cdot \eta_{YPHA}$
P 19					1	$-Y_{PHA} \cdot \eta_{YPHA}$						$3.23 - 0.6 \cdot Y_{PHA} \cdot \eta_{YPHA}$
P 20					1	$-Y_{PHA} \cdot \eta_{YPHA}$						$3.23 - 0.6 \cdot Y_{PHA} \cdot \eta_{YPHA}$
P 21					1	$-Y_{PHA} \cdot \eta_{YPHA}$						$3.23 - 0.6 \cdot Y_{PHA} \cdot \eta_{YPHA}$
P 22				1		$-\frac{1}{Y_{PAO}}$						$i_{TSS,BM} - 0.6 \cdot \frac{1}{Y_{PAO}}$
P 23				1		$-\frac{1}{Y_{PAO} \cdot \eta_{YPAO}}$						$i_{TSS,BM} - 0.6 \cdot \frac{1}{Y_{PAO} \cdot \eta_{YPAO}}$
P 24				1		$-\frac{1}{Y_{PAO} \cdot \eta_{YPAO}}$						$i_{TSS,BM} - 0.6 \cdot \frac{1}{Y_{PAO} \cdot \eta_{YPAO}}$
P 25				1		$-\frac{1}{Y_{PAO} \cdot \eta_{YPAO}}$						$i_{TSS,BM} - 0.6 \cdot \frac{1}{Y_{PAO} \cdot \eta_{YPAO}}$
P 26				1		$-\frac{1}{Y_{PAO} \cdot \eta_{YPAO}}$						$i_{TSS,BM} - 0.6 \cdot \frac{1}{Y_{PAO} \cdot \eta_{YPAO}}$
P 27	f_{XI}	$1 - f_{XI}$		-1								$-i_{TSS,BM} + f_{XI} \cdot i_{TSS,XI}$ $+(1 - f_{XI}) \cdot i_{TSS,XS}$
P 28					-1							-3.23
P 29						-1						-0.6

Appendix G Stoichiometric matrix of ASMG2d (continued)

	X_I	X_S	X_H	X_{PAO}	X_{PP}	X_{PHA}	X_{AOB}	X_{NOB}	X_{ij}	X_{MeOH}	X_{MeP}	X_{TSS}
P 30							1					$i_{TSS,BM}$
P 31								1				$i_{TSS,BM}$
P 32							1					$i_{TSS,BM}$
P 33							1					$i_{TSS,BM}$
P 34	f_{XI}	$1 - f_{XI}$					-1					$-i_{TSS,BM} + f_{XI} \cdot i_{TSS,XI}$ $+ (1 - f_{XI}) \cdot i_{TSS,XS}$
P 35	f_{XI}	$1 - f_{XI}$					-1					$-i_{TSS,BM} + f_{XI} \cdot i_{TSS,XI}$ $+ (1 - f_{XI}) \cdot i_{TSS,XS}$
P 36										$\frac{107}{151} \cdot \frac{1}{0.205}$	$\frac{1}{0.205}$	$\frac{44}{151} \cdot \frac{1}{0.205}$
P 37										$\frac{107}{151} \cdot \frac{1}{0.205}$	$\frac{1}{0.205}$	$-\frac{44}{151} \cdot \frac{1}{0.205}$

Appendix H Kinetic equations of ASMG2d

Process Number	Description	Kinetic equation (ρ)
Heterotrophic processes		
P 1	Aerobic hydrolysis	$k_{h,Temp} \cdot \frac{S_O}{K_{O,Hyd} + S_O} \cdot \frac{X_S}{K_X + X_S} \cdot X_H$
P 2	Anoxic hydrolysis	$\rho_{P1} \cdot \eta_{Hyd} \cdot \frac{K_{O,Hyd}}{S_O} \cdot \frac{S_{NOx}}{K_{NOx,Hyd} + S_{NOx}} \cdot X_H$
P 3	Anaerobic hydrolysis	$\rho_{P1} \cdot \eta_{fe} \cdot \frac{K_{O,Hyd}}{S_O} \cdot \frac{K_{NOx,Hyd}}{K_{NOx,Hyd} + S_{NOx}} \cdot X_H$
P 4	Heterotrophic aerobic growth on S_F	$\mu_{R,H} \cdot \frac{S_O}{K_{OH1} + S_O} \cdot \frac{S_F}{K_{F1} + S_F} \cdot \frac{S_{NH4}}{S_{NH4} + S_{NH4}} \cdot \frac{S_{PO4}}{K_{PO4,H} + S_{PO4}} \cdot \frac{S_{Alk}}{K_{Alk,H} + S_{Alk}} \cdot X_H$
P 5	Heterotrophic aerobic growth on S_A	$\mu_{R,H} \cdot \frac{S_O}{K_{OH1} + S_O} \cdot \frac{S_A}{K_{F1} + S_F} \cdot \frac{S_{NH4}}{K_{NH4,H} + S_{NH4}} \cdot \frac{S_{PO4}}{K_{PO4,H} + S_{PO4}} \cdot \frac{S_{Alk}}{K_{Alk,H} + S_{Alk}} \cdot X_H$
P 6	Heterotrophic denitrification of $NO_3^- \rightarrow NO_2^-$ on S_F	$\rho_{R4} \cdot \eta_{H2} \cdot \frac{K_{OH1} + S_O}{S_O} \cdot \frac{K_{F1} + S_F}{K_{F2} + S_F} \cdot \frac{K_{OH2}}{K_{OH2} + S_O} \cdot \frac{S_{NO3,H}}{K_{NO3,H} + S_{NO3}}$
P 7	Heterotrophic denitrification of $NO_2^- \rightarrow NO$ on S_F	$\rho_{R4} \cdot \eta_{H3} \cdot \frac{K_{OH1} + S_O}{S_O} \cdot \frac{K_{F1} + S_F}{K_{F3} + S_F} \cdot \frac{K_{OH3}}{K_{OH3} + S_O} \cdot \frac{S_{NO2,H}}{K_{NO2,H} + S_{NO2}} \cdot \frac{K_{I3NO,H}}{K_{I3NO,H} + S_{NO}}$
P 8	Heterotrophic denitrification of $NO \rightarrow N_2O$ on S_F	$\rho_{R4} \cdot \eta_{H4} \cdot \frac{K_{OH1} + S_O}{S_O} \cdot \frac{K_{F1} + S_F}{K_{F4} + S_F} \cdot \frac{K_{OH4}}{K_{OH4} + S_O} \cdot \frac{S_{NO}}{K_{NO,H} + S_{NO} + S_{NO}^2 / K_{I4NO,H}}$

Appendix H Kinetic equations of ASMG2d (continued)

Process Number	Description	Kinetic equation (ρ)
Heterotrophic processes		
P 9	Heterotrophic denitrification of $N_2O \rightarrow N_2$ on S_F	$\rho_{P9} \cdot \eta_{H5} \cdot \frac{K_{OH1} + S_O}{S_O} \cdot \frac{K_{F1} + S_F}{K_{F5} + S_F} \cdot \frac{K_{OH5}}{K_{OH5} + S_O} \cdot \frac{S_{N2O,H}}{K_{N2O,H} + S_{N2O}} \cdot \frac{K_{ISNO,H}}{K_{ISNO,H} + S_{NO}}$
P 10	Heterotrophic denitrification of $NO_3^- \rightarrow NO_2^-$ on S_A	$\rho_{P10} \cdot \eta_{H2} \cdot \frac{K_{OH1} + S_O}{S_O} \cdot \frac{K_{A1} + S_F}{K_{A2} + S_F} \cdot \frac{K_{OH2}}{K_{OH2} + S_O} \cdot \frac{S_{NO3,H}}{K_{NO3,H} + S_{NO3}}$
P 11	Heterotrophic denitrification of $NO_2^- \rightarrow NO$ on S_A	$\rho_{P11} \cdot \eta_{H3} \cdot \frac{K_{OH1} + S_O}{S_O} \cdot \frac{K_{A1} + S_F}{K_{A3} + S_F} \cdot \frac{K_{OH3}}{K_{OH3} + S_O} \cdot \frac{S_{NO2,H}}{K_{NO2,H} + S_{NO2}} \cdot \frac{K_{ISNO,H}}{K_{ISNO,H} + S_{NO}}$
P 12	Heterotrophic denitrification of $NO \rightarrow N_2O$ on S_A	$\rho_{P12} \cdot \eta_{H4} \cdot \frac{K_{OH1} + S_O}{S_O} \cdot \frac{K_{A1} + S_F}{K_{A4} + S_F} \cdot \frac{K_{OH4}}{K_{OH4} + S_O} \cdot \frac{S_{NO}}{K_{NO,H} + S_{NO} + S_{NO}^2 / K_{I4NO,H}}$
P 13	Heterotrophic denitrification of $N_2O \rightarrow N_2$ on S_A	$\rho_{P13} \cdot \eta_{H5} \cdot \frac{K_{OH1} + S_O}{S_O} \cdot \frac{K_{A1} + S_F}{K_{A5} + S_F} \cdot \frac{K_{OH5}}{K_{OH5} + S_O} \cdot \frac{S_{N2O,H}}{K_{N2O,H} + S_{N2O}} \cdot \frac{K_{ISNO,H}}{K_{ISNO,H} + S_{NO}}$
P 14	Fermentation	$q_{fe,Temp} \cdot \frac{K_{O,Ferm}}{K_{O,Ferm} + S_O} \cdot \frac{K_{NOx,Ferm}}{K_{NOx,Ferm} + S_{NOx}} \cdot \frac{S_F}{K_{fe} + S_F} \cdot \frac{S_{Alk}}{K_{Alk,H} + S_{Alk}} \cdot X_H$
P 15	Lysis of heterotrophs	$b_{H,Temp} \cdot \left(\frac{S_O}{K_{O,H,b} + S_O} + \eta_{H,b} \cdot \frac{K_{O,H,b}}{K_{O,H,b} + S_O} \cdot \frac{S_{NOx}}{K_{NOx,H,b} + S_{NOx}} \right) \cdot X_H$

Appendix H Kinetic equations of ASMG2d (continued)

Process Number	Description	Kinetic equation (ρ)
PAO processes		
P 16	Storage of X_{PHA}	$q_{PHA,Temp} \cdot \frac{S_A}{K_{A,PHAStor} + S_A} \cdot \frac{S_{Alk}}{K_{Alk,PAO} + S_{Alk}} \cdot \frac{X_{PP} / X_{PAO}}{K_{PP} + X_{PP} / X_{PAO}} \cdot X_{PAO}$
P 17	Aerobic storage of X_{PP}	$q_{PP,Temp} \cdot \frac{S_{PO4}}{K_{O,PAO} + S_{O_2}} \cdot \frac{S_{Alk}}{K_{P,PPStor} + S_{PO4}} \cdot \frac{X_{PP}}{K_{Alk,PAO} + S_{Alk}} \cdot \frac{X_{PHA}}{K_{PHA} + X_{PHA}}$ $\cdot \frac{K_{MAX} - X_{PP} / X_{PAO}}{K_{IPP} + K_{MAX} - X_{PP} / X_{PAO}} \cdot X_{PAO}$
P 18	Anoxic storage of X_{PP} with denitrification of $NO_3^- \rightarrow NO_2^-$	$\rho_{P17} \cdot \eta_{PAO2} \cdot \frac{K_{O,PAO}}{S_{O_2}} \cdot \frac{S_{NO3}}{K_{NO3,PAO} + S_{NO3}}$
P 19	Anoxic storage of X_{PP} with denitrification of $NO_2^- \rightarrow NO$	$\rho_{P17} \cdot \eta_{PAO3} \cdot \frac{K_{O,PAO}}{S_{O_2}} \cdot \frac{S_{NO2}}{K_{NO2,PAO} + S_{NO2}} \cdot \frac{K_{ISNO,PAO}}{K_{ISNO,PAO} + S_{NO}}$
P 20	Anoxic storage of X_{PP} with denitrification of $NO \rightarrow N_2O$	$\rho_{P17} \cdot \eta_{PAO4} \cdot \frac{K_{O,PAO}}{S_{O_2}} \cdot \frac{S_{NO}}{K_{NO,PAO} + S_{NO} + S_{NO}^2 / K_{IHNO,PAO}}$
P 21	Anoxic storage of X_{PP} with denitrification of $N_2O \rightarrow N_2$	$\rho_{P17} \cdot \eta_{PAO5} \cdot \frac{K_{O,PAO}}{S_{O_2}} \cdot \frac{S_{N2O}}{K_{N2O,PAO} + S_{N2O}} \cdot \frac{K_{ISNO,PAO}}{K_{ISNO,PAO} + S_{NO}}$
P 22	Aerobic growth on X_{PHA}	$\mu_{R,PAO} \cdot \frac{S_{O_2}}{K_{O,PAO} + S_{O_2}} \cdot \frac{X_{PHA}}{K_{PHA} + X_{PHA}} \cdot \frac{S_{NH4}}{K_{NH4,PAO} + S_{NH4}} \cdot \frac{S_{PO4}}{K_{P,PAO} + S_{PO4}} \cdot \frac{S_{Alk}}{K_{Alk,PAO} + S_{Alk}} \cdot X_{PAO}$
P 23	Anoxic growth on X_{PHA} with denitrification of $NO_3^- \rightarrow NO_2^-$	$\rho_{P22} \cdot \eta_{PAO2} \cdot \frac{K_{O,PAO}}{S_{O_2}} \cdot \frac{S_{NO3}}{K_{NO3,PAO} + S_{NO3}}$

Appendix H Kinetic equations of ASMG2d (continued)

Process Number	Description	Kinetic equation (p)
PAO processes		
P 24	Anoxic growth on X_{PHA} with denitrification of $NO_2^- \rightarrow NO$	$\rho_{P22} \cdot \eta_{PAO3} \cdot \frac{K_{O,PAO}}{S_O} \cdot \frac{S_{NO2}}{K_{NO2,PAO} + S_{NO2}} \cdot \frac{K_{ISNO,PAO}}{K_{ISNO,PAO} + S_{NO}}$
P 25	Anoxic growth on X_{PHA} with denitrification of $NO \rightarrow N_2O$	$\rho_{P22} \cdot \eta_{PAO4} \cdot \frac{K_{O,PAO}}{S_O} \cdot \frac{S_{NO}}{K_{NO,PAO} + S_{NO} + S_{NO}^2 / K_{I4NO,PAO}}$
P 26	Anoxic growth on X_{PHA} with denitrification of $N_2O \rightarrow N_2$	$\rho_{P22} \cdot \eta_{PAO5} \cdot \frac{K_{O,PAO}}{S_O} \cdot \frac{S_{N2O}}{K_{N2O,PAO} + S_{N2O}} \cdot \frac{K_{ISNO,PAO}}{K_{ISNO,PAO} + S_{NO}}$
P 28	Lysis of X_{PP}	$b_{PAO,Temp} \cdot \left(\frac{S_O}{K_{O,PAO,b} + S_O} + \eta_{PAO,b} \cdot \frac{K_{O,PAO,b}}{K_{O,PAO,b} + S_O} \cdot \frac{S_{NOx}}{K_{NOx,PAO,b} + S_{NOx}} \right) \cdot \frac{S_{Alk}}{K_{Alk,PAO} + S_{Alk}} \cdot X_{PAO}$
P 29	Lysis of X_{PHA}	$b_{PAO,Temp} \cdot \left(\frac{S_O}{K_{O,PAO,b} + S_O} + \eta_{PAO,b} \cdot \frac{K_{O,PAO,b}}{K_{O,PAO,b} + S_O} \cdot \frac{S_{NOx}}{K_{NOx,PAO,b} + S_{NOx}} \right) \cdot \frac{S_{Alk}}{K_{Alk,PAO} + S_{Alk}} \cdot X_{PAO}$
Autotrophic processes		
P 30	Growth of X_{AOB} with nitrification of $NH_4^+ \rightarrow NO_2^-$	$\mu_{R,AOB} \cdot \frac{S_{FA}}{K_{FA} + S_{FA} + S_{FA}^2 / K_{IFA,1}} \cdot \frac{K_{IFNA,1}}{K_{IFNA,1} + S_{FNA}} \cdot \frac{S_O}{K_{OA1} + S_O} \cdot \frac{S_{PO4}}{K_{P,Aut} + S_{PO4}} \cdot \frac{S_{Alk}}{K_{Alk,Aut} + S_{Alk}} \cdot X_{AOB}$
P 31	Growth of X_{NOB} with nitrification of $NO_2^- \rightarrow NO_3^-$	$\mu_{R,NOB} \cdot \frac{S_{FNA}}{K_{FNA} + S_{FNA} + S_{FNA}^2 / K_{IFNA,2}} \cdot \frac{K_{IFA,2}}{K_{IFA,2} + S_{FA}} \cdot \frac{S_O}{K_{OA2} + S_O} \cdot \frac{S_{PO4}}{K_{P,Aut} + S_{PO4}} \cdot \frac{S_{Alk}}{K_{Alk,Aut} + S_{Alk}} \cdot X_{NOB}$
P 32	AOB denitrification of $NO_2^- \rightarrow NO$	$\mu_{R,AOB} \cdot \eta_{AOBden1} \cdot \frac{S_{FNA}}{K_{FNA,AOBden} + S_{FNA}} \cdot \frac{S_{FA}}{K_{FA,AOBden} + S_O} \cdot DO_{Haldane} \cdot \frac{S_{PO4}}{K_{P,Aut} + S_{PO4}} \cdot \frac{S_{Alk}}{K_{Alk,Aut} + S_{Alk}} \cdot X_{AOB}$

Appendix H Kinetic equations of ASMG2d (continued)

Process Number	Description	Kinetic equation (p)
Autotrophic processes		
P 33	AOB denitrification of $\text{NO} \rightarrow \text{N}_2\text{O}$	$\mu_{r,\text{AOB}} \cdot \eta_{\text{AOBden}2} \cdot \frac{S_{\text{NO}}}{K_{\text{NO,AOBden}2} + S_{\text{FNA}} + S_{\text{NO}}} \cdot \frac{S_{\text{FA}}}{K_{\text{FA,AOBden}} + S_{\text{O}}} \cdot \text{DO}_{\text{Haldane}} \cdot \frac{S_{\text{PO4}}}{K_{\text{P,Aut}} + S_{\text{PO4}}} \cdot \frac{S_{\text{Alk}}}{K_{\text{Alk,Aut}} + S_{\text{Alk}}} \cdot X_{\text{AOB}}$
P 34	Lysis of X_{AOB}	$b_{\text{AOB,Temp}} \cdot \left(\frac{S_{\text{O}}}{K_{\text{O,AOB,b}} + S_{\text{O}}} + \eta_{\text{AOB,b}} \cdot \frac{K_{\text{O,AOB,b}}}{K_{\text{O,AOB,b}} + S_{\text{O}}} \cdot \frac{S_{\text{NOx}}}{K_{\text{NOx,AOB,b}} + S_{\text{NOx}}} \right) \cdot X_{\text{AOB}}$
P 34	Lysis of X_{AOB}	$b_{\text{AOB,Temp}} \cdot \left(\frac{S_{\text{O}}}{K_{\text{O,AOB,b}} + S_{\text{O}}} + \eta_{\text{AOB,b}} \cdot \frac{K_{\text{O,AOB,b}}}{K_{\text{O,AOB,b}} + S_{\text{O}}} \cdot \frac{S_{\text{NOx}}}{K_{\text{NOx,AOB,b}} + S_{\text{NOx}}} \right) \cdot X_{\text{AOB}}$
P 35	Lysis of X_{NOB}	$b_{\text{NOB,Temp}} \cdot \left(\frac{S_{\text{O}}}{K_{\text{O,NOB,b}} + S_{\text{O}}} + \eta_{\text{NOB,b}} \cdot \frac{K_{\text{O,NOB,b}}}{K_{\text{O,NOB,b}} + S_{\text{O}}} \cdot \frac{S_{\text{NOx}}}{K_{\text{NOx,NOB,b}} + S_{\text{NOx}}} \right) \cdot X_{\text{NOB}}$

Appendix H Kinetic equations of ASMG2d (continued)

Process Number	Description	Kinetic equation (p)
Precipitation and Redissolution		
P 36	Precipitation	$k_{\text{PRE}} \cdot S_{\text{PO4}} \cdot X_{\text{MeOH}}$
P 37	Redissolution	$k_{\text{RED}} \cdot \frac{S_{\text{Alk}}}{K_{\text{Alk,RED}} + S_{\text{Alk}}} \cdot X_{\text{MeP}}$

Note:

- $$\text{DO}_{\text{Haldane}} = \frac{S_{\text{O}}}{K_{\text{SO,AOBden}} + \left(1 - 2 \cdot \sqrt{K_{\text{O,AOBden}} / K_{\text{IO,AOBden}}}\right) \cdot S_{\text{O}} + S_{\text{O}}^2 / K_{\text{IO,AOBden}}}$$
- $$k_{h, \text{Temp}} = k_h \cdot \theta_{\text{kh}}^{T - T_{\text{reference}}}, \quad q_{\text{fe,Temp}} = q_{\text{fe}} \cdot \theta_{\text{qfe}}^{T - T_{\text{reference}}}, \quad b_{\text{H,Temp}} = b_{\text{H}} \cdot \theta_{\text{bH}}^{T - T_{\text{reference}}}$$
- $$q_{\text{PHA,Temp}} = q_{\text{PHA}} \cdot \theta_{\text{qPHA}}^{T - T_{\text{reference}}}, \quad q_{\text{PP,Temp}} = q_{\text{PP}} \cdot \theta_{\text{qPP}}^{T - T_{\text{reference}}}, \quad b_{\text{PAO,Temp}} = b_{\text{PAO}} \cdot \theta_{\text{bPAO}}^{T - T_{\text{reference}}}$$
- $$b_{\text{AOB,Temp}} = b_{\text{AOB}} \cdot \theta_{\text{bAOB}}^{T - T_{\text{reference}}}, \quad b_{\text{NOB,Temp}} = b_{\text{NOB}} \cdot \theta_{\text{bNOB}}^{T - T_{\text{reference}}}$$
- $$S_{\text{NOx}} = S_{\text{NO3}} + S_{\text{NO2}}$$
- $f_{\text{P\#}}$ stands for the kinetic equation of process P#.

Appendix I Component matrix of ASMG2d

Component	Unit	COD (g COD)	N (g N)	P (g P)	Charge (mol)	Mass (g TSS)
S _O	g O ₂	-1	0	0	0	0
S _F	g COD	1	$i_{N,SF}$	$i_{P,SF}$	0	0
S _A	g COD	1	0	0	-1/64	0
S _{NH4}	g N	0	1	0	1/14	0
S _{NO3}	g N	64/14	1	0	-1/14	0
S _{NO2}	g N	48/14	1	0	-1/14	0
S _{NO}	g N	40/14	1	0	0	0
S _{N2O}	g N	31/14	1	0	0	0
S _{N2}	g N	24/14	1	0	0	0
S _{PO4}	g P	0	0	1	-3/62	0
S _I	g COD	1	$i_{N,SI}$	$i_{N,SI}$	0	0
S _{Alk}	mol HCO ₃ ⁻	0	0	0	-1	0
X _I	g COD	1	$i_{N,XI}$	$i_{N,XI}$	0	$i_{TSS,XI}$
X _S	g COD	1	$i_{N,XS}$	$i_{N,XS}$	0	$i_{TSS,XS}$
X _H	g COD	1	$i_{N,HB}$	$i_{N,HB}$	0	$i_{TSS,HB}$
X _{PAO}	g COD	1	$i_{N,HB}$	$i_{N,HB}$	0	$i_{TSS,HB}$
X _{PP}	g P	0	0	1	-1/31	3.23
X _{FHA}	g COD	1	0	0	0	0.6
X _{AOB}	g COD	1	$i_{N,HB}$	$i_{N,HB}$	0	$i_{TSS,HB}$
X _{NOB}	g COD	1	$i_{N,HB}$	$i_{N,HB}$	0	$i_{TSS,HB}$
X _{TSS}	g TSS	0	0	0	0	-1
X _{MeOH}	g TSS	0	0	0	0	1
X _{MeP}	g TSS	0	0	0.205	0	1

Appendix J Publications and conferences

1. Journal papers

Guo L. and Vanrolleghem P.A. (2013) Calibration and validation of an Activated Sludge

Model for Greenhouse gases No. 1 (ASMG1) - Prediction of temperature dependent

N₂O emission dynamics. *Bioprocess and Biosystems Engineering*, 37, 151-163.

Guo L., Porro J., Sharma K.R., Amerlinck Y., Benedetti L., Nopens I., Shaw A., Van Hulle

S.W., Yuan Z. and Vanrolleghem P.A. (2012) Towards a benchmarking tool for

minimizing wastewater utility greenhouse gas footprints. *Water Science and*

Technology, 66 (11), 2483-2495.

Guo L., Lamaire-Chad C., Bellandi G., Daelman M., Amerlinck Y., Maere T., Nous J.,

Flameling T., Weijers S., van Loosdrecht M.C.M., Volcke E.I.P., Nopens I. and

Vanrolleghem P.A. (2014) Full-scale field measurement of nitrous oxide (N₂O) gas

emissions and its relationship with other nitrogen species under dry and wet weather

conditions. Submitted.

Guo L. and Vanrolleghem P.A. (2014) Interaction of weather conditions and ammonia-

based feedforward and feedback control strategies on N₂O emissions at full-scale

wastewater treatment plants. In preparation.

Guo L. and Vanrolleghem P.A. (2013) Full-scale simulation of N₂O emissions with ASMG2d and elucidation of its different production and emission sources in nitrogen (N) and phosphorus (P) removed systems. Submitted.

Flores-Alsina X., Arnell M., Amerlinck Y., Corominas L., Gernaey K.V., **Guo L.**, Lindblom E., Nopens I., Porro J., Shaw A., Snip L., Vanrolleghem P.A. and Jeppsson U. (2014) Balancing effluent quality, economic cost and greenhouse gas emissions during the evaluation of (plant-wide) control/operational strategies in WWTPs. Science of The Total Environment, 466-467, 616-624.

2. Conferences

2.1 Oral presentations

Spérandio M., Pocquet M., **Guo L.**, Vanrolleghem P.A., Ni B.-J. and Yuan Z. (2013) Calibration of nitrous oxide production models with continuous long-term process data. In proceedings of the 4th IWAWEF Wastewater Treatment Modelling Seminar 2014 (WWTmod2014). Spa, Belgium, March 30 - April 2 2014.

Vanrolleghem P.A., Flores-Alsina X., **Guo L.**, Solon K., Ikumi D., Batstone D., Brouckaert C., Takács I., Grau P., Ekama G., Jeppsson Ulf and Gernaey K.V. (2013) Towards BSM2-GPS-X: A plant-wide benchmark simulation model not only for carbon and nitrogen, but also for greenhouse gases (G), phosphorus (P), sulphur (S) and

micropollutants (X), all within the fence of WWTPs/WRRFs. In proceedings of the 4th IWA/WEF Wastewater Treatment Modelling Seminar 2014 (WWTmod2014), Spa, Belgium, March 30 - April 2 2014.

Rehman U., Vesvikar M., Maere T., **Guo L.**, Vanrolleghem P.A. and Nopens I. (2013) Effect of sensor location on controller performance in a wastewater treatment plant. In proceedings of the 11th IWA conference on instrumentation control and automation, Narbonne, France, September 18-20 2013.

Guo L., Lamaire-Chad C., Bellandi G., Daelman M., Amerlinck Y., Maere T., Nous J., Flameling T., Weijers S., van Loosdrecht M.C.M., Volcke E.I.P., Nopens I. and Vanrolleghem P.A. (2013) High-frequency field measurement of nitrous oxide (N₂O) gas emissions and influencing factors at WWTPs under dry and wet weather conditions. In proceedings of IWA Nutrient Removal and Recovery 2013: Trends in Resource Recovery and Use, Vancouver, Canada, July 28-31 2012.

Pocquet M., Filali A., Bessiere Y., **Guo L.**, Queinnec I., Vanrolleghem P.A. and Spérandio M. (2012) Modelisation de la production de protoxyde d'azote pendant les processus de nitrification/dénitrification: application a un réacteur granulaire aérobie. In proceedings of Le 9ème Congrès International du GRUTTEE, Aix en Provence, France, Octobre 29-31 2012. (In French)

Guo L., Martin C., Nopens I. and Vanrolleghem P.A. (2012) Climate change and WWTPs: Controlling greenhouse gas (GHG) emissions and impacts of increased wet weather disturbances. In proceedings of IWA Nutrient Removal and Recovery 2012: Trends in NRR, Harbin, China, September 23-25 2012.

Flores-Alsina X., Arnell M., Amerlinck Y., Corominas Ll., Gernaey K.V., **Guo L.**, Lindblom E., Nopens I., Porro J., Shaw A., Snip L., Vanrolleghem P.A. and Jeppsson U. (2012) Balancing effluent quality, economical cost and greenhouse gas emissions during the evaluation of plant-wide wastewater treatment control strategies. In proceedings of IWA Nutrient Removal and Recovery 2012: Trends in NRR, Harbin, China, September 23-25 2012.

Pocquet M., Filali A., Bessiere Y., **Guo L.**, Queinnec I., Vanrolleghem P.A. and Sperandio M. (2012) Analysis and modelling of process conditions influencing N₂O emission by aerobic granular sludge processes for N/DN treatment. In proceeding of IWA Nutrient Removal and Recovery 2012: Trends in NRR, Harbin, China, September 23-25 2012.

Flores-Alsina X., Arnell M., Amerlinck Y., Corominas Ll., Gernaey K.V., **Guo L.**, Lindblom E., Nopens I., Porro J., Shaw A., Vanrolleghem P.A. and Jeppsson U. (2012) A dynamic modelling approach to evaluate GHG emissions from wastewater treatment plants. In proceeding of IWA World Congress on Water, Climate and Energy, Dublin, Ireland, May 13-18 2012.

Guo L. and Vanrolleghem P.A. (2012) Full-scale N₂O model calibration using BSM2. In: N₂O Workshop at the 3rd IWAWEF Wastewater Treatment Modelling Seminar (WWTmod2012), Québec, Canada, February 26-28 2012.

Guo L., Amerlinck Y., Nopens I., Porro J. and Vanrolleghem P.A. (2012) Greenhouse gases from and impact of climate change on wastewater treatment plants. In: 47th Central Canada Symposium on Water Quality Research, Burlington, Canada, February 21-22 2012.

Vanrolleghem P.A., **Guo L.**, Porro J., Amerlinck Y., Shaw A. and Nopens I. (2011) Mitigating wastewater utility greenhouse gas footprints - Development of a benchmark simulation model. In: First International Symposium on Microbial Resource Management in Biotechnology: Concepts & Applications, Ghent, Belgium, June 30 – July 1 2011.

Guo L., Vanrolleghem P.A., Amerlinck Y. and Nopens I. (2011) Plant-wide inspection of integrated N₂O pathway models. In: the 8th International IWA Symposium on Systems Analysis and Integrated Assessment (Watermatex 2011). San Sebastián, Spain, June 19-22 2011.

Porro J., **Guo L.**, Sharma K., Benedetti L., Van Hulle S., Vanrolleghem P.A., Amerlinck Y., Yuan Z., Shaw A. and Nopens I. (2011) Towards a benchmarking tool for minimizing wastewater utility greenhouse gas footprints. In proceedings of 8th International IWA

Symposium on Systems Analysis and Integrated Assessment (WATERMATEX2011).

San Sebastian, Spain, June 20-22 2011.

2.3 Posters

Guo L. and Vanrolleghem P.A. (2012) Controlling greenhouse gas emissions from wastewater treatment plants. In: Climate Change Day - Faculty of Bioscience Engineering Ghent University. Gent, Belgium, 17 March 17 2011.